SD

USAAVLABS TECHNICAL REPORT 68-22A

IN-FLIGHT MEASUREMENT AND CORRELATION WITH THEORY OF BLADE AIRLOADS AND RESPONSES ON THE XH-51A COMPOUND HELICOPTER ROTOR

VOLUME I
MEASUREMENT AND DATA REDUCTION OF AIRLOADS AND STRUCTURAL LOADS

By
E. A. Bartsch

May 1968

U. S. ARMY AVIATION MATERIEL LABORATORIES
FORT EUSTIS, VIRGINIA

CONTRACT DA 44-177-AMC-357(T)
LOCKHEED-CALIFORNIA COMPANY
BURBANK, CALIFORNIA

Disclaimers

The findings in this report are not to be construed as an official Department of the Army position unless so designated by other authorized documents.

When Government drawings, specifications, or other data are used for any purpose other than in connection with a definitely related Government procurement operation, the United States Government thereby incurs no responsibility nor any obligation whatsoever; and the fact that the Government may have formulated, furnished, or in any way supplied the said drawings, specifications, or other data is not to be regarded by implication or otherwise as in any manner licensing the holder or any other person or corporation, or conveying any rights or permission. manufacture, use, or sell any patented invention that may in any way be related thereto.

Disposition Instructions

Destroy this report when no longer needed. Do not return it to the originator.

DEPARTMENT OF THE ARMY
U. S. ARMY AVIATION MATERIEL LABORATORIES
FORT EUSTIS, VIRGINIA 23604

Under Army contract, the Lockheed Aircraft Corporation has conducted an investigation of blade aerodynamic pressures and strains and other associated flight characteristics on an XH-51A compound helicopter. The flight tests and theoretical analyses which were performed during the program were monitored by Army personnel, and the final report has been reviewed to ensure basic technical accuracy.

This report is published for the dissemination of information and the stimulation of further research.

Task 1F125901A14608
Contract DA 44-177-AMC-357(T)
USAAVLABS Technical Report 68-22A
May 1968

IN-FLIGHT MEASUREMENT AND CORRELATION WITH THEORY OF BLADE AIRLOADS AND RESPONSES ON THE XH-51A COMPOUND HELICOPTER ROTOR

LR 21072

VOLUME I
MEASUREMENT AND DATA REDUCTION OF AIRLOADS AND STRUCTURAL LOADS

By

E. A. Bartsch

Prepared by

Lockheed-California Company
Burbank, California

for

U. S. ARMY AVIATION MATERIEL LABORATORIES
FORT EUSTIS, VIRGINIA

ABSTRACT

This report presents the results of a two-phase research program consisting of (1) in-flight measurement of aerodynamic pressures and structural loads on a compound, rigid-rotor helicopter and (2) correlation of these data with theoretical results.

Flight test data obtained in Phase I and recorded on an oscillograph were read on an oscillograph reading machine and were processed in an automatic data reduction program. This data processing consisted of integration of the pressure data to obtain the distribution of aerodynamic lift and pitching moments over the rotor blade, as functions of azimuth position. Airload and structural load data were harmonically analyzed.

Output of the data reduction program was used in Phase II as input to the correlation program. The measured airloads were used to compute the theoretical bending and torsion responses of the blade. The measured torsion moments were used in the theoretical prediction of the airloads. The results of the applied theories are compared with the flight measurements.

FOREWORD

This report describes a two-phase research program consisting of (1) flight test measurements of helicopter rotor blade structural loads and aerodynamic pressures and (2) correlation of these measurements with data obtained from current theories. This research program was conducted by the Lockheed-California Company under Contract DA 44-177-AMC-357(T) to the U.S. Army Aviation Materiel Laboratories (USAAVLABS), Fort Eustis, Virginia.

The research program was performed during the period from June 1966 to October 1967. Technical monitoring of the project for USAAVLABS was by W. E. Nettles.

The report covering the program is presented in three volumes. Volume I is entitled "Measurement and Data Reduction of Airloads and Structural Loads". It contains the main body of the report plus Appendixes I through IV. Volume II contains Appendixes V through IX, with all flight test data in tabular form. The correlation of the measured airloads and structural loads with theoretical data is covered in Volume III, "Theoretical Prediction of Airloads and Structural Loads and Correlation with Flight Test Measurements".

The Lockheed program was under the technical direction of A. W. Turner and W. E. Spreuer, engineering managers, and J. E. Sweers, project leader. The test pilot was R. Goudey. Additional Lockheed personnel associated with the program included W. H. Foulke and R. A. Berry, flight test; C. J. Buzzetti, E. A. Bartsch, S. H. Lomax, and T. H. Oglesby, structural flight measurement; R. H. Cook and R. G. Murison, instrumentation; R. D. Baker and W. C. Weddle, data processing; R. E. Donham and D. H. Janda, rotary wing dynamics; C. H. Ranschau, programming; and R. P. Boal, editor.

Appreciation is due USAAVLABS for their help in providing assistance and advice in planning and executing the entire research program.

CONTENTS

VOLUME I

VOLUME II

VOLUME III

LIST OF ILLUSTRATIONS

LIST OF TABLES

INTRODUCTION

Under contract to the U. S. Army Transportation Research Command,* Lockheed has conducted a series of research flight test programs to determine the capabilities of compound helicopters in high-speed flight (References 1 through 3). The objective of the program reported herein was to investigate rotor blade loads especially in the high-speed range.

The test vehicle for these programs was an XH-51A helicopter modified to the compound configuration. This modification consisted principally of adding a 70-square-foot wing and an auxiliary jet engine to the basic helicopter. No changes were made to the rotor system. Because of its ability to provide control power throughout the high-speed range with an unloaded rotor, the rigid-rotor concept is the key design feature in this compound helicopter.

From 1958, when Lockheed started developing the rigid-rotor helicopter, until the start of this contract, all blade loads were measured by strain gages only.

With rapidly approaching compound helicopter application, additional rotor blade structural loads data, aerodynamic pressure data, and correlation of these measurements with data obtained from current theories as presented in this report are needed to assist designers of future compound helicopters.

The overall purpose of this program was to investigate rotor blade loads on a compound helicopter. Specific objectives were:

- To obtain measured airload distributions for use in correlation with theoretical airload distributions and for calculation of the dynamic response of the rotor blade.
- To obtain measured blade response for these same conditions for correlation with theoretical response.
- To evaluate and demonstrate the applicability of numerical computation methods to the prediction of blade fatigue loads.

---

* Name changed to U.S. Army Aviation Materiel Laboratories in March 1965.

DESCRIPTION OF TEST ARTICLE

TEST VEHICLE

The test vehicle was the Lockheed XH-51A rigid-rotor helicopter, S/N 1002, modified to a compound helicopter configuration. The major modifications included the installation of a short-span wing and a J-60 jet engine, as shown in Figure 1. These modifications permitted the evaluation of a wide range of rotor lift and speed combinations from hover to speeds producing transonic Mach numbers at the advancing blade tips. Table I presents a detailed breakdown of the pertinent configuration items. Photographs of the test vehicle are presented in Figures 2 and 3. Photographs of the transducer installations on the blade are presented in the Instrumentation section.

The basic helicopter was a standard model XH-51A helicopter with a 35-foot-diameter rigid rotor, a Canadian Pratt and Whitney PT6B-9 engine, and retractable skid landing gear. In the experimental configuration used for these tests, the passenger space was utilized for the instrumentation equipment and extra fuel. The significant item for this program was the installation of special pressure transducers on the instrumented rotor blade (No. 1) and a special set of 162 instrumentation sliprings. Refer to the instrumentation section of this report for a detailed description of the transducer installations on the blade.

FATIGUE ANALYSIS AND TEST OF THE PERFORATED ROTOR BLADE

A fatigue analysis of the modified main rotor blade was performed using actual laboratory test data and predicted flight loading. The method used to evaluate the effect of holes in the rotor blade was as follows:

1. An S-N curve was derived from the results of spectrum fatigue testing on a Model 286 main rotor blade root specimen.
2. A stress spectrum was derived from the anticipated loading spectrum for the flight test program.
3. A cumulative damage calculation was performed using the above data.

The estimated fatigue life of 18.1 hours before a crack starts, indicated by the above calculation, is sufficient to substantiate the safety of the flight test program by analytical methods.

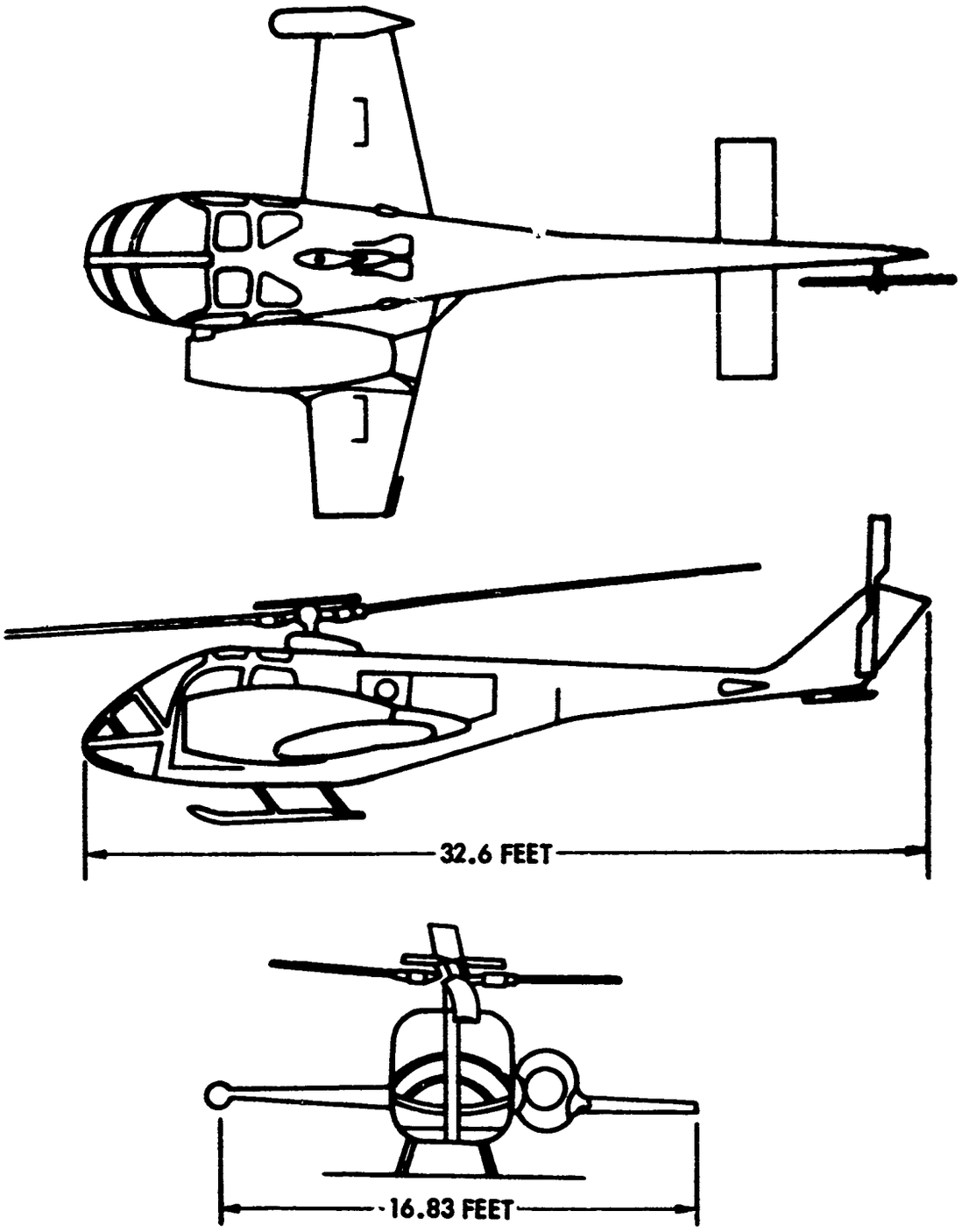

Figure 1. XH-51A Compound Helicopter General Arrangement

TABLE I. COMPOUND HELICOPTER DESCRIPTION

General	
Design gross weight	4,500 lb
Fuel capacity (includes 220-lb-capacity torso tank)	700 lb
Normal crew (plus research instrumentation)	one with torso tank
Overall length	42.58 ft
Maximum ground attitude (tail low)	6°
Roll mass moment of inertia (including rotor)	1,500 slug-ft^2
Pitch mass moment of inertia (including rotor)	3,180 slug-ft^2
Yaw mass moment of inertia (including rotor)	3,800 slug-ft^2
Main Rotor	
Type	Rigid
Diameter	35 ft
Number of blades	4
Blade chord	13 in.
Blade weight	86 lb/blade
Airfoil section	Modified NACA 0012
Blade taper	0
Blade twist (root to tip)	-5°
Rotational axis tilt	6° forward
Hub precone	$+3.2^{\circ}$
Preset blade droop at sta 27.85	-1°
Disc area	962 ft^2
Solidity	.0818
Disc loading	4.68 lb/ft^2
Polar moment of inertia	1,013 slug-ft^2
Normal operating speed	355 rpm
Blade sweep	1.4° forward
Control Gyro	
Diameter	72 in.
Number of arms	4
Polar moment of inertia	7.5 slug-ft^2
Incidence angle of arms	5.0

TABLE I (cont'd)	
Tail Rotor	
Diameter	72 in.
Number of blades	2
Blade chord	8.5 in.
Hub type	Teetering
Airfoil section	NACA 0012
Blade taper	0
Blade twist (root to tip)	-4.35°
Feathering moment balance weights:	
weight	2.25 lb/blade
arm	3.0 in.
Delta -3 hinge	15°
Disc area	28.27 ft^2
Solidity	.1503
Pitch change travel	27° to -8°
Normal operating speed	2,085 rpm
Wing	
Span	16.83 ft
Taper ratio	.5
Area	70 ft^2
Aspect ratio	4.05
Sweepback (.25c)	0
Chord (MAC)	51.72 in.
Airfoil	NACA 23012
Incidence (fixed)	$-.9^{\circ}$
Horizontal Stabilizer	
Span	108 in.
Chord (constant)	26.4 in.
Area	19.8 ft^2
Aspect ratio	4.1
Incidence	-0.25°
Airfoil section	NACA 0015

TABLE I (concluded)	
Tip weights	8 lb/side
Vertical stabilizer	
Span	41.75 in.
Chord (tip)	38.5 in.
Chord (root)	51.5 in.
Area	12.68 ft^2
Taper ratio	.70
Aspect ratio	.95
Airfoil section	Modified NACA 4424
Powerplants	
Primary	
Type	Turboshaft PT6B-9
Maximum power (takeoff)	550 SHP @ sea level
Military power (30-minute limit)	500 SHP @ sea level
Fuel type	JP-4
Oil type	Turbo 35
Auxiliary	
Type	Turbojet J-60-P-2
Military thrust @ 200 knots	2,490 lb @ sea level
Fuel type	JP-4
Oil type	Turbo 35
Thrust axis inclination	$+7^{\circ}$

In addition to the fatigue analysis, a spectrum-type fatigue test was conducted on an XH-51A blade root sample with a set of holes identical to that of the flight vehicle. The stress spectrum derived for rotor station 115 was simulated on a cross section of the specimen corresponding to rotor station 52. The test duration corresponded to 20 hours of flight time. After this, the fatigue test was continued for another 20 hours of flight time with a 10-percent increase of varying stresses. No cracks due to the fatigue loading were observed, and the test was discontinued.

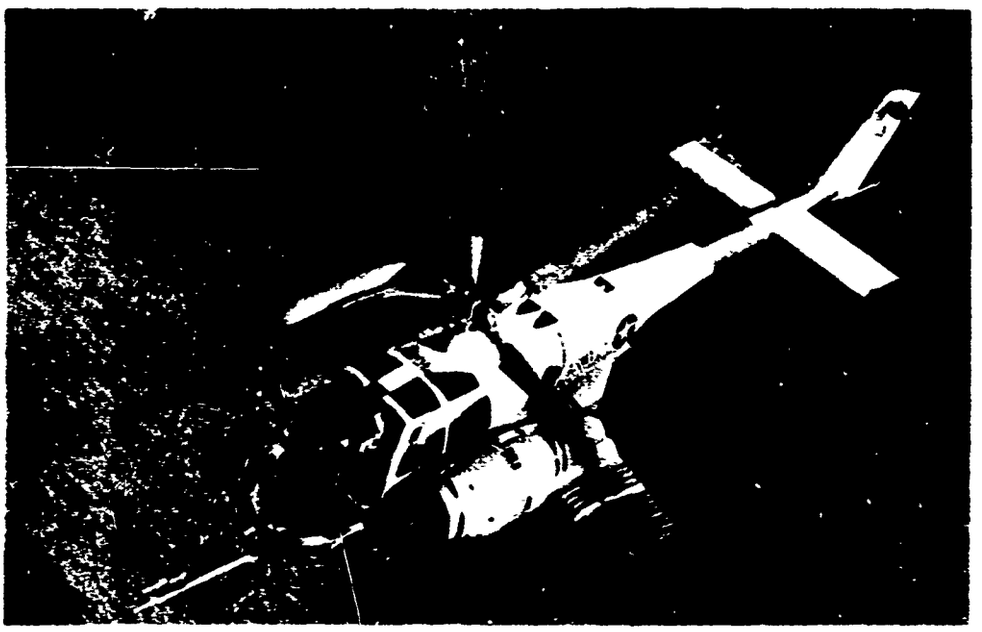

Figure 2. Test Vehicle in Flight

Figure 3. Front View of Test Vehicle

INSTRUMENTATION

INSTRUMENTATION SYSTEM

Conventional instrumentation methods and proven instruments were used in this flight loads research program in order to assure measurement accuracy and reliability throughout the flight test program. Except for the blade differential pressure transducers, only conventional transducers and strain gages well proven in the past were used. The blade differential pressure transducers are a relatively new product and represent the state of the art in this type of measurement. These transducers were tested both in the laboratory and in the whirl tower to prove their accuracy and integrity under all expected environmental conditions. Dynamic pressure fluctuations to 60 cycles per second and static blade pressures were measured. Instrumentation and transducer system signal phase shift was investigated, and phase shift correction was found to be unnecessary for the frequencies of interest.

The instrumented main rotor blade differential pressure transducer and moment-measuring strain gage bridge signals were routed through a 162-slipring assembly to two 50-channel oscillographs. Conventional series, shunt, and calibration resistors and controlling equipment were used with the oscillographs to provide proper recording trace height and calibration. One of the main sources of helicopter instrumentation system noise is the slipring assembly. Signal amplification is often necessary to produce a satisfactory signal-to-noise ratio, but careful design of the slipring assembly used in this program provided microvolt noise level and signal amplification was unnecessary.

Additional measurement parameters were provided by photo recordings of the pilot's instrument panel. Photographic speed was variable from one picture every 5 seconds to 10 frames per second.

MEASUREMENT PARAMETERS

The compound helicopter instrumentation utilized two 50-channel oscillographs and one photo recorder (photographing the pilot's instrument panel) as the recording devices.

Time correlation of the three recorders was obtained from a time coordination system driving counters simultaneously on the photo panel and in the two oscillographs.

The following rotor blade measurements were recorded in the oscillographs:

- 46 Differential pressure sensors, Figure 4

- Blade flapwise bending moments measured at the 6-, 24-, 45-, 73-, 115-, 140-, 157-, 172-, and 185-inch radial stations for a total of nine measurements, Figure 5
- Blade chordwise bending moments measured at the 6-, 45-, 115-, and 157-inch radial stations for a total of four measurements, Figure 5
- Blade torsional moment measured at radial stations 115 and 185 inches for a total of two measurements, Figure 5
- Flapwise and chordwise acceleration measured by two accelerometers located at the blade tip
- Pitch link axial load.

The following transmission gearbox velocity measurements were recorded in the oscillographs:

- One vertical velocity at the top of the gearbox
- Two lateral velocities, one each on the top and bottom of the gearbox
- Two fore and aft velocities, one each on the left and right sides of the gearbox.

The following vehicle parameters were recorded in the oscillographs:

- Angle of attack
- Main rotor blade pitch angle
- Collective pitch control position
- Longitudinal cyclic pitch control position
- Lateral cyclic pitch control position
- Tail rotor pedal position
- Main rotor shaft torque
- Roll rate
- Pitch rate
- Yaw rate
- Rotor load
- Wing root bending moment
- Horizontal stabilizer root bending moment
- Main rotor pip (azimuth)
- Normal acceleration at the center of gravity
- Sideslip angle.

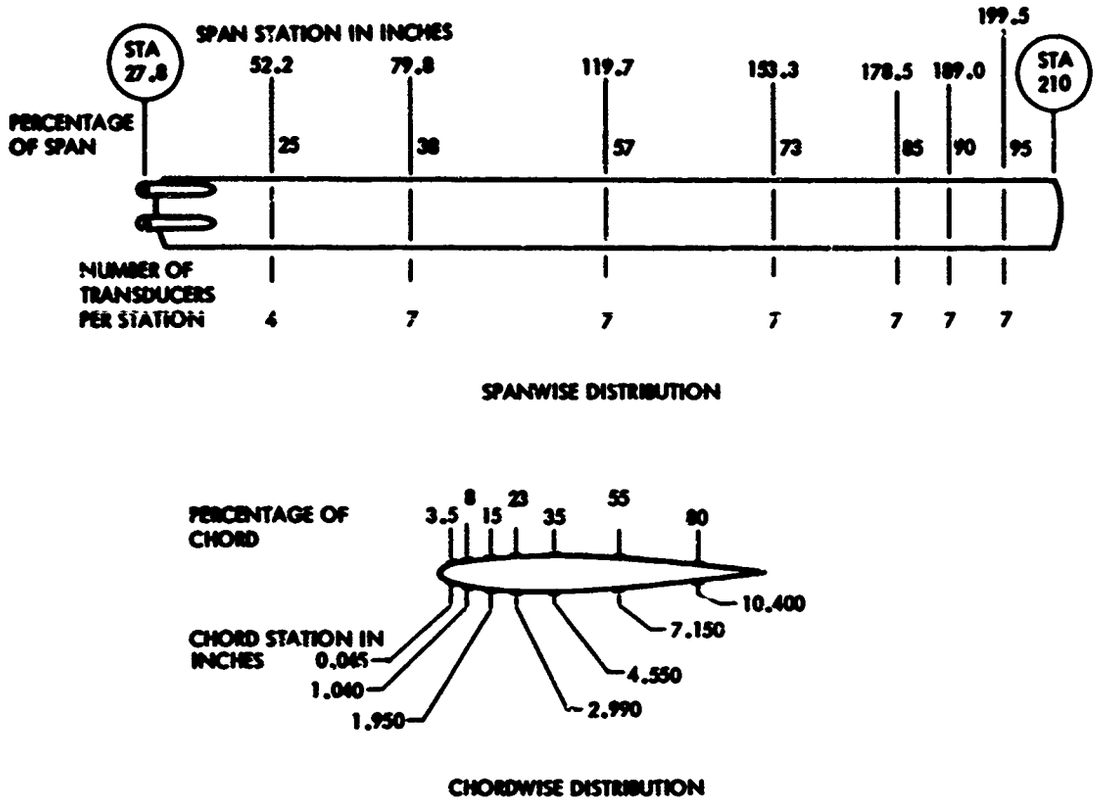

Figure 4. Location of Pressure Measurements on Main Rotor Blade

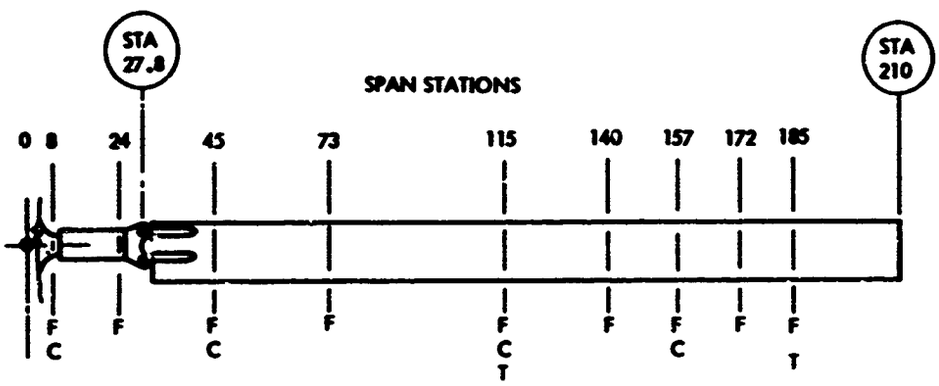

Figure 5. Location of Strain Gage Measurements on Main Rotor Blade

The following measurements were made in the photo recorder panel (time-phased, photographic record of pilot's instrument indications), Figure 6:

- Airspeed
- Altitude
- Outside air temperature
- Exhaust gas temperature of the main rotor powerplant (PT-6)
- Exhaust gas temperature for the auxiliary propulsion unit (J-60)
- Compressor inlet temperature for the main rotor powerplant (PT-6)
- Time
- Fuel quantity (total)
- J-60 engine rpm
- J-60 engine pressure ratio
- Main rotor power turbine rpm
- Main rotor power turbine torque
- Main rotor shaft rpm.

Other instruments were also located on the pilot's instrument panel for control of the helicopter. Figure 7 shows an oscillograph and the pilot's instrument panel, while Figure 6 shows a closeup view of the pilot's instrument panel as seen by the camera.

TECHNICAL APPROACH

Blade Pressure Measurements

Pressure transducers were mounted at seven chordwise blade stations at each of the six outboard spanwise stations located at 38, 57, 73, 85, 90, and 95 percent of blade radius. In addition, tranducers were mounted at four chordwise stations on the inboard spanwise station (at 25 percent of blade radius). The table below shows this distribution and the pressure ranges in psid (in parentheses) of the transducers.

Chordwise location in percent chord	Spanwise location in percent of blade radius						
	25	38	57	73	85	90	95
3.5	(5)	(5)	(10)	(10)	(15)	(15)	(15)
8		(5)	(10)	(10)	(15)	(15)	(15)
15	(5)	(5)	(5)	(10)	(15)	(15)	(15)
23		(5)	(5)	(5)	(10)	(10)	(10)
35	(5)	(5)	(5)	(5)	(5)	(5)	(5)
55		(2)	(2)	(2)	(2)	(2)	(2)
80	(2)	(2)	(2)	(2)	(2)	(2)	(2)

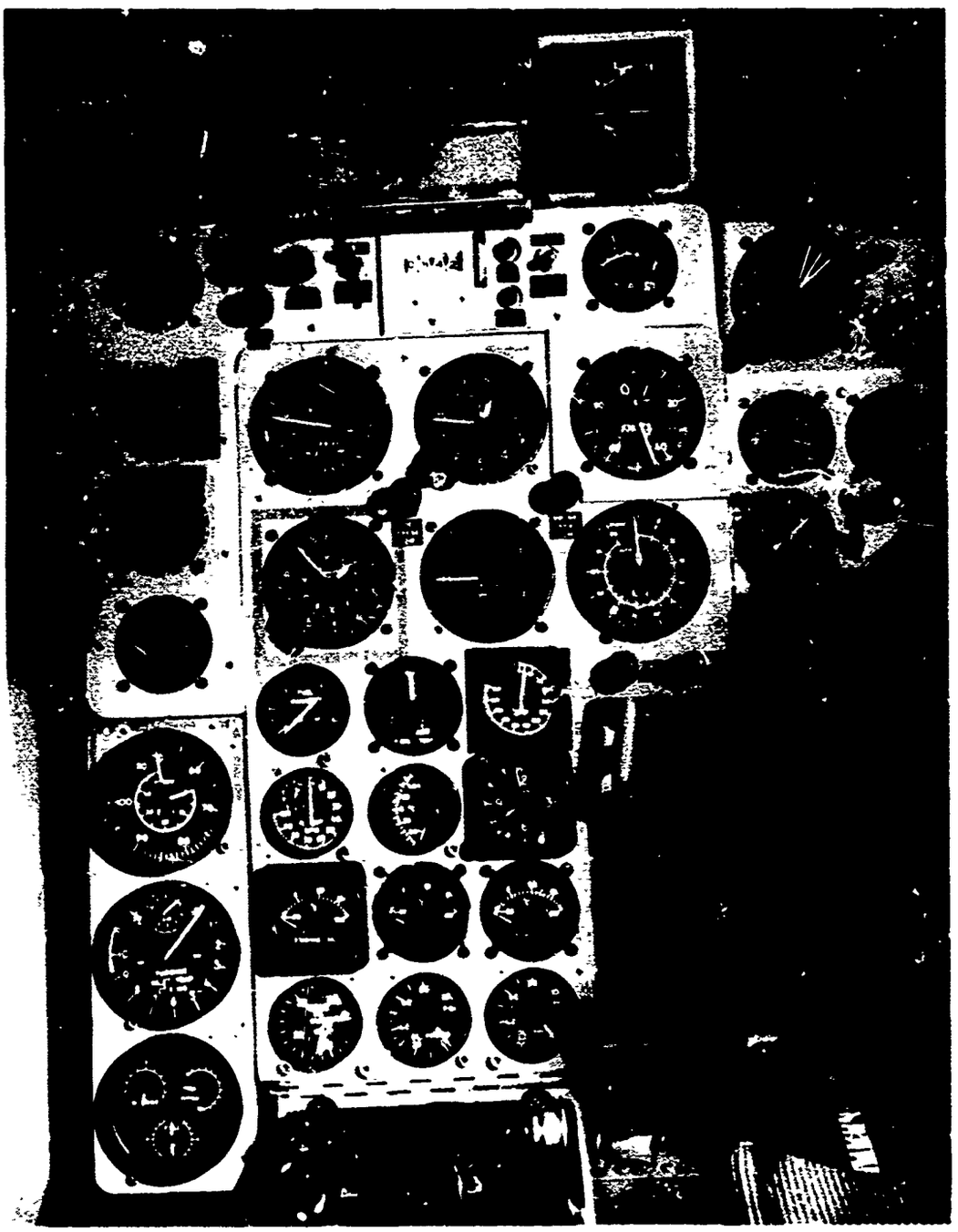

Figure 6. Photo Recorder Panel

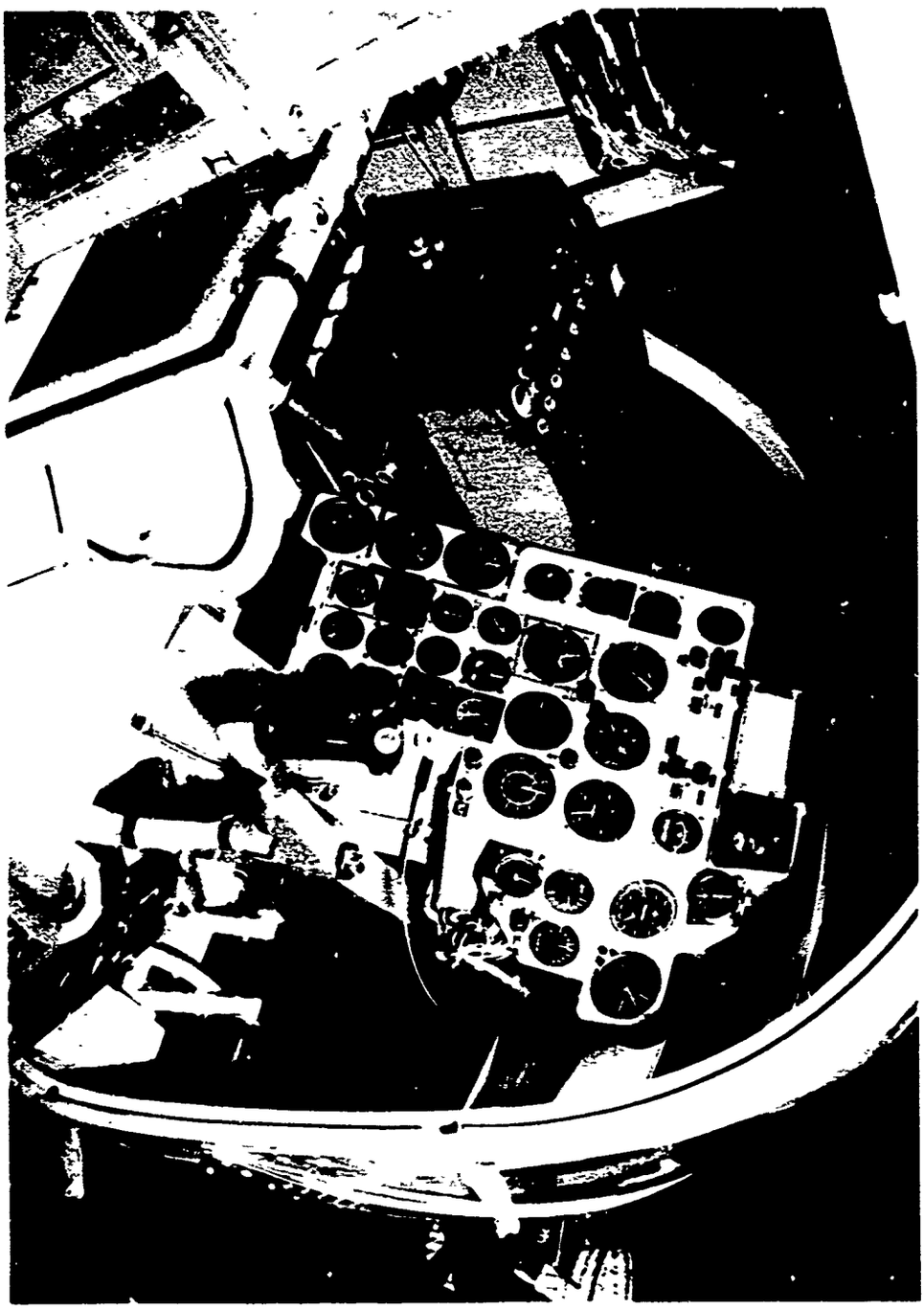

Figure 7. Oscillograph and Photo Panel

Pressure transducer selection was extremely limited because of the very limited space available in the helicopter blade and the small pressure port desired. The pressure transducers selected were manufactured by Scientific Advances Incorporated, model SA-SDM-7F. These transducers constitute the very latest in an improved line of very subminiature semiconductor strain gage pressure transducers. These transducers incorporate temperature compensation, external to the sensing diaphragm, by thermistors located on the transducer paddle (see Figures 8 and 9).

Tests revealed a relatively simple technique for mounting the differential pressure transducers that practically eliminated the effects of blade strain on the transducers. This technique utilized a mounting tube which fitted through the helicopter blade (see Figures 8 and 10) and held the pressure transducer by its rugged reference pressure stem. The actual mounting of the transducers can be seen in Figures 9 and 11.

After the pressure transducers were mounted, it was necessary to add a fairing to cover the transducers (see Figure 8) on the top of the blade. This was accomplished by putting a rubber pressure sealing boot around the transducer (see Figures 12 and 13 for additional fairing details). The rubber fairing was originally covered with a stainless steel sheath, but it could not be made tight enough to prevent air leakage. Instead, shim

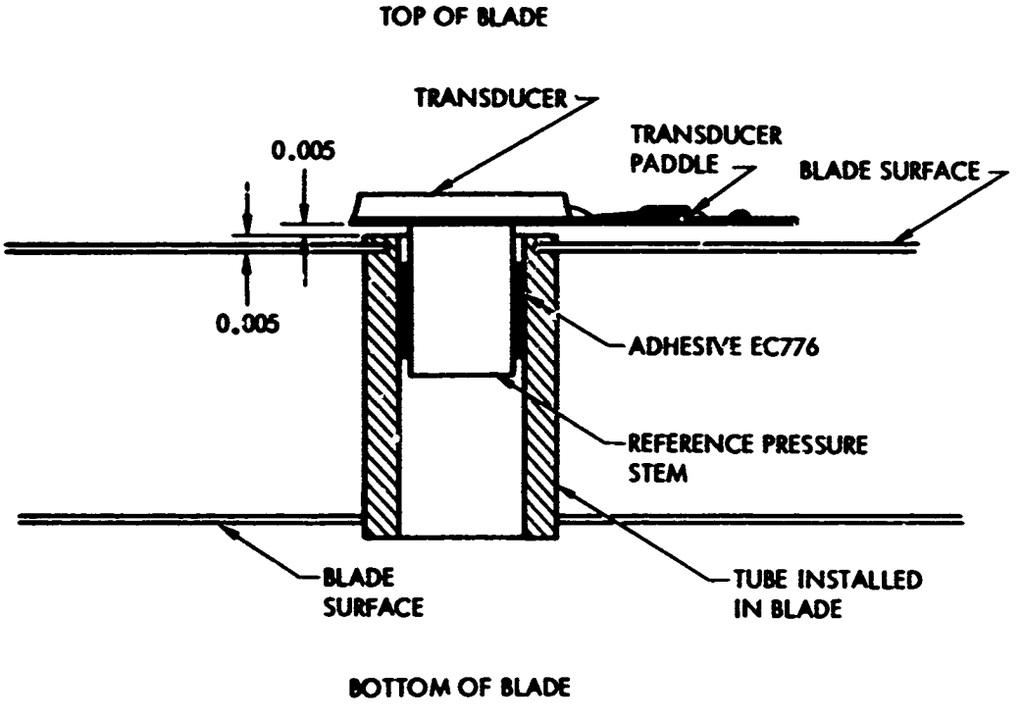

Figure 8. Blade Pressure Transducer Tube Installation

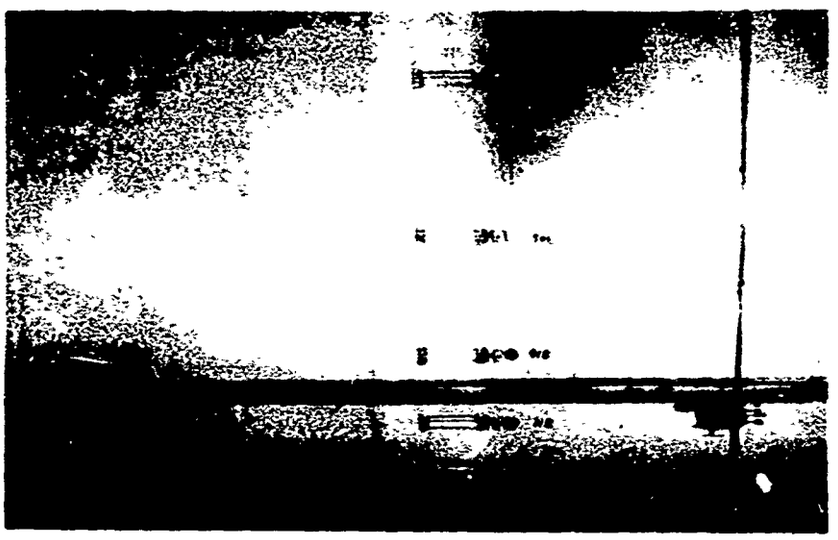

Figure 9. Seven Differential Pressure Transducers Exposed in Mounting Holes

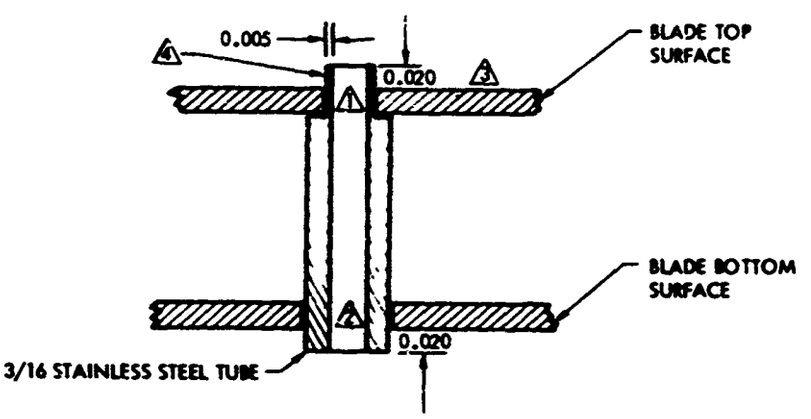

NOTES: DIMENSIONS IN INCHES

1. TOP HOLE IN BLADE SKIN 0.144
2. BOTTOM HOLE IN BLADE SKIN 0.189
3. TUBE SHANK TURNED DOWN TO 0.005 WALL THICKNESS AND PROTRUDES 0.020 ABOVE BLADE SURFACE. BLADE SURFACE THICKNESS VARIES; THEREFORE, EACH TUBE HAD TO BE FITTED
4. SWAGE TO TOP BLADE SURFACE WITH SPECIAL TOOL DEVELOPED SPECIFICALLY FOR THIS PURPOSE

Figure 10. Blade Pressure Transducer Tube Installation

Pressure transducer selection was extremely limited because of the very limited space available in the helicopter blade and the small pressure port desired. The pressure transducers selected were manufactured by Scientific Advances Incorporated, model SA-SDM-7F. These transducers constitute the very latest in an improved line of very subminiature semiconductor strain gage pressure transducers. These transducers incorporate temperature compensation, external to the sensing diaphragm, by thermistors located on the transducer paddle (see Figures 8 and 9).

Tests revealed a relatively simple technique for mounting the differential pressure transducers that practically eliminated the effects of blade strain on the transducers. This technique utilized a mounting tube which fitted through the helicopter blade (see Figures 8 and 10) and held the pressure transducer by its rugged reference pressure stem. The actual mounting of the transducers can be seen in Figures 9 and 11.

After the pressure transducers were mounted, it was necessary to add a fairing to cover the transducers (see Figure 8) on the top of the blade. This was accomplished by putting a rubber pressure sealing boot around the transducer (see Figures 12 and 13 for additional fairing details). The rubber fairing was originally covered with a stainless steel sheath, but it could not be made tight enough to prevent air leakage. Instead, shim

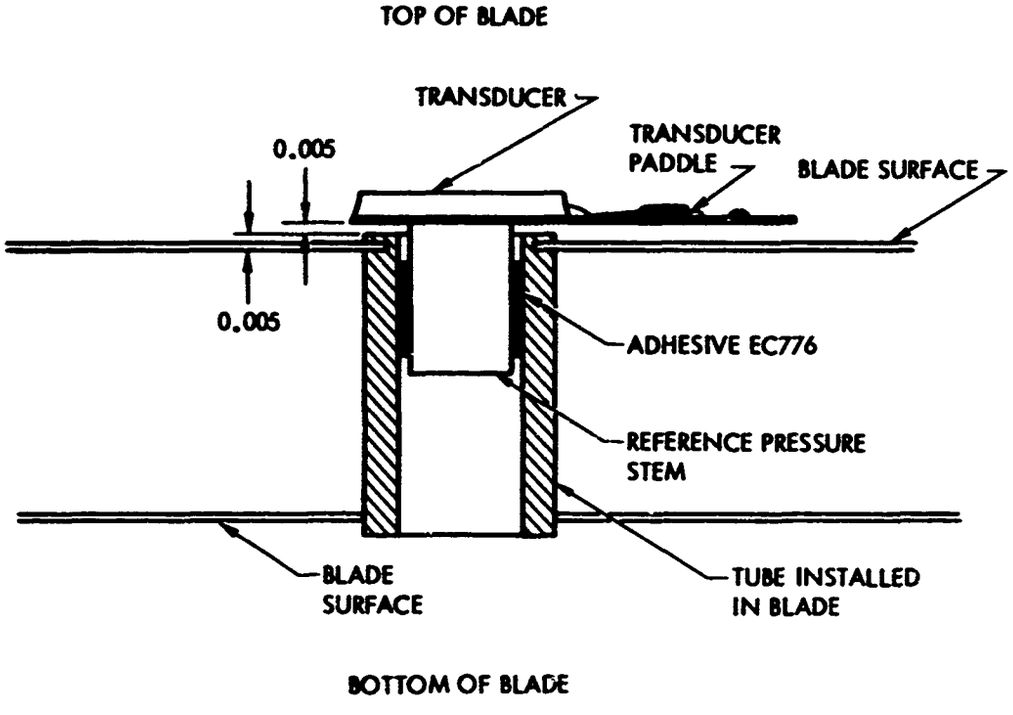

Figure 8. Blade Pressure Transducer Tube Installation

Figure 9. Seven Differential Pressure Transducers Exposed in Mounting Holes

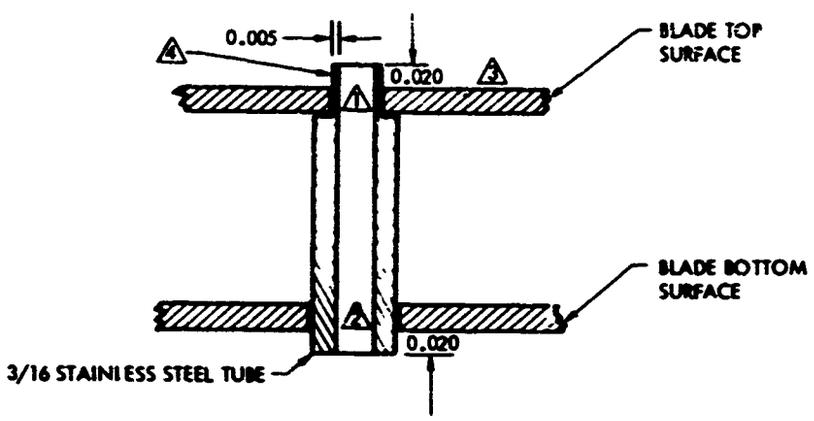

NOTES: DIMENSIONS IN INCHES

1. TOP HOLE IN BLADE SKIN 0.144
2. BOTTOM HOLE IN BLADE SKIN 0.189
3. TUBE SHANK TURNED DOWN TO 0.005 WALL THICKNESS AND PROTRUDES 0.020 ABOVE BLADE SURFACE. BLADE SURFACE THICKNESS VARIES; THEREFORE, EACH TUBE HAD TO BE FITTED
4. SWAGE TO TOP BLADE SURFACE WITH SPECIAL TOOL DEVELOPED SPECIFICALLY FOR THIS PURPOSE

Figure 10. Blade Pressure Transducer Tube Installation

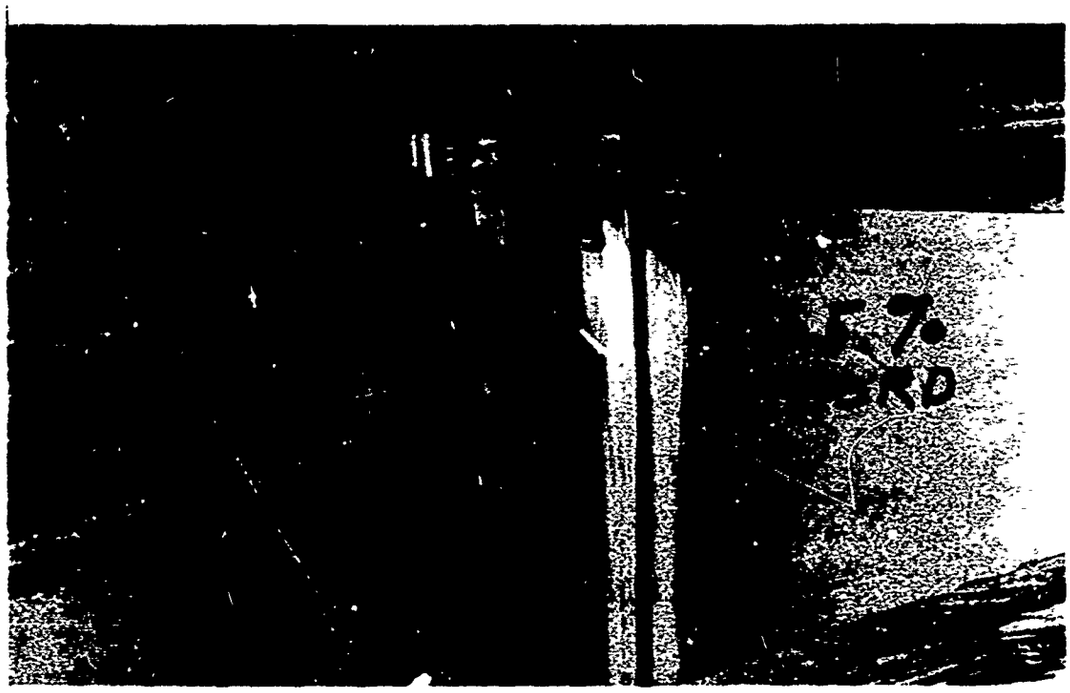

Figure 11. Blade with 3.5 Percent Chord Differential Pressure Transducer and Mounting Hole for 15 Percent Chord Transducer

Figure 12. Rubber Pressure Sealing Booting Around Transducers (Top Blade Surface)

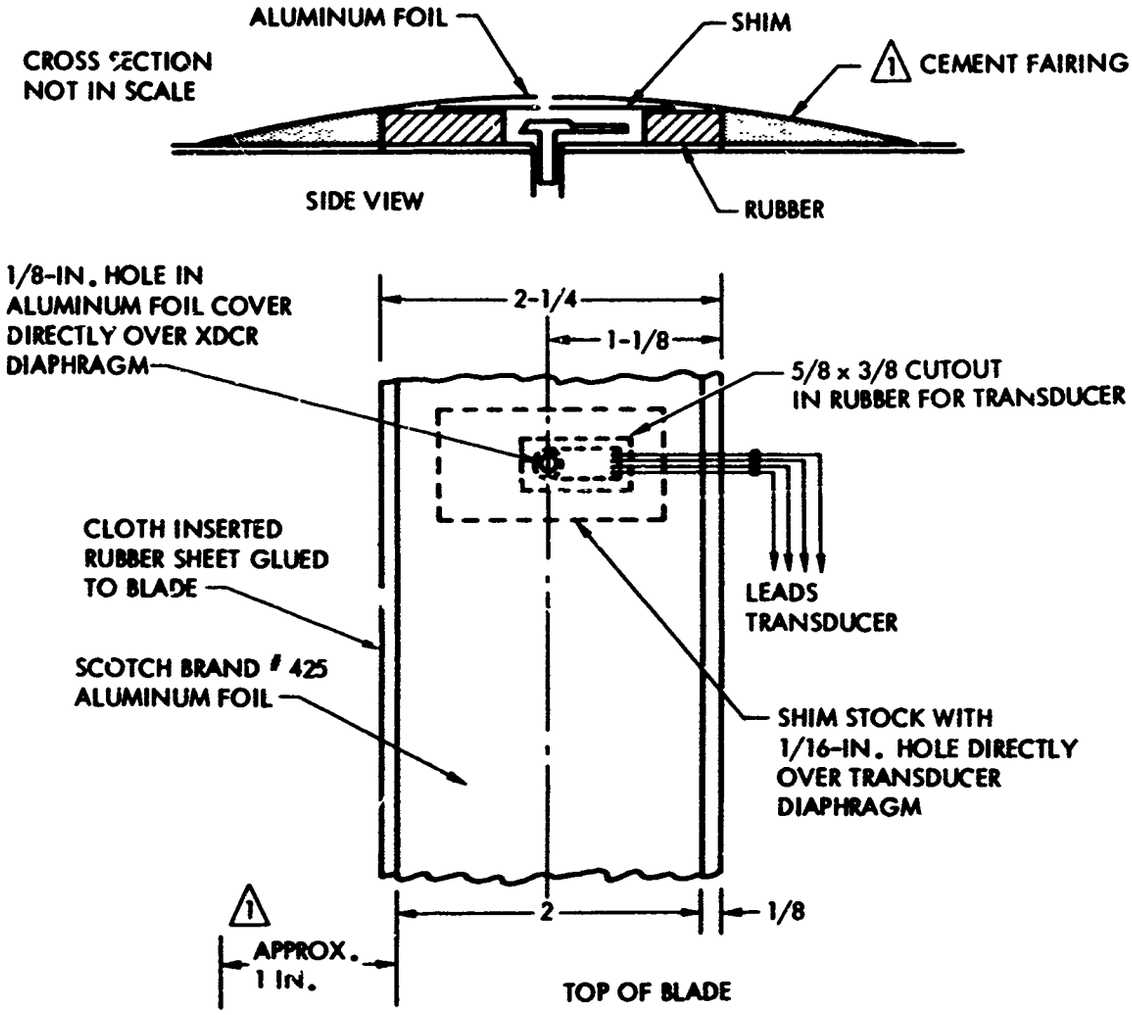

NOTES:

1. C-3 CEMENT FAIRING FROM ALUMINUM FOIL TO BLADE SURFACE
2. FAIRING IS AROUND COMPLETE BLADE
3. BOTTOM SURFACE HOLES IN RUBBER SHEET ARE TIGHTLY FITTED ON TUBE EXTENSION
4. BOTTOM SURFACE HOLES IN ALUMINUM FOIL ARE 1/16-IN. SIZE

DIMENSIONS IN INCHES

Figure 13. Blade Fairing for Transducer Installation

stock (with a 1/16-inch port) large enough to overlap the rubber boot cut-out area surrounding the transducer was placed over the transducer and sealed to the rubber boot. Then an adhesive-backed aluminum foil was placed over the rubber boot and tightly bonded. Epoxy cement was used to fair in the edges of the completed assembly, which can be seen in Figures 14 and 15. Periodically during flight testing, the metallic tape covering the transducer installation had to be replaced because of dust particle erosion. This was relatively easy to accomplish, and the problem was minimized by reducing operating time under dusty conditions.

The accepted transducers (six were rejected) were all well within the manufacturer's specification for thermal zero shift (less than 0.05 percent full scale per degree F) and sensitivity change due to temperature change (average of 0.08 percent full scale per degree F). All pressure transducers, 2, 5, 10, and 15 psid, were calibrated and tested throughout the operational temperature range for comparison with manufacturer's performance specifications. The tests included linearity and hysteresis checks as well as a sensitivity determination. Test results indicated that the performance was within the specifications, but additional testing was performed to determine stability under expected operating conditions.

Transducer installation development was carried out by installation of three transducers in a test blade. This blade and the installation were subjected to twisting, bending, and vibrating inputs simulating flight conditions. This blade was X-rayed before the tests began and during the testing to verify that the transducer tube installations, Figures 8 and 10, did not affect the structural integrity of the blade. Results of all these tests were satisfactory, and installation of the transducers in the flight blade began immediately.

As each pressure transducer was installed on the blade, the sensitivity to blade stress was checked and a leak test was conducted. After the transducer installation and checkout were completed, wiring runs and terminations were accomplished and the protective transducer fairings were installed.

To prove the mounting technique a single pressure transducer was installed on a special test blade. Output from this transducer was recorded on an oscillograph during whirl tests of the blade on a whirl stand through normal operating ranges. The fact that the operation and output of this transducer were satisfactory during these tests provided a basis for confidence in the installation method.

Shake tests were performed on the nonrotating, completely instrumented rotor blades to determine the natural flapwise and chordwise bending mode frequencies and to determine the response of pressure pickups. Shake tests were also performed on the noninstrumented blades. The measured mode shapes of the instrumented blade were compared with the calculated mode shapes (Figure 16). Ballast weights were installed in the noninstrumented blades to compensate for the difference in mass distribution between the blades.

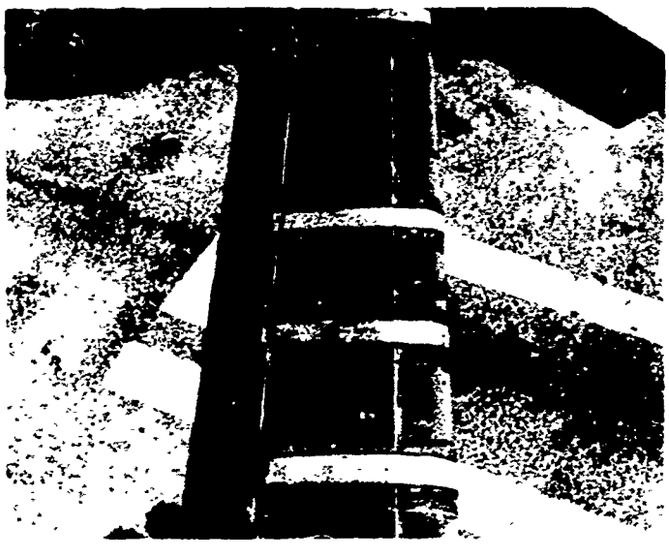

Figure 14. Transducer Installation Completed
(Top Surface of Blade)

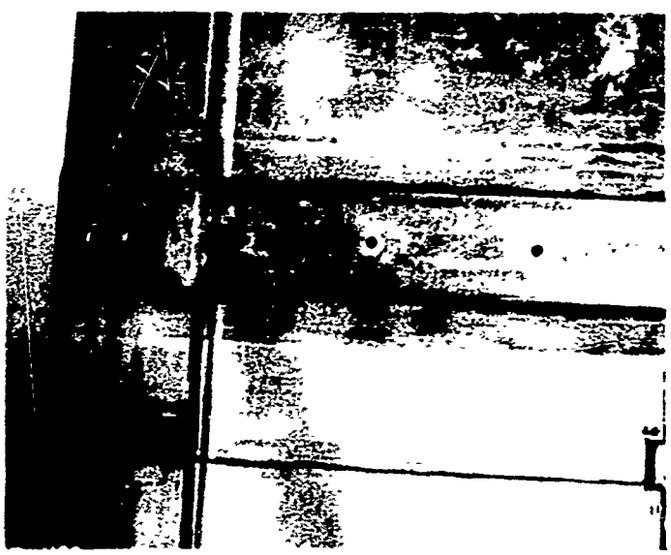

Figure 15. Transducer Installation Completed
(Bottom Surface of Blade)

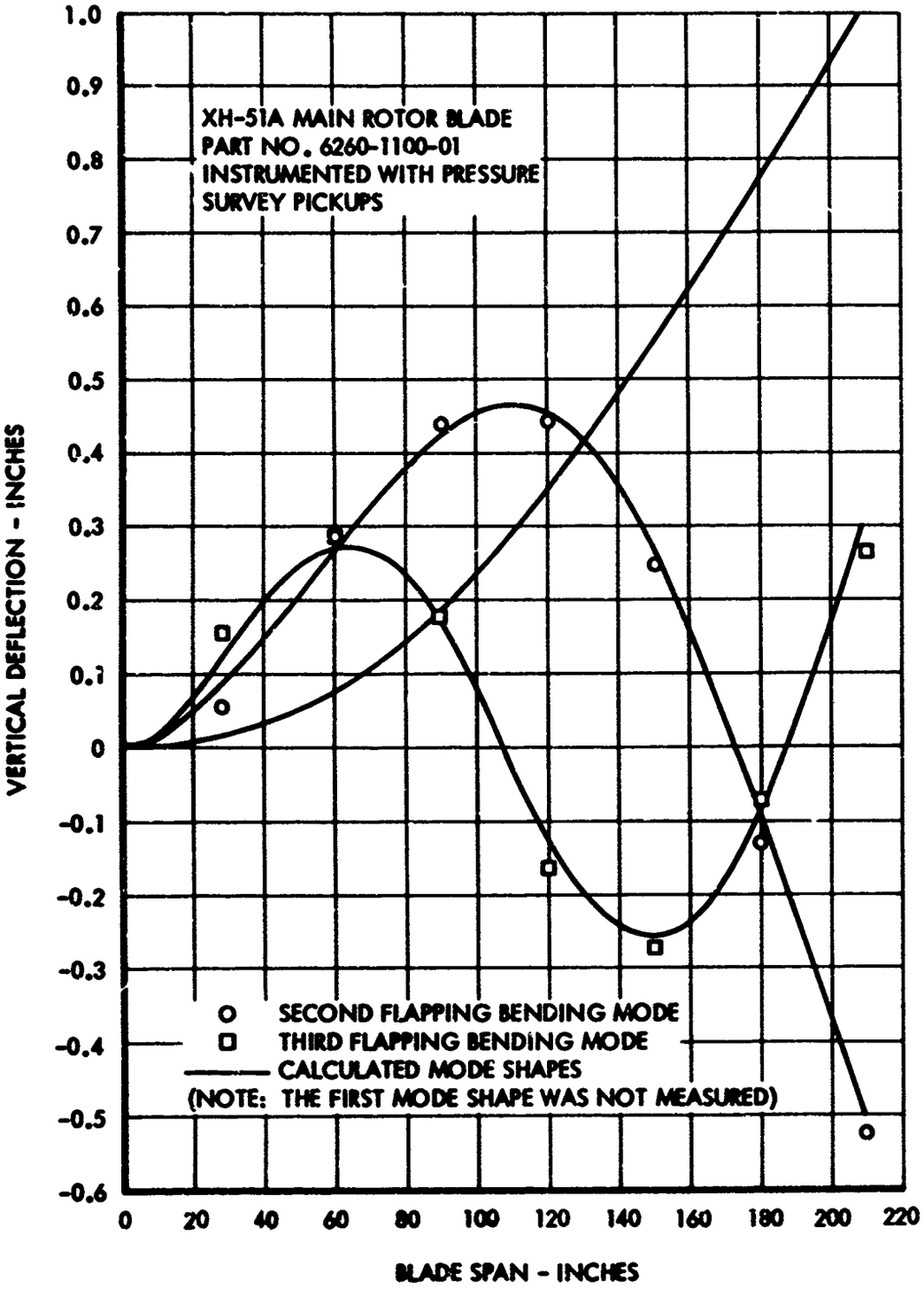

Figure 16. Comparison of Measured and Calculated Mode Shapes

After the shake test, the completely instrumented blade was X-ray inspected to check blade structural integrity in the area of the holes bored for transducer installation. The X-ray inspection was also used to provide a reference for later X-ray inspections which were performed periodically during the flight testing.

A frequency response test was performed on a typical pressure transducer installation in the range of interest for the program. The test was conducted by applying an oscillating pressure first to the diaphragm side (top of blade) and then to the vent side (bottom of blade) of the transducer. The outputs of the transducer as well as of a reference transducer of known characteristics were recorded on an oscillograph and monitored for phase and amplitude. The results indicated an essentially flat response and minimal phase shift up to 150 Hz, which is well above the frequencies of interest on this program.

In reducing flight data it was found that in-flight zero shifts were occurring on some of the blade pressure measurements. Zeros recorded before and after the flight showed differences of approximately 4 percent of full scale on the pressure gages with a range of 15, 10, and 5 psid and about 9 percent on the low-range pressure gages of 2 psid. The differences were larger than would have been predicted on the basis of laboratory tests. A thorough investigation of the possible parameters causing the undesired zero shift was initiated. This investigation showed that the semiconductor strain gages tended to drift from one stable condition to another. Oscillograph recordings taken in the hangar at different time intervals indicated that some of the transducers drifted more than others. This was partially due to the transducer's use of external temperature compensation. Quite a number of transducers were fairly stable. Readings at zero rotor speed and at 100-percent operating rpm with collective set for nearly zero blade angle showed considerable differences on some elements which could not be explained by the small pressure differences due to the blade twist. Readings of the mean values of two different hovering conditions on the same flight also showed the effect of zero shift. Similar but smaller differences were observed when repeated readings were made of the same flight condition, specifically 160 knots level flight, on different flights. On these flights, the readings were taken at the same azimuth position for each spanwise station, where a very low pressure difference could be expected.

The effect of rotor rpm (centrifugal load) on the transducers was investigated by covering the openings to the transducers with brass sheet metal and by sealing with tape, thus reducing or eliminating the response to pressure variation during runup of the rotor, hovering, and rotor rundown. Large zero shift on some of the transducers was observed during the runup and rundown phase, while the shift from one hovering condition to a second hovering condition of the same test was fairly small. The results of all these tests indicated that the conventional method of recording zeros before and after the flight did not produce reasonable zeros for data

reduction. Since zero shift affects only the static components of the pressure measurements, transducer zeros were obtained by data analysis, as is explained in more detail in the Reduction of Data section. The dynamic components of the pressure measurements, the more important portion of the correlation program, are not affected by the zero shift.

Blade Load Measurements

One of the blades of the main rotor was instrumented with strain gages, as shown in Figures 5, 9, 12, 14, and 15. This blade contained the airload differential pressure transducers. Blade loads were measured with 350-ohm foil strain gage bridges located to define the spanwise distribution of flapping and in-plane bending moments. As previously noted, a slipring assembly of 162 active sliprings was used, allowing simultaneous recording of all main rotor-rotating measurements.

Blade Tip Acceleration

The instrumented blade also contained two Statham strain gage accelerometers to measure flapwise and chordwise acceleration at the blade tip as shown in the following sketch:

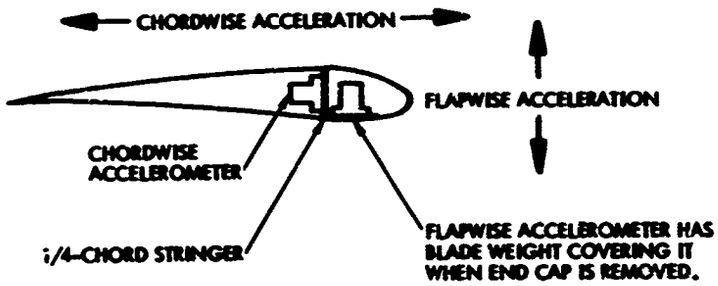

Transmission Gearbox Velocity

Five gearbox velocities (one vertical, two lateral, and two fore and aft) were measured with MB Model 120 transducers. The inset area in Figure 17 shows this installation.

Photo Recorder Panel (Pilot's Instrument Panel)

The pilot's instrument panel with conventional aircraft indicators and special flight test indicators was used as photo recorder panel. Figures 6 and 7 show the typical photo recorder panel instrumentation configuration used in the airloads program. Pictures of the photo recorder panel were taken with a 16mm camera at a rate of 2 frames per second. Synchronization of the photo panel data and the oscillograph record occurred by use of synchronized frame counters.

Oscillograph Recorder

The oscillograph was a Consolidated Electrodynamics Corporation type 5-119P3 operating on 28-volt dc aircraft power. The galvanometers used were Consolidated Electrodynamics Corporation type 7-315 which have a flat response (5 percent) in the frequency range from 0 to 60 cycles per second.

Signal Conditioning

Although the pressure transducer signals (~3 mv full scale) and blade-mounted strain gage signals were relatively low level signals, no attempt was made to amplify the signals to a higher level. Instead, a carefully specified and designed slipring assembly was used which had less than 10 microvolts peak-to-peak noise. The slipring assembly incorporated aligning bearings between the brushes and rings to minimize brush movement. The slipring assembly was completely enclosed to prevent the entrance of dirt and dust (see Figure 17). A slipring assembly consisting of 162 sliprings was selected for these tests to provide sufficient capacity for all rotating measurements. Galvanometers with flat response from 0 to 60 cycles per second filtered high-frequency electrical noise and minimized the effects of 400-cycle pickup. RC filters were used in the cg vertical accelerometer circuit and in the pitch, roll, and yaw rate signals to eliminate the 4-per-revolution rotor-induced signal.

Conventional series and shunt calibration resistors and controlling equipment were used with the oscillographs to provide proper recording trace height and calibration. The main recording devices were two 50-channel oscillographs and one photo recorder which photographed the pilot's instrument panel. Time correlation of the data was obtained from a master unit driving a counter on the pilot's panel and a pulse on the oscillograph.

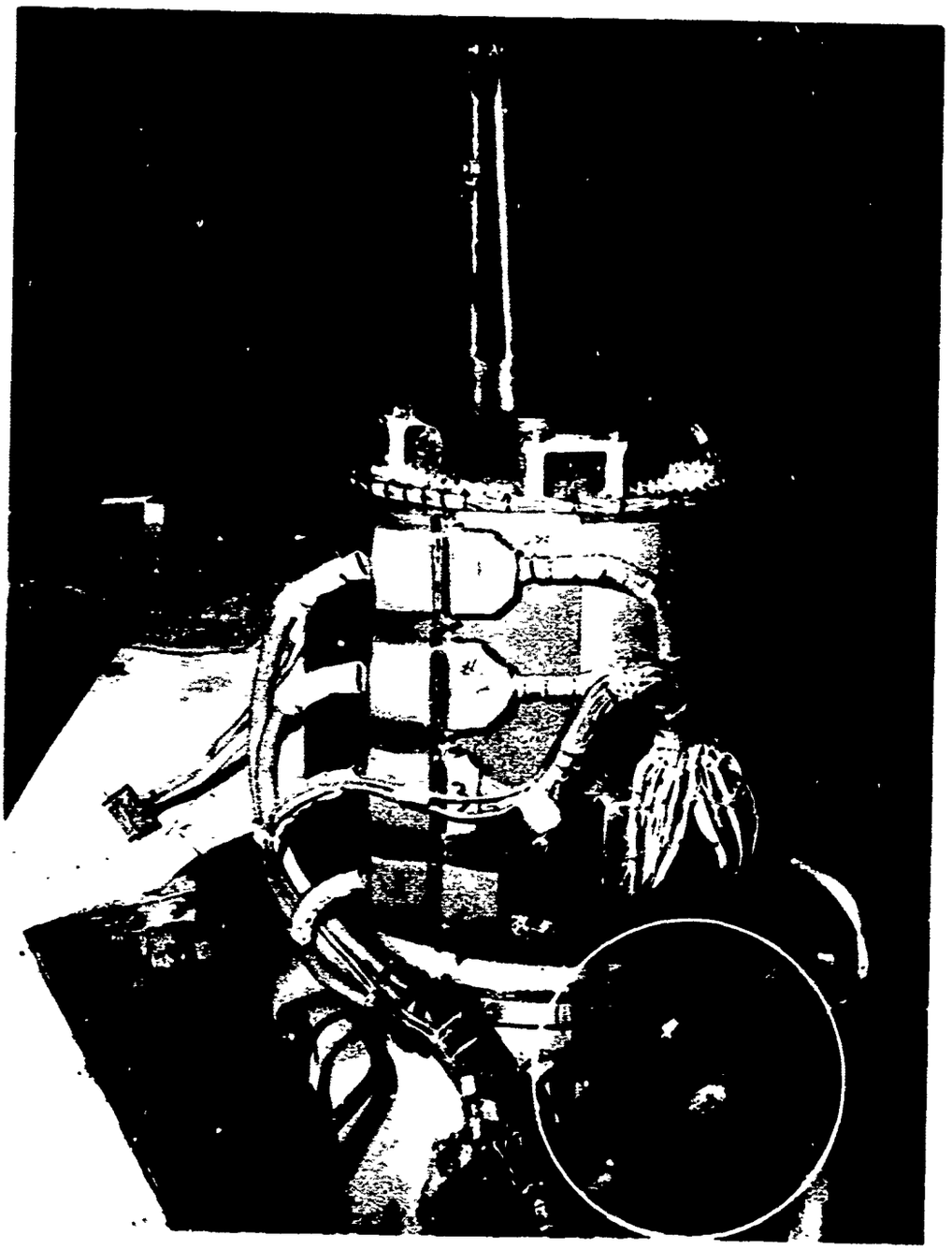

Figure 17. Slipring Assembly on Main Rotor Shaft

DESCRIPTION OF TESTS

SAFETY OF FLIGHT

Safety of flight was a prime consideration in the program. Thorough preflight and postflight inspections were conducted on each test. The oscillograph records were surveyed after each flight to assure that the measured parameters were within allowable limits and that the required measurements were operable. The instrumented blade was removed and X-rayed after every two hours of flight time to assure its structural integrity. A chase plane with a qualified Lockheed pilot and engineering observer accompanied the helicopter on every flight to observe the test vehicle closely. The chase plane observers also provided radio assistance with the airspace controllers and steered the test vehicle away from other aircraft.

FLIGHT TESTS

The flight test program consisted of recording the outputs of the blade pressure transducers and load strain gages during approximately 50 test conditions (or test points). These conditions were divided into two general modes: the helicopter mode in which the auxiliary jet engine was inoperative, and the compound mode in which the auxiliary jet engine thrust was used as required to obtain the test conditions. In general, the helicopter mode included hover, low-speed forward flight, transition, steady turns, and maneuvering pullup flight conditions. The compound mode of operation included a range of level-flight speed conditions, pullups to maximum load factors, and maneuvers with various rates of control applications. Table II lists the conditions tested together with pertinent details. Test condition 32 has been deleted, since the maximum level-flight speed was reached under test condition 31. The tests covered a range of altitudes from sea level to 10,000 feet and speeds from zero to the maximum of 232 knots true airspeed. The compound configuration tests were executed with a constant collective pitch setting of 4 degrees which resulted in low rotor lift at the high-speed condition. All tests were flown with a forward cg offset of 1.6 inches and a lateral cg position of 4.1 inches.

The following paragraphs amplify the procedures used for the flight test of each condition. An oscillograph record was made by the pilot when the aircraft was in the specified flight condition.

Helicopter Mode

Test Condition 1 - Hover. To satisfy condition 1 the helicopter was positioned a few feet above the ramp in a steady hover condition. Condition 1 was used as a baseline for instrumentation purposes and was performed at the beginning and end of each flight.

Test Conditions 2 through 4 - Collective Pullups. Rapid applications of the collective control were made by the pilot from a steady hover to obtain the target load factor.

Test Conditions 5 through 8 - Level Flight. The level-flight test points were taken in statilized level flight in smooth air with the helicopter trimmed at the specified speeds and altitudes.

Test Conditions 9 through 12 - Steady Turning Flight. Steady turns were set up by the pilot at the scheduled airspeed, altitude, and load factor. Airload data were taken after the turn was stabilized.

Test Conditions 13 through 15 - Pullups at 80 Knots. The pullup maneuver was accomplished by pushing over and then pulling slowly up to obtain the target load factor and speed as the nose pitched up through the horizon.

Test Conditions 16 and 17 - Autorotation. Data recordings for the autorotative entries were made by setting up the test conditions, turning on the oscillograph, and then performing the entry. The oscillograph was then turned off. Another recording was made during the stabilized descent.

Test Conditions 18 through 20 - Transition. These conditions were started from a low hover. The oscillograph was turned on; the pilot then pitched the aircraft nose down to the desired attitudes (estimated) and accelerated to 45 knots (airspeed indicator off the peg).

Test Conditions 21 and 22 - Landing Approach Flare. The landing approach flare condition was set up by accelerating at a constant altitude from a hover to the desired speed. The oscillograph was then turned on and the deceleration to hover was accomplished.

Compound Mode

Test Conditions 23 through 50. These test conditions were accomplished in the same manner as in the helicopter mode but with J-60 thrust as required to maintain the test condition. A collective setting of 4 degrees and a rotor rpm of 100 percent were used for all conditions. Test condition 32, level flight at maximum speed, has been deleted because this condition was obtained under test condition 31.

TABLE II. FLIGHT TEST CONDITI

TEST CONDITION NO.	DESCRIPTION OF TEST CONDITION	COMPUTER RUN NO.	TEST NO.	OSCILLOGRAPH COUNTER	MEASURED ROTOR LOAD, LB	CG VERT ACCEL, G	ANGLE OF ATTACK, DEG	CO B A
01	HOVER	53.0	502	536	4980	1.00	-	1
02	COLLECTIVE PULLUP	31.0	497	53-	5180	1.19	-	1
03	COLLECTIVE PULLUP	30.0	497	5-5	5771	1.31	-	1
04	COLLECTIVE PULLUP	37.0	498	5-3	6850	1.54	-	1
05	FORWARD FLIGHT	50.1	502	354	4720	1.02	3.62	
06	FORWARD FLIGHT	49.0	502	327	4612	0.98	1.21	
07	FORWARD FLIGHT	51.0	504	257	4683	0.98	-1.51	
08	FORWARD FLIGHT	48.1	502	306	5330	1.04	-2.11	1
09	LEFT TURN	34.0	498	404	6260	1.42	3.47	
10	RIGHT TURN	35.0	498	419	5996	1.32	2.56	
11	LEFT TURN	52.0	504	269	5890	1.33	1.51	
12	RIGHT TURN	53.0	504	276	5800	1.27	1.36	
13	COLLECTIVE PULLUP	54.0	504	311	5973	1.38	2.27	
14	COLLECTIVE PULLUP	55.0	504	329	7020	1.73	5.44	1
15	COLLECTIVE PULLUP	57.0	494	338	7700	2.06	6.84	
16	AUTOROTATION	60.0	505	354	4650	1.0	-	
17	AUTOROTATION	59.0	503	307	3837	1.08	18.90	
18	TRANSITION	52.1	502	417	5115	1.03	-	1
19	TRANSITION	50.1	503	351	5320	1.07	-	1
20	TRANSITION	29.0	497	404	5134	1.05	-15.86	1
21	FLARE	36.0	498	494	4650	1.02	12.70	
22	FLARE	51.1	502	383	4942	1.07	-	
23	LEVEL FLIGHT	42.0	501	346	2870	1.02	10.79	
24	LEVEL FLIGHT	43.1	502	163	2471	0.97	9.06	
25	LEVEL FLIGHT	22.1	494	184	1948	1.08	7.45	
26	LEVEL FLIGHT	11.0	494	264	1040	1.05	5.47	
27	LEVEL FLIGHT	39.0	500	458	810	1.15	4.20	
28	LEVEL FLIGHT	26.0	497	416	1636	1.03	6.80	
29	LEVEL FLIGHT	27.0	497	373	1091	1.01	4.83	
30	LEVEL FLIGHT	28.0	497	394	863	1.10	5.13	
31	LEVEL FLIGHT	40.0	500	570	654	1.13	4.80	
33	LEVEL FLIGHT	32.0	498	250	2280	1.05	10.50	
34	LEVEL FLIGHT	33.0	498	276	1210	1.02	7.10	
35	LEVEL FLIGHT	41.0	501	246	839	1.03	6.08	
36	PULLUP	44.1	502	175	3290	1.32	11.63	
37	PULLUP	45.1	502	188	3900	1.61	13.44	
38	PULLUP	58.0	503	190	3183	1.69	10.35	
39	PULLUP	8.0	494	220	1450	1.38	6.54	
40	PULLUP	25.0	497	256	1545	1.63	7.55	
41	PULLUP WITH	54.0	503	120	2311	1.30	8.85	
42	VARIOUS RATES	55.0	503	140	2616	1.56	9.75	
43	OF CONTROL	6.0	494	151	2054	1.54	9.27	
44	APPLICATION	7.0	494	174	2220	1.21	8.21	
45	LEFT TURNS	46.0	502	226	3078	1.25	10.72	
46	LEFT TURNS	56.0	503	163	2530	1.34	8.70	
47	LEFT TURNS	9.0	494	244	1495	1.37	6.08	
48	RIGHT TURNS	47.0	502	242	3338	1.30	11.33	
49	RIGHT TURNS	57.0	503	178	2020	1.49	9.45	
50	RIGHT TURNS	10.0	494	256	1586	1.38	6.23	

H

TABLE II. FLIGHT TEST CONDITIONS

TEST NO.	OSCILLOGRAPH COUNTER	MEASURED ROTOR LOAD, LB	CG VERT ACCEL, G	ANGLE OF ATTACK, DEG	COLLECT. BLADE ANGLE, DEG	GROSS WT, LB	V_T, KT	ALT, FT	JET	INTEGRATED ROTOR LOAD, LB	TEST CONDITION ANALYSIS PERFORMED
502	538	4980	1.00	-	10.61	4990	-	-	OFF	4587	FULL
497	536	5180	1.19	-	11.1	4841	-	GROUND	OFF	4609	PARTIAL
497	545	5771	1.31	-	12.1	4836	-	GROUND	OFF	4752	PARTIAL
498	563	6850	1.54	-	13.27	4871	-	GROUND	OFF	6331	FULL
502	354	4720	1.02	3.62	7.56	5010	51	805	OFF	4145	FULL
502	327	4812	0.98	1.21	8.0	5006	59.5	1065	OFF	3746	PARTIAL
504	257	4883	0.98	-1.51	9.2	5051	80.5	1060	OFF	4739	PARTIAL
502	306	5330	1.04	-2.11	10.93	5010	105	1060	OFF	4354	FULL
498	404	6260	1.42	3.47	9.0	4906	61	975	OFF	5789	PARTIAL
496	419	5990	1.32	2.56	8.9	4896	58	860	OFF	5500	PARTIAL
504	269	5890	1.33	1.51	9.54	5050	84	1025	OFF	5819	FULL
504	278	5800	1.27	1.36	9.21	5040	82	1005	OFF	5317	PARTIAL
504	311	5973	1.38	2.27	9.3	5036	84.5	1005	OFF	5825	PARTIAL
504	329	7020	1.73	5.44	10.0	5031	86	1070	OFF	6972	PARTIAL
494	338	7700	2.06	6.84	9.0	4915	87	975	OFF	8015	PARTIAL
505	354	4650	1.0	-	3.49	4900	-	115	OFF	3855	FULL
503	307	3837	1.08	18.90	3.20	4986	83	1075	OFF	2780	PARTIAL
502	417	5115	1.03	-	10.7	5241	-	GROUND	OFF	4670	PARTIAL
503	351	5320	1.07	-	11.09	4990	-	-	OFF	4418	FULL
497	494	5134	1.05	-15.86	10.6	4861	-	GROUND	OFF	3817	PARTIAL
498	494	4650	1.02	12.70	4.93	4891	60	-	OFF	4205	FULL
502	383	4942	1.07	-	9.7	5006	-	GROUND	OFF	4283	PARTIAL
501	346	2870	1.02	10.79	3.61	4940	109	1105	ON	2129	FULL
502	163	2471	0.97	9.06	3.6	5156	124.5	1045	ON	1528	PARTIAL
494	184	1948	1.08	7.45	3.27	5100	163.5	1180	ON	1363	FULL
494	264	1040	1.05	5.47	3.15	4980	207	1245	ON	282	FULL
500	458	610	1.15	4.20	3.24	5110	227	1220	ON	-426	FULL
497	418	1636	1.03	6.80	3.70	4891	170	3530	ON	923	PARTIAL
497	373	1091	1.01	4.83	3.80	4936	215.5	3745	ON	-106	PARTIAL
497	394	863	1.10	5.13	3.80	4906	219.5	3720	ON	161	PARTIAL
500	570	654	1.13	4.80	3.34	4940	232	3655	ON	72	FULL
498	250	2280	1.05	10.50	3.37	5026	157	10100	ON	1683	FULL
498	278	1210	1.02	7.10	3.50	4996	202.5	10105	ON	395	PARTIAL
501	246	839	1.03	6.08	3.80	5011	219	10370	ON	276	PARTIAL
502	175	3290	1.32	11.63	3.52	5150	126	1025	ON	2565	FULL
502	188	3900	1.61	13.44	3.76	5150	124	1005	ON	3576	FULL
503	190	3183	1.69	10.35	4.00	5091	160	955	ON	2670	PARTIAL
494	226	1450	1.38	6.54	3.17	5030	206	1390	ON	851	FULL
497	256	1545	1.63	7.55	3.56	5096	206	1025	ON	727	FULL
503	120	2311	1.39	8.85	3.80	4986	83	1075	ON	1810	PARTIAL
503	140	2616	1.56	9.75	3.70	5151	166	1290	ON	2071	PARTIAL
494	151	2854	1.54	9.27	3.60	5115	163	1110	ON	2666	PARTIAL
494	174	2220	1.21	8.21	3.30	5100	162	1175	ON	1336	PARTIAL
502	228	3078	1.25	10.72	3.40	5111	124	1050	ON	2344	PARTIAL
503	163	2530	1.34	8.70	3.60	5140	161	1175	ON	1705	FULL
494	244	1495	1.37	6.08	3.50	5005	207.5	1385	ON	1036	PARTIAL
502	242	3338	1.36	11.33	3.70	5091	124	905	ON	2550	PARTIAL
503	176	2620	1.49	9.45	3.70	5110	164	1105	ON	1620	PARTIAL
494	256	1586	1.38	6.23	3.23	4995	208	1265	ON	1212	FULL

REDUCTION OF DATA

GENERAL

A minimum of 49 different flight conditions listed in Table II was selected for data reduction. On 20 of these conditions, a complete data analysis was performed with the purpose of theoretical correlation. A partial data reduction was performed on the remaining test conditions.

The complete (full) data analysis of the 20 selected conditions was done on all pressure data and all structural load data. By partial data reduction is meant that all pressure data were analyzed, but the only load data reduced were flapwise and chordwise bending moments at span stations 6 and 115. Air pressure data were read entirely in order to obtain complete input data for the partial response analysis of the correlation program.

The data reduction program served the main objective of the research project, namely, the correlation of the measured and calculated airloads and structural loads data. The reduced data had to be presented in a form most suitable for the comparison. Some of the data generated in the data reduction program for flight test data were punched in cards so that they could be used directly as input data in the correlation program. Other data were presented in plotted form to be used for comparison with theoretical data. These requirements and the way that the measured data were recorded were important factors governing the data reduction program and the sequence in which individual computing steps were conducted.

Airload and structural load data for presentation in comparison with theoretical data in Phase II of the research program were plotted versus azimuth position. In order to obtain the airload versus span and versus azimuth position, the integration along the chord was performed prior to the determination of harmonic components.

The airload data obtained from flight test were also integrated in sections as lumped loads for discrete span stations. The harmonic components of these loads were punched in IBM cards and used in this form as input data for the correlation program.

The data reduction program was designed to process all types of data, including those which describe the flight test conditions, pressure data which have to be integrated to airload data, and structural load data which have to be compared with theoretical data.

FLIGHT TEST CONDITIONS

A complete description of the actual flight test conditions were necessary for the correlation program. Data were taken from the oscillograph and from the pilot's instrument panel photo recorder. The following data were determined: gross weight, rotor rpm, true airspeed, altitude, cg vertical acceleration, angle of attack, main rotor shaft torsion, roll rate, pitch rate, yaw rate, and collective blade angle.

Data from the photo recorder were obtained by reading the frame nearest to the cycle selected from the oscillograph record. The weight was calculated from takeoff weight and corrected for fuel consumed. True airspeed was obtained from indicated airspeed. Oscillograph records of test condition data were read as mean values during the selected cycle.

The main parameters describing the 49 flight conditions tested are listed in Table II.

AIRLOADS

Determination of Zero Reference Lines

A difficulty encountered in the use of the differential pressure transducers concerned the quality of the data obtained during the course of any flight testing. An examination of oscillograph trace recordings from early tests indicated that a drift higher than desired was present on about one-third of the pressure recordings. This condition was particularly noticeable when preflight and postflight zeros were compared for repeatability. In many cases the zero-condition reading differences were larger than expected on the basis of previous laboratory tests.

The cause of the trace shift was later determined to be a combination of several factors which were discussed previously in the Instrumentation section under Technical Approach. Briefly, such factors included the effects of centrifugal force, temperature, and time on the response.

Based on observations of the drift behavior made during stabilized flight conditions, an effective method of data reduction was realized by developing correction functions to be applied to the pressure data obtained at the various conditions. For instance, the zero reference level for each pressure output was determined from the ground condition of 100-percent rpm with full down collective. Preflight and postflight oscillograph trace levels obtained at this condition were in fair agreement, as opposed to a similar comparison of the nonrotating condition. In addition, this condition was selected as the one that most nearly approximated an actual zero-pressure output case, differing only by an amount due to the effect of blade twist in the rotating environment. This blade twist pressure distribution, or desired correction function, was derived in th following manner: The blade angle was varied from +3 to +10 degrees at the root, corresponding to -2 to +5 degrees at the tip, keeping the rotor speed constant at 100-percent rpm. From plots of the differential pressure versus blade angle

for all 46 pressure transducers, the pressure distribution due to twist was determined by interpolation and extrapolation toward zero blade angle. This method was based on the assumption that the differential pressure is zero at zero blade angle, since the profile of the blade is symmetrical. The pressure distribution due to 5-degree twist which is presented in Figure 18 (solid curves) was used as the correction function for the derivation of the zero reference line for each element at 100-percent-rpm operating condition.

In order to check whether this pressure distribution represented the expected zero lift condition of the rotor, the integration program was applied and a result of 30 pounds was obtained, a negligible total lift. The correction of the pressure due to twist was small compared to the pressure measured during hover. At span station 199.5 and 3.5 percent chord, for example, the pressure ratio was 0.21 to 7.0.

The correction function due to blade twist, Figure 18, was used to derive the zero reference lines of the pressure transducers for all hovering and near-ground conditions close to the 100-percent-rpm zero lift condition on the ground.

Differences between before and after flight zeros, using the correction function described above, indicated that the zero reference lines were shifting during the flight, probably due to time and temperature effect.

In order to compensate for zero shift between the ground condition and the in-flight condition, a zero correction similar to the one described above was applied for all flight conditions, especially at high speed. The correction function for in-flight conditions was based on a loading condition of very low local pressure differences. Such a condition could be found, for example, on the retreating blade of the partially unloaded rotor at a speed of 160 knots. At this speed, the retreating blade experiences nearly zero speed at span station 76 in the azimuth range from about 240 degrees to 300 degrees. This is also the area of nearly zero differential pressure. Inboard of station 76, the area of reversed flow, the tangential speed is very low and the pressure is also nearly zero. Outboard of this station the pressure is gradually increasing because of increasing speed toward the tip. The azimuth range from 240 degrees to 300 degrees is the range of a very flat minimum of tangential speed and very low change of differential pressure (Figures 19 and 20). Readings of the differential pressure at 250 degrees azimuth position, using the corrected zeros at 100-percent rpm on the ground, were plotted for repeated test runs at 160 knots true airspeed, with the same collective blade setting. A typical sample is shown in Figure 21 (dashed lines). Differences of the plottings for the different runs were fairly small. Families of curves faired in the directions of span and chord giving best fit for all plots of the same condition were drawn. Plots versus rotor span station are presented in Figure 21 (solid lines).

This family of curves representing the pressure distribution of the blade at 250 degrees azimuth position for the 160 knots true airspeed condition

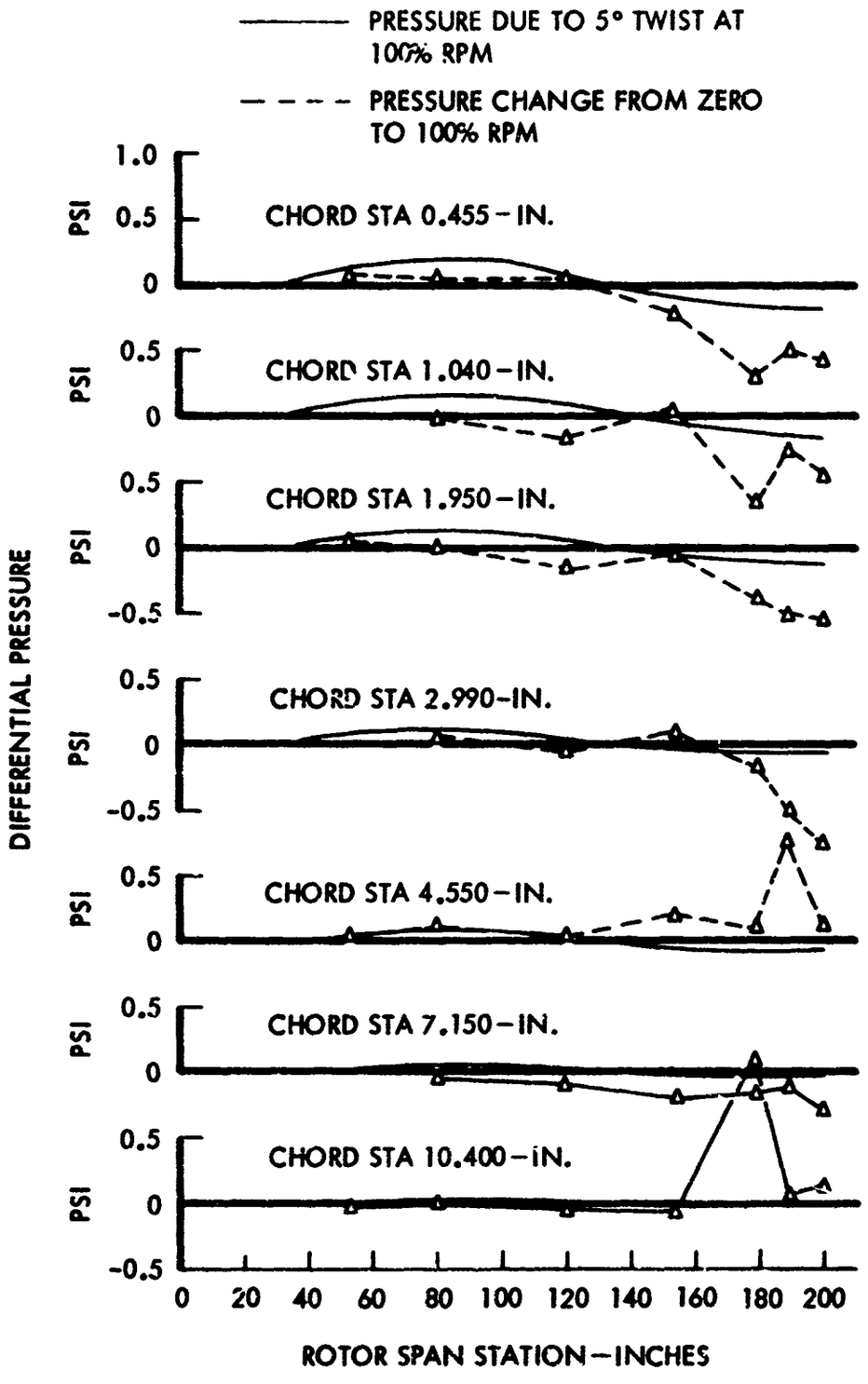

Figure 18. Blade Differential Pressure Distribution at Zero Lift Condition

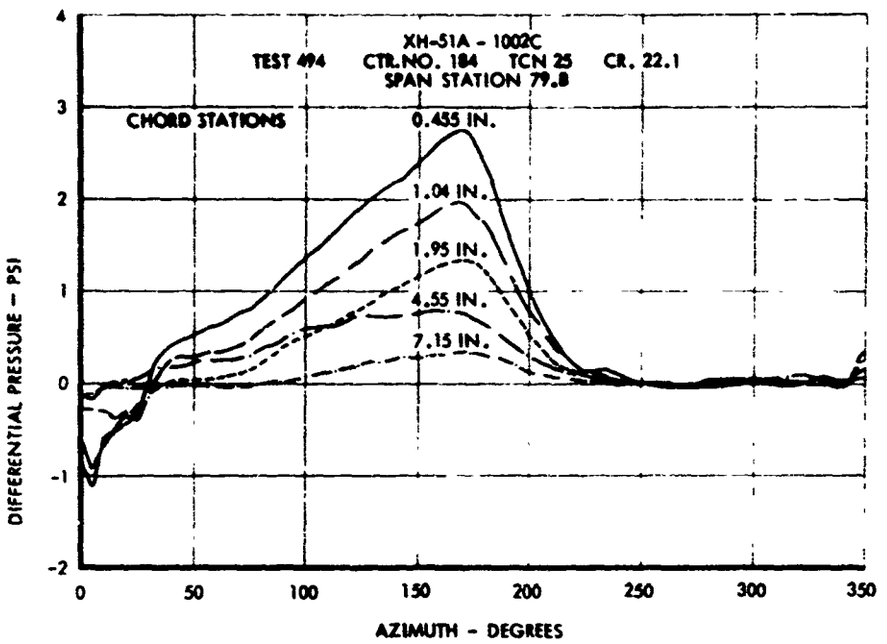

Figure 19. Blade Differential Pressure at 160 Knots Level-Flight Condition - Span Station 79.8

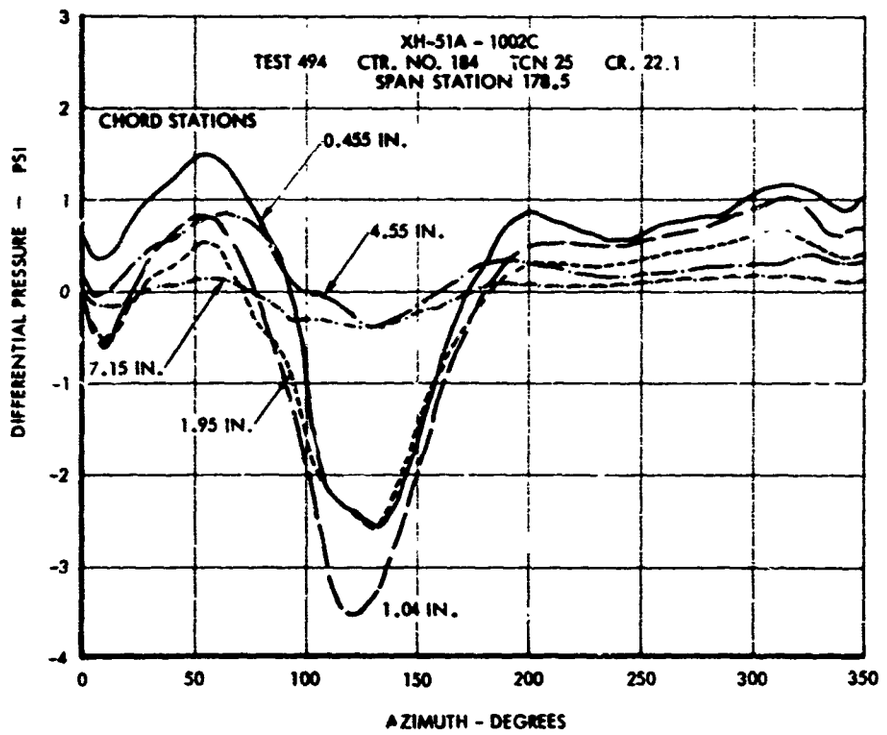

Figure 20. Blade Differential Pressure at 160 Knots Level-Flight Condition - Span Station 178.5

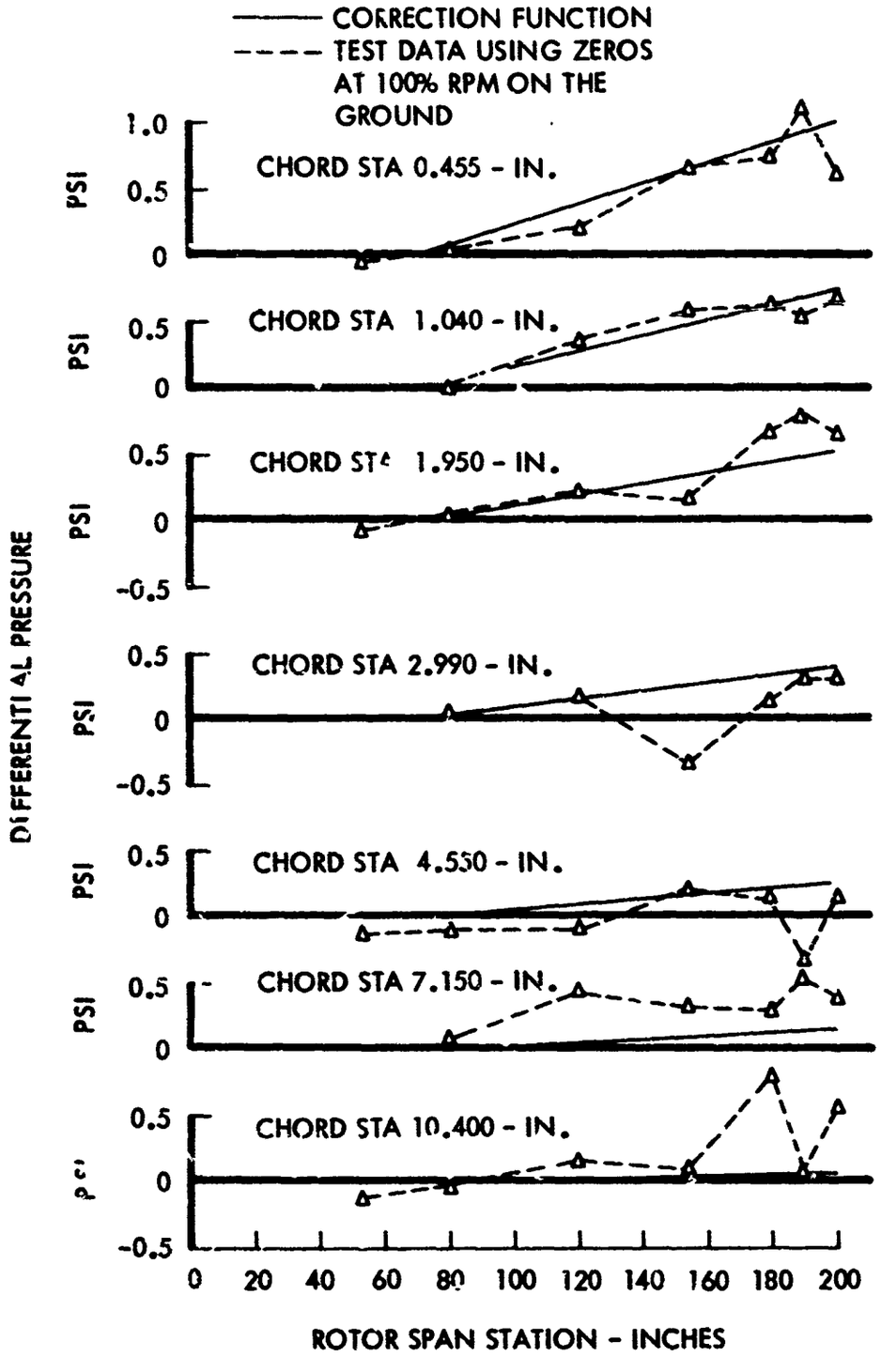

Figure 21. Blade Differential Pressure Distribution at 160 Knots Level-Flight Condition for Blade Azimuth 250 Degrees

was used to derive the zero reference lines of the pressure transducers for all in-flight conditions.

The reference condition, 160 knots true airspeed and low collective blade setting, was repeatedly recorded, two or three times during each flight for each altitude. Tests conducted at 1000 and 3500 feet did not show any significant difference. However, the 10,000-foot data showed slightly higher pressures. Therefore, another correction function was established for the 10,000-foot altitude.

The shift of the zero reference line is a slow process, noticeable only in a longer period of time between test runs, but not effective during the short period of one revolution. Therefore, the zero shift does not affect the cyclic variation of the pressure (dynamic component); it can affect only the steady-state (static) component. Plots and crossplots of differences between maximum and minimum pressure during one revolution of a typical forward flight condition showed no noticeable effect on the sensitivity of the transducers.

In order to minimize further the possible remaining effect of zero shift, dynamic components, not affected by zero shift, and static components, corrected for zero shift, were separated throughout the entire data reduction program.

Automatic Data Handling

The determination of the airloads and the preparation of the flight test data for the correlation phase of the research program required a special data reduction program which included a number of calculation steps and subroutines. A detailed description of the program written in the computer language Fortran IV for the IBM 360/75 digital computer is presented in Appendix I.

The basic steps of the automatic data handling program were:

- Preparation of the input data for the following computing steps.
- Integration of the pressure data to obtain loads, pitching moments, and total lift.
- Harmonic analysis of airloads, pitching moments, and structural loads.
- Preparation of output data for presentation and for input purposes in the correlation computing program.

The input data read from the oscillograph, in small time increments at arbitrarily spaced points of sufficient number to describe the time function accurately, were converted into engineering units (psi) and interpolated by a third-degree polynomial interpolation routine to obtain 72 equally spaced data points per cycle. The interpolation routine is described in Appendix I. The 72 interpolated data points, sufficient to describe ten harmonics adequately, were used in all subsequent computing

steps instead of the actual data points. Plots of test data after the interpolation process was applied are presented in Figures 19 and 20. They are directly comparable with the data recorded on oscillograph. Structural load data and calculated airload data obtained after the interpolation are used for comparison in Volume III in plots versus azimuth angle. A few samples of airload plots are shown in Figures 22 through 31. Harmonic analysis was applied in a later step of the program. The dynamic and static components of the differential pressures, respectively, are tabulated in Appendixes V and VI.

Before the pressure along the chord was integrated to obtain airload distribution versus span, the same interpolation routine as above was applied. However, only seven measured points at the seven pressure gage stations were available. Assumptions for the leading edge and trailing edge were made. The pressure at the trailing edge can be assumed to be zero. Slightly different assumptions for the leading edge were necessary in order to simulate the pressure peak near the leading edge. Wind tunnel data from NASA 0012 airfoil indicate that the maximum differential pressure for positive angles of attack is ahead of chord station 3.5 percent, the first pressure gage station, and that there is a steep slope of the pressure between the leading edge and the pressure peak. The pressure peak between the leading edge and the first pressure gage station was simulated by the interpolation routine, assuming that, if the pressure at 3.5 percent chord was higher than at 8 percent chord, the pressure would rise to a peak, return at the leading edge to the same level as at station 3.5 percent chord, and drop to zero on a vertical line at the leading edge.

In the cases where the measured pressure at 3.5 percent chord was lower than at 8 percent, no assumption for the pressure at station zero was made and the pressure distribution between zero and 3.5 percent was obtained by extrapolation.

The interpolation and extrapolation of the pressure along the chord were applied in increments of 1/4 inch for a total of 53 points, thus providing sufficient points for the integration process along the chord to obtain blade loads and pitching moments. The integration method used is described in Appendix I. Integrated blade loads are presented in Appendix VII for seven span stations in pounds per inch. The first 72 lines (0.0 degree through 355.00 degrees) represent the dynamic components of the airload, while the bottom line contains the static components.

Prior to the integration along the span, the same interpolation routine as mentioned above was applied to obtain 106 data points in increments of 2 inches. The assumption was made that the airload at the tip, at blade station 26, and inboard of that station is zero. There is no lift in the area of the cuffs. This interpolation step was applied to the airload (normal to the blade) and to the pitching moment about the 1/4-chord line. Plots of airload and pitching moment versus blade station are presented in Appendix II for the dynamic components and in Appendix III for the static components.

The integration along the span was done in segments in order to obtain lumped loads of lift (normal to the blade) and pitching moments at discrete span stations. The width and the mean span station of the segments are listed in Table III (see Appendix I).

After integration, harmonic analysis was applied to the lumped loads of lift (in pounds) and pitching moment (in inch-pounds). These data, presented in Appendix VIII, were used as input in the correlation phase of the research program. The total integrated load of the rotor, i.e., the load of the four blades, is listed in Table II.

In order to present the spanwise distribution of the steady-state and first three harmonic components of the blade loads along the span (in pounds per inch), the harmonic analysis was applied to the running loads in increments of 2 inches of span. Plotted results are shown in Appendix IV.

STRUCTURAL LOADS

The structural load data have been read in the same manner as the pressure data. A large number of data points along the trace were selected such that the time function could be described by 72 data points per cycle applying the third-degree polynomial interpolation routine (see Appendix I). With 72 points per cycle, the harmonic components were computed up to the tenth harmonic. Plotted time histories are presented in Volume III of the report in the correlation of theoretical and measured structural response. Results of the harmonic analysis are given in Appendix IX of this report.

All but one of the structural load measurements were analyzed. Because of crosstalk to other loads which could not be compensated for, the strain gage for flapwise bending moment at station 24 did not produce reliable measurements.

DISCUSSION OF RESULTS

Several different methods of data reading and data reduction were applied in order to check the reliability of the procedures. All of them were on a comparative basis, with flight test data being compared with flight test data. One method used was to perform the same data reduction for more than one cycle of the same steady-state condition in order to check the repeatability of the flight test data. Another way was to apply the data reduction on repeated test runs of the same condition. A third method was to compare data obtained throughout the data reduction process with data obtained by derivation from other measured data.

Comparison of Cycles from Same Test Run

The repeatability of flight test data was checked by performing the same data reduction on two additional cycles for each of five selected steady-state conditions. The conditions selected were hover, left and right turn maneuvers, and three different level-flight speed runs. Plots made of the blade load variations occurring during three successive rotor cycles for each condition are shown in Figures 22 through 26. The blade load data shown are the result of the integration along the chord for four different blade stations, performed on 72 azimuth positions.

In general, data repeatability is good for all of the selected conditions, particularly those in low-speed regions. In hover condition, a slight periodicity can be observed which is mainly due to the cg offset, some wind, and tail rotor interference. At the high-speed condition, Figure 25, slight differences appear in the higher harmonic content, becoming more noticeable at the outboard blade stations. Probably these small differences are due primarily to tip vortexes and tip Mach effect in these regions.

The highest tip Mach number reached at test condition 31 was 0.93, a value at which the structural loads also show higher harmonics due to tip Mach number effect.

The integrated rotor load of the second and third cycle deviates in general from the load obtained in the first cycle by an amount within the accuracy of the data acquisition system. The differences among the three cycles for the test conditions 1, 11, 25, and 50 are less than 2 percent of the gross weight. For the test condition 31 where the highest tip Mach number of 0.93 was measured, however, the differences among the three cycles of the integrated load are between 3 percent and 4 percent, still within the reading accuracy of the oscillograph data. A deviation of the reference line of the pressure gages of 0.01 [illegible] for example, would result in a difference of the integrated lift of 196 pounds, which is approximately 4 percent of the gross weight of the vehicle.

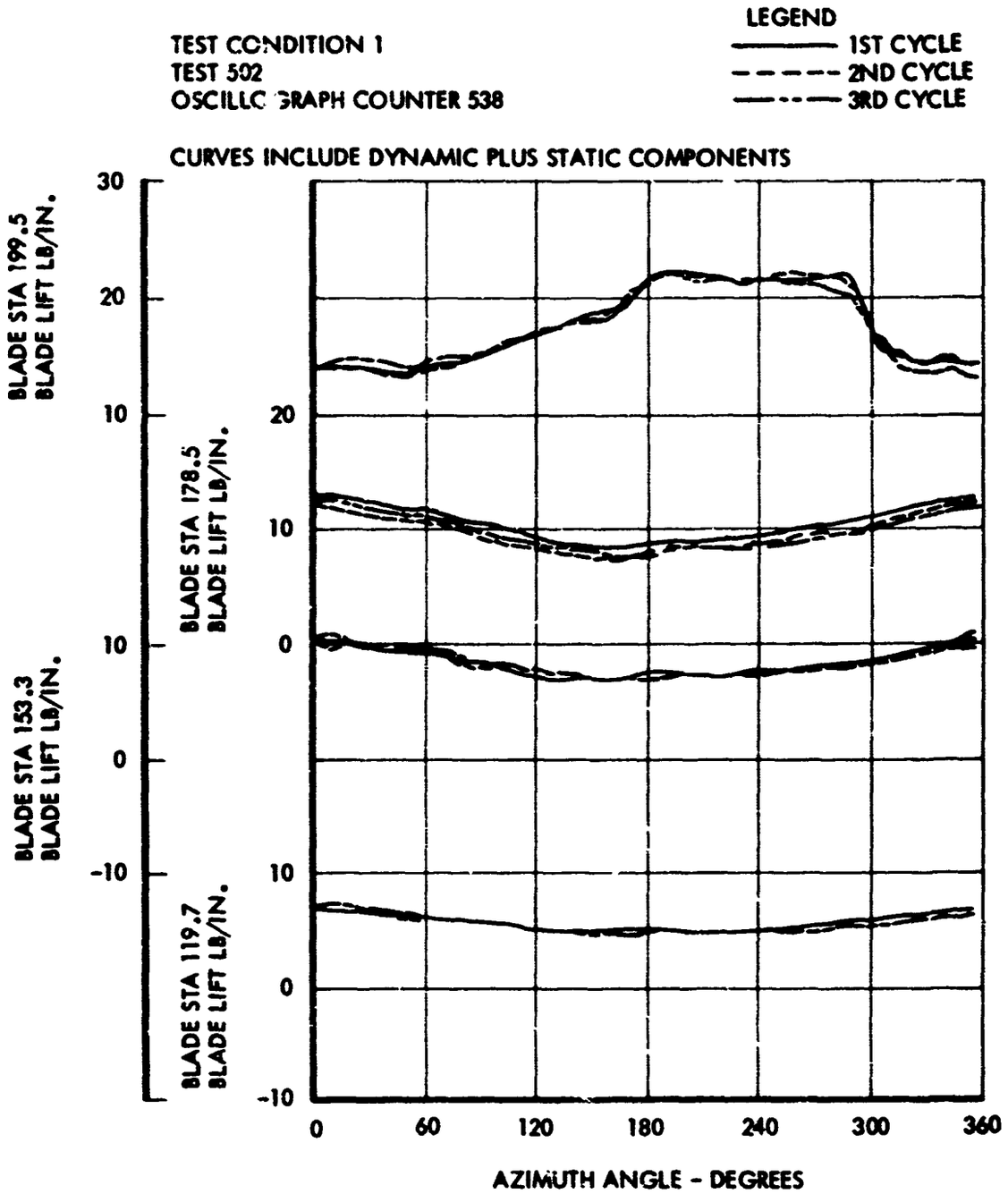

Figure 22. Comparison of Blade Section Load for Three Successive Rotor Cycles During Hover Condition

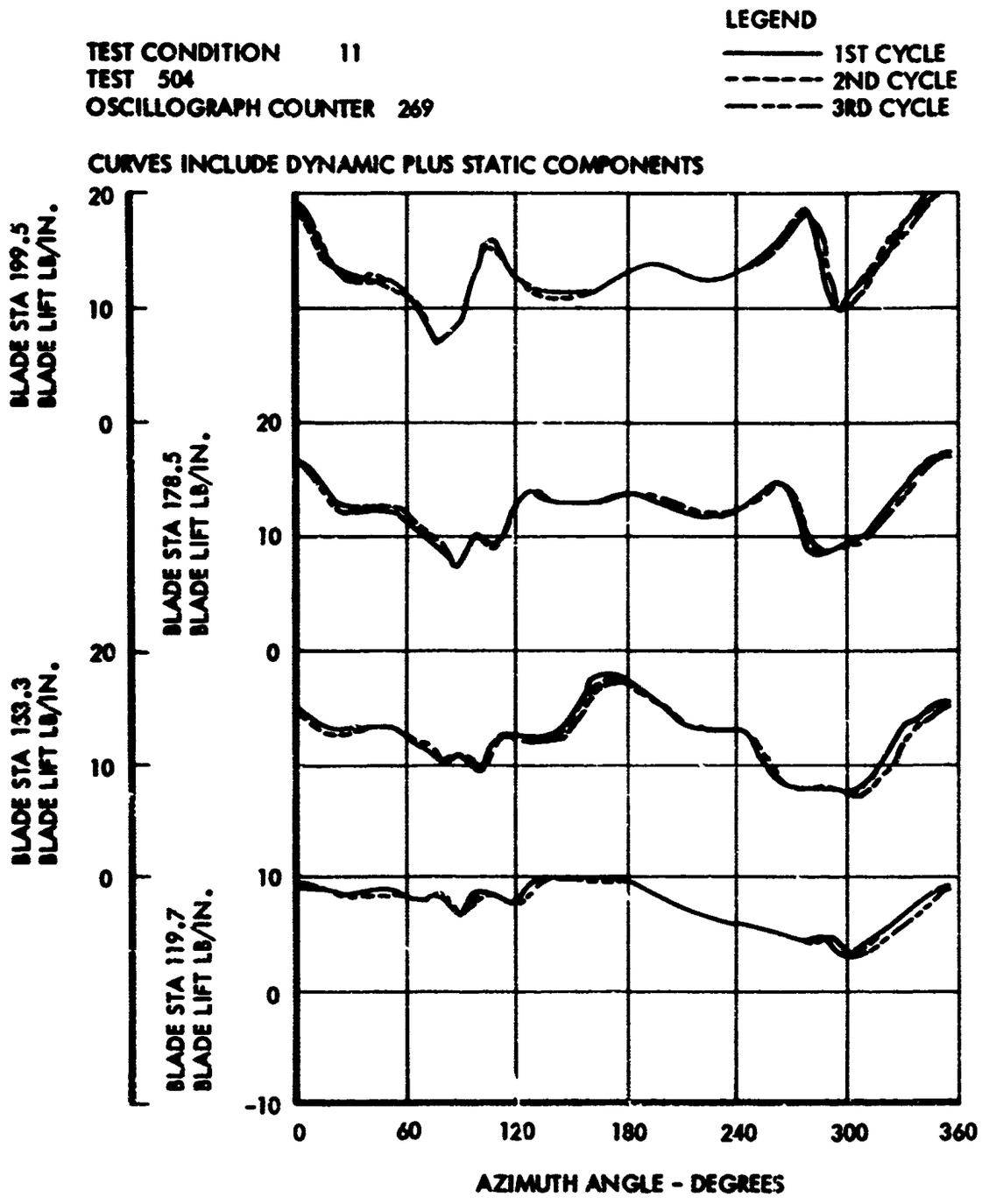

Figure 23. Comparison of Blade Section Load for Three Successive Rotor Cycles During a Left Turn Maneuver

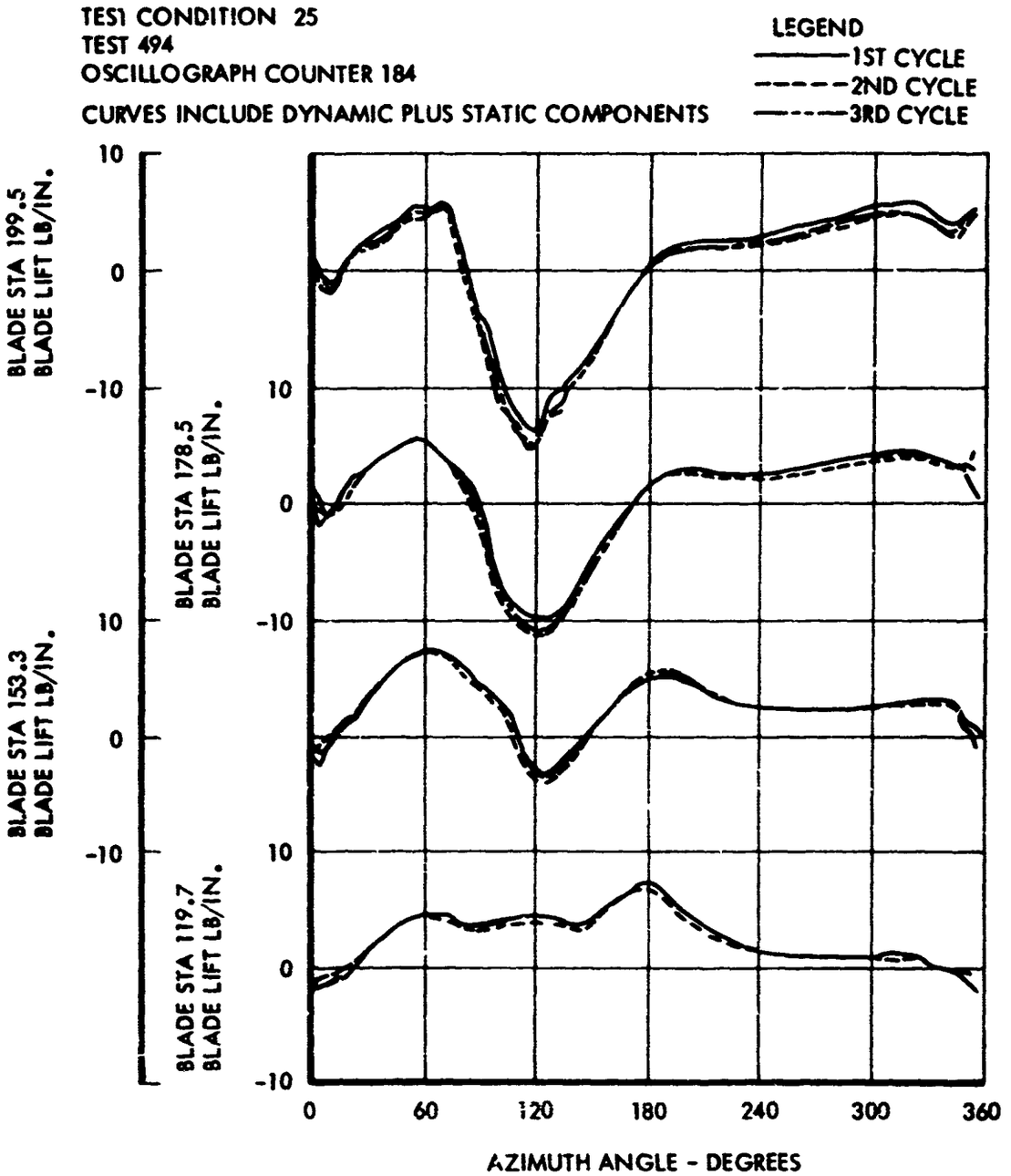

Figure 24. Comparison of Blade Section Load for Three Successive Rotor Cycles During Level Flight at 163.5 Knots True Airspeed

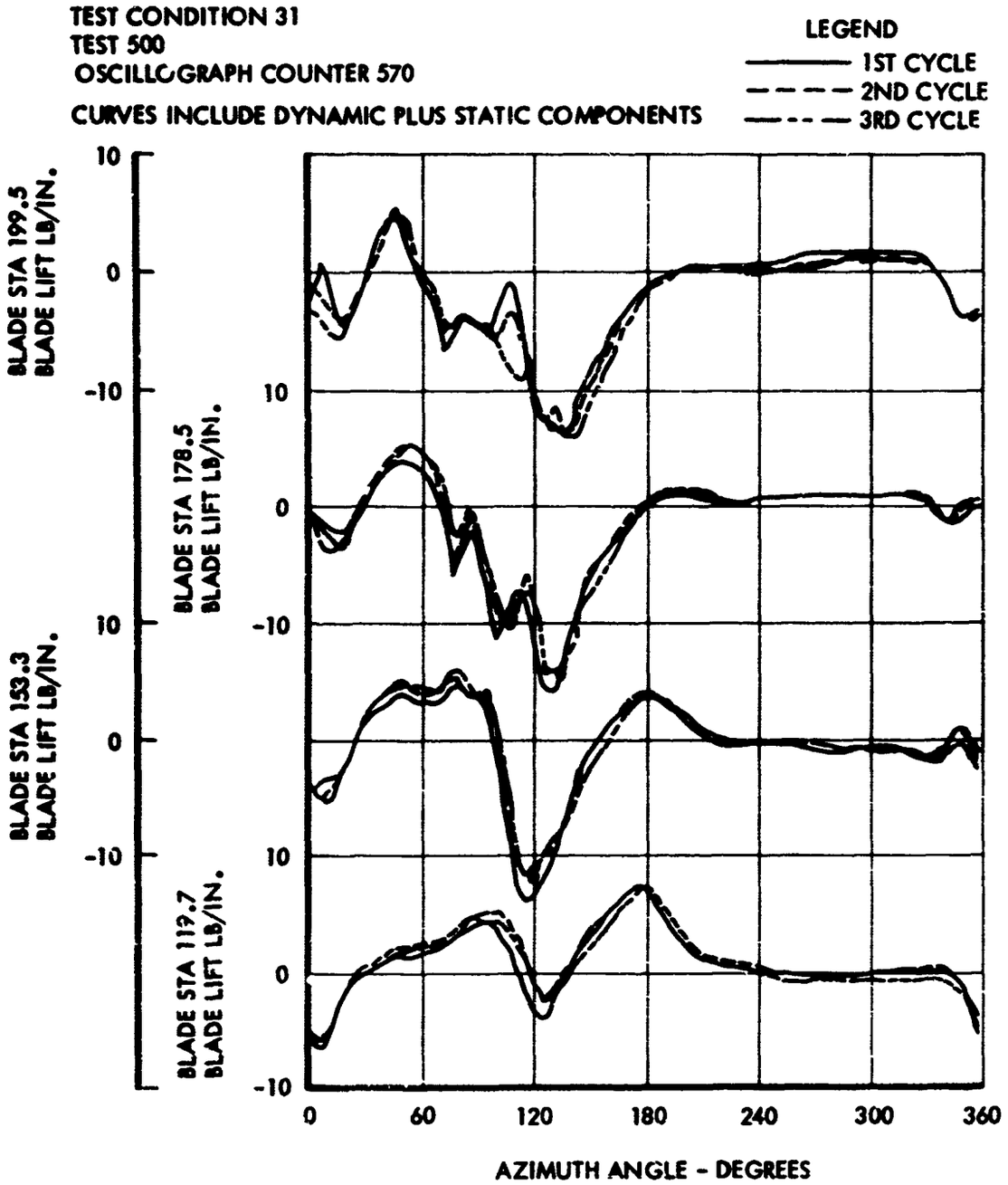

Figure 25. Comparison of Blade Section Load for Three Successive Rotor Cycles During Level Flight at 232 Knots True Airspeed

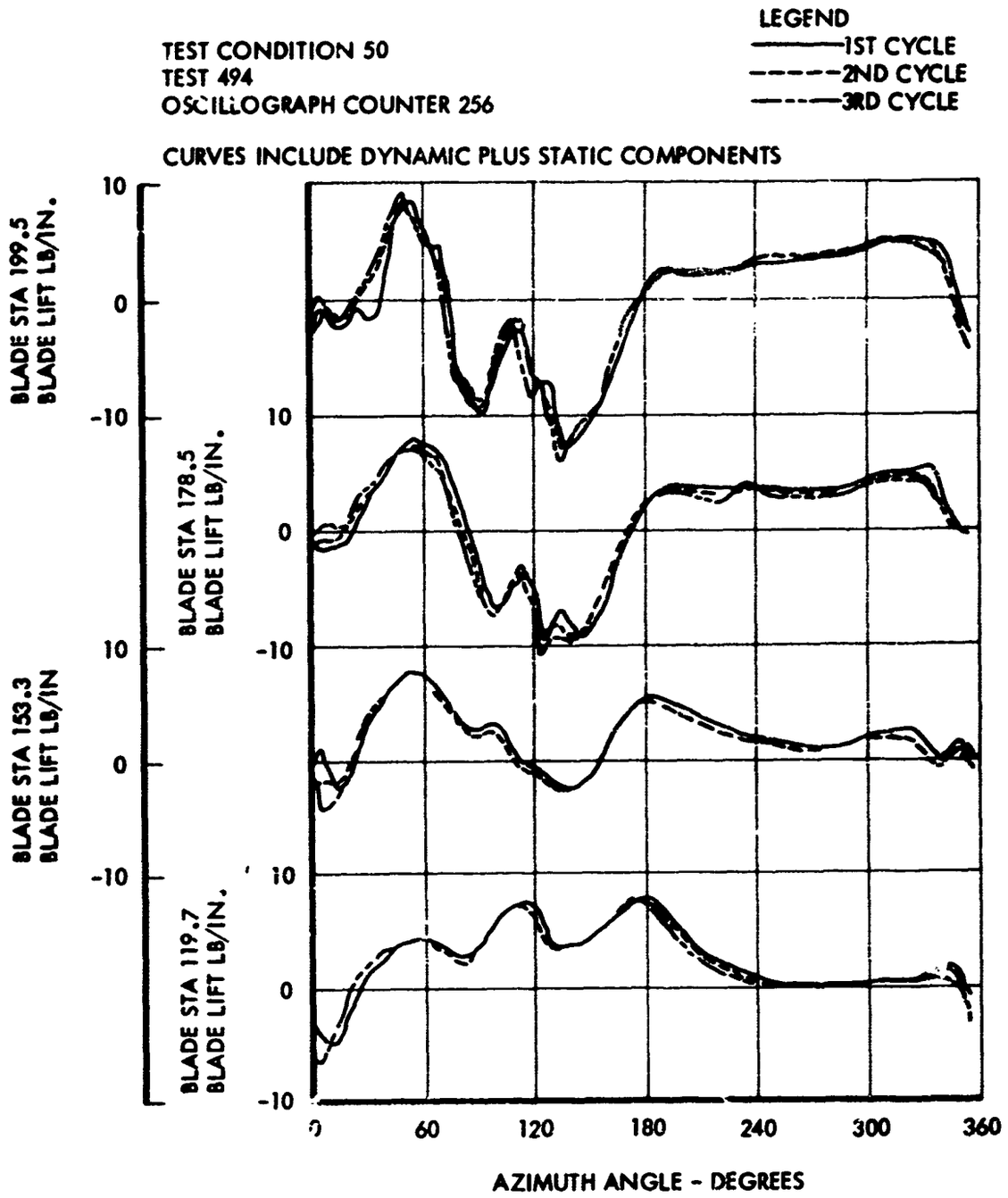

Figure 26. Comparison of Blade Section Load for Three Successive Rotor Cycles During a Right Turn Maneuver

Repeatability Comparison from Separate Runs

Repeatability comparisons were also made of blade load variations obtained on separate runs of the same test condition. Figure 27 shows such a comparison of blade section lift for three repeated speed runs at approximately 164 knots true airspeed. The differences observed among these three runs are equal or even less than the differences among the three cycles of the same test condition. Also the integrated load varies less than 3 percent of the gross weight.

Figures 28, 29, and 30 show the gradual change of blade loads with an increasing speed in level-flight conditions. Figure 28 compares blade section load for three different level-flight runs covering the medium-speed range. In these curves the outboard blade stations in particular reflect the increase in dynamic component activity as speed is increased. A similar comparison is shown in Figure 29, where the high-speed region is covered. Again the outboard stations reflect the effects of increased speed as higher harmonic content becomes more pronounced. Figure 30 is essentially similar to Figure 29; only the test altitude is different. There is no apparent change in the curve characteristics due to the difference in altitude, however. Figure 31 compares the blade section lift of a left and a right turn at essentially the same speed. The curves are very similar in nature, exhibiting some higher harmonic content due to speed and blade loading in the turn.

Comparison of Measured and Integrated Rotor Load

In order to have one direct measurement which represents the rotor load, the sum of the axial loads of the four vertical links between fuselage and gear box was measured. This measurement, however, can be used for comparison with the integrated load in level-flight conditions only, because it includes dynamic loads from the gearbox and rotor hub and some control loads from the collective control which cannot be separated from the rotor load by direct measurement. In hover and in low-speed level-flight conditions, the measured rotor load agrees fairly well with the gross weight while it deviates in high-speed flight and in dynamic conditions because of load sharing by the fixed wing.

The comparison of the integrated rotor load with the measured rotor load reveals that the integrated load is in general lower than the measured load. The difference in hover condition is 393 pounds and in higher altitude forward flight above 100 knots flying in the compound mode, the differences are about 700 pounds as shown in Figure 32. Both loads, however, decrease with nearly the same rate with increasing forward speed.

The consistent differences seem to indicate that the instrumented blade produces less lift than the other three blades. It should be noted that the integrated load is calculated as four times the integral of the static components of the blade loads versus span measured normal to the blade.

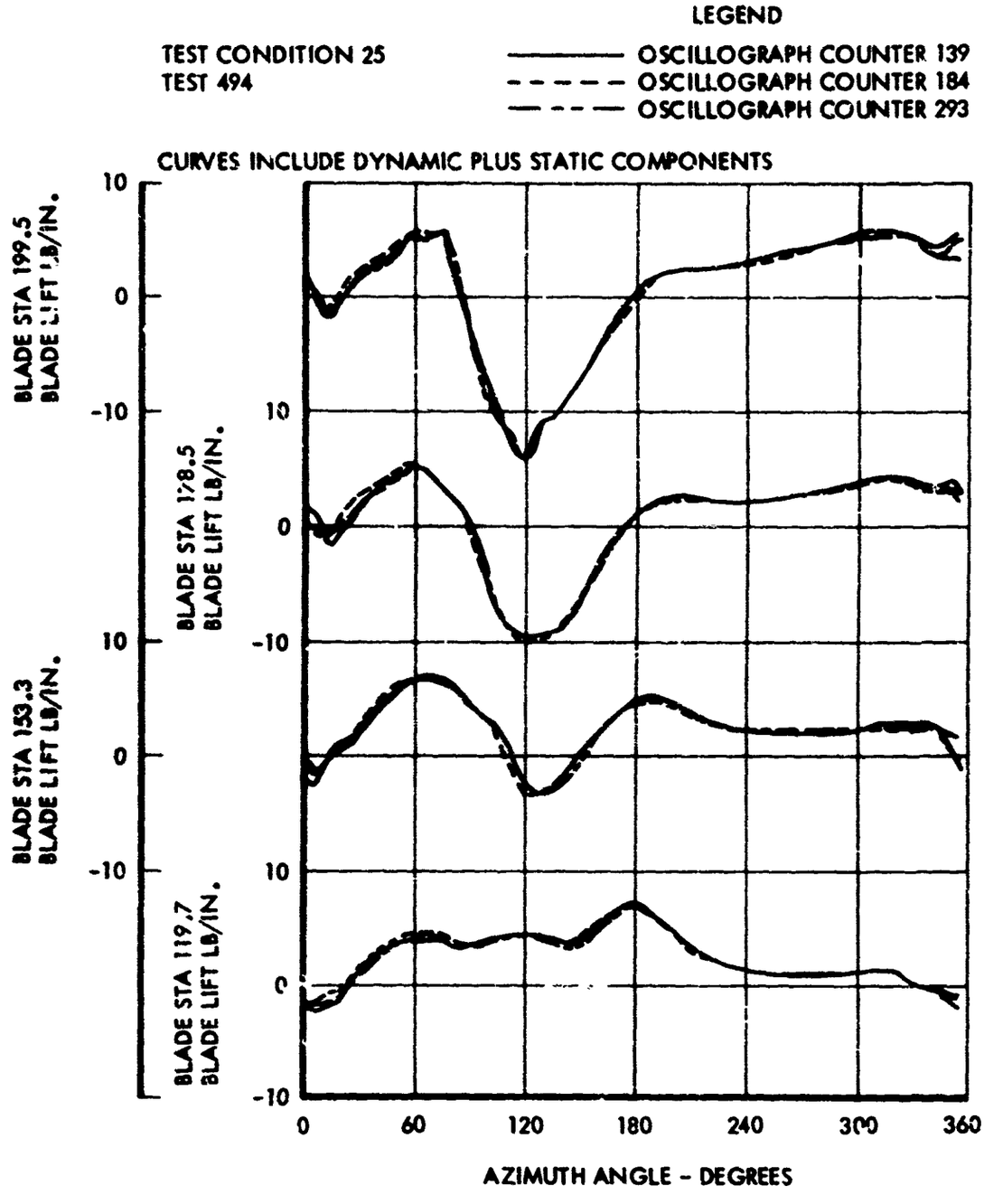

Figure 27. Comparison of Blade Section Load for Three Repeated Speed Runs at 164 Knots True Airspeed

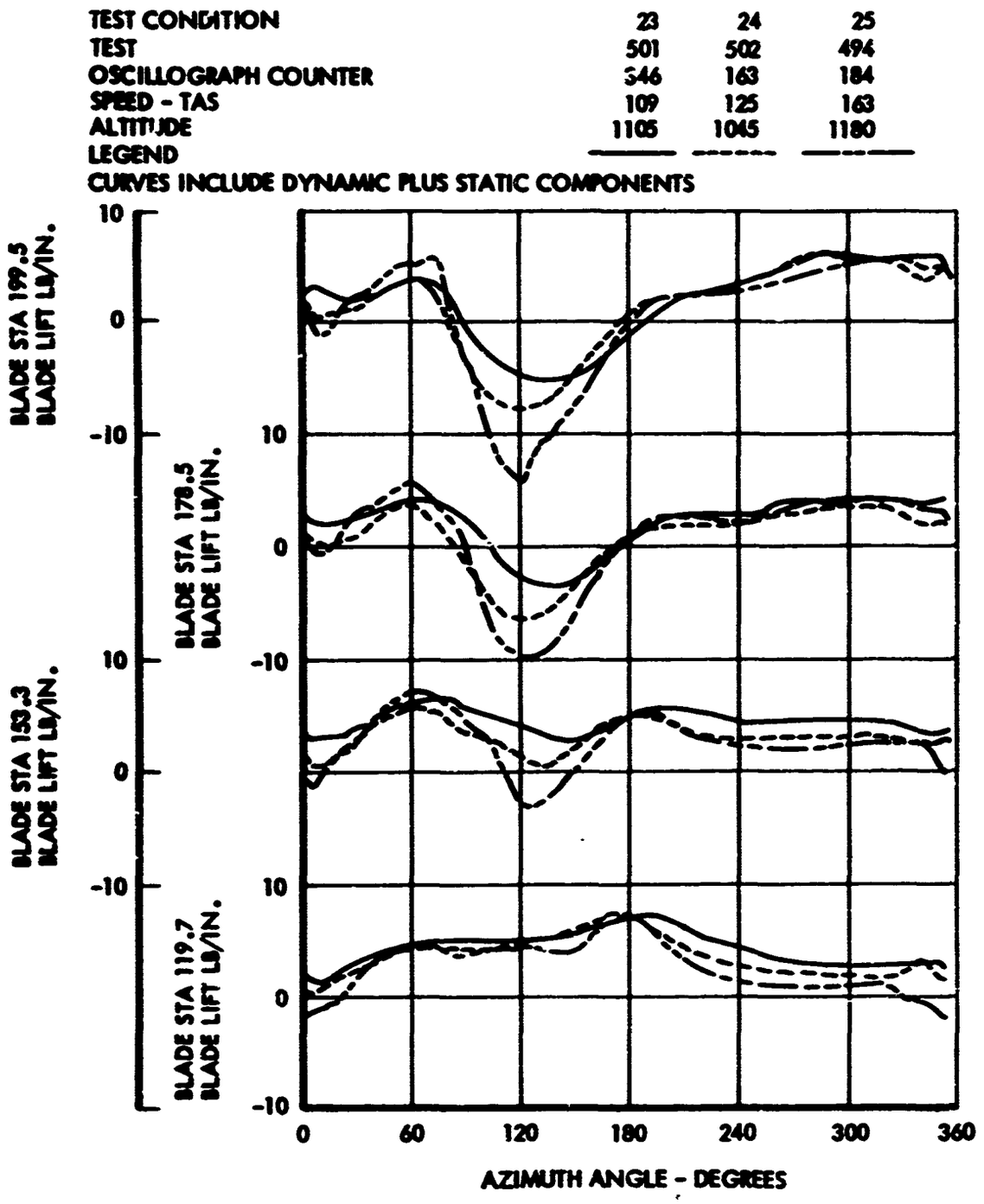

Figure 28. Comparison of Blade Section Load for Three Level-Flight Speed Conditions - 23, 24, and 25

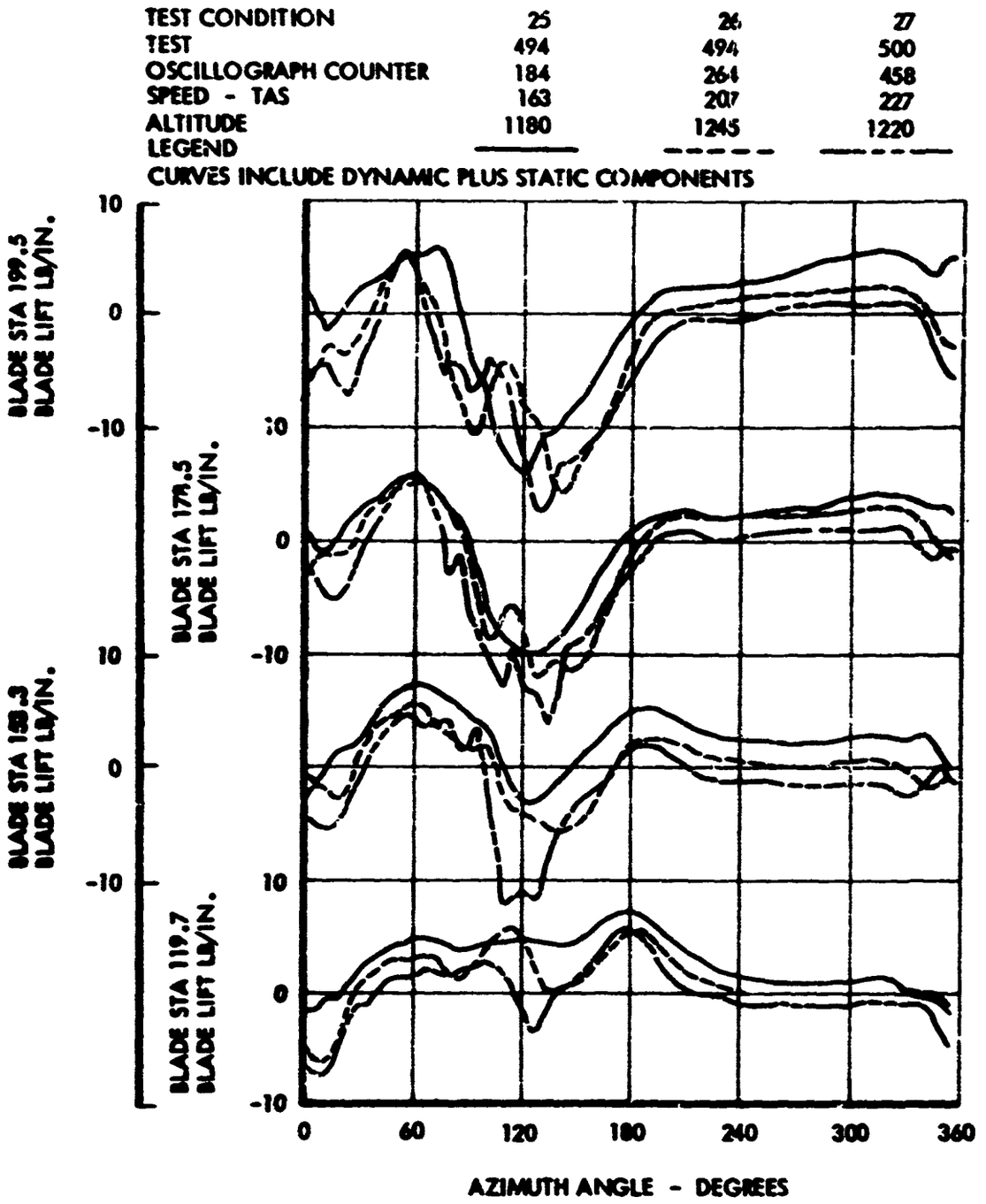

Figure 29. Comparison of Blade Section Load for Three Level-Flight Speed Conditions - 25, 26, and 27

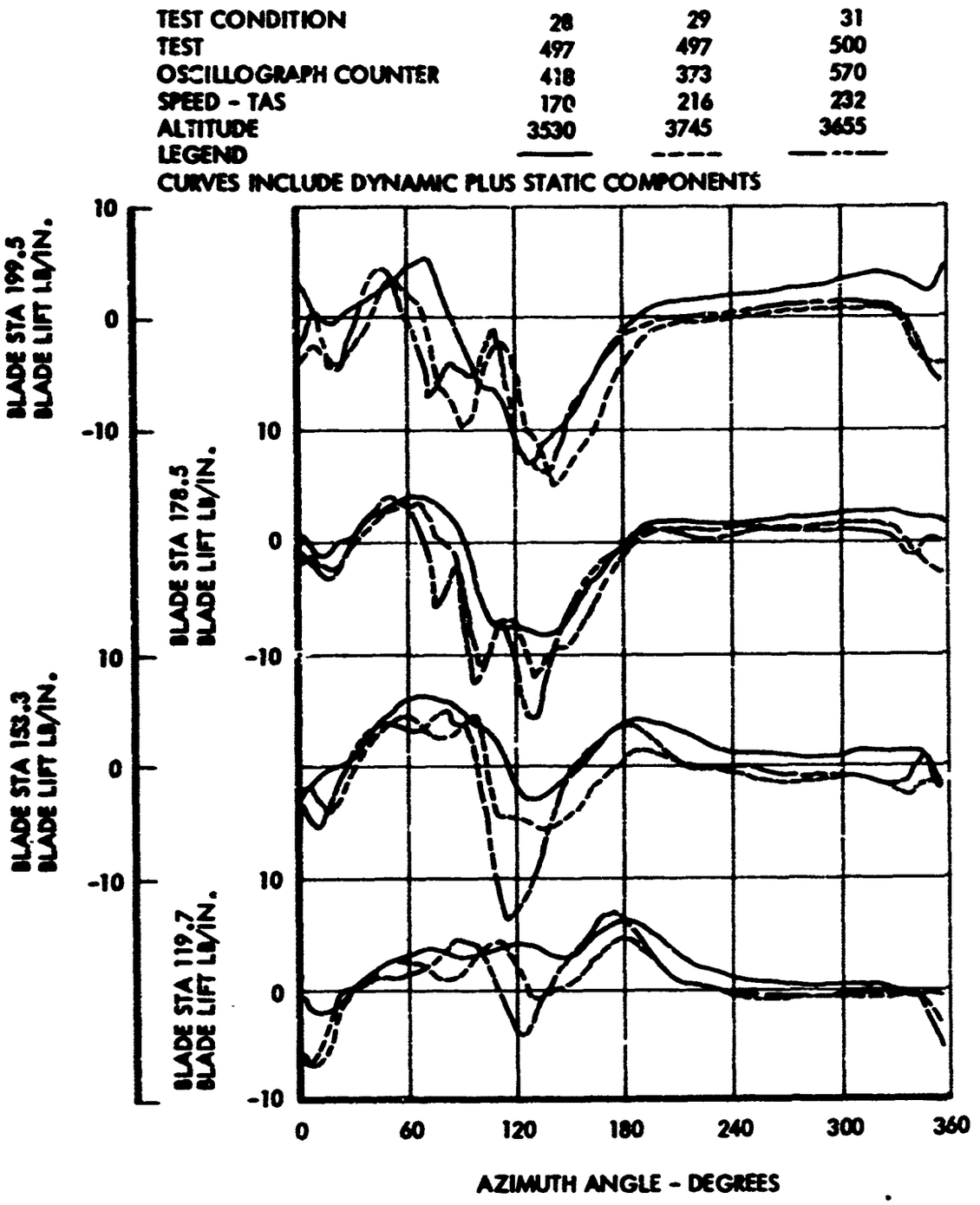

Figure 30. Comparison of Blade Section Load for Three Level-Flight Speed Conditions - 28, 29, and 31

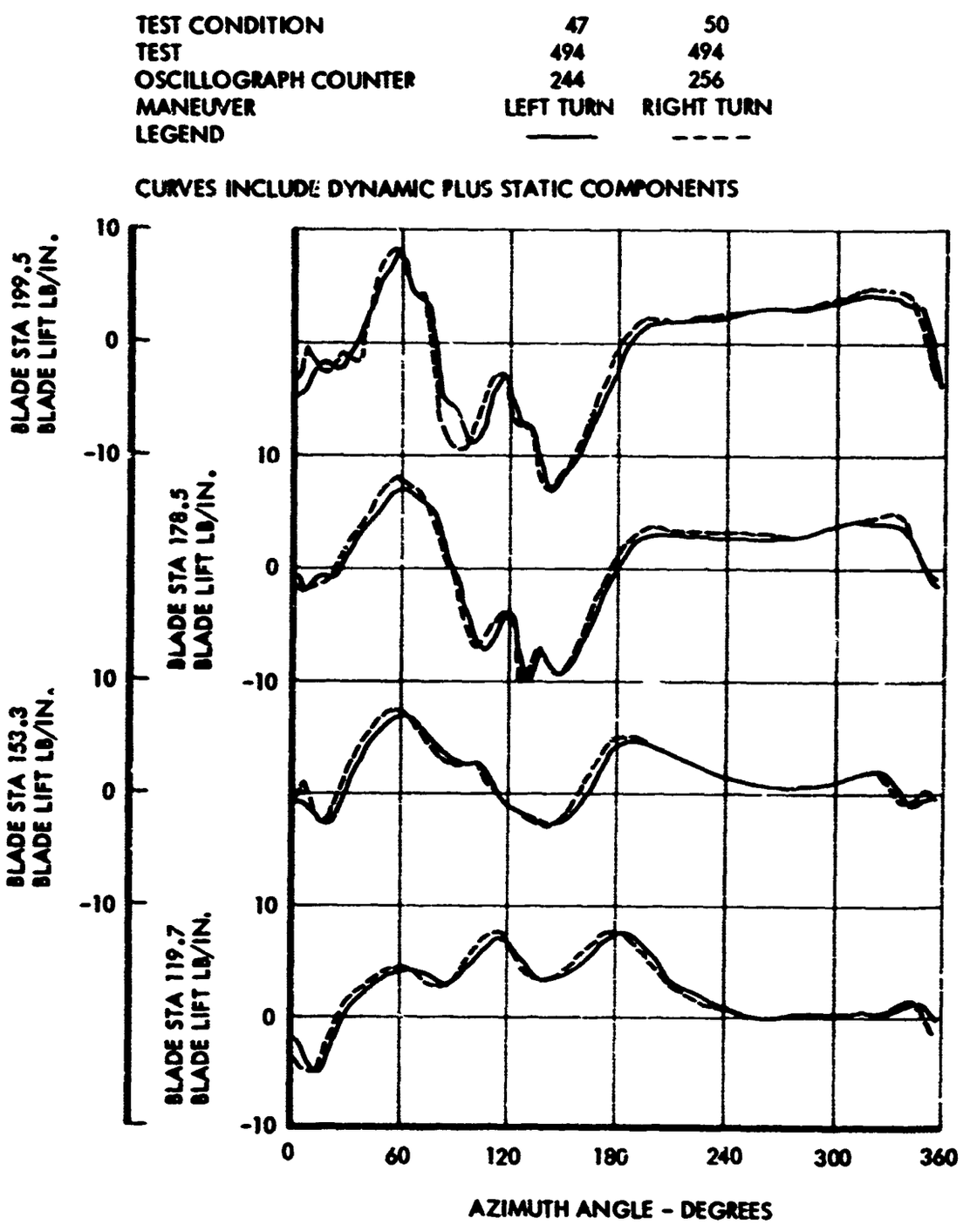

Figure 31. Comparison of Blade Section Load During Turning Maneuvers

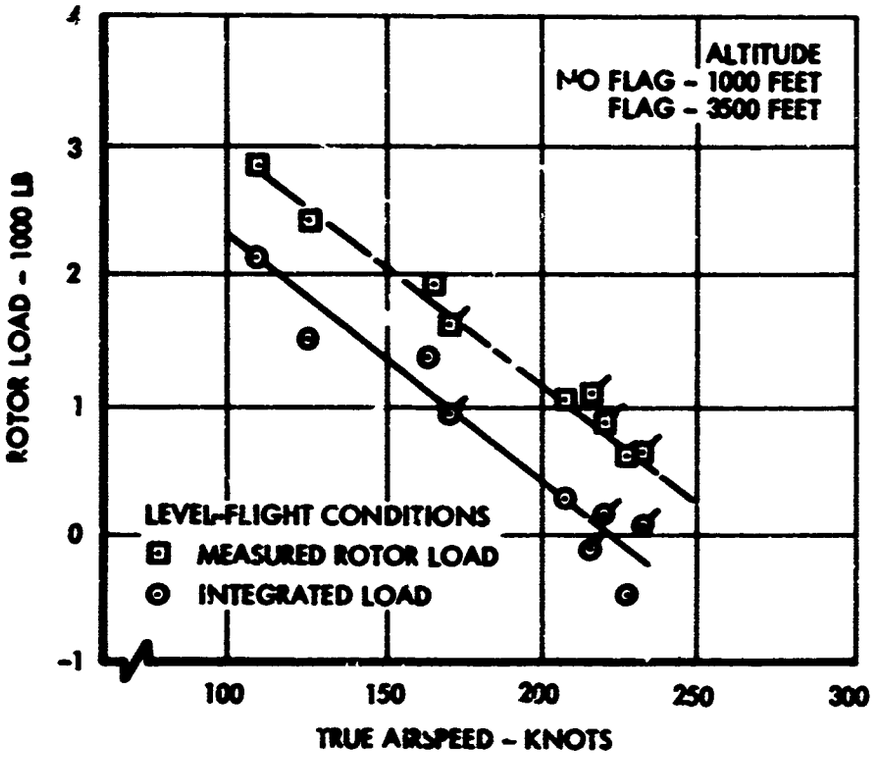

Figure 32. Main Rotor Load Versus True Airspeed

This means that any load difference between the instrumented blade and the other noninstrumented blades appears with a factor of 4 in the total difference between the integrated and the measured load.

A probable cause for loss of lift on the instrumented blade lies in its physical deviations from the noninstrumented blades. The mounting of the pressure transducers with the fairing around them can influence the pressure distribution by a certain amount. The added weight of the sleeves and the wiring for the instruments shifted the center of gravity backward. Counterweights at the tip of the blade near the leading edge were necessary to move the cg of the blade forward, resulting in a change of the blade angle. In order to balance the rotor, corresponding weights were attached on the opposite blade at the quarter-chord point. During the balancing and tracking procedure, the tip weights on the instrumented blade and the counterweights on the opposite blade were varied until the rotor appeared to be balanced, and the four blade tips followed the same track during the ground run and hover condition. In order to keep the blades in track during forward flight conditions, the trim tab at the trailing edge near the tip of the blade was deflected and the pitch link was adjusted. The tracking and balancing procedure by changing weights and trim tab deflections was continued until the residual imbalance was acceptable for all flight conditions.

The final configuration of the instrumented blade after tracking and balancing resulted in a different weight, airload, and twist distribution compared with the other three blades. It is therefore very likely that the static component of the airload of the instrumented blade was shifted in order to keep all static moment components in balance.

Some of the differences might be explained by losses in the integration process. The actual pressure peak near the leading edge was probably higher than could be simulated by the interpolation process discussed in the Automatic Data Handling section. Also the assumption that the airload was zero inboard of blade station 26, the start of the airfoil, might not be true in all cases.

Another probable source for differences in the total load is the zero-shift sensitivity of the pressure gages which can also be the source for the scatter in the data.

It is unlikely that only one of the parameters mentioned above is to blame for the differences between measured and integrated rotor load. The largest contribution, however, seems to be the dissymmetry in the rotor system.

BIBLIOGRAPHY

1. Foulke, W.K., Exploration of High-Speed Flight With the XH-51A Rigid Rotor Helicopter, Lockheed Report 18374, USAAVLABS 65-25, U.S. Army Aviation Materiel Laboratories, Fort Eustis, Virginia, June 1965.

2. Wyrick, D.R., Extension of the High-Speed Envelope of the XH-51A Compound Helicopter, Lockheed Report 18917, USAAVLABS 65-71, U.S. Army Aviation Materiel Laboratories, Fort Eustis, Virginia, May 1965.

3. Lentine, F.P., Groth, W.P., and Oglesby, T.H., Research in Maneuverability of the XH-51A Compound Helicopter, Lockheed Report 20894, U.S. Army Aviation Materiel Laboratories, Fort Eustis, Virginia (in publication).

4. Hildebrand, F.B., Introduction to Numerical Analysis, McGraw-Hill Book Co., New York, N.Y., 1956.

5. Sokolnikoff, I.S., and Redheffer, R.M., Mathematics of Physics and Modern Engineering, McGraw-Hill Book Co., New York, N.Y.

APPENDIX I

XH-51A AIRLOADS COMPUTER PROGRAM

INTRODUCTION

This program was designed to process the pressure oscillograph data to obtain airload and pitching moment with their harmonics. After the trace readings were calibrated, the dynamic component was separated from the static component, and both were tabulated. From the instrumentation geometry a chordwise pressure distribution map of the blade pressures at the instrumented span stations was built for every 5 degrees of blade azimuth. Some of the pressure distribution maps were plotted, and all were integrated to obtain airload and pitching moment per inch of span. With these airloads and pitching moments per inch of span and the two known end-point values, a spanwise airload and pitching moment distribution map was built for every 5 degrees of blade azimuth. Some of these were plotted. A harmonic analysis was performed and plotted on the airload distribution every 2 inches of span. At preassigned span segments, the airload and pitching moment distributions were integrated spanwise from the lower to the upper segment limit to obtain the airload in pounds and pitching moment in inch-pounds for that particular segment. These are called lumped loads. A harmonic analysis of these lumped loads was performed, tabulated, and punched in cards for input into a matrix analysis program.

DEFINITION OF SYMBOLS

Parameters

Ψ	azimuth angle, deg
t	elapsed time of data reading from timing reference, sec
T	period of one blade revolution (elapsed time from one timing reference to the next), sec
P	differential pressure, psi
Ps	mean differential pressure static component, psi
Pd	differential pressure dynamic component, psi
Al	airload, lb/in. of span
AL	lift (lumped load), lb

Pm pitching moment, in.-lb/in.

PM pitching moment (lumped load), in.-lb

S span station, in.

C chord station, in.

Subscripts

r reading point

e oscillograph element (trace)

i 5-degree azimuth increments

s instrumented span stations

c instrumented chord stations

k interpolated chord stations (1/4-inch increments)

j interpolated span stations (2-inch increments)

l harmonic

m blade segment

DIFFERENTIAL PRESSURES

The data traces are read by machine as a time history. The program calibrates the data readings to engineering units and converts time to blade azimuth angle.

$$\Psi_{r,e} = \frac{t_{r,e}}{T} \quad 360.$$

This yields a table of $P_{r,e}$ and $\Psi_{r,e}$. Entering this table at 5-degree azimuth increments, the program interpolates for $P_{i,e}$ using a cubic polynomial derived from the third-order difference equation; i.e., Newton's interpolation formula with divided differences. Hereafter, this is called cubic interpolation.

The mean, Ps_e, of each trace is calculated and tabulated.

$$Ps_e = \sum_{i=1}^{72} \left(P_{i,e}\right) /72$$

These tabulations are labeled Differential Pressure - Static Components (Appendix VI). The dynamic differential pressure, $Pd_{i,e}$, is calculated ($Pd_{i,e} = P_{i,e} - Ps_e$, where i = 1,2...72 and e = 1,2...46) and tabulated. These tabulations are labeled Differential Pressure - Dynamic Components (Appendix V).

PRESSURE DISTRIBUTION

Dynamic Component

At the seven instrumented span stations, there were four or seven pressure transducers aligned chordwise in the blade. This allowed the e indices to be changed to s and c indices, since each transducer was located at a specific span and chord station. Thus for each of seven instrumented span stations, there is a table of dynamic pressure versus chord station for every 5 degrees of blade rotation. These tables of pressure and chord station were modified so that the pressure at chord station 13.0 (blade trailing edge) was set equal to zero. At chord station zero (blade leading edge), the pressure was set equal to the pressure at the first transducer reading (3.5 percent chord) when this reading was higher than the second transducer reading (8.0 percent chord). When the pressure at chord station 3.5 was lower than at 8.0 percent chord station, the cubic extrapolation routine was applied.

Entering the modified table of $Pd_{i,s,c,}$ at 1/4-inch increments of chord station, the program cubic interpolates for

$$Pd_{i,s,k}; \; k = 1,2...53.$$

If plots were required for checking purposes, the values of $Pd_{i,s,k}$ were plotted versus C_k.

Static Component

The same interpolation routine as described for the dynamic blade pressure was applied on the mean pressure to obtain the table $Ps_{s,k}$.

AIRLOAD AND PITCHING MOMENT

Dynamic Component

At each instrumented span station and at every 5 degrees of azimuth, airload, $Al_{i,s}$, and pitching moment about the 1/4 chord, $Pm_{i,s}$, were calculated by numerically integrating $Pd_{i,s,k}$;

$$Al_{i,s} = \int_{o}^{13} (Pd_s)\, dx$$

$$Pm_{i,s} = \int_{o}^{13} Pd_s (3.25 - x)\, dx$$

The first three terms of Newton's interpolation formula were integrated which were sufficient to establish the accuracy of interpolation.

The airloads, $Al_{i,s}$, were tabulated at each 5-degree increment of blade azimuth and labeled Blade Loads - Dynamic Components (Appendix VII).

The tables of airload and pitching moment were modified. Since the hub area makes no contribution to lift and pitching moment, Al and Pm at span stations zero and 26 were set to zero. At the tip, Al and Pm were set to zero and folded (the load at span station 199 was multiplied by -1 and entered again at span station 226). Entering the modified tables of $Al_{i,s}$ and $Pm_{i,s}$ at 2-inch increments of span station, the program cubic interpolated for $Al_{i,j}$ and $Pm_{i,j}$, where $j = 13,14...106$, and $i = 1,2...72$. At eight azimuth angles, these two parameters were plotted versus span station, S_j. These plots were labeled Blade Loads Versus Span - Dynamic Components (Appendix II).

Airload $Al_{i,j}$ was plotted versus azimuth angle Ψ_i, at four selected span stations.

Static Component

The tables $Ps_{s,k}$ were then integrated to find the mean airload and mean pitching moment. These data were stored in the 73rd position of the pitching moment tables.

$$Al_{73,s} = \int_{o}^{13} Ps_s\, dx$$

$$Pm_{73,s} = \int_{o}^{13} Ps_s\, (3.25 - x)\, dx$$

These two parameters were cubically interpolated spanwise to obtain $Al_{73,j}$ and $Pm_{73,j}$, plotted, and labeled Blade Loads Versus Span - Static Components (Appendix III).

Harmonics

The first three harmonic components of the total airload were calculated and plotted at every 2 inches of span. Total airload is the sum of the dynamic and static airload components. (The plot of these parameters is labeled Blade Load Harmonics.) The cosine terms are labeled A_o, A_1, A_2 and A_3 and the sine terms are labeled B_1 , B_2 and B_3 . The techniques of harmonic analysis are described on page 63 under Methods. These components are plotted versus span station S_j. This plot is labeled Blade Load Harmonics Versus Span (Appendix IV).

Segmented Loads

For 20 preselected span segments, lift Al and pitching moment Pm were calculated by integrating, spanwise, $Al_{i,j}$ and $Pm_{i,j}$. The integration technique is described under Methods on page 62.

$$\left.\begin{aligned} Al_{m,i} &= \int_Q^R Al_i \, dy \\ Pm_{m,i} &= \int_Q^R Pm_i \, dy \end{aligned}\right\}$$ Where R and Q are the limits of the preselected span segments as defined in Table III

The first ten harmonics of lift and pitching moment for these blade segments were calculated, tabulated, and punched in cards for input into a matrix analysis program. Table III shows the limits of integration and the mean span station for each segment number. The tabulated harmonic components of airloads and pitching moments are shown in Appendix VIII.

TABLE III. SEGMENTS OF SPAN FOR LUMPED LOADS

Segment No. (m)	Span station increments (Q - R)	Mean span station
1	0 - 4	*
2	4 - 12	*
3	12 - 22	*
4	22 - 26	*
5	26 - 32	29
6	32 - 40	36
7	40 - 50	45
8	50 - 66	58
9	66 - 80	73
10	80 - 96	88
11	96 - 110	103
12	110 - 120	115
13	120 - 130	125
14	130 - 150	140
15	150 - 164	157
16	164 - 180	172
17	180 - 190	185
18	190 - 200	195
19	200 - 208	204
20	208 - 211.3	209

*This is the hub area; therefore, no airload.

PROGRAM DESIGN

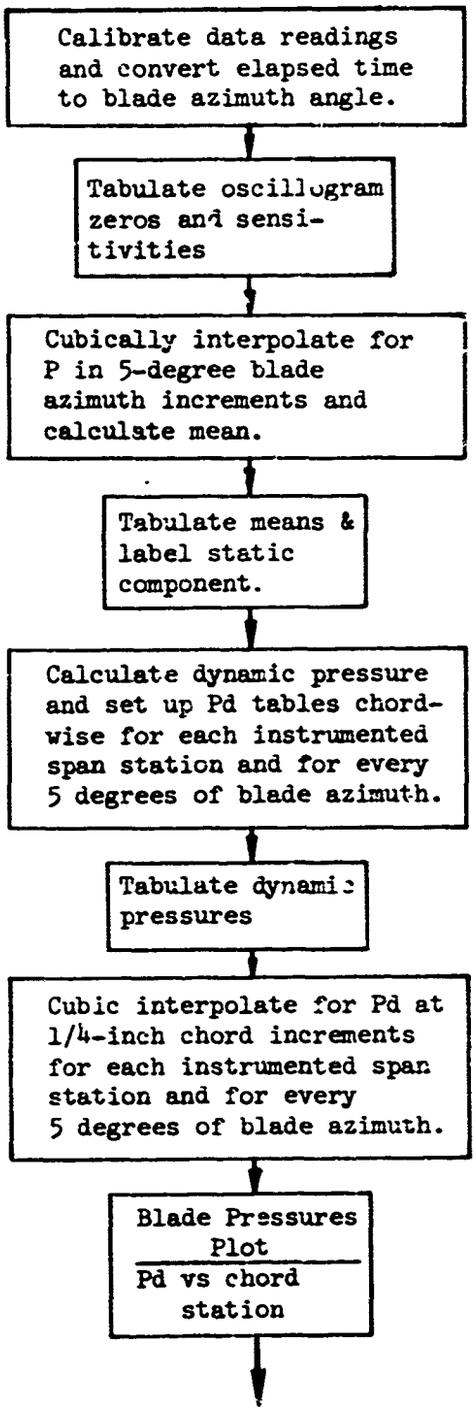

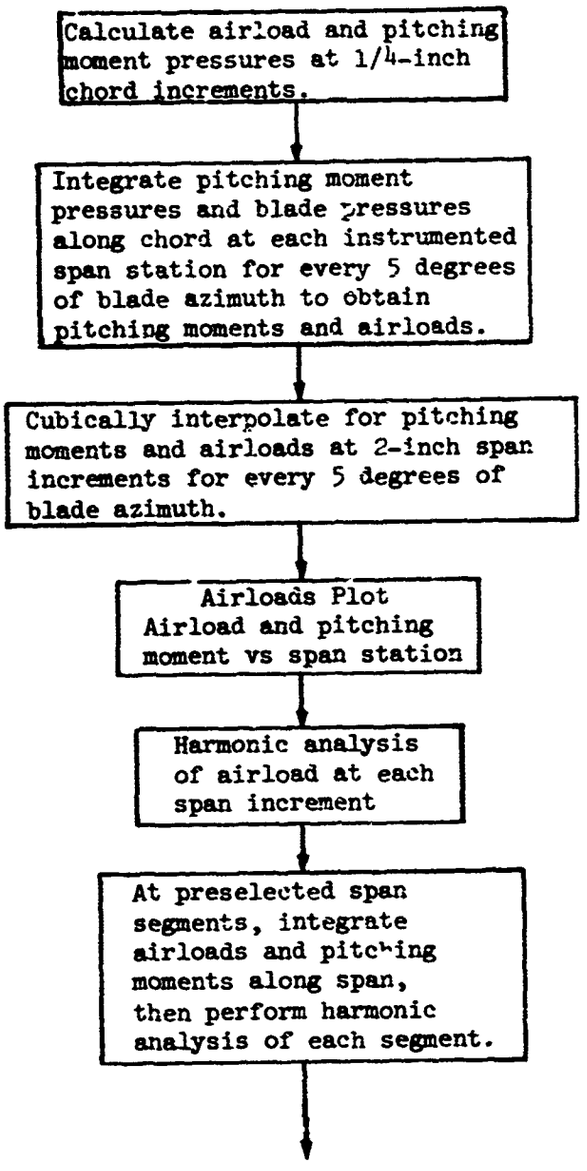
Calculate airload and pitching moment pressures at 1/4-inch chord increments.
Integrate pitching moment pressures and blade pressures along chord at each instrumented span station for every 5 degrees of blade azimuth to obtain pitching moments and airloads.
Cubically interpolate for pitching moments and airloads at 2-inch span increments for every 5 degrees of blade azimuth.
Airloads Plot
Airload and pitching moment vs span station
Harmonic analysis of airload at each span increment
At preselected span segments, integrate airloads and pitching moments along span, then perform harmonic analysis of each segment.

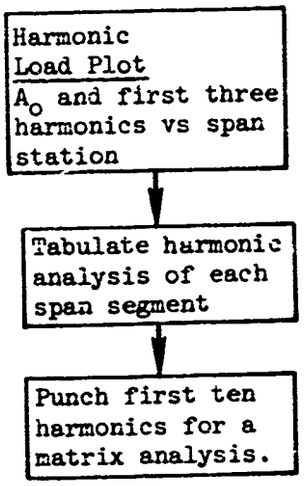
Harmonic
Load Plot
A_o and first three harmonics vs span station
Tabulate harmonic analysis of each span segment
Punch first ten harmonics for a matrix analysis.

METHODS

Newton's Interpolation Formula with Divided Differences (Reference 4).

In general

$$f(x)=f(x_0)+(x-x_0)f[x_0,x_1]+(x-x_0)(x-x_1)f[x_0,x_1,x_2]$$
$$+(x-x_0)\ \ldots\ (x-x_{n-1})f[x_0,\ \ldots\ ,x_n]$$

where

$$f[x_0] = f(x_0)$$

$$f[x_0,x_1] = \frac{f[x_1]-f[x_0]}{x_1-x_0}$$

$$f[x_0,\ \ldots\ x_n] = \frac{f[x_1,\ \ldots\ ,x_n] - f[x_0,\ \ldots\ ,x_{n-1}]}{x_n-x_0}$$

When n = 3 this reduces to

$$f(x)=f(x_0)+\frac{x-x_0}{x_1-x_0}\left(f(x_1)-f(x_0)\right)+\frac{(x-x_0)(x-x_1)}{x_2-x_0}\left[\frac{f(x_2)-f(x_1)}{x_2-x_1}-\frac{f(x_1)-f(x_0)}{x_1-x_0}\right]$$
$$+\frac{(x-x_0)(x-x_1)(x-x_2)}{x_3-x_0}\left[\frac{1}{x_3-x_1}\left(\frac{f(x_3)-f(x_1)}{x_3-x_2}-\frac{f(x_2)-f(x_1)}{x_2-x_1}\right)\right.$$
$$\left.-\frac{1}{x_2-x_0}\left(\frac{f(x_2)-f(x_1)}{x_2-x_1}-\frac{f(x_1)-f(x_0)}{x_1-x_0}\right)\right]$$

where x_0,x_1,x_2, and x_3 are any known values with corresponding known values of $f(x_0),f(x_1),f(x_2)$, and $f(x_3)$ when $f(x)$ is required at x.

Integration by Integrating the First Three Terms of Newton's Interpolation Formula

The first three terms of Newton's interpolation formula are

$$f(x)=f(x_0)+\frac{x-x_0}{x_1-x_0}[f(x_1)-f(x_0)]+\frac{(x-x_0)(x-x_1)}{x_2-x_0}\left[\frac{f(x_2)-f(x_1)}{x_2-x_1}-\frac{f(x_1)-f(x_0)}{x_1-x_0}\right]$$

Integrating

$$\int_{x_0}^{x_2}f(x)dx=\int_{x_0}^{x_2}f(x_0)dx+\frac{f(x_1)-f(x_0)}{x_1-x_0}\int_{x_0}^{x_2}(x-x_0)dx+$$
$$\frac{1}{x_2-x_0}\left[\frac{f(x_2)-f(x_1)}{x_2-x_1}-\frac{f(x_1)-f(x_0)}{x_1-x_0}\right]\int_{x_0}^{x_2}(x-x_0)\ (x-x_1)dx$$

$$\int_{x_0}^{x_2} f(x)dx = (x_2-x_0)\left[f(x_0)-Cx_0+Bx_0x_1\right] + \frac{x_2^2-x_0^2}{2}\left[C-B(x_1-x_0)\right] + \frac{1}{3}B(x_2^3-x_0^3)$$

where

$$C = \frac{f(x_1)-f(x_0)}{x_1-x_0}$$

$$B = \frac{1}{x_2-x_0}\left[\frac{f(x_2)-f(x_1)}{x_2-x_1} - \frac{f(x_1)-f(x_0)}{x_1-x_0}\right]$$

This is used numerically by adding the index i to all subscripts; i.e., x_2 now is x_{2+i}.

$$\int f(x)dx = \sum_{j=0}^{n} \int_{x_{0+i}}^{x_2+i} f(x)dx$$

where $i = 2j$ and $n = \begin{cases} (N-1)/2; \text{ if } N \text{ is odd} \\ (N-2)/2; \text{ if } N \text{ is even} \end{cases}$

Harmonic Analysis (Reference 5)

The Fourier Series of $y = f(x)$ is

$$y = A_0 + \sum_{j=1}^{n} A_j \cos jx + \sum_{j=1}^{n} B_j \sin jx$$

or in the complex form

$$y = A_0 + \sum_{j=1}^{n} C_j \cos (jx - \phi_j)$$

If N is the number of equally spaced input points (not including 360°),

$$A_0 = \frac{1}{N}\sum_{i=1}^{n} y_i$$

$$A_j = \frac{2}{N}\sum_{i=1}^{n} y_i \cos\left[\frac{2(i-1)j\pi}{N}\right] \qquad ,j = 1,2,\ldots,\frac{N}{2}$$

$$B_j = \frac{2}{N}\sum_{i=1}^{n} y_i \sin\left[\frac{2(i-1)j\pi}{N}\right] \qquad ,j = 1,2,\ldots,\frac{N}{2}$$

$$C_j = (A_j^2 + B_j^2)^{1/2} \qquad ,j = 1,2,\ldots,\frac{N}{2}$$

$$\phi_j \text{(or PHI}_j\text{C)} = \tan^{-1}\left(\frac{B_j}{A_j}\right) \qquad ,j = 1,2,\ldots,\frac{N}{2}$$

$$\text{FREQUENCY}_j = j\left(\frac{1}{T}\right) \qquad ,j = 1,2,\ldots,\frac{N}{2}$$

APPENDIX II

BLADE LOADS VERSUS SPAN - DYNAMIC COMPONENTS

The plottings presented in this appendix show the dynamic components of the airloads (in pounds per inch) and pitching moments (in inch-pounds per inch) versus blade station for eight azimuth positions, as indicated, of the 20 test conditions selected for full analysis.

The corresponding static components are shown in Appendix III. A complete set of the dynamic components of blade loads for 72 azimuth positions is tabulated in Appendix VII.

BLADE LOADS VERSUS SPAN - DYNAMIC COMPONENTS

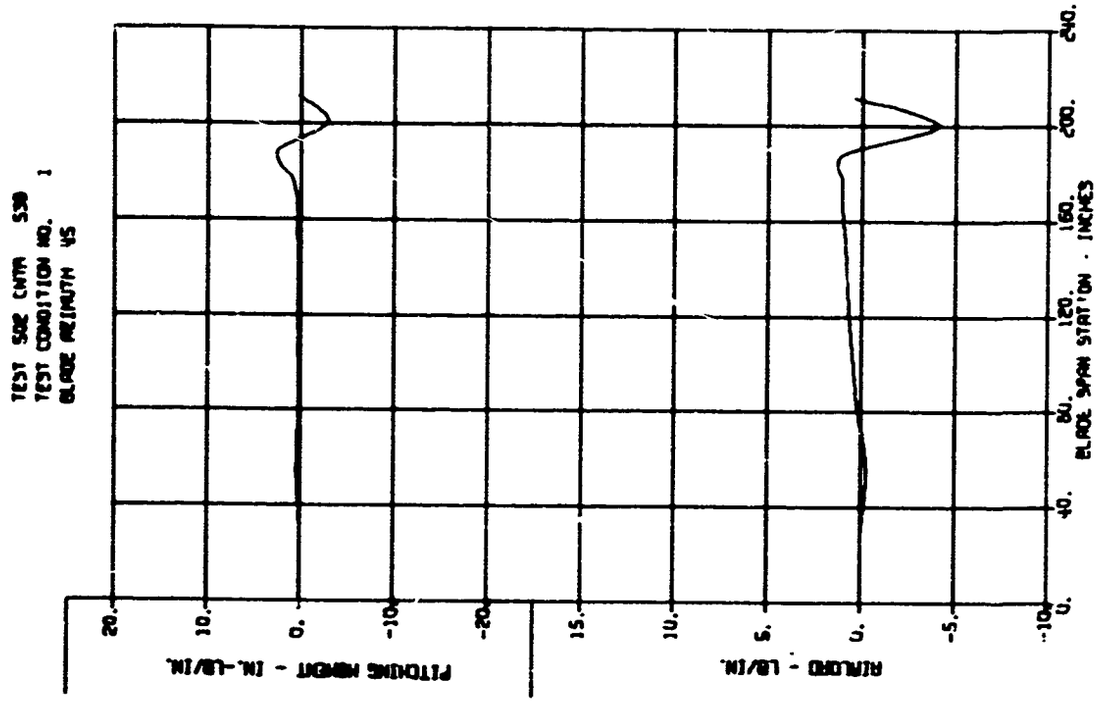

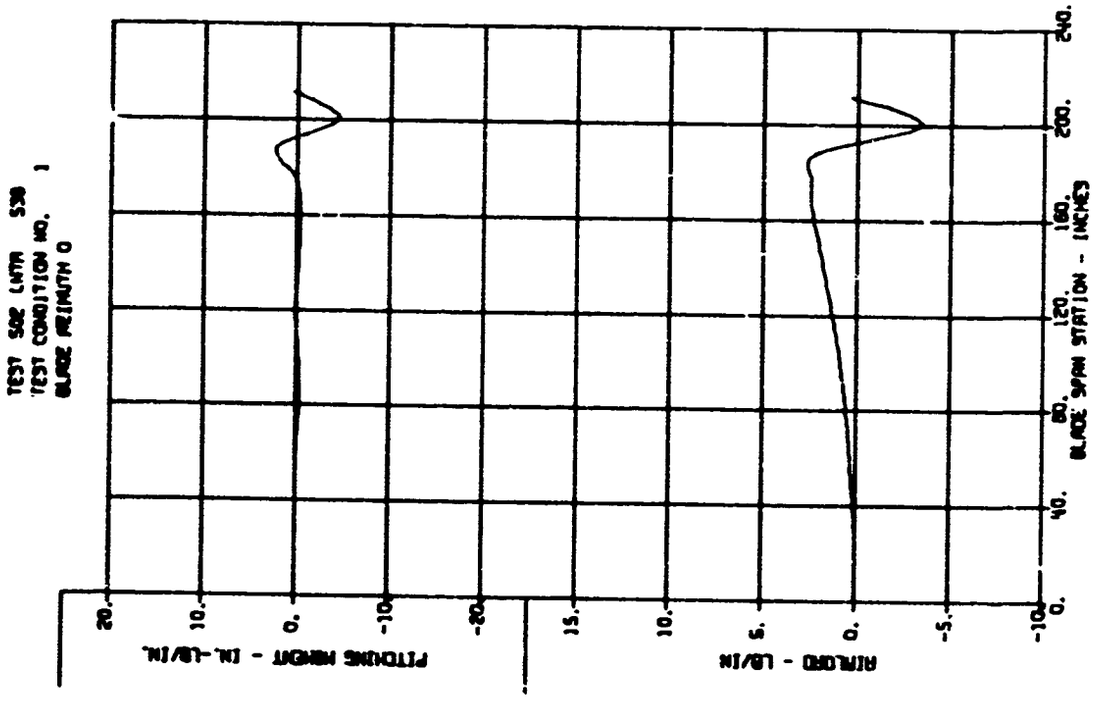

BLADE LOADS VERSUS SPAN - DYNAMIC COMPONENTS

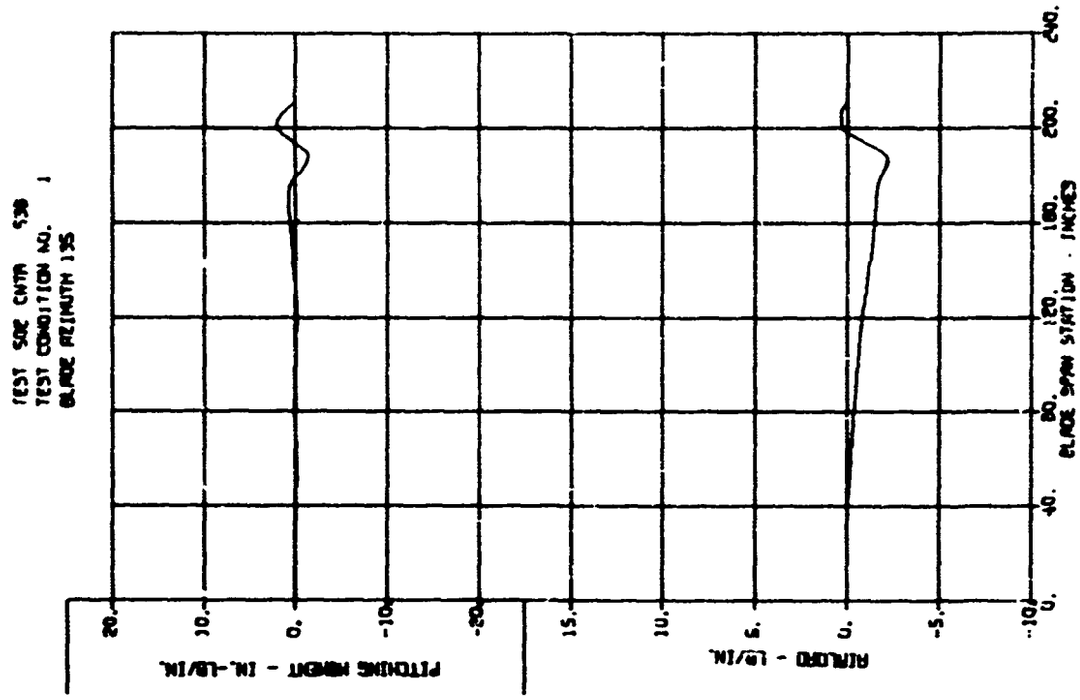

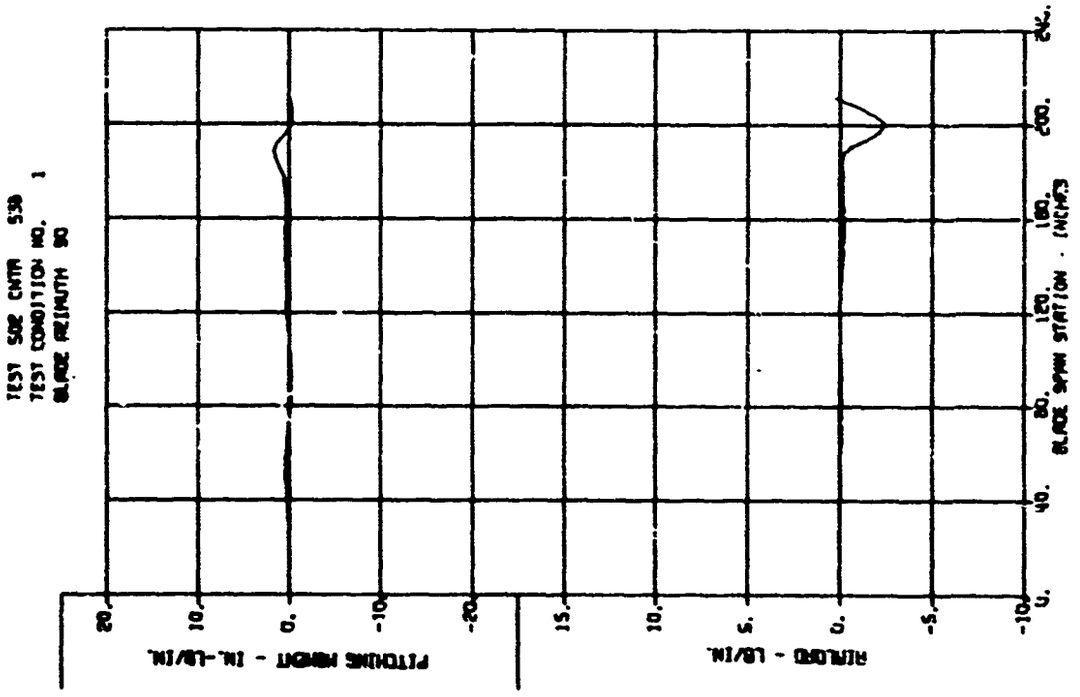

BLADE LOADS VERSUS SPAN - DYNAMIC COMPONENTS

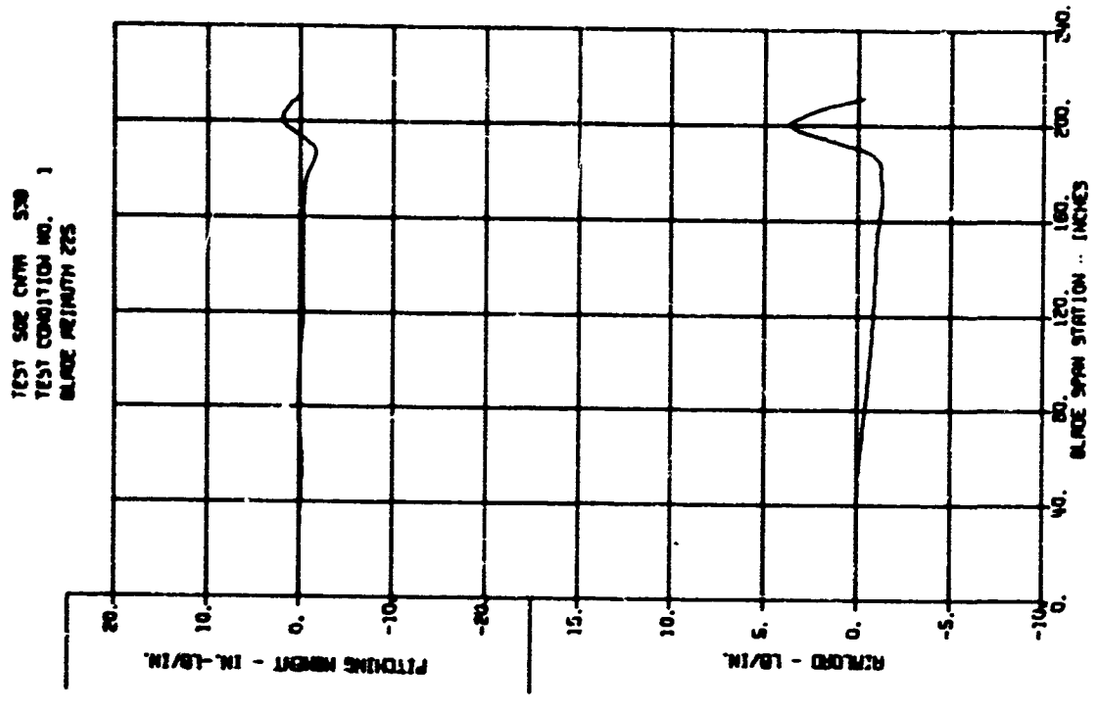

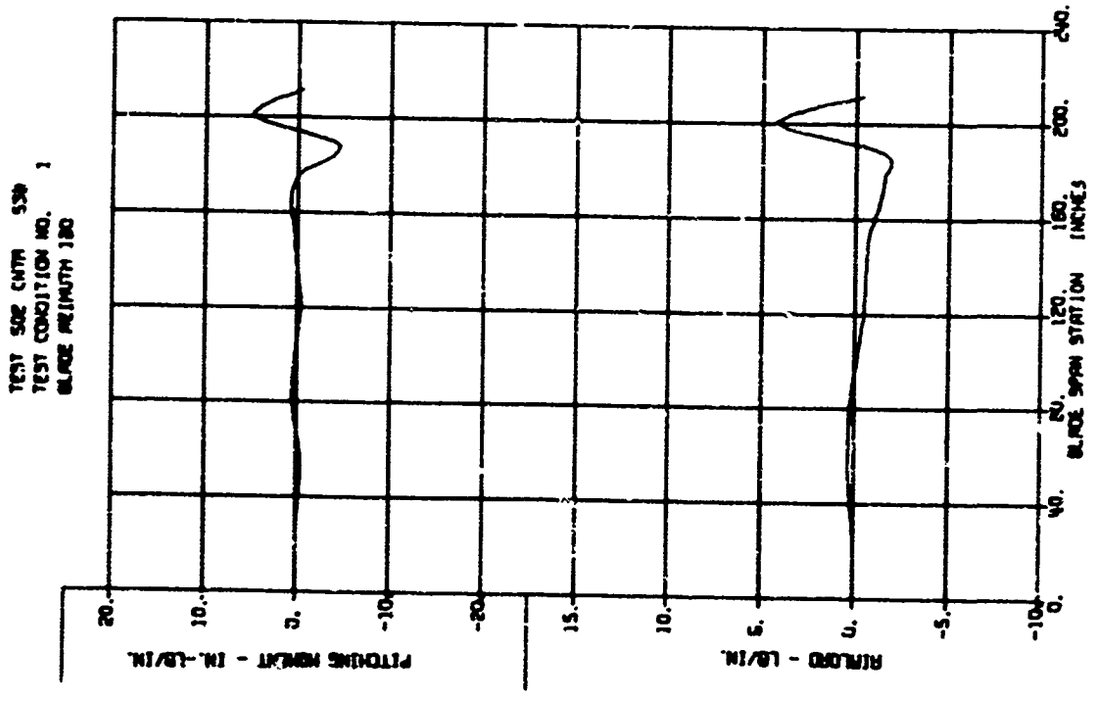

BLADE LOADS VERSUS SPAN - DYNAMIC COMPONENTS

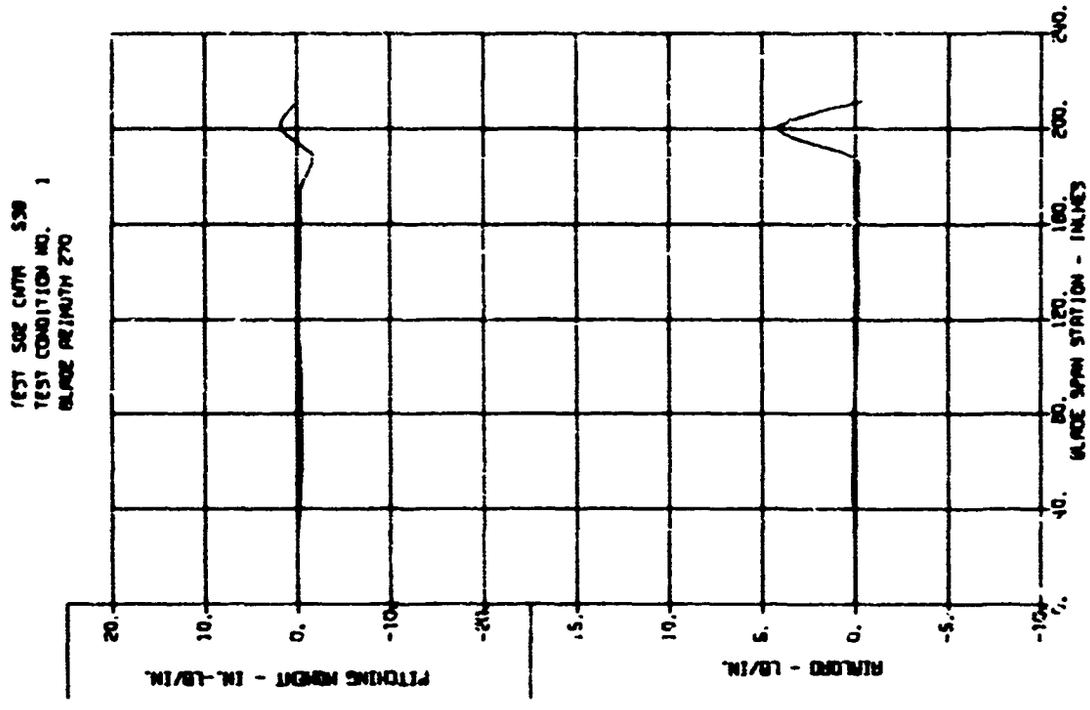

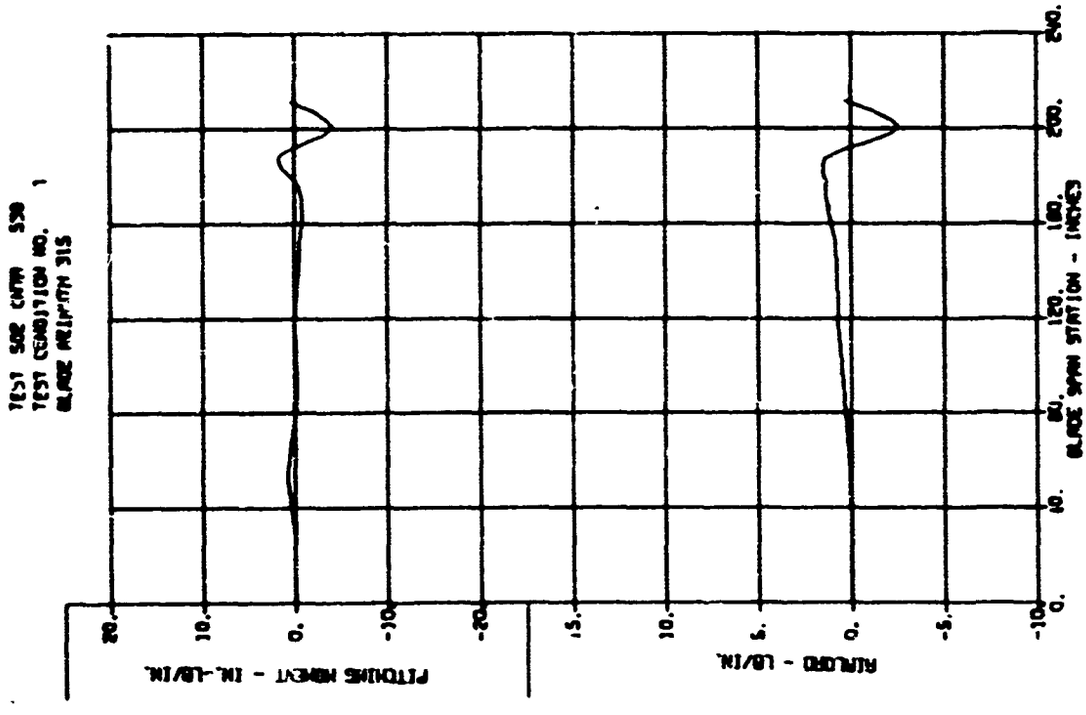

BLADE LOADS VERSUS SPAN - DYNAMIC COMPONENTS

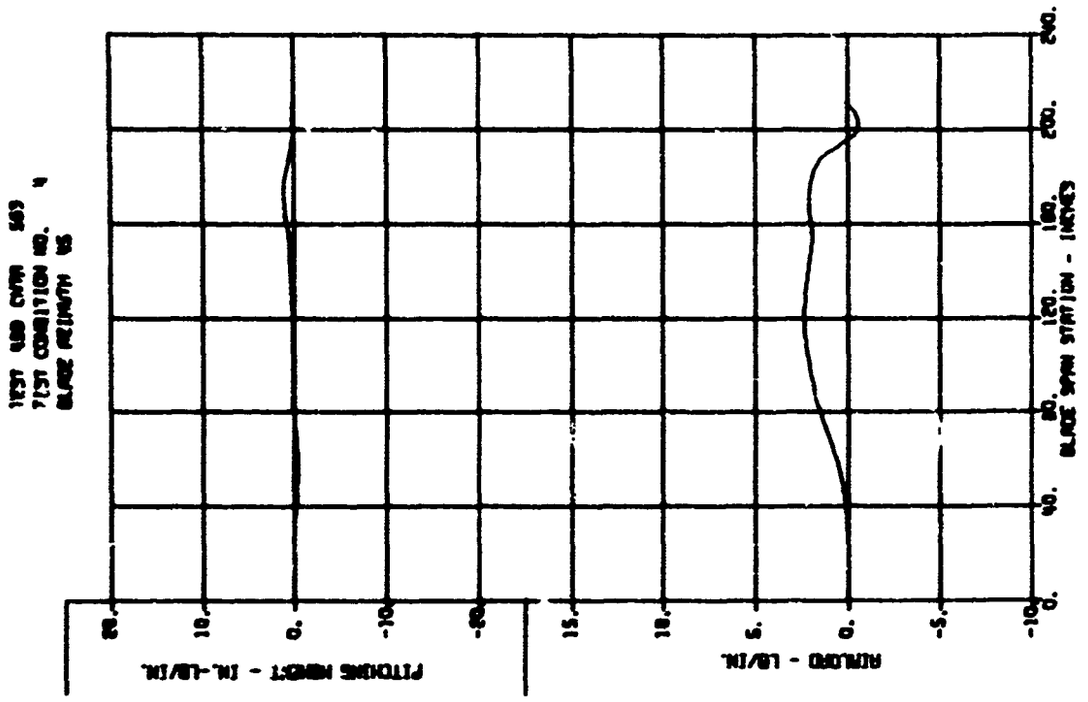

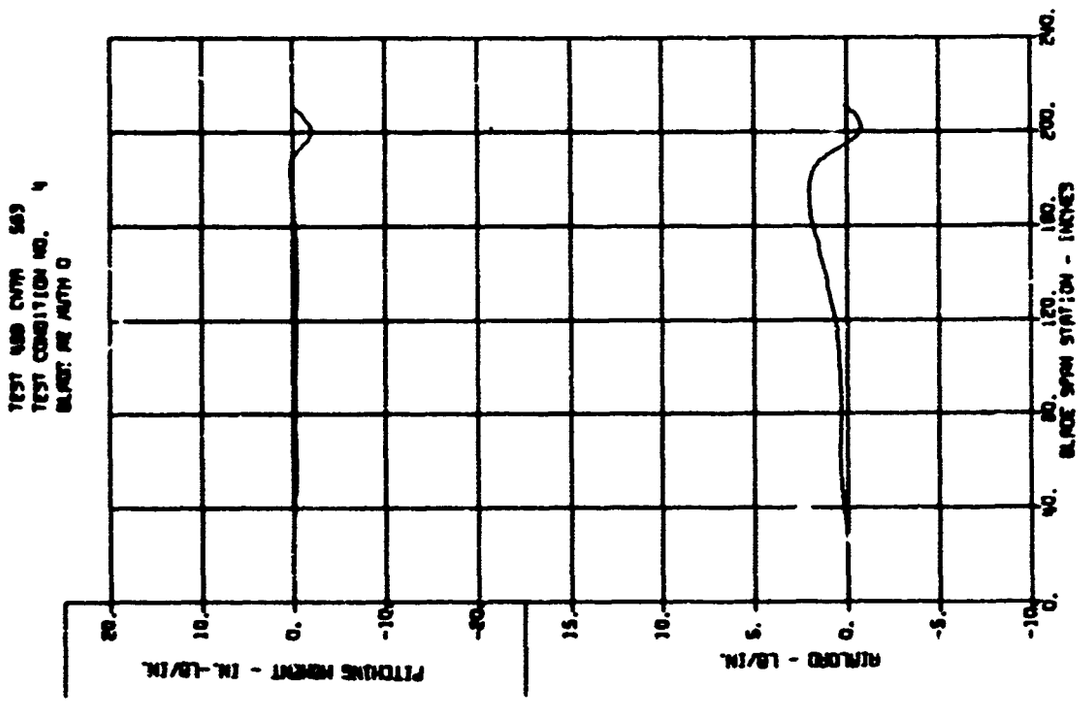

BLADE LOADS VERSUS SPAN - DYNAMIC COMPONENTS

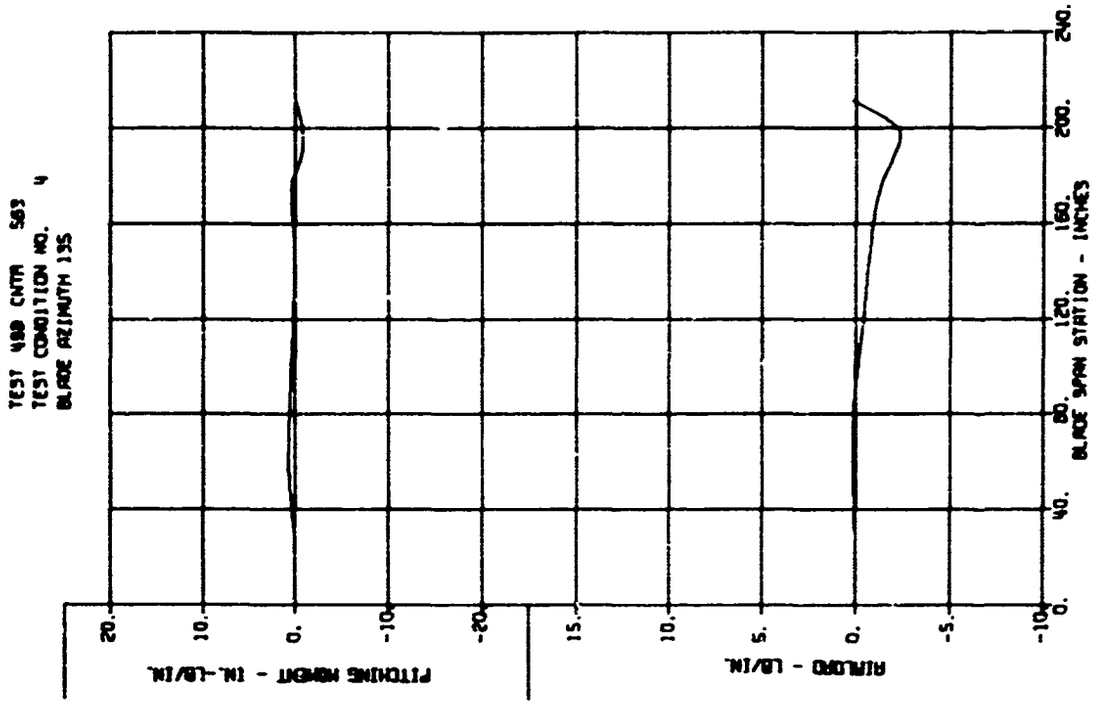

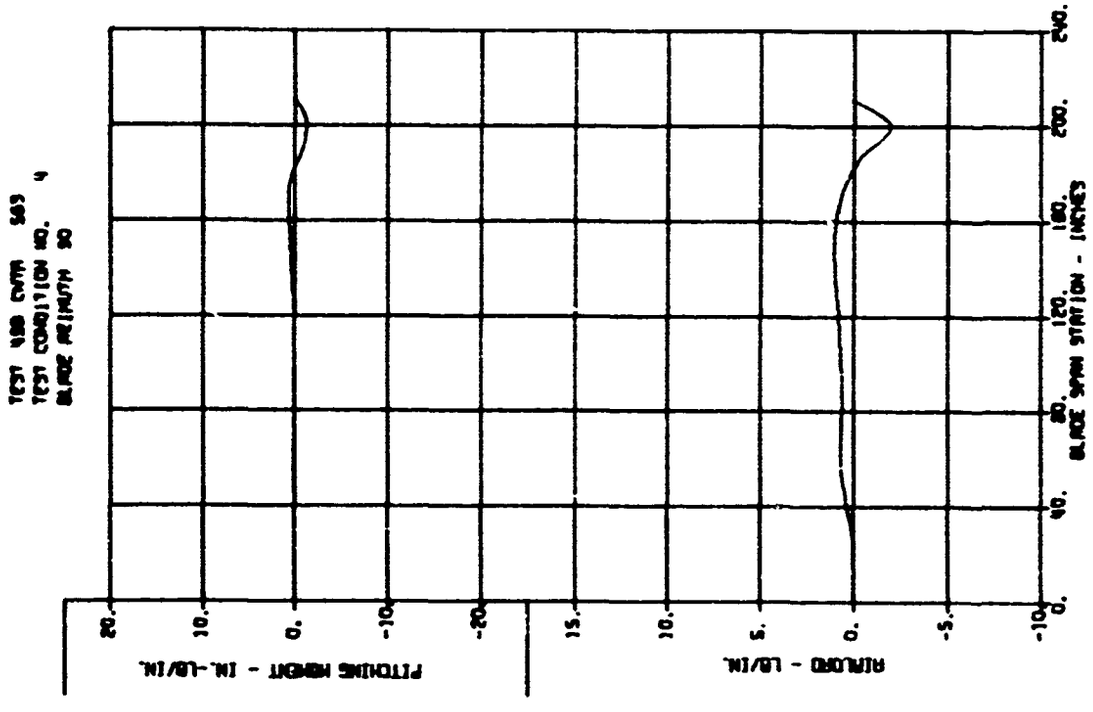

BLADE LOADS VERSUS SPAN - DYNAMIC COMPONENTS

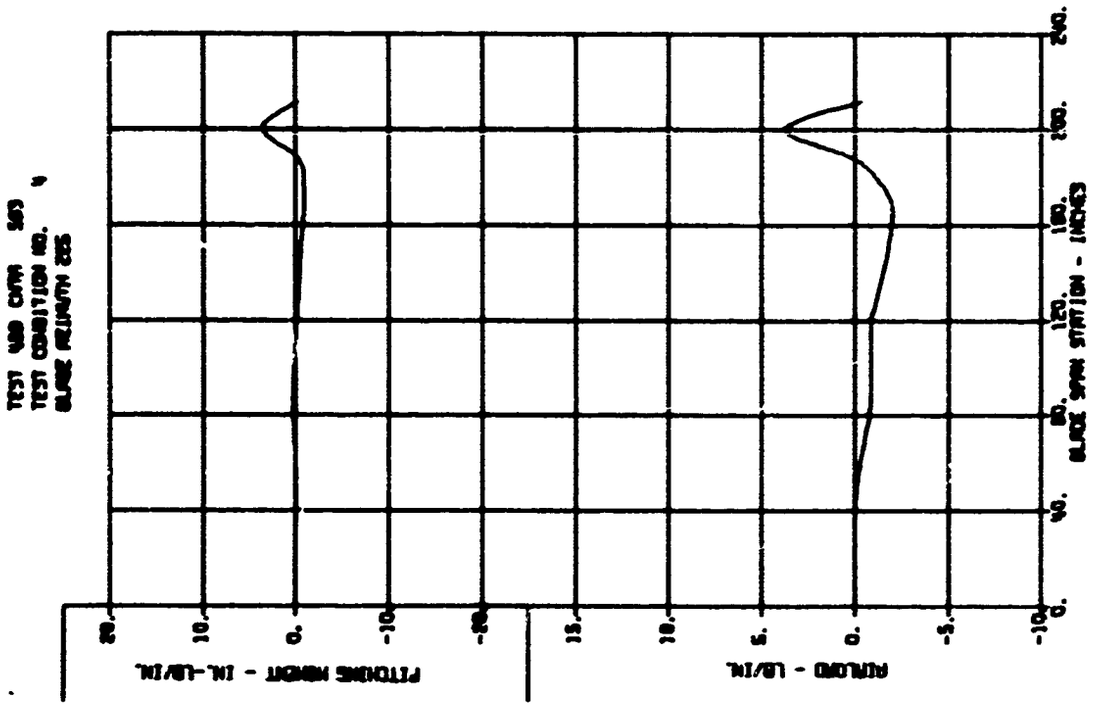

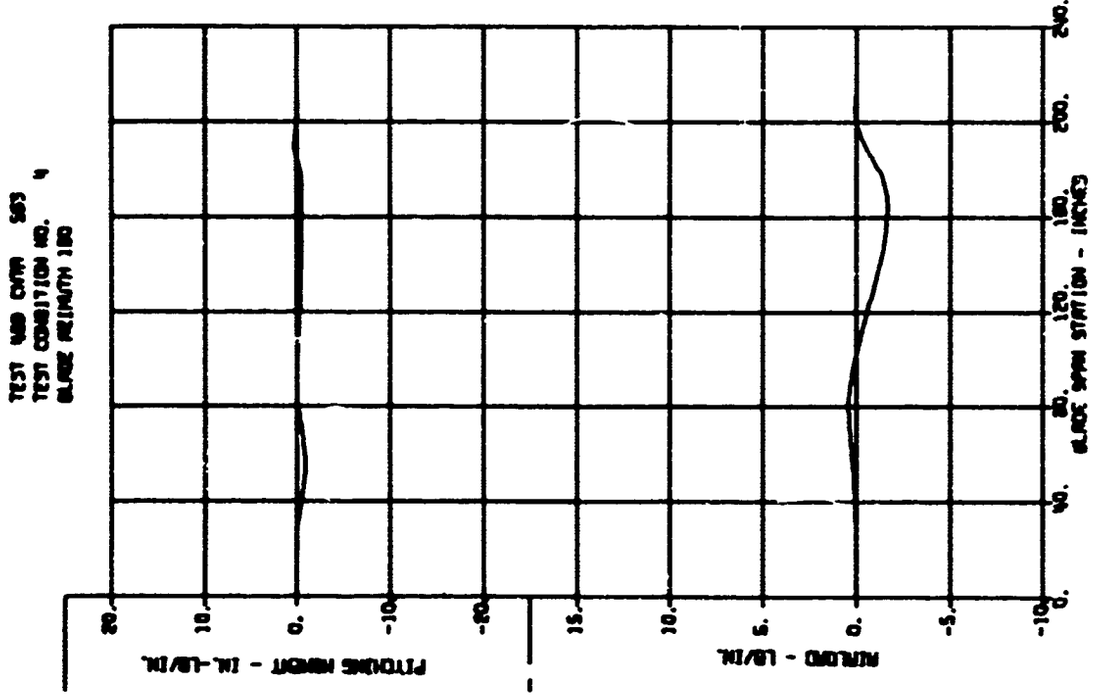

BLADE LOADS VERSUS SPAN - DYNAMIC COMPONENTS

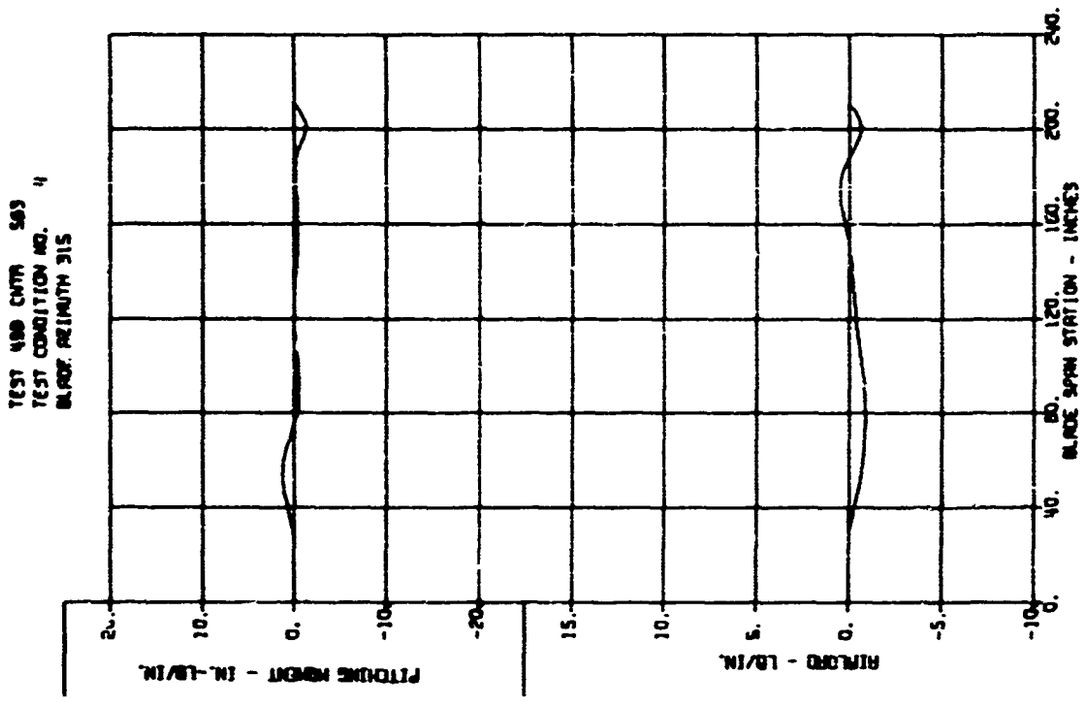

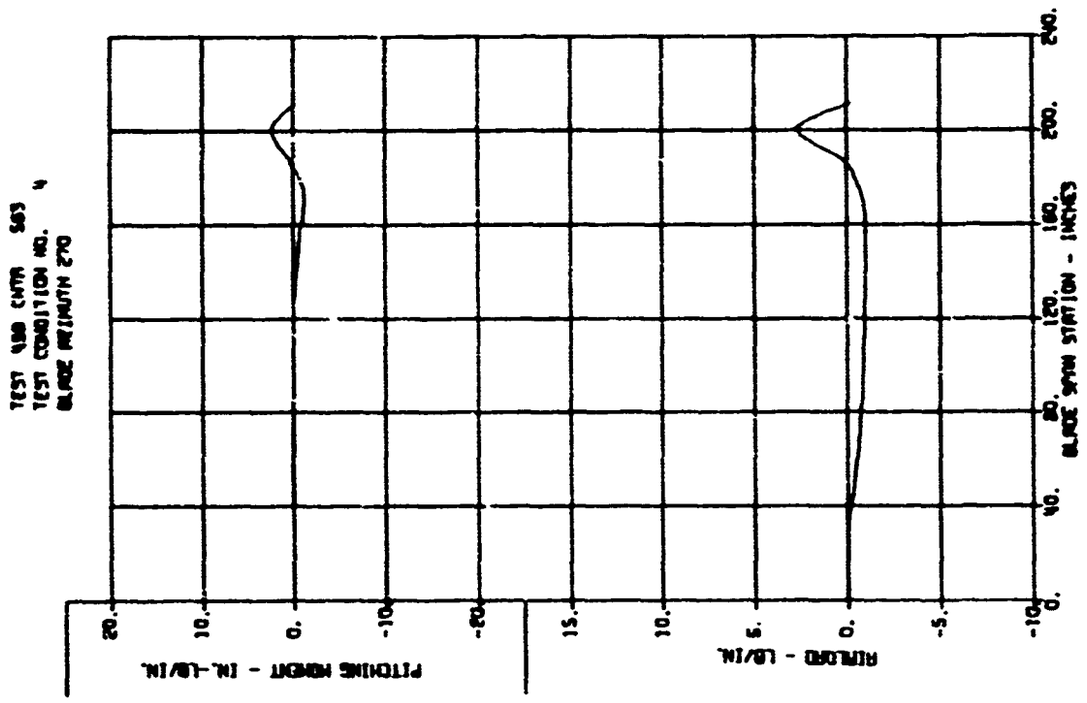

BLADE LOADS VERSUS SPAN - DYNAMIC COMPONENTS

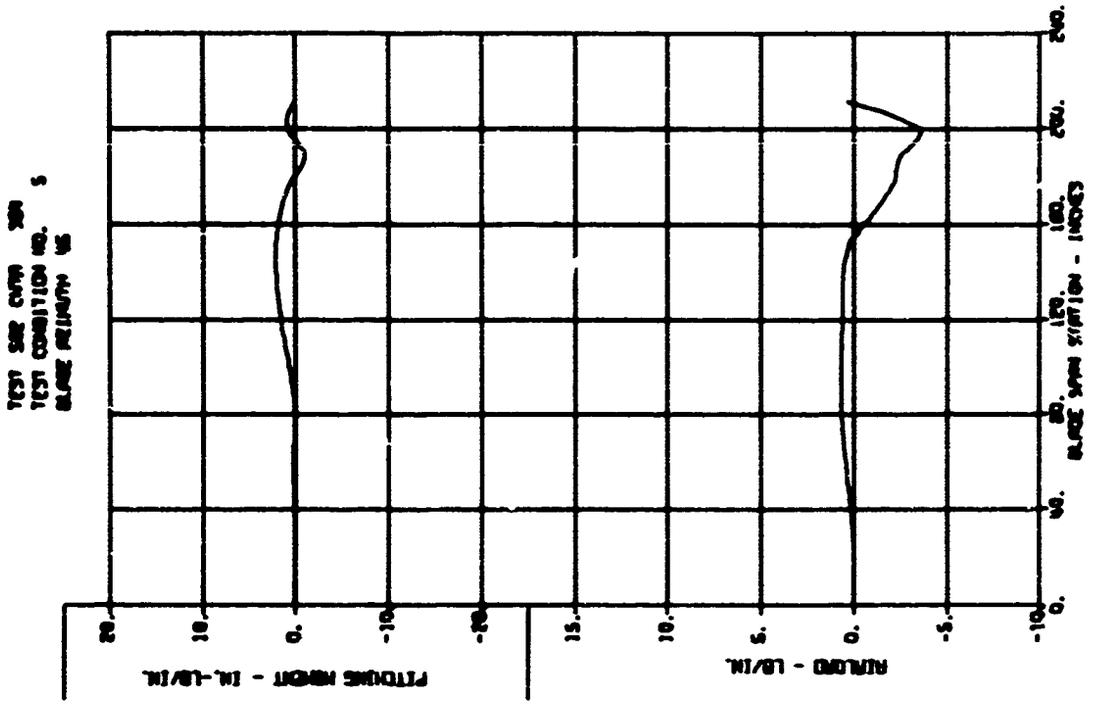

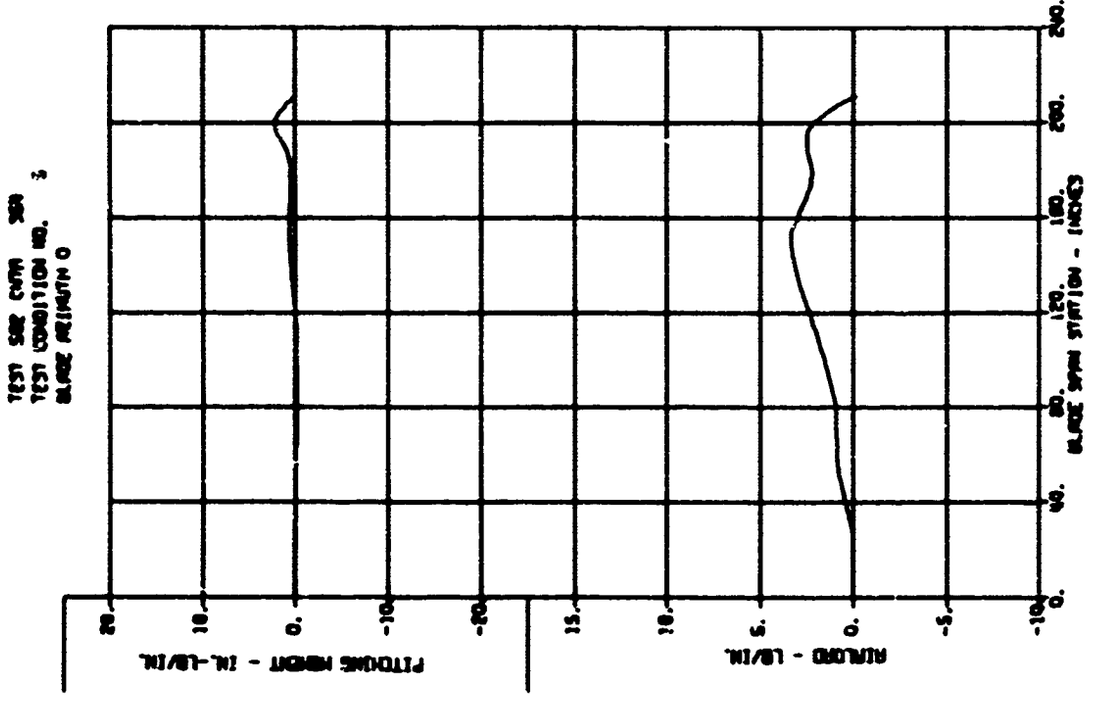

BLADE LOADS VERSUS SPAN - DYNAMIC COMPONENTS

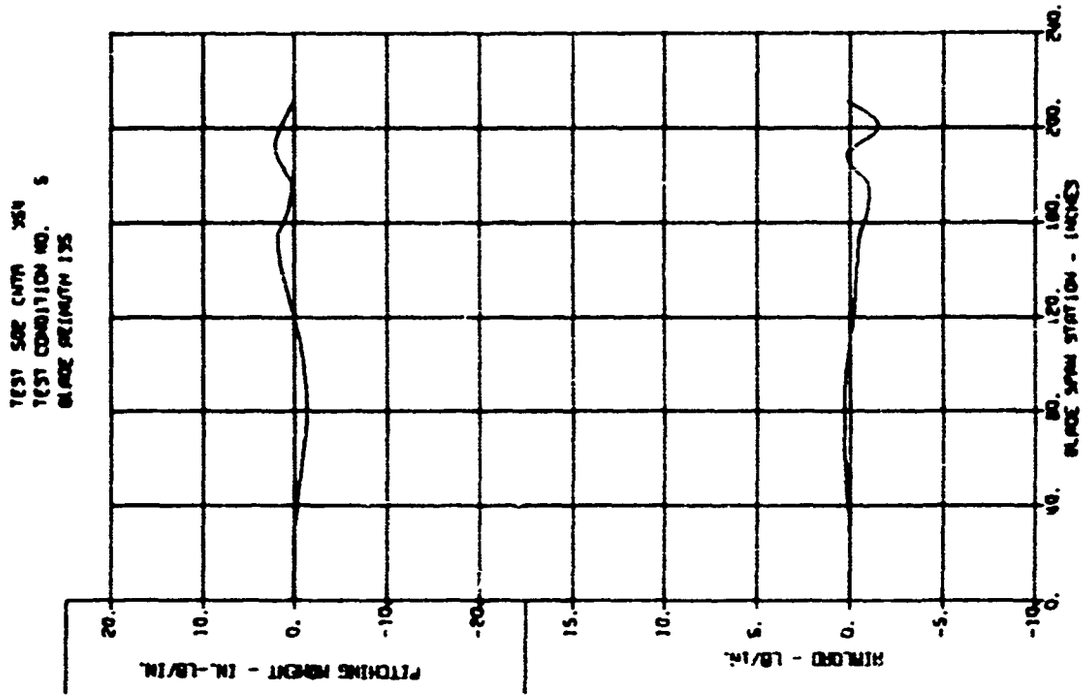

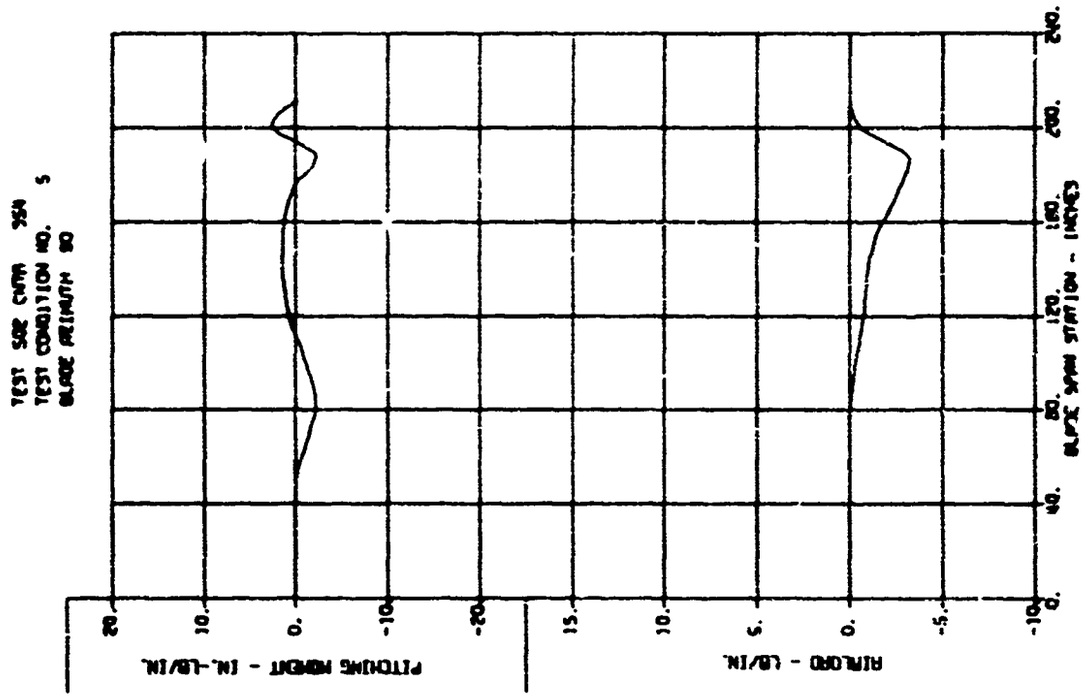

BLADE LOADS VERSUS SPAN - DYNAMIC COMPONENTS

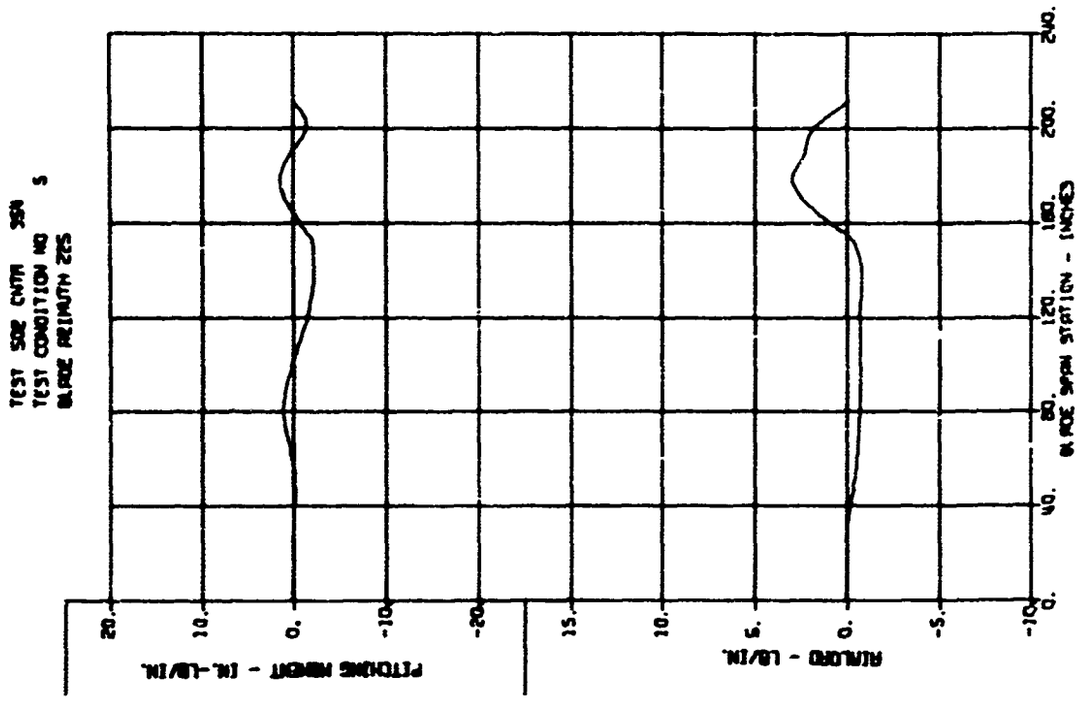

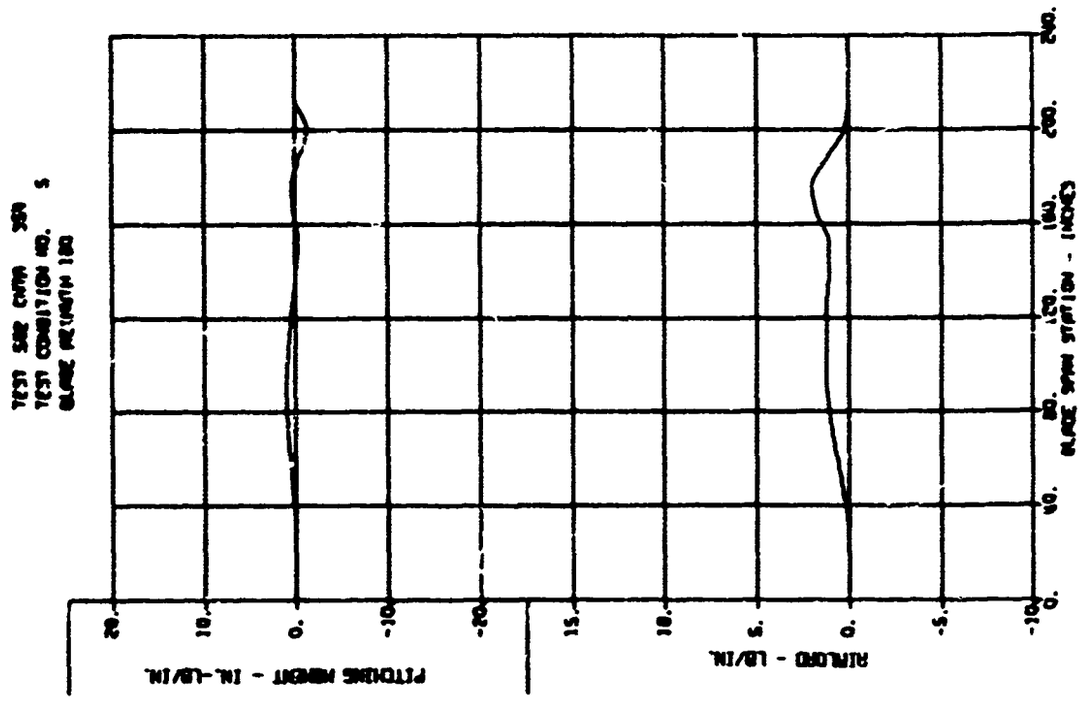

BLADE LOADS VERSUS SPAN - DYNAMIC COMPONENTS

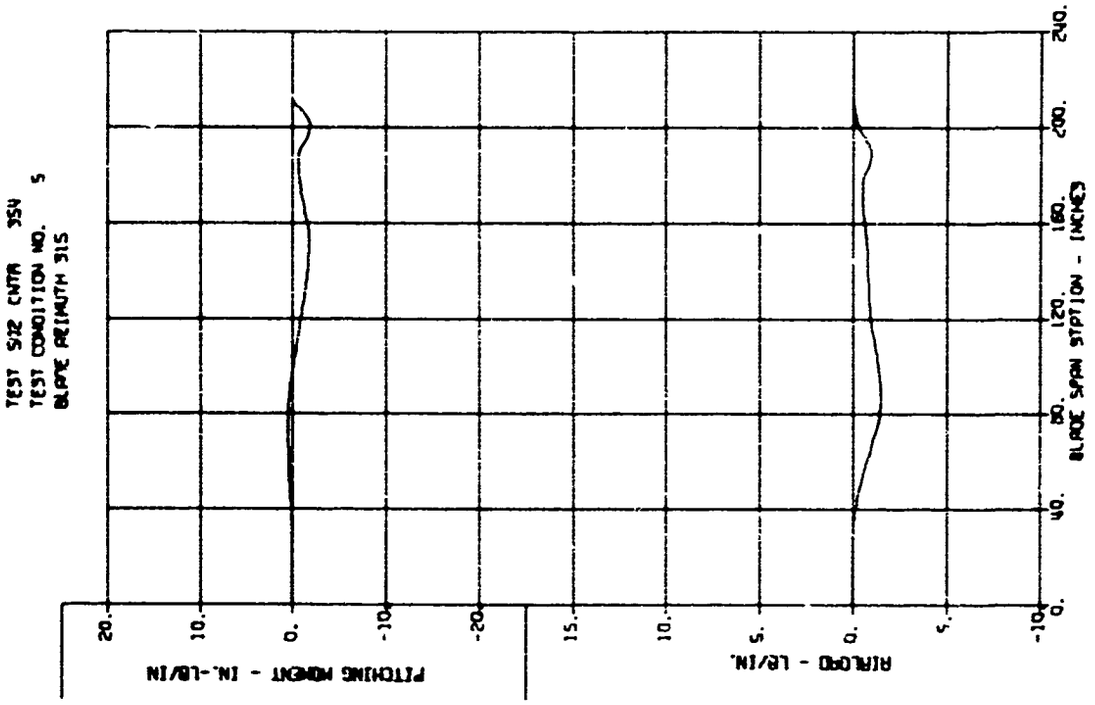

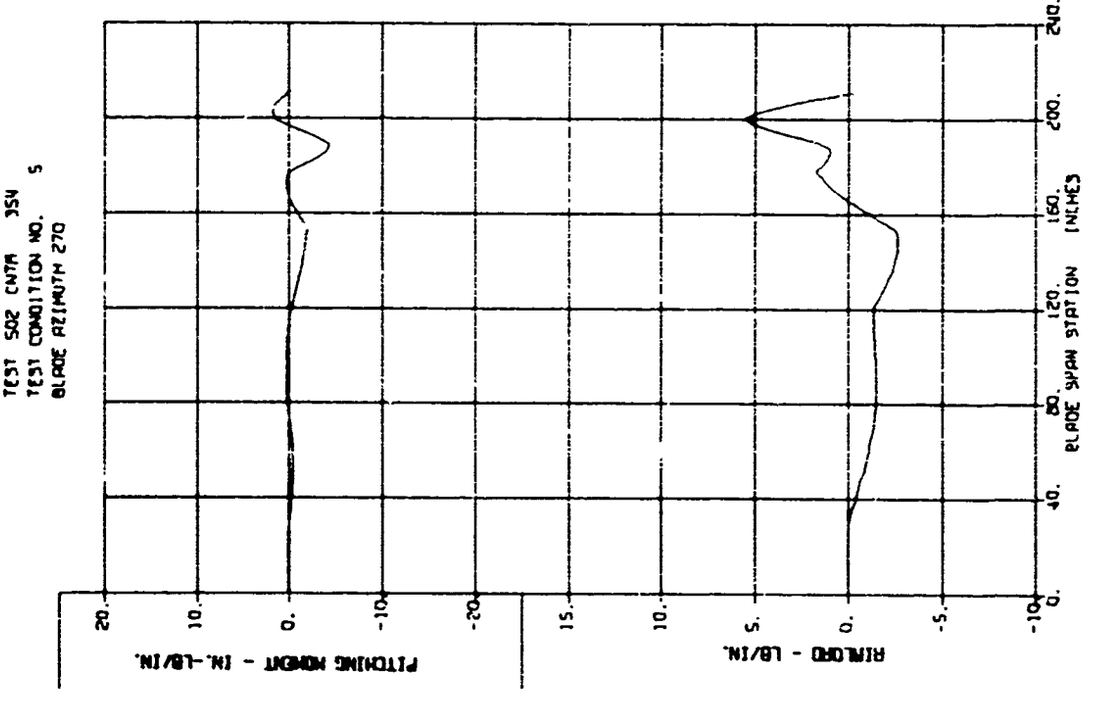

BLADE LOADS VERSUS SPAN - DYNAMIC COMPONENTS

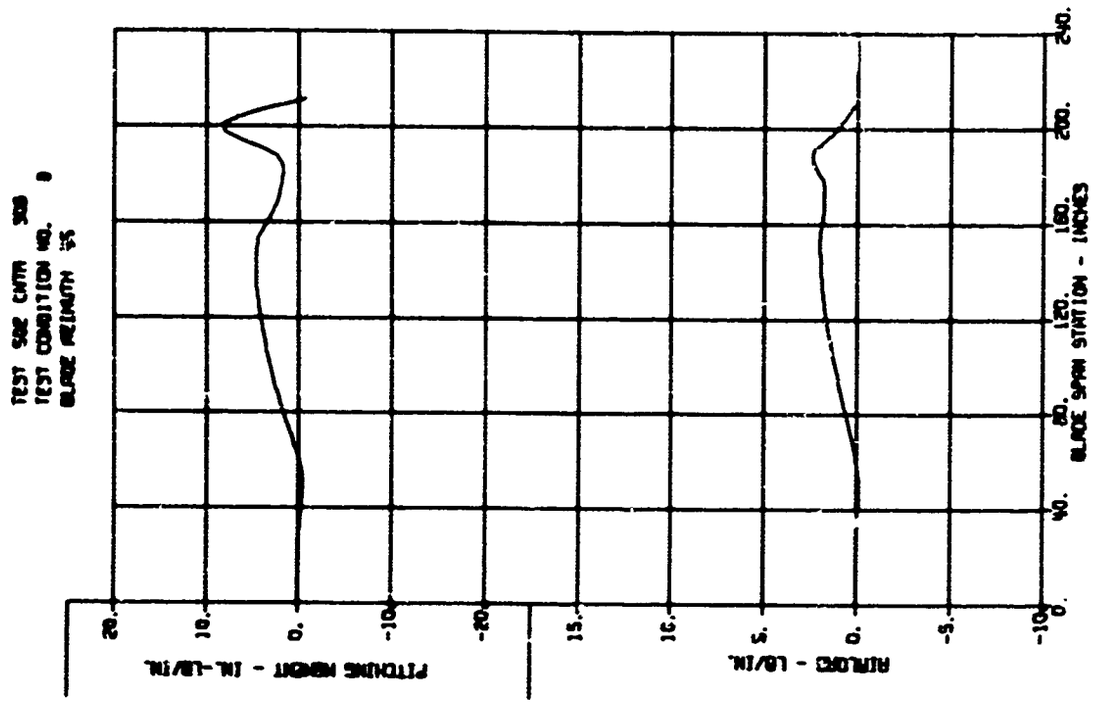

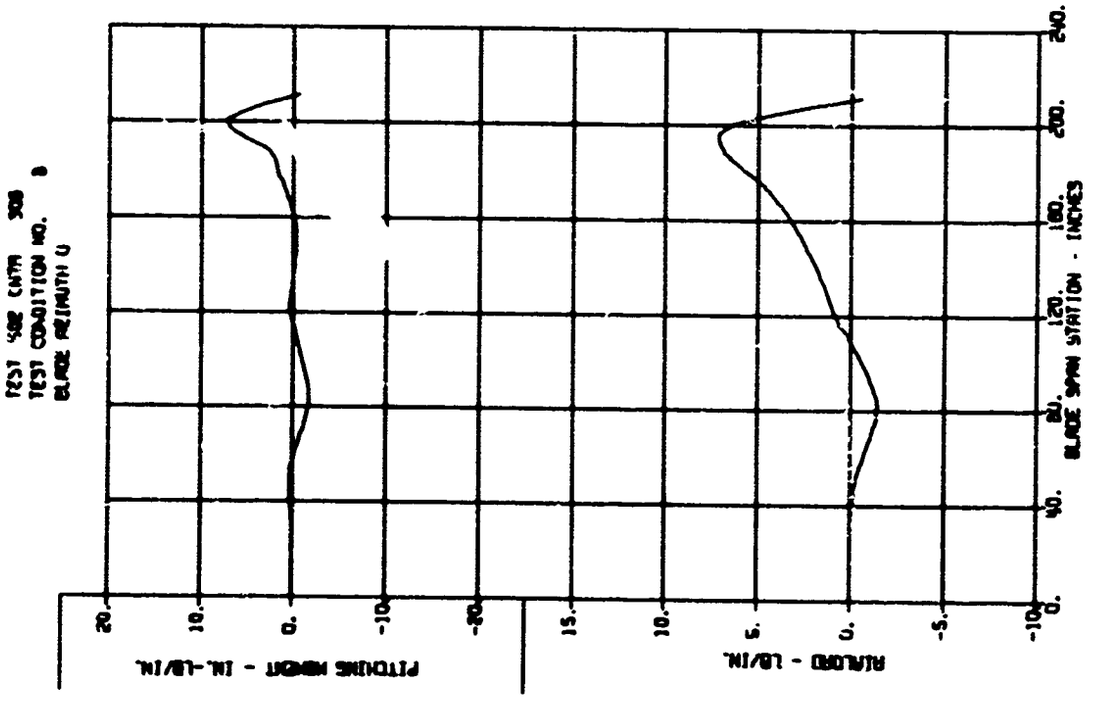

BLADE LOADS VERSUS SPAN - DYNAMIC COMPONENTS

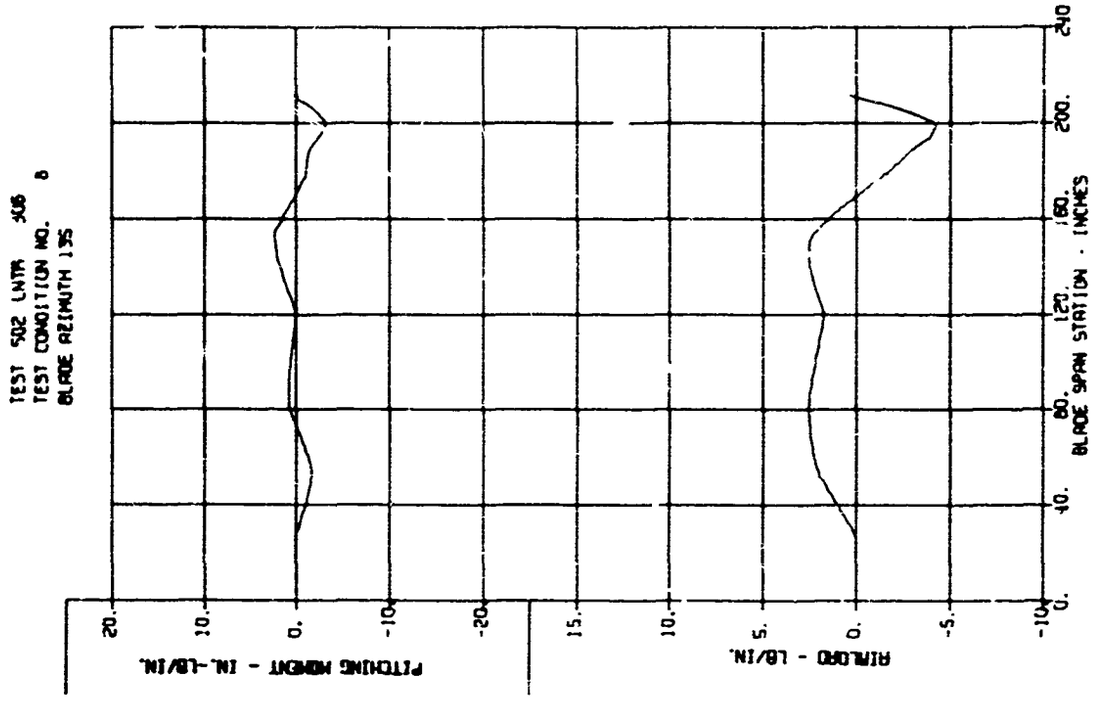

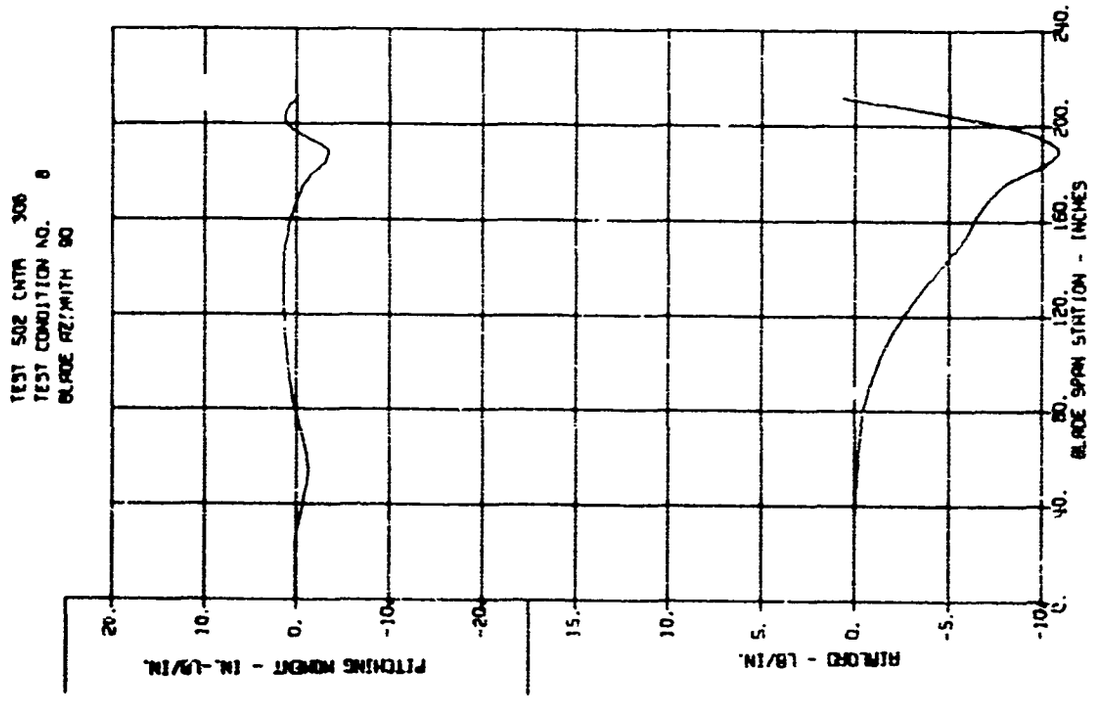

BLADE LOADS VERSUS SPAN - DYNAMIC COMPONENTS

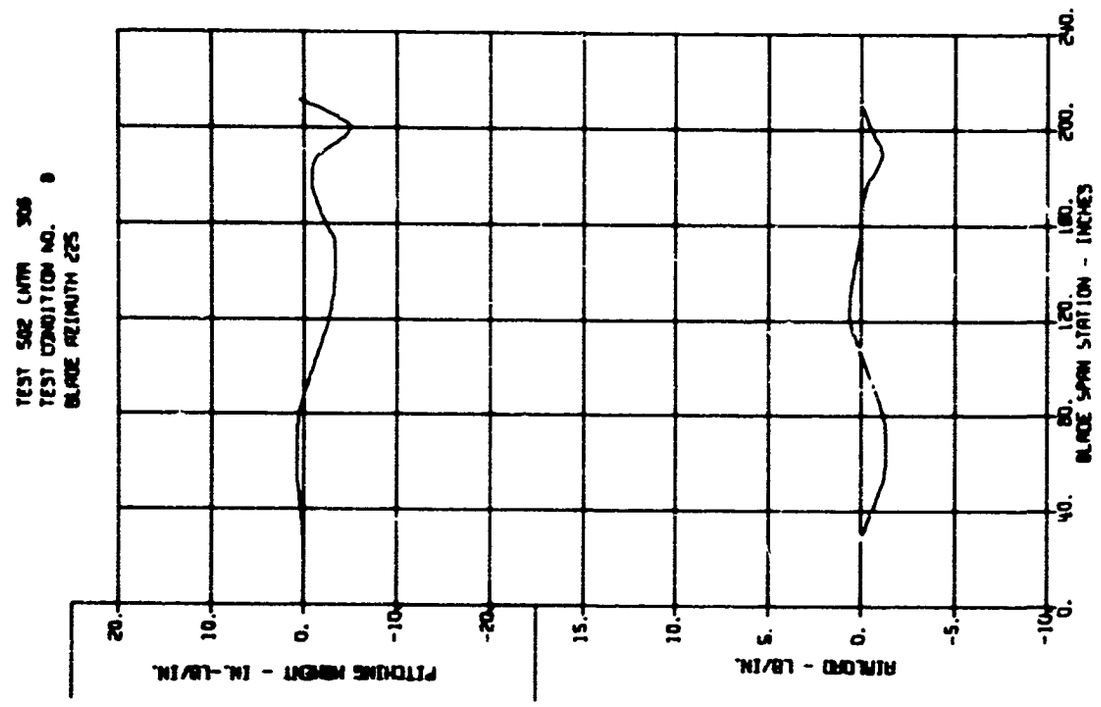

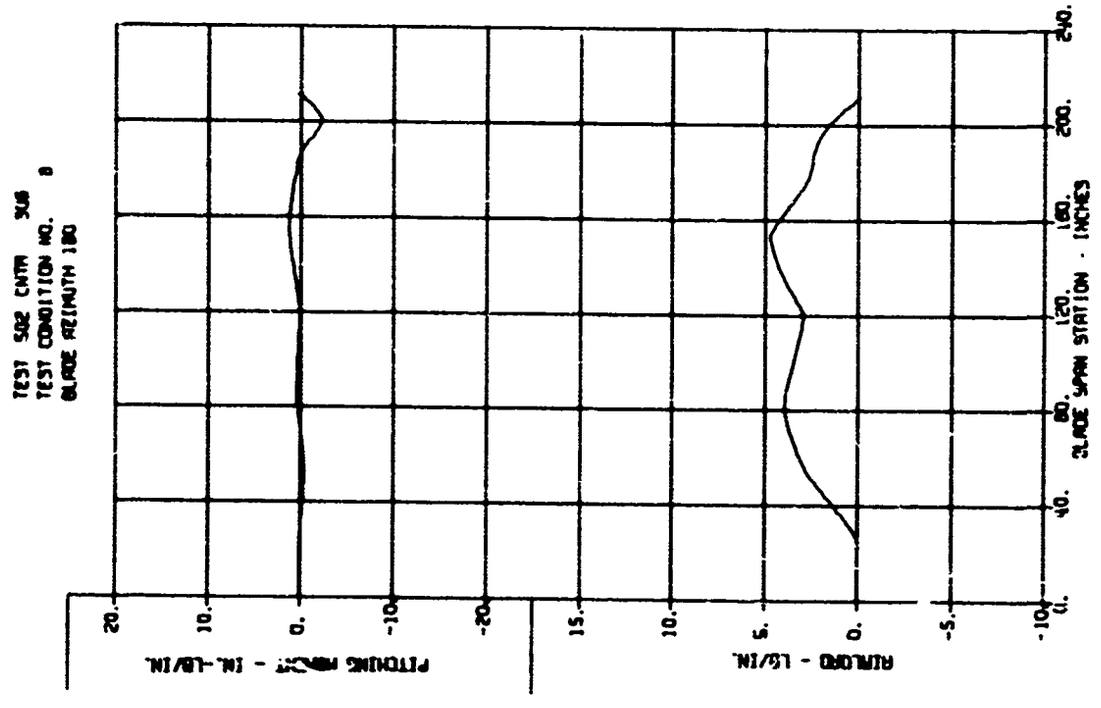

BLADE LOADS VERSUS SPAN - DYNAMIC COMPONENTS

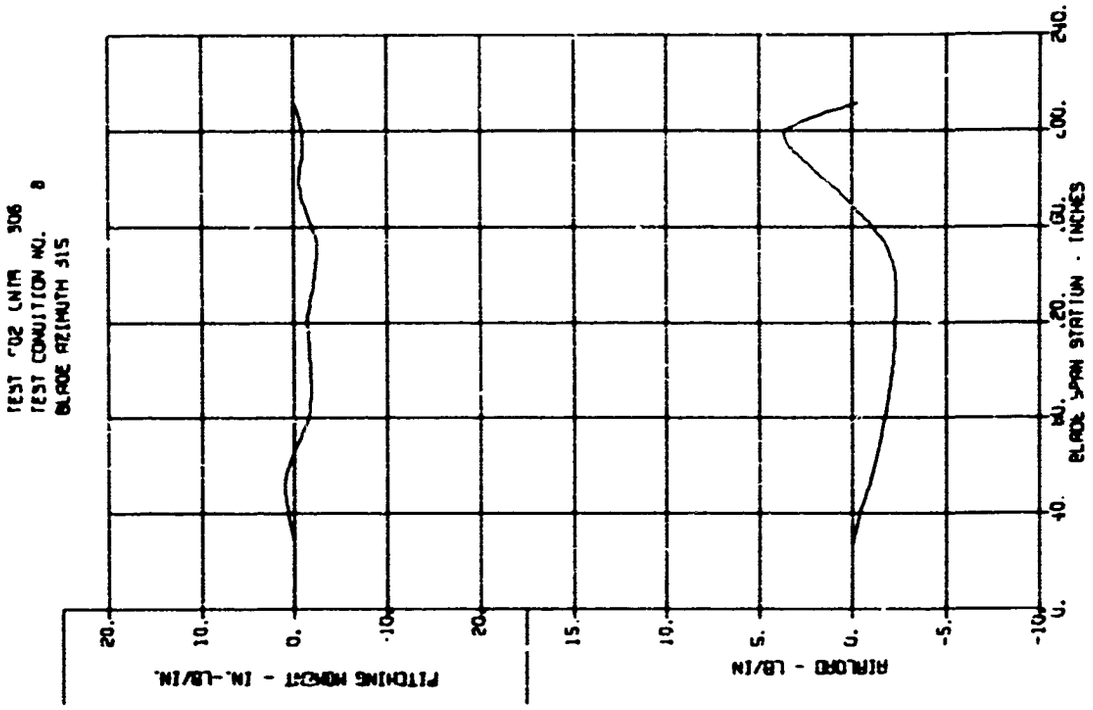

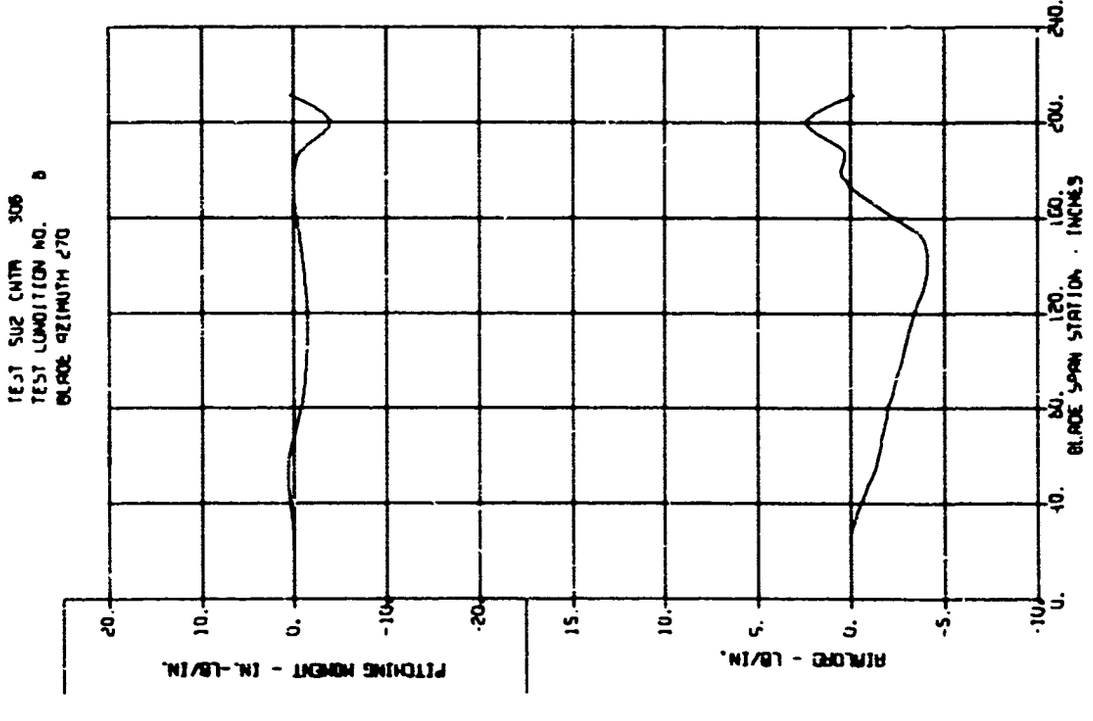

BLADE LOADS VERSUS SPAN - DYNAMIC COMPONENTS

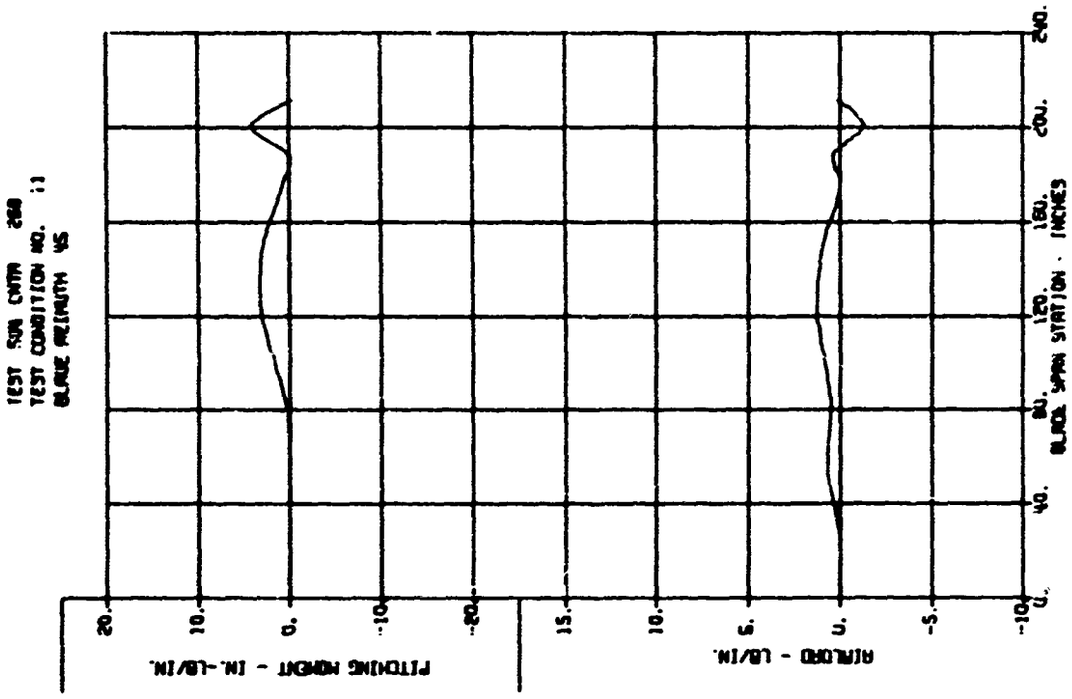

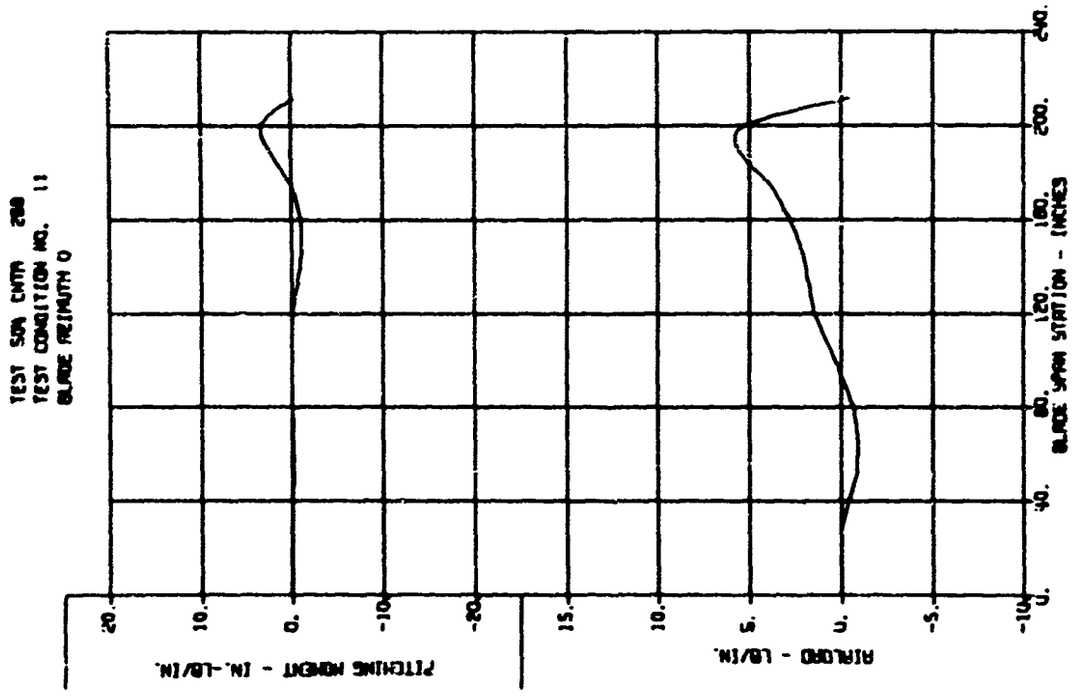

BLADE LOADS VERSUS SPAN - DYNAMIC COMPONENTS

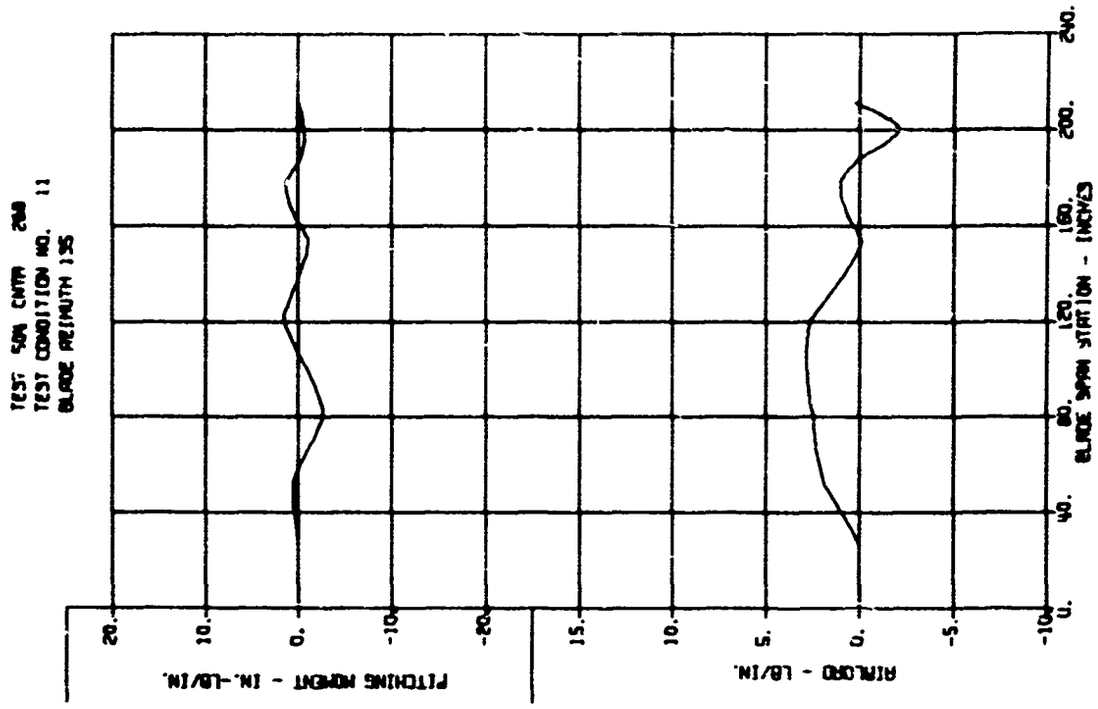

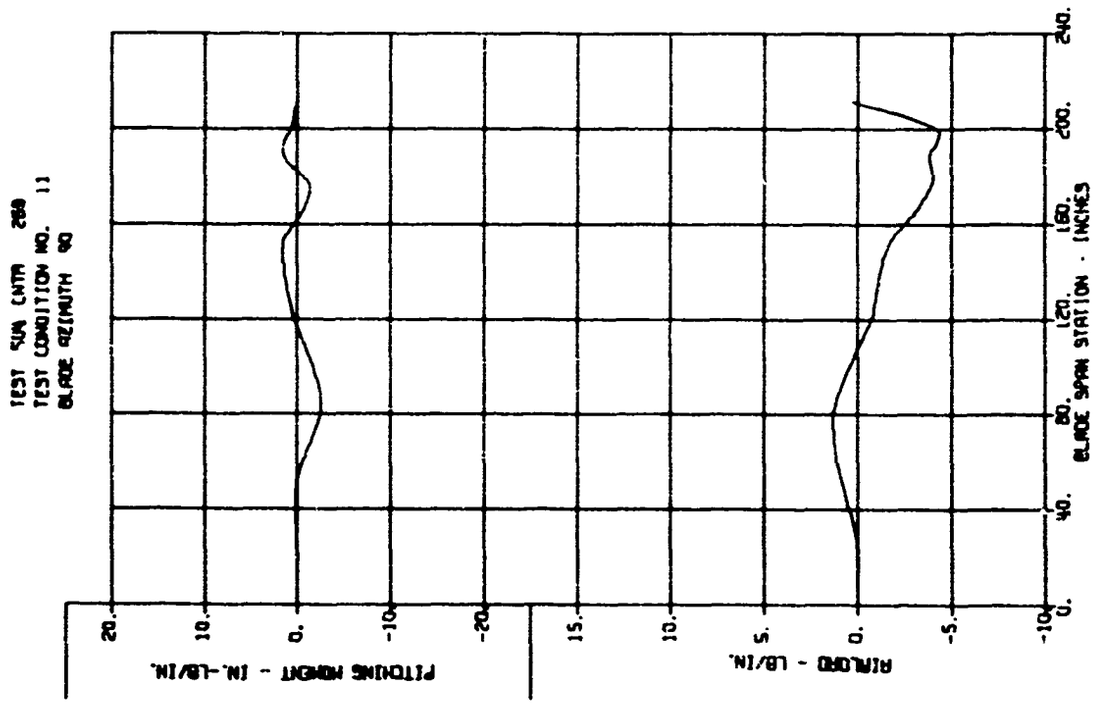

BLADE LOADS VERSUS SPAN - DYNAMIC COMPONENTS

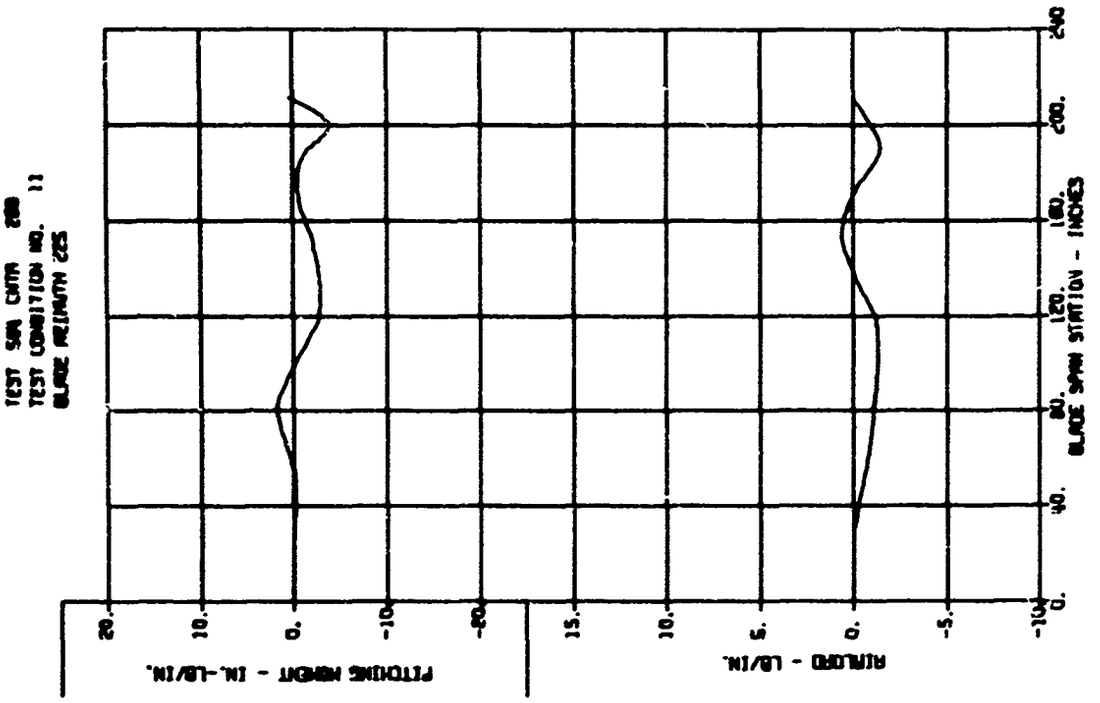

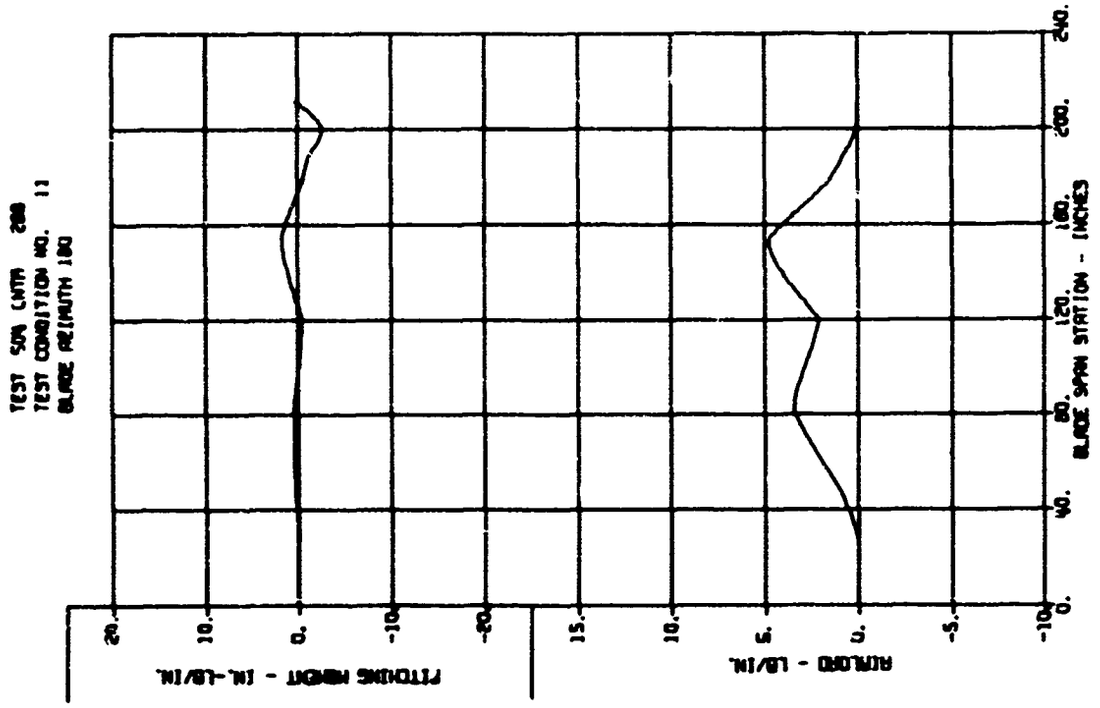

BLADE LOADS VERSUS SPAN - DYNAMIC COMPONENTS

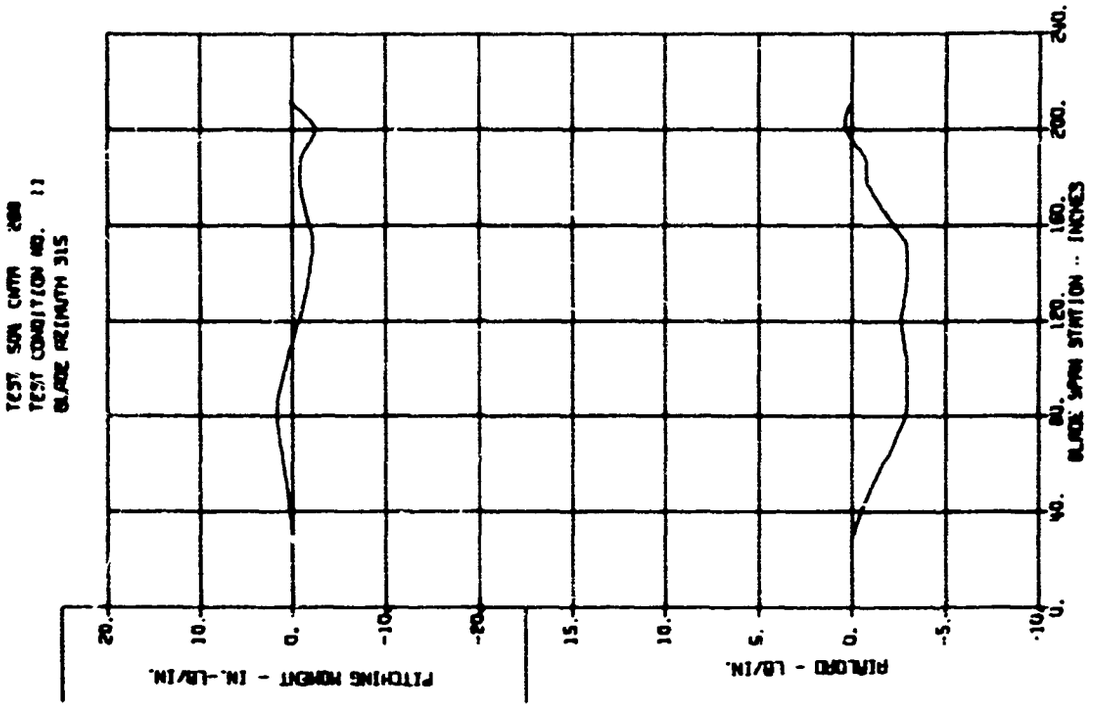

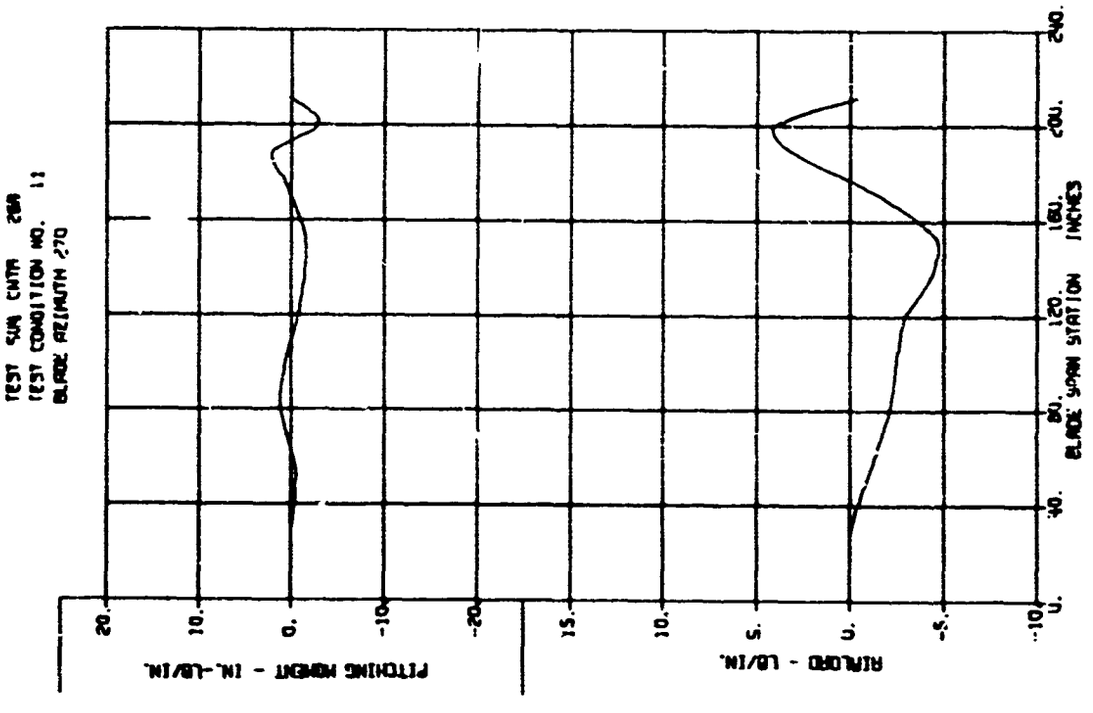

BLADE LOADS VERSUS SPAN - DYNAMIC COMPONENTS

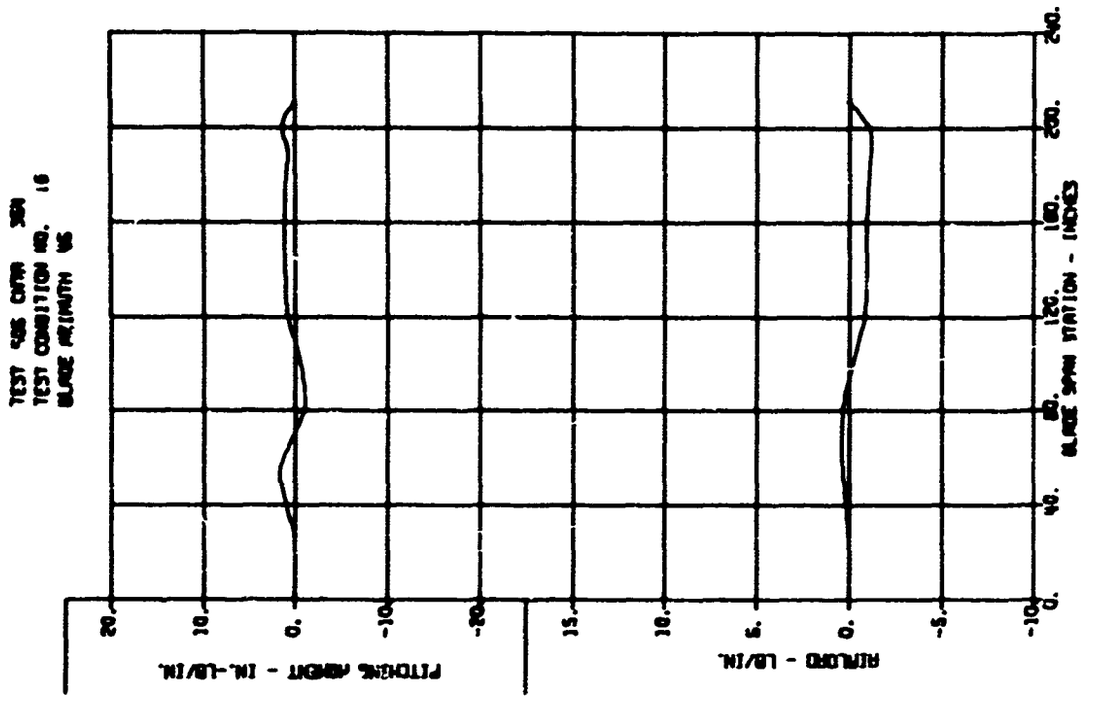

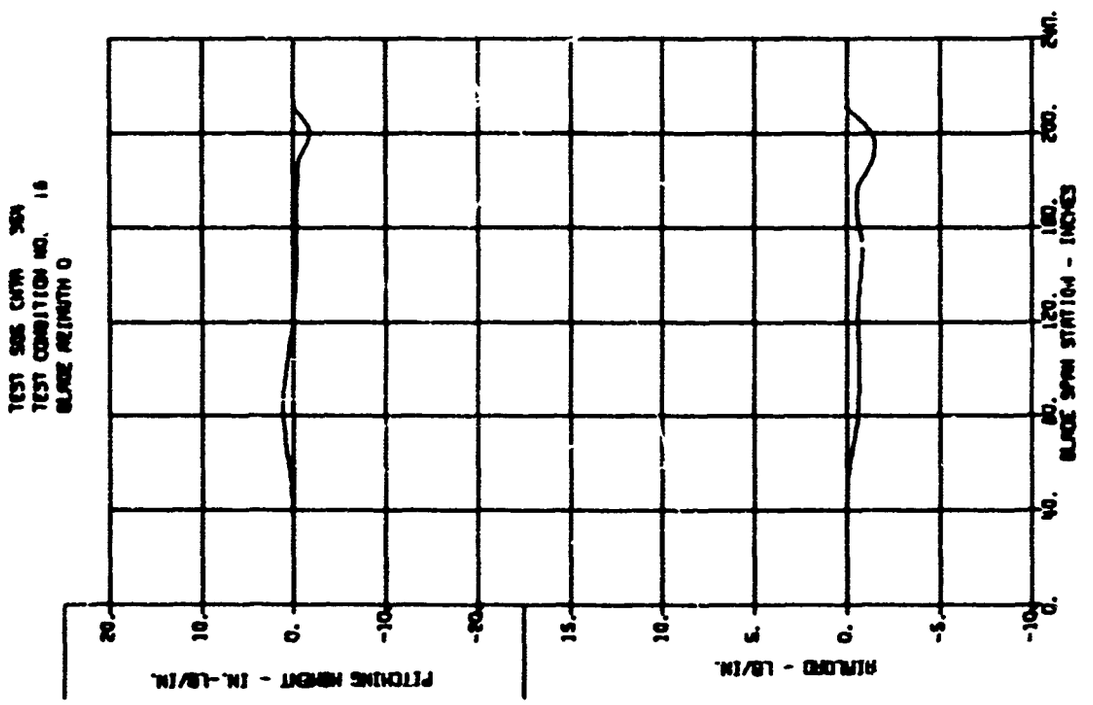

BLADE LOADS VERSUS SPAN - DYNAMIC COMPONENTS

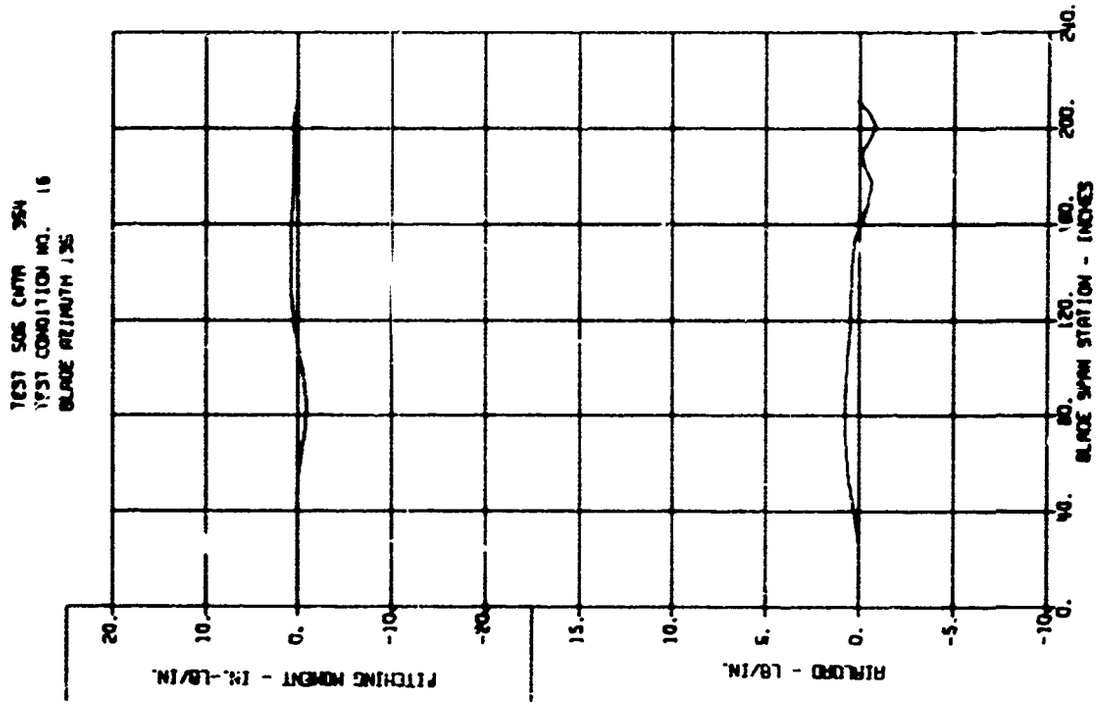

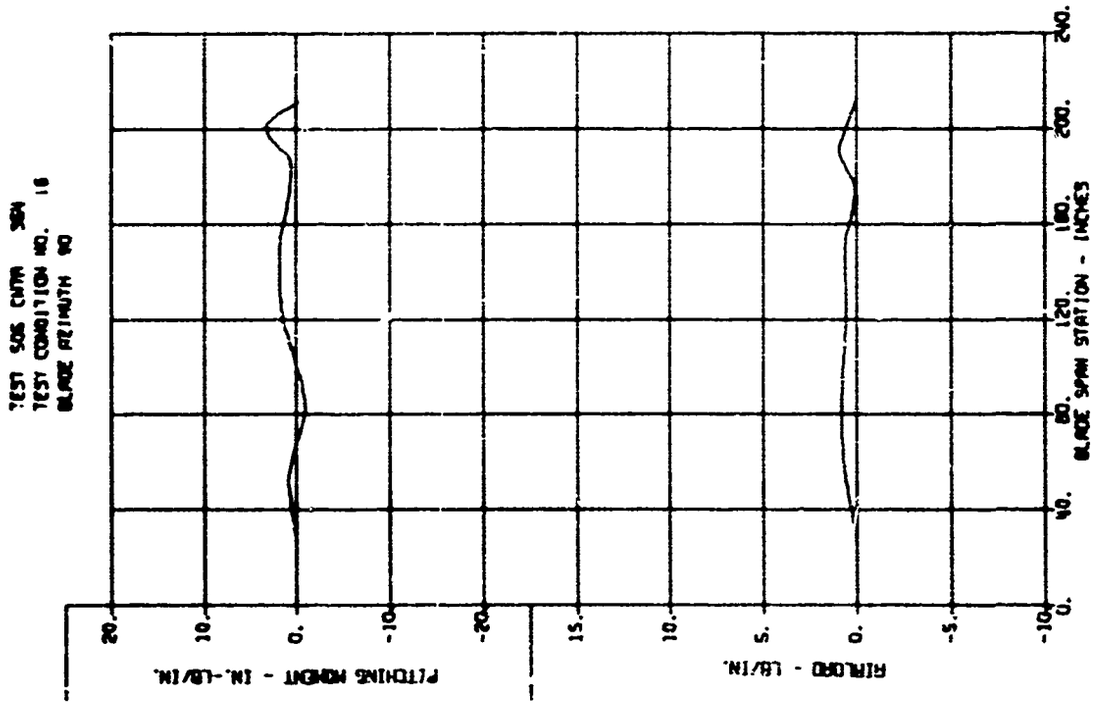

BLADE LOADS VERSUS SPAN - DYNAMIC COMPONENTS

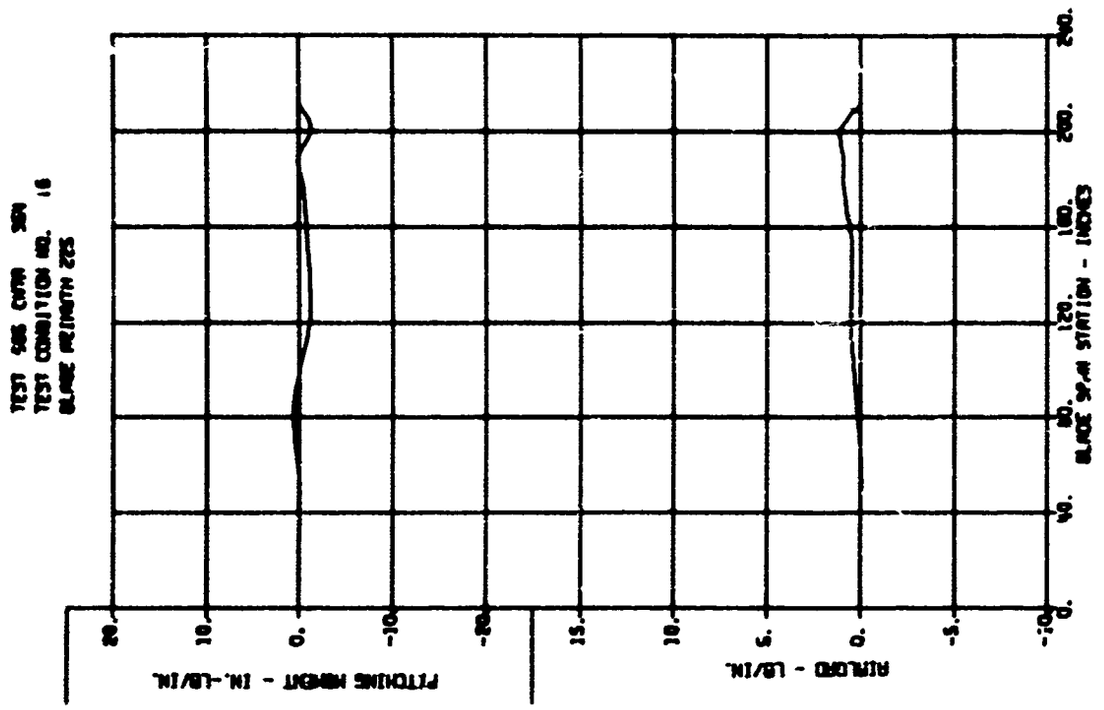

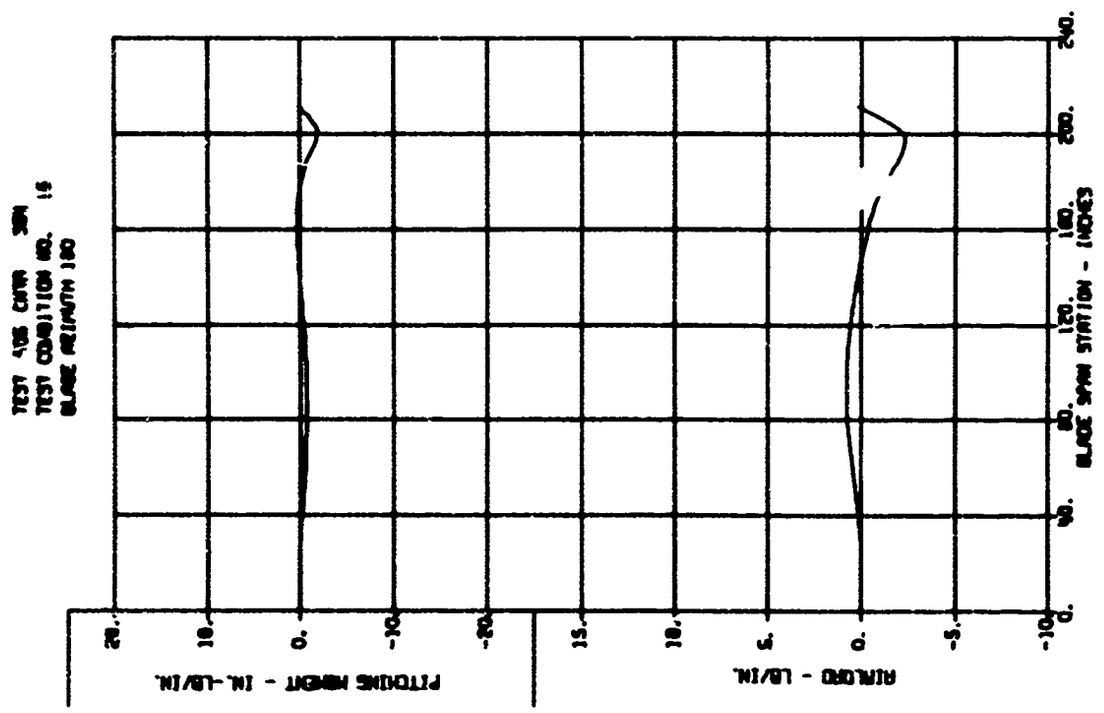

BLADE LOADS VERSUS SPAN - DYNAMIC COMPONENTS

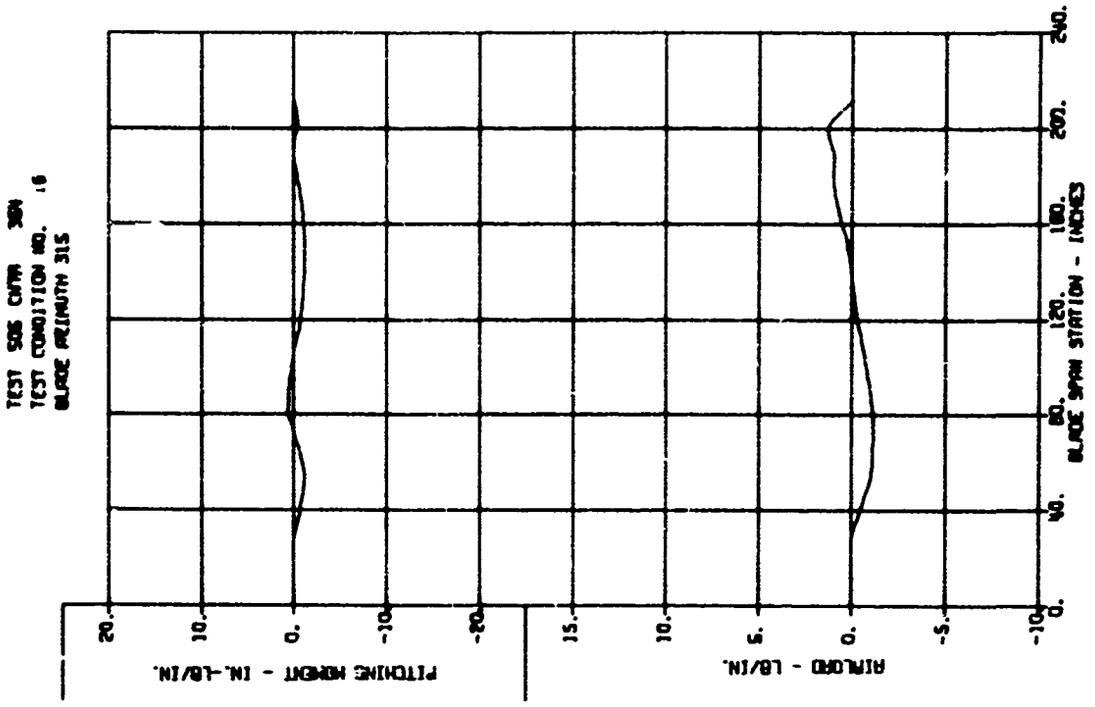

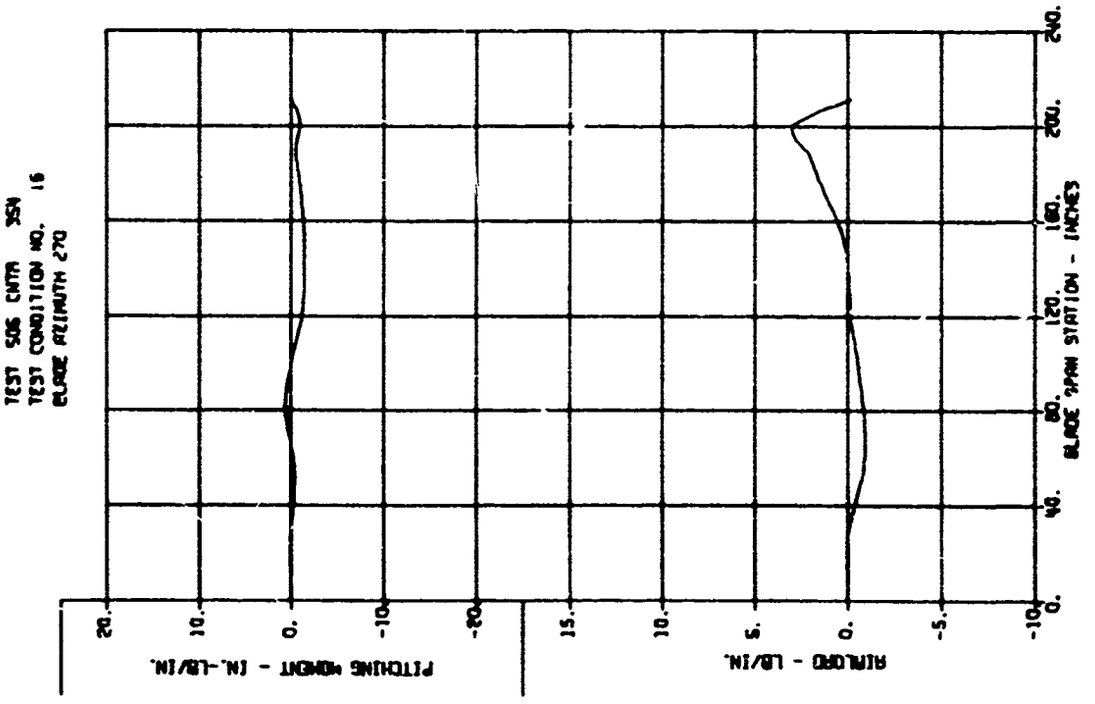

BLADE LOADS VERSUS SPAN - DYNAMIC COMPONENTS

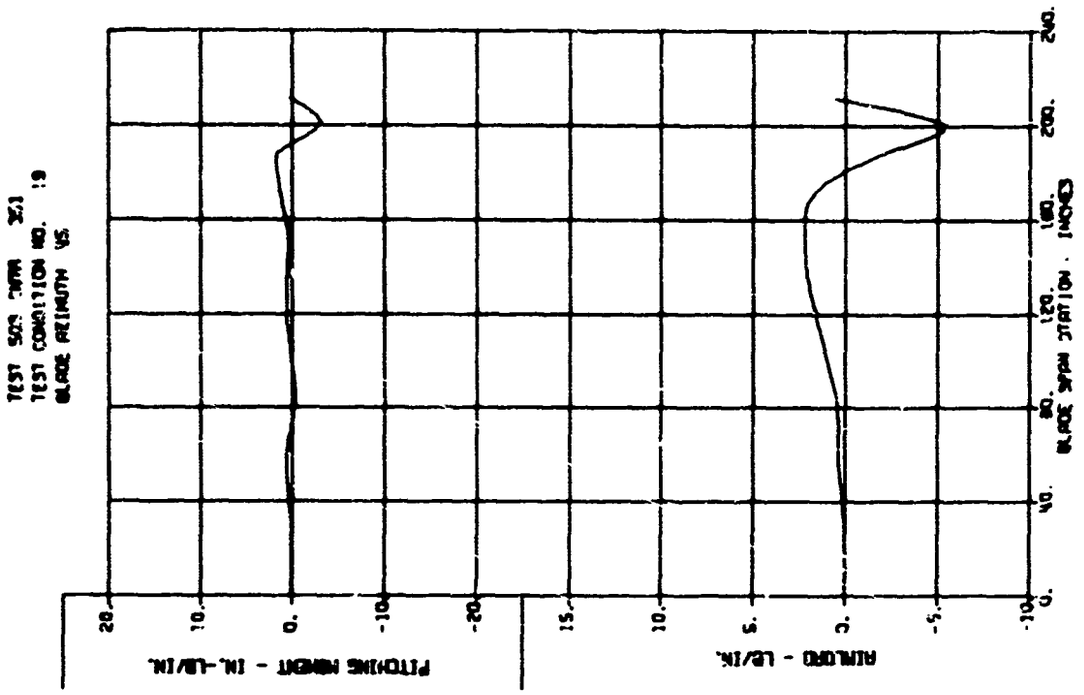

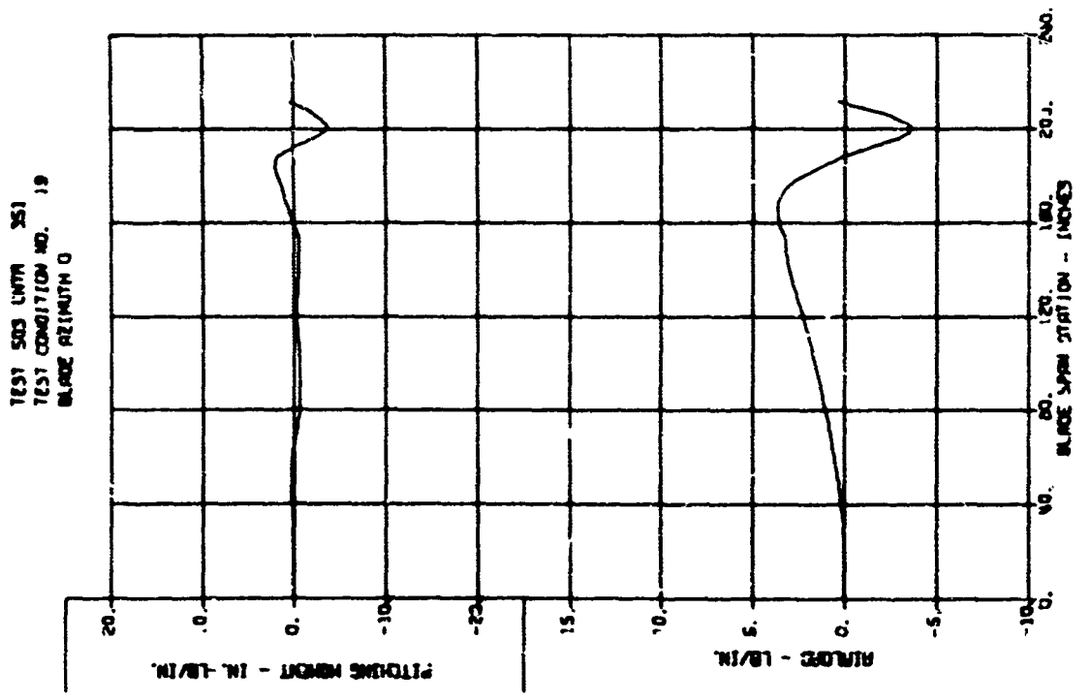

BLADE LOADS VERSUS SPAN - DYNAMIC COMPONENTS

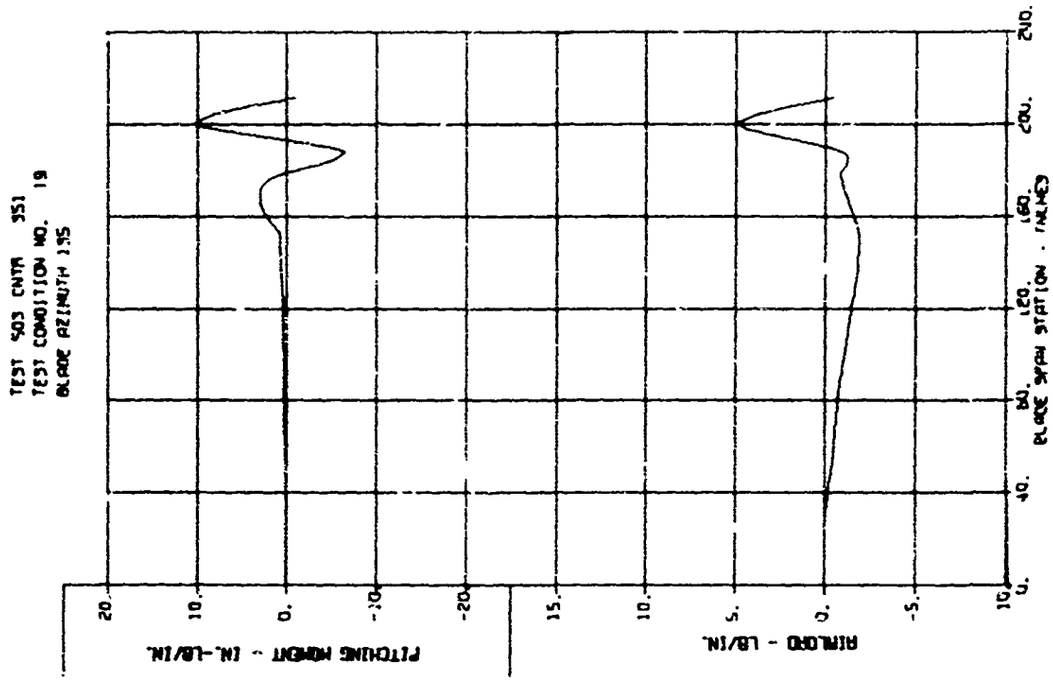

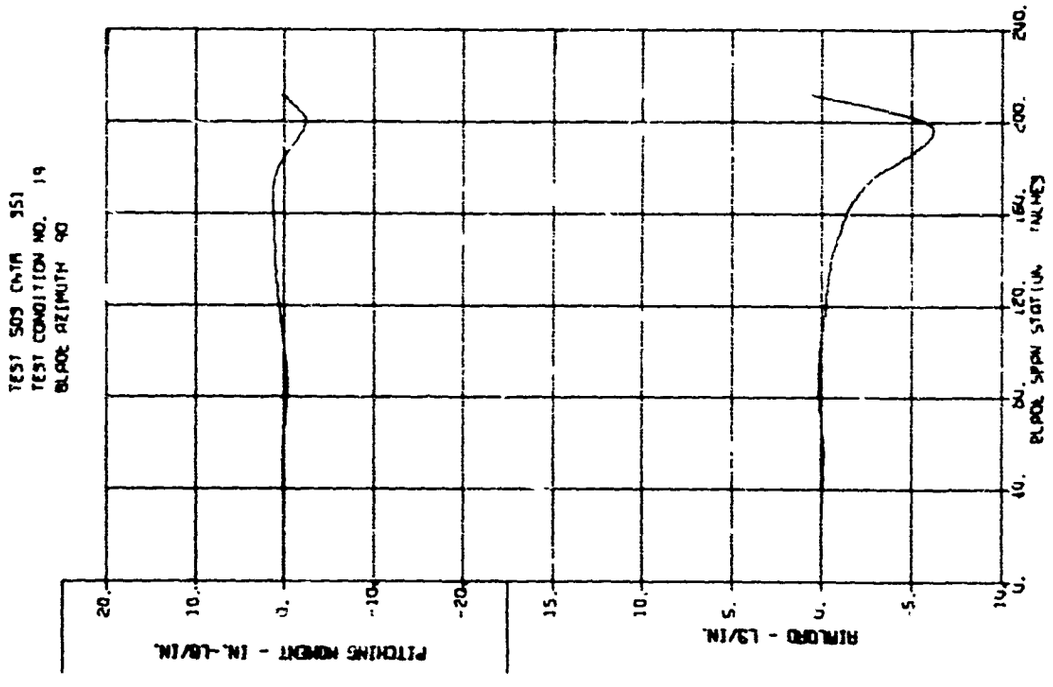

BLADE LOADS VERSUS SPAN - DYNAMIC COMPONENTS

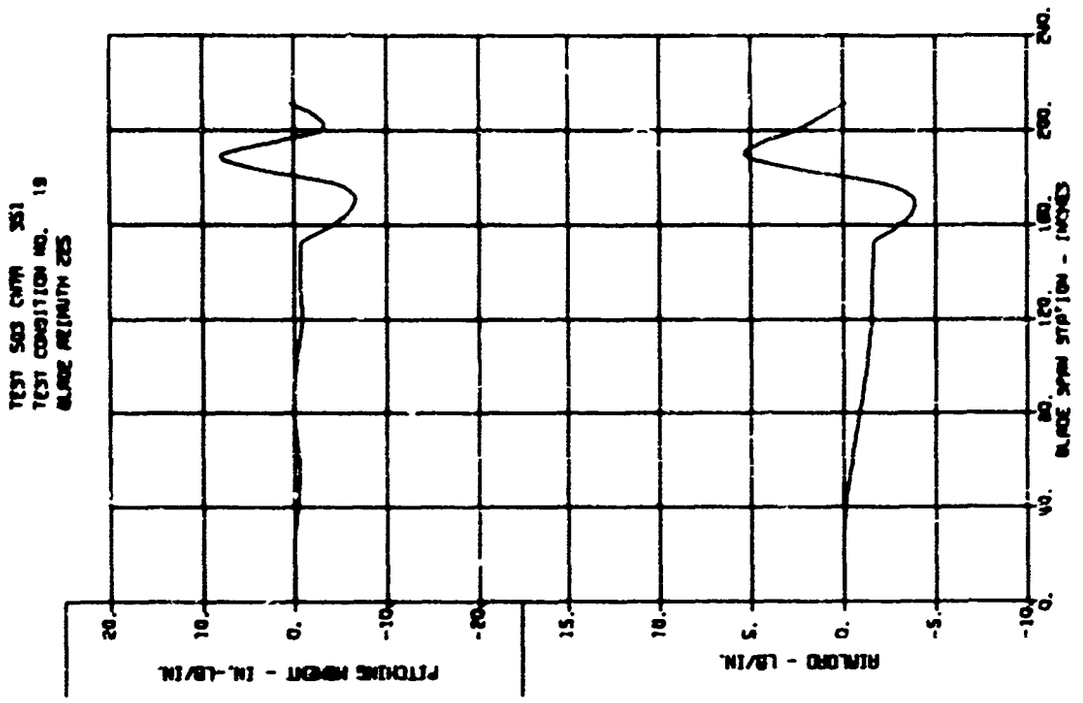

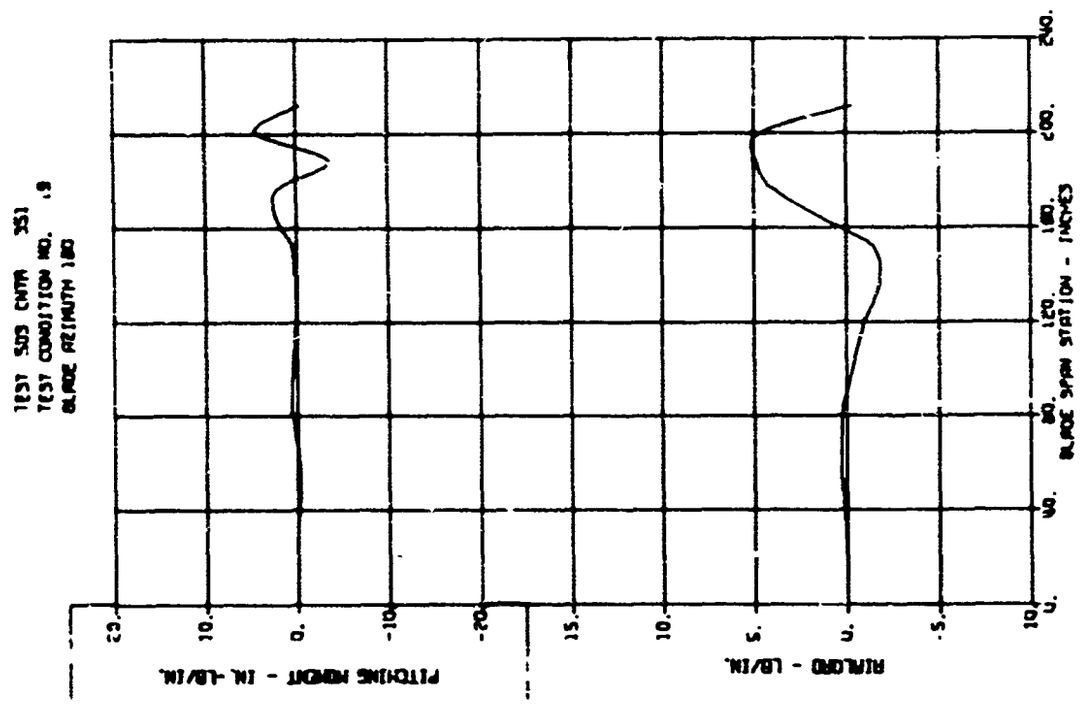

BLADE LOADS VERSUS SPAN - DYNAMIC COMPONENTS

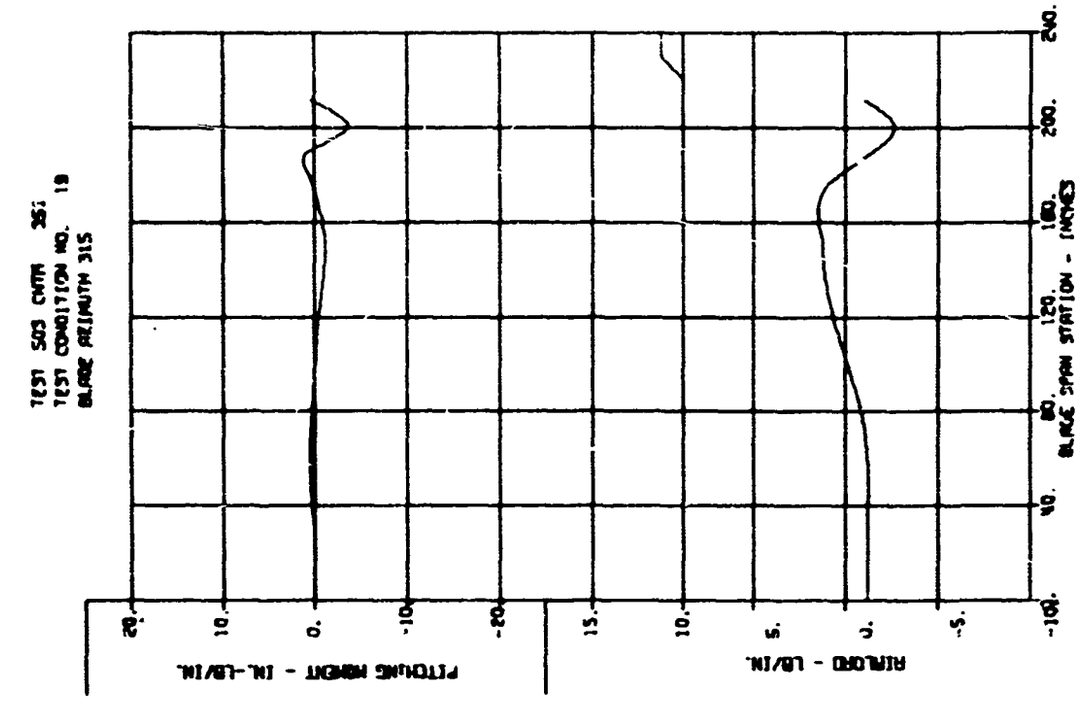

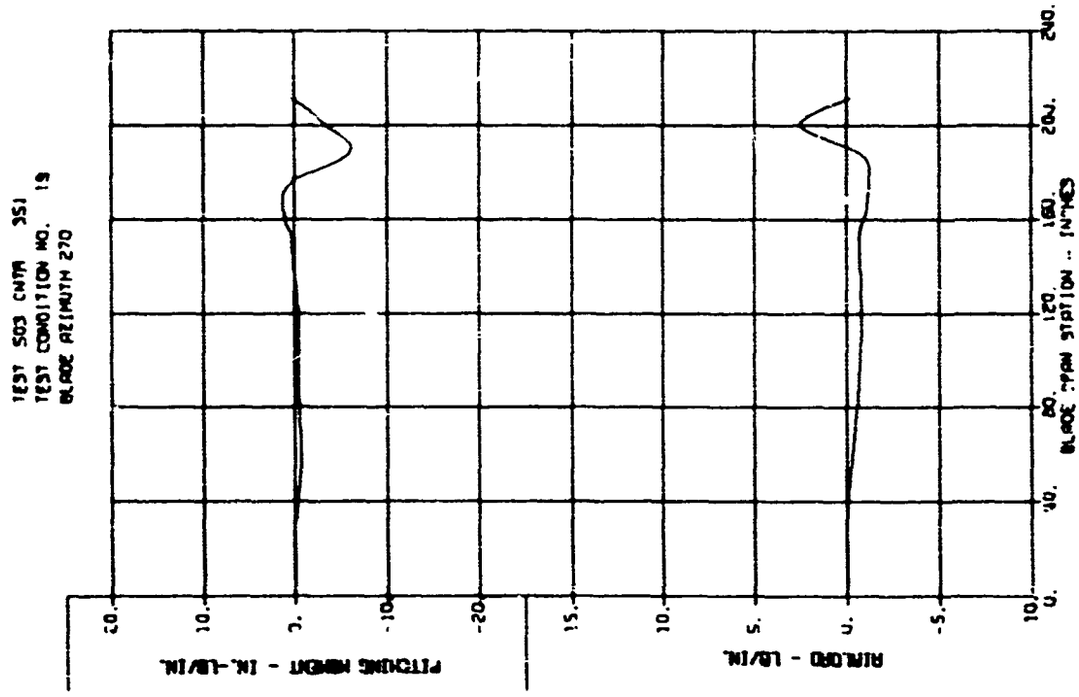

BLADE LOADS VERSUS SPAN - DYNAMIC COMPONENTS

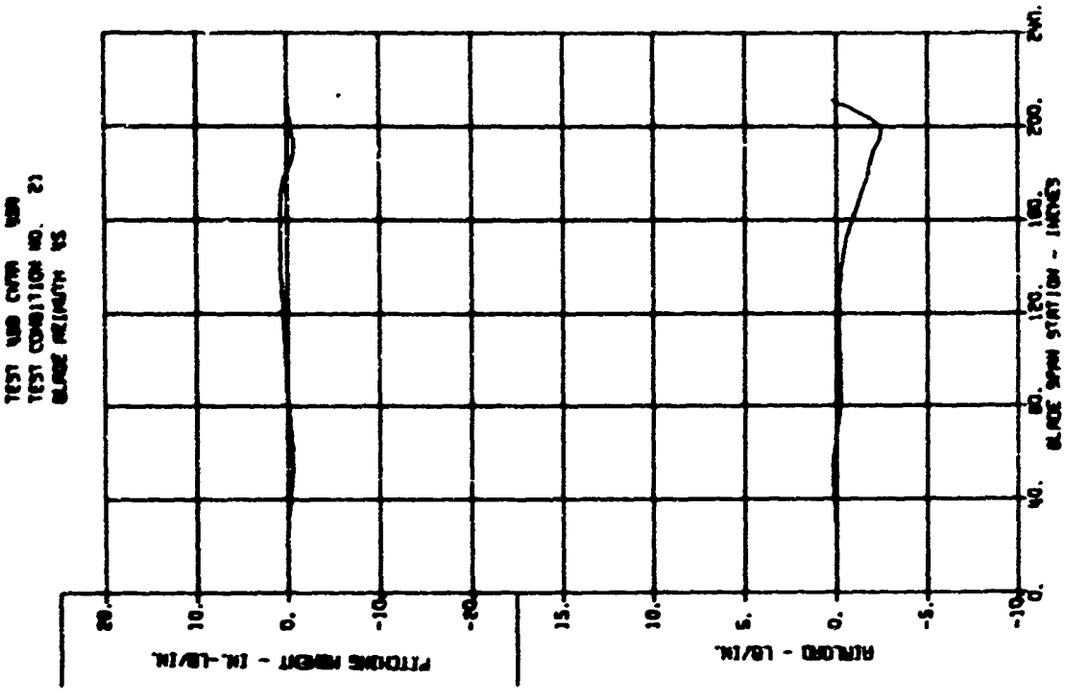

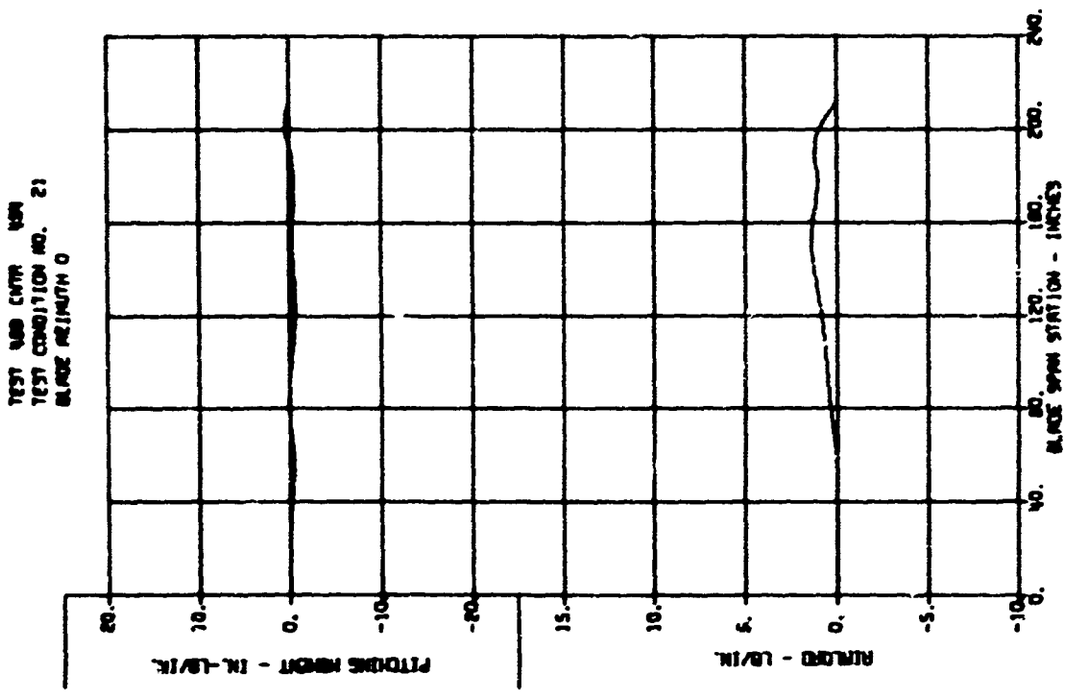

BLADE LOADS VERSUS SPAN - DYNAMIC COMPONENTS

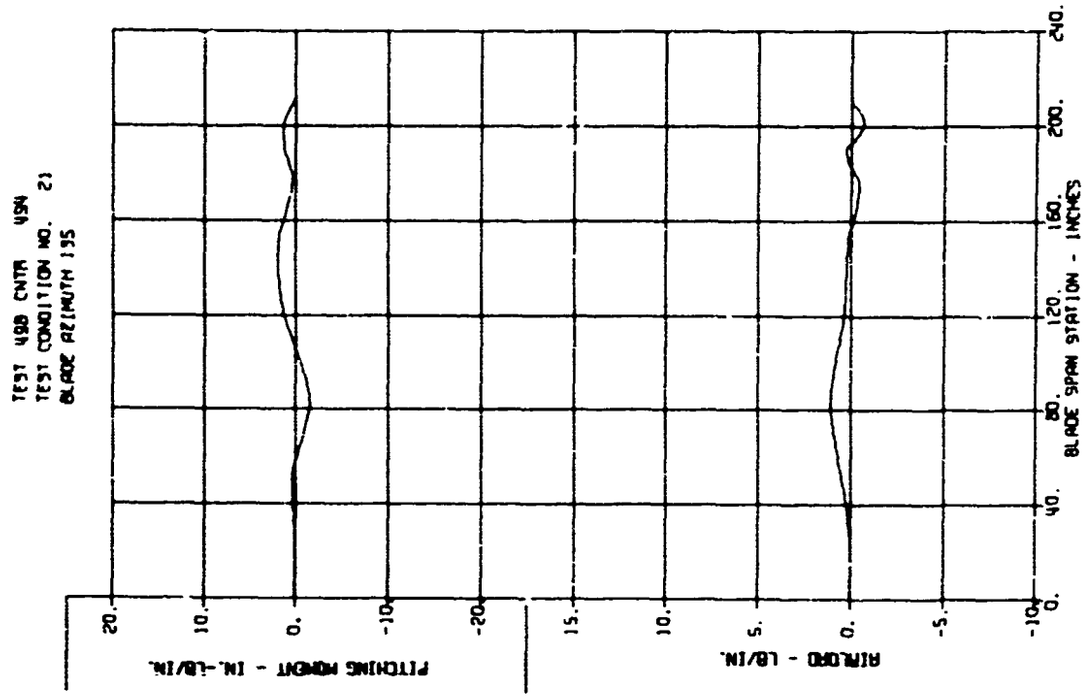

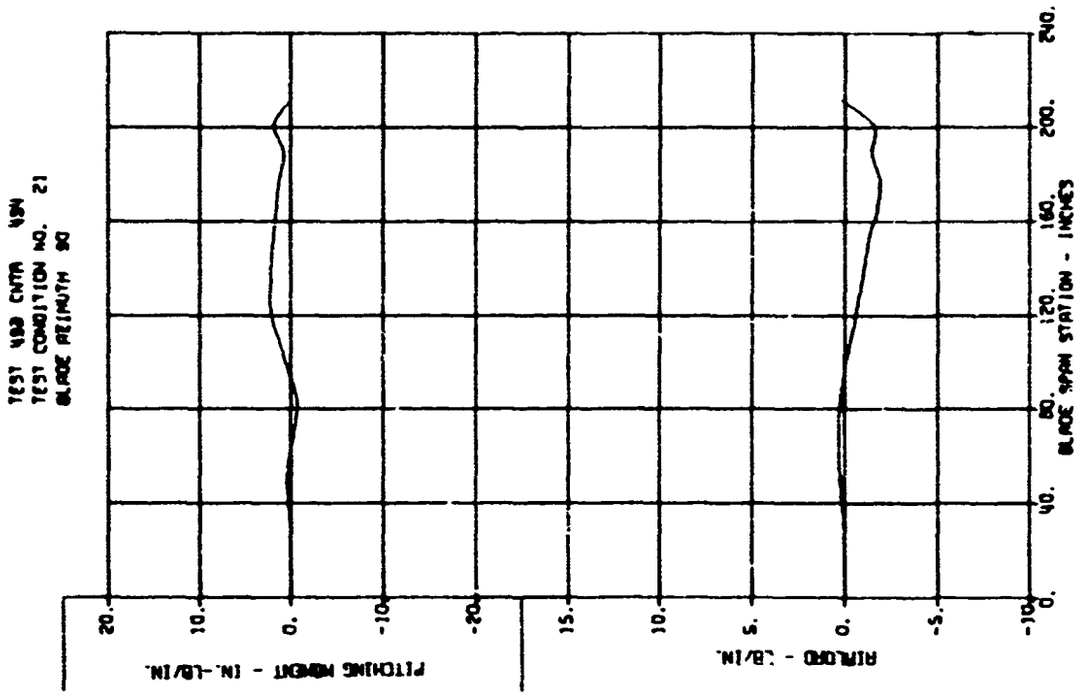

BLADE LOADS VERSUS SPAN - DYNAMIC COMPONENTS

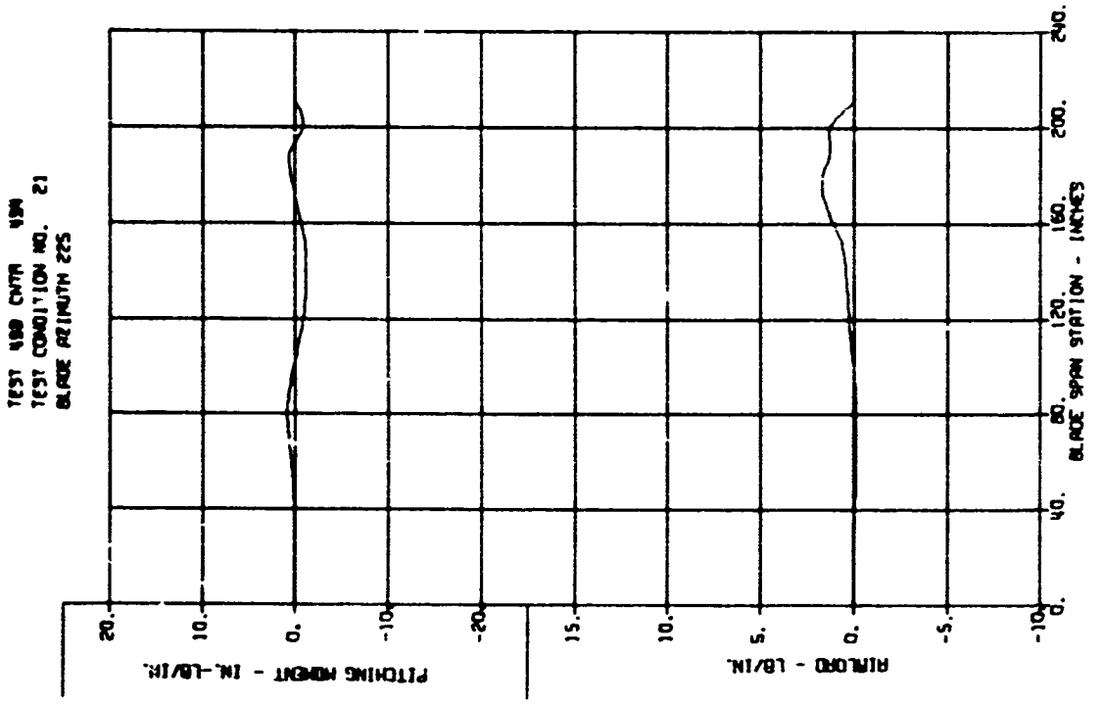

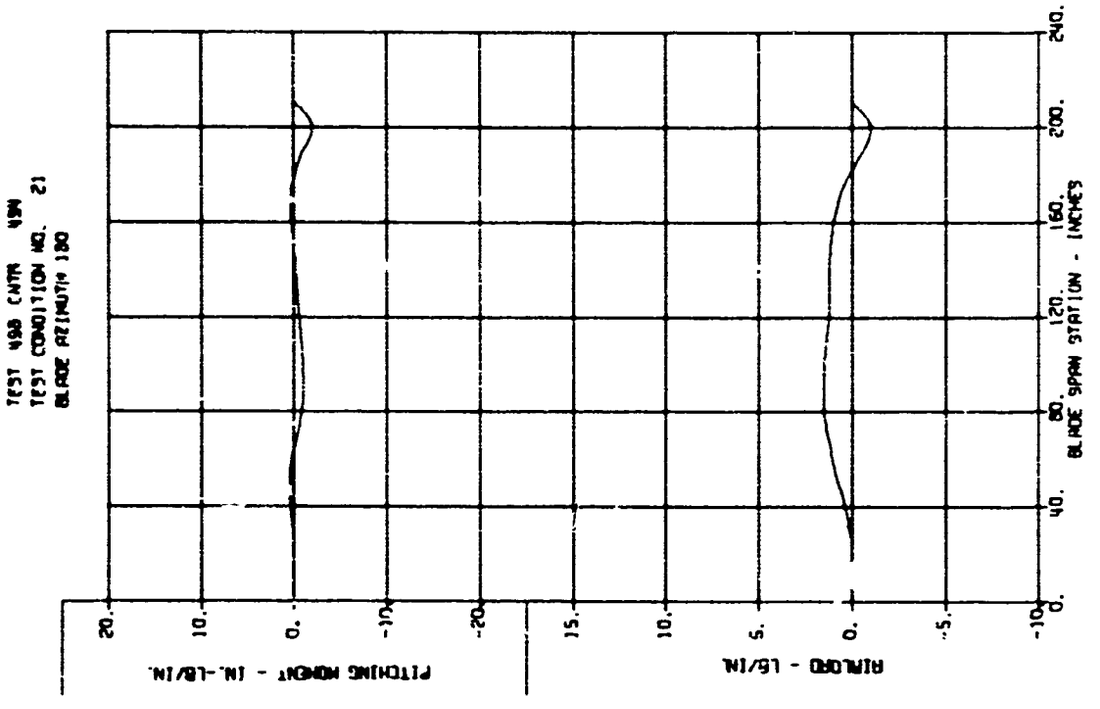

BLADE LOADS VERSUS SPAN - DYNAMIC COMPONENTS

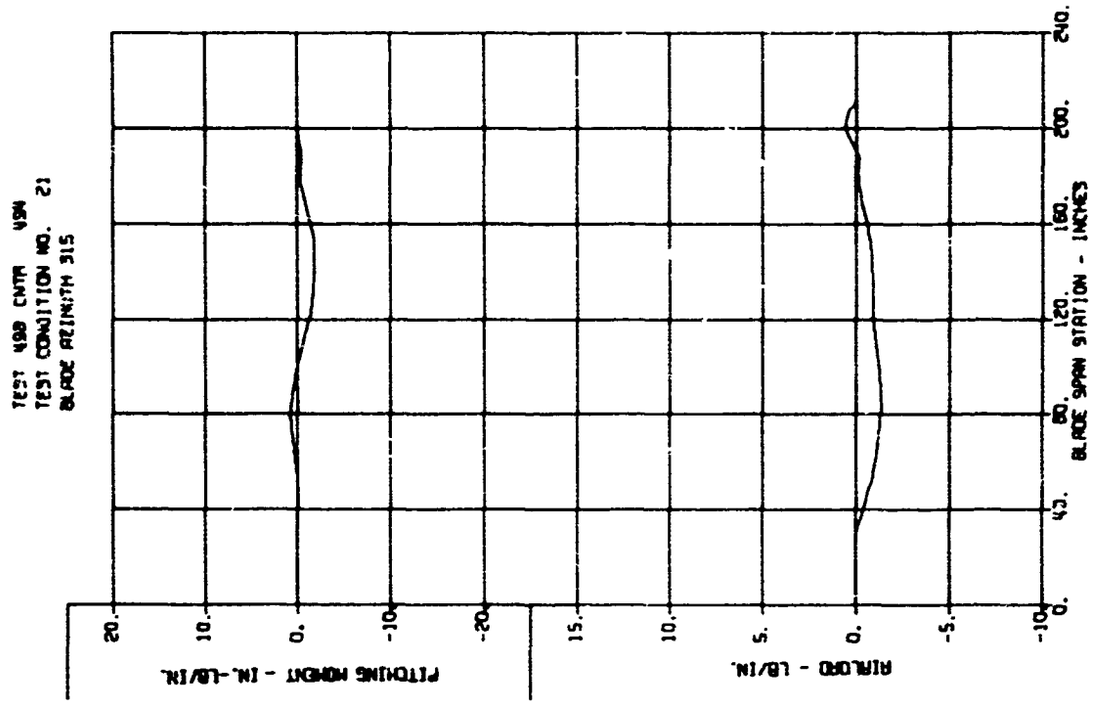

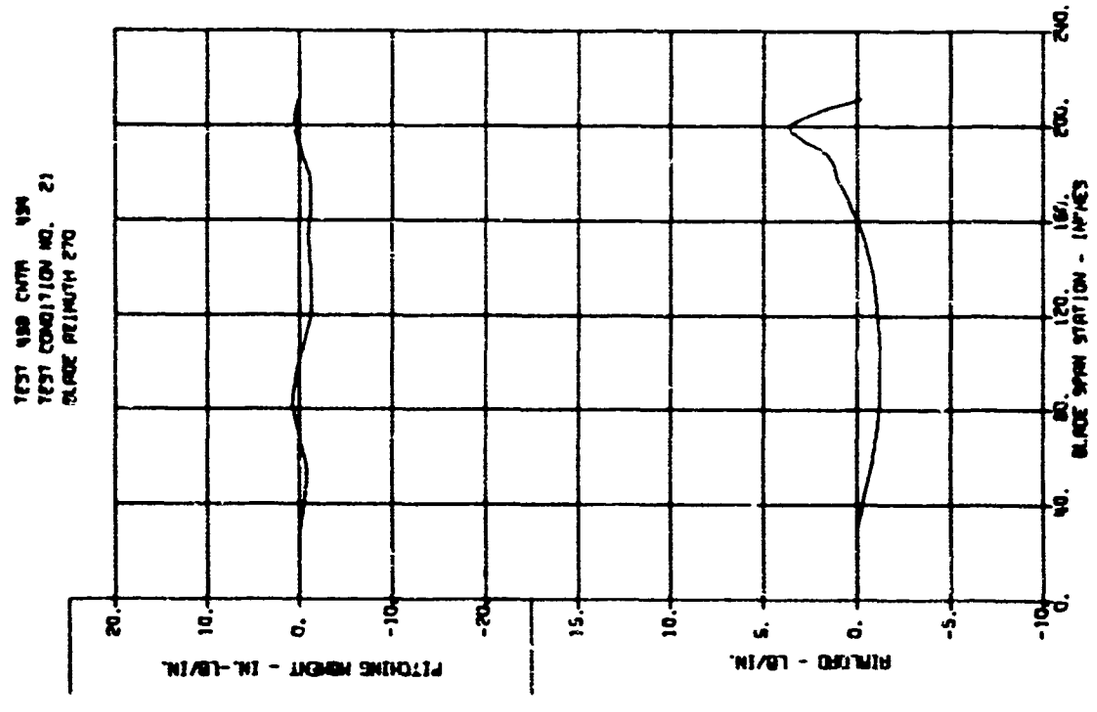

BLADE LOADS VERSUS SPAN - DYNAMIC COMPONENTS

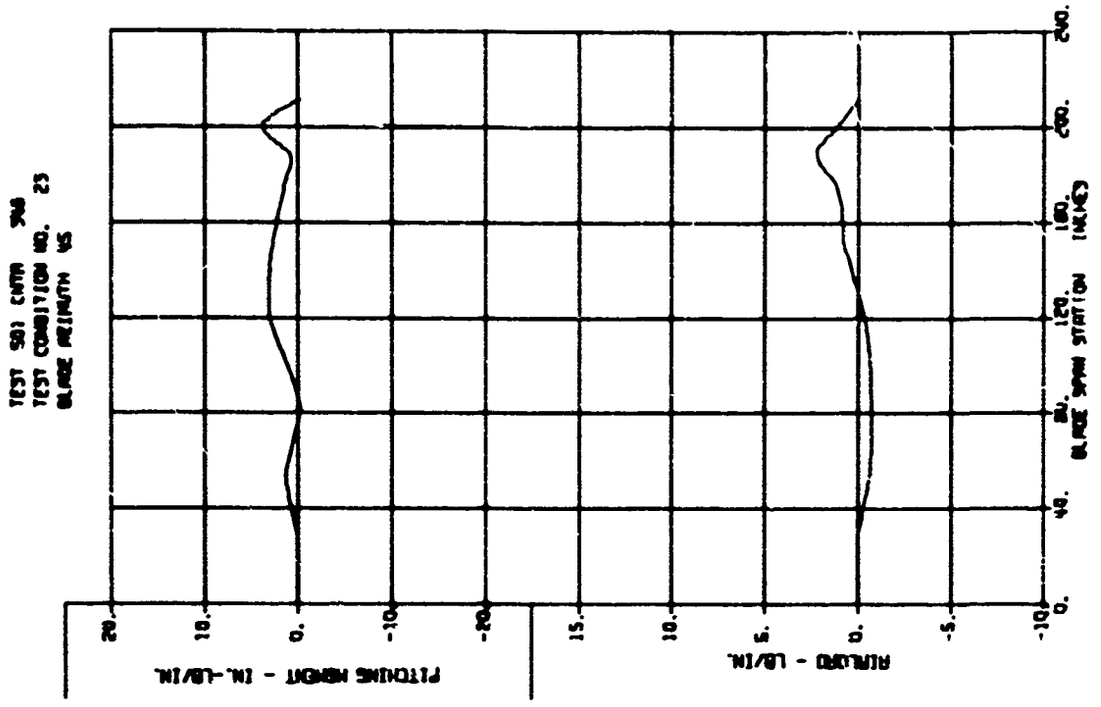

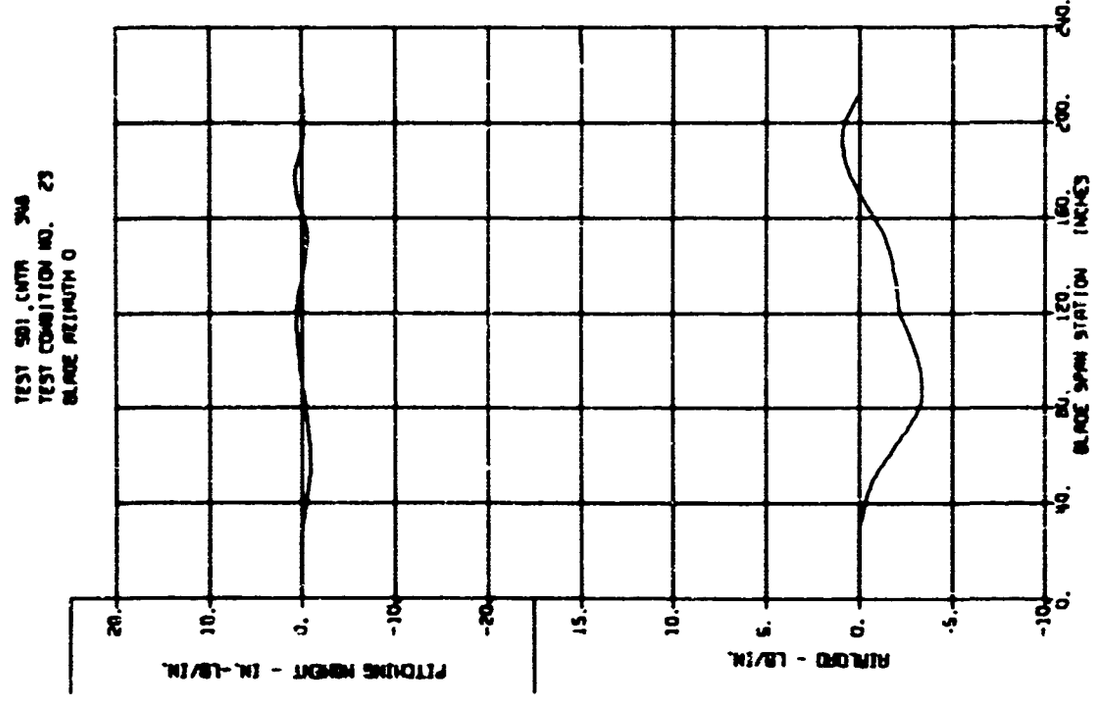

BLADE LOADS VERSUS SPAN - DYNAMIC COMPONENTS

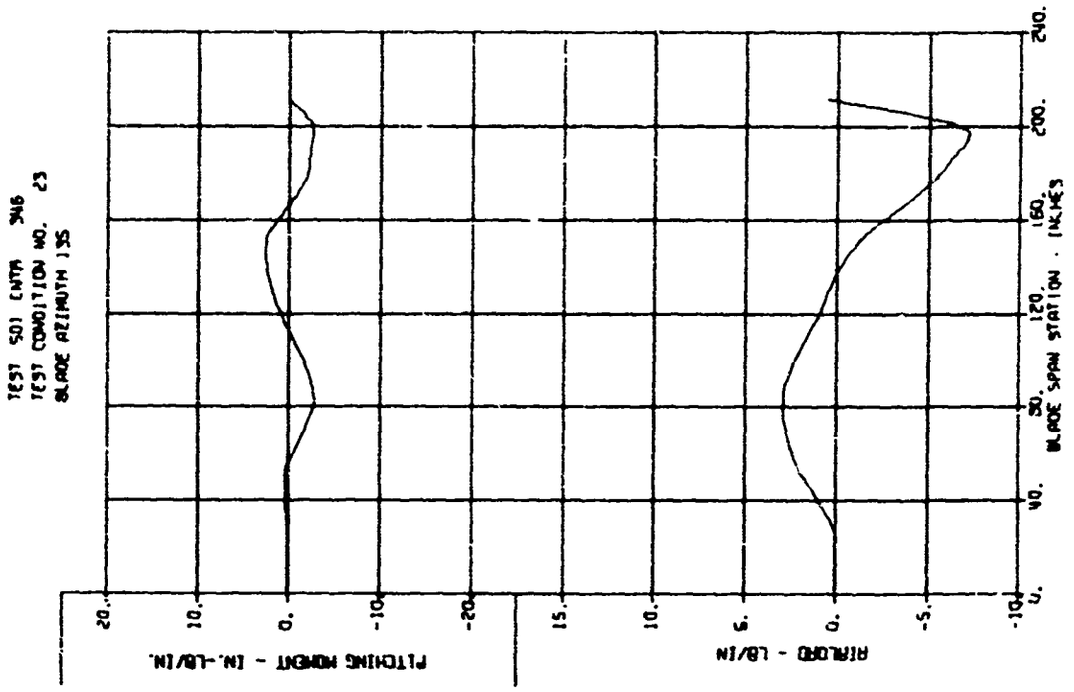

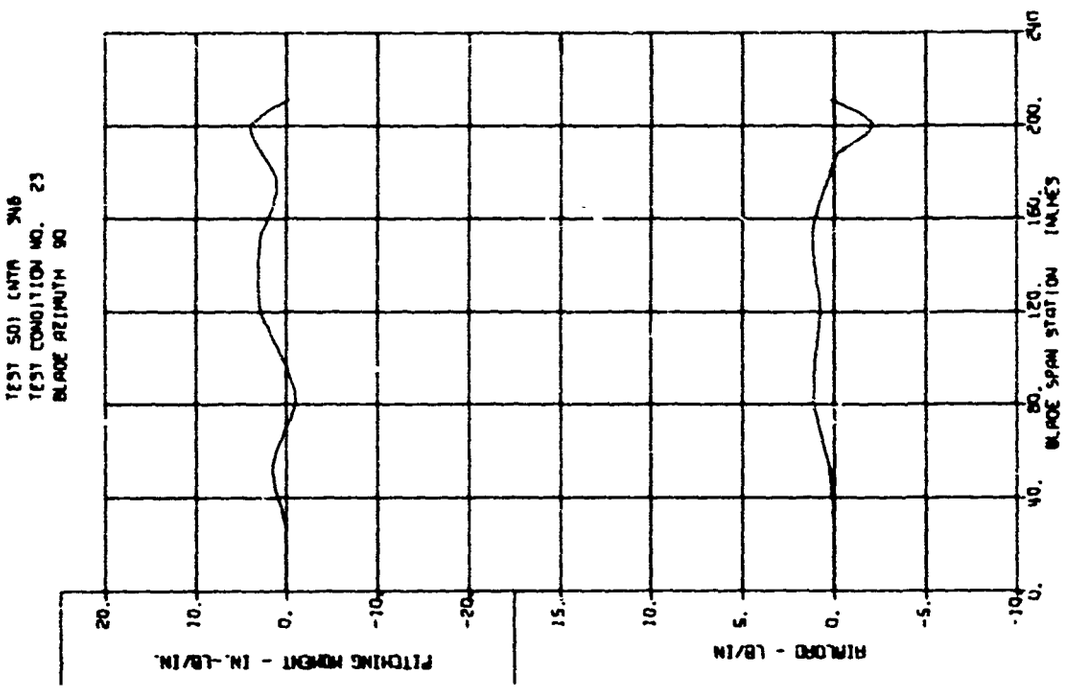

BLADE LOADS VERSUS SPAN - DYNAMIC COMPONENTS

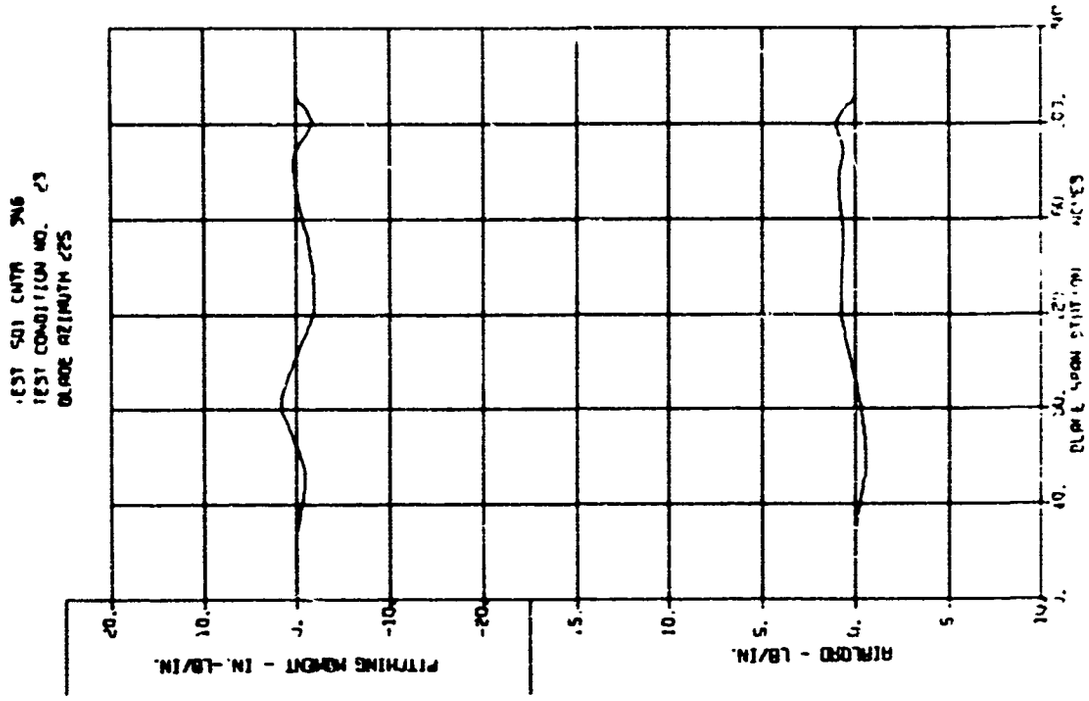

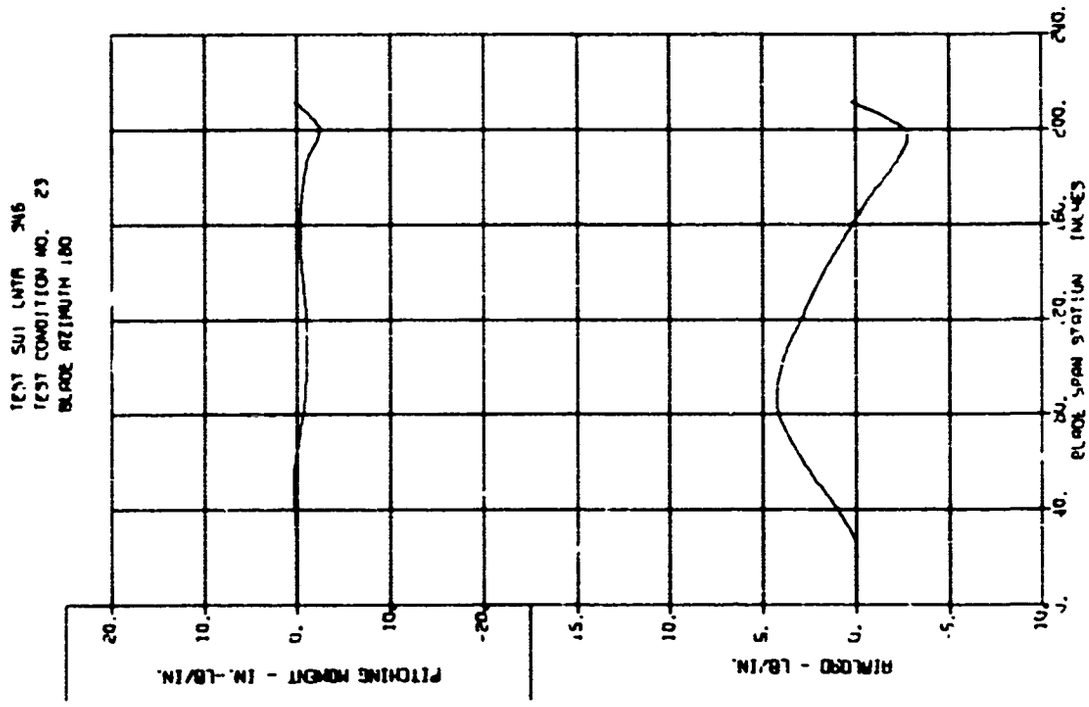

BLADE LOADS VERSUS STAT. - DYNAMIC COMPONENTS

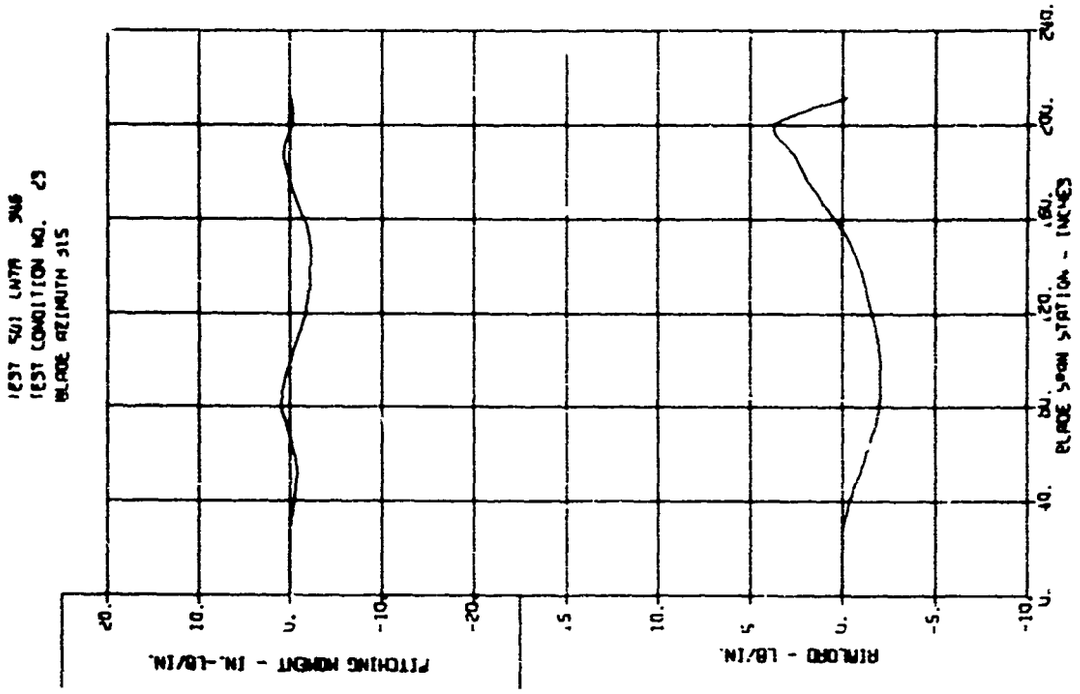

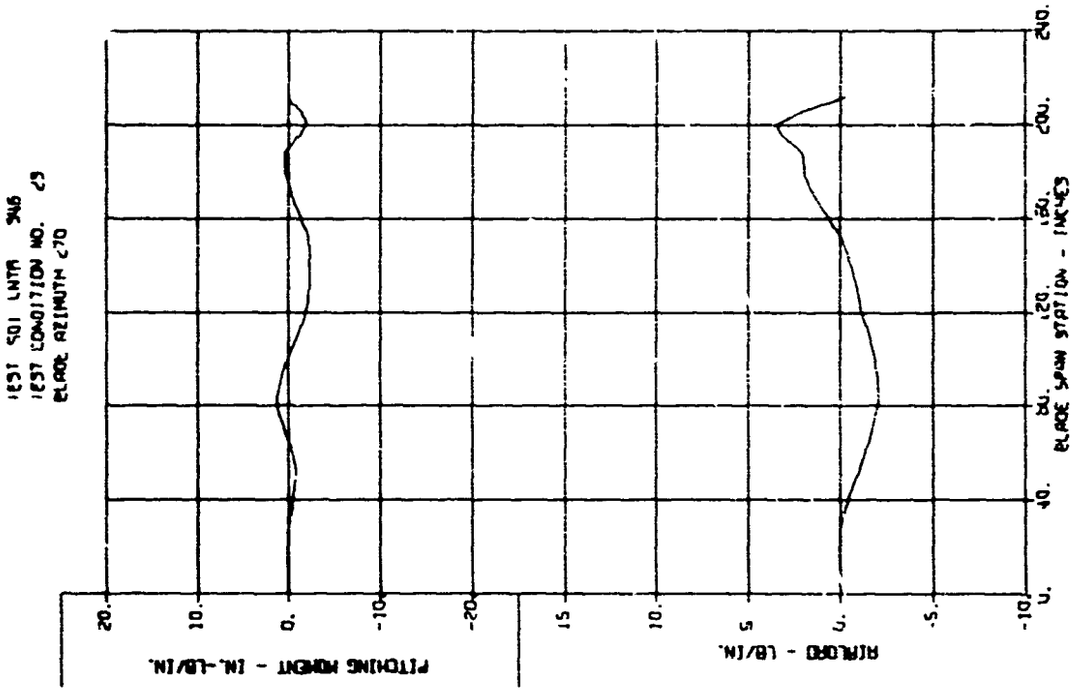

BLADE LOADS VERSUS SPAN - DYNAMIC COMPONENTS

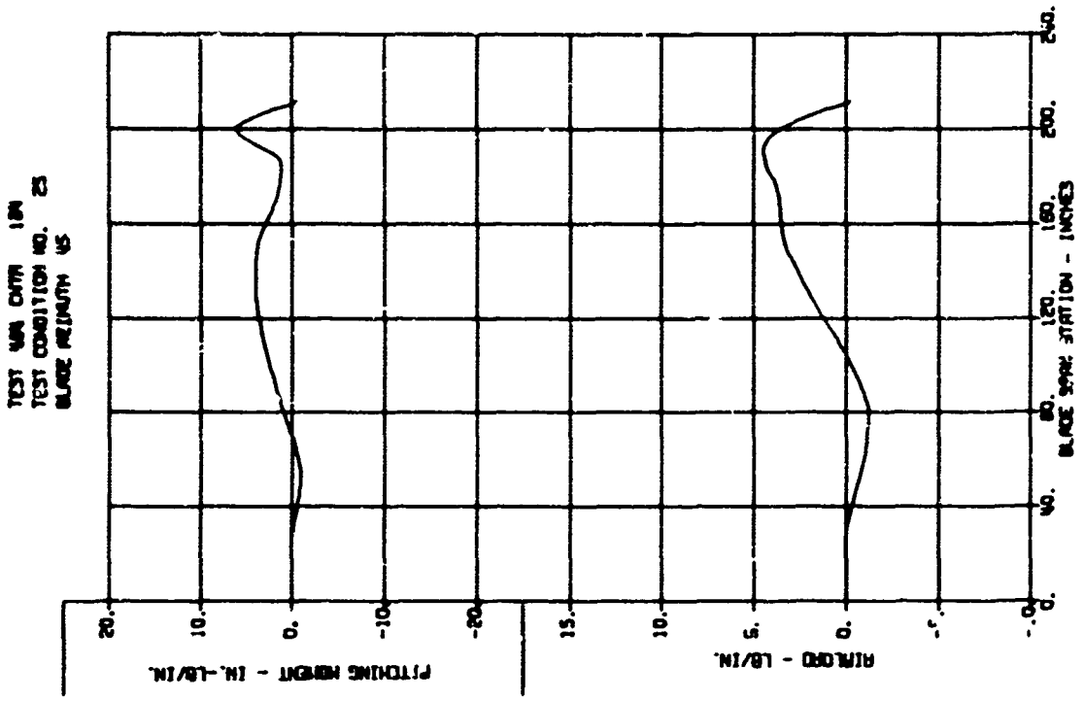

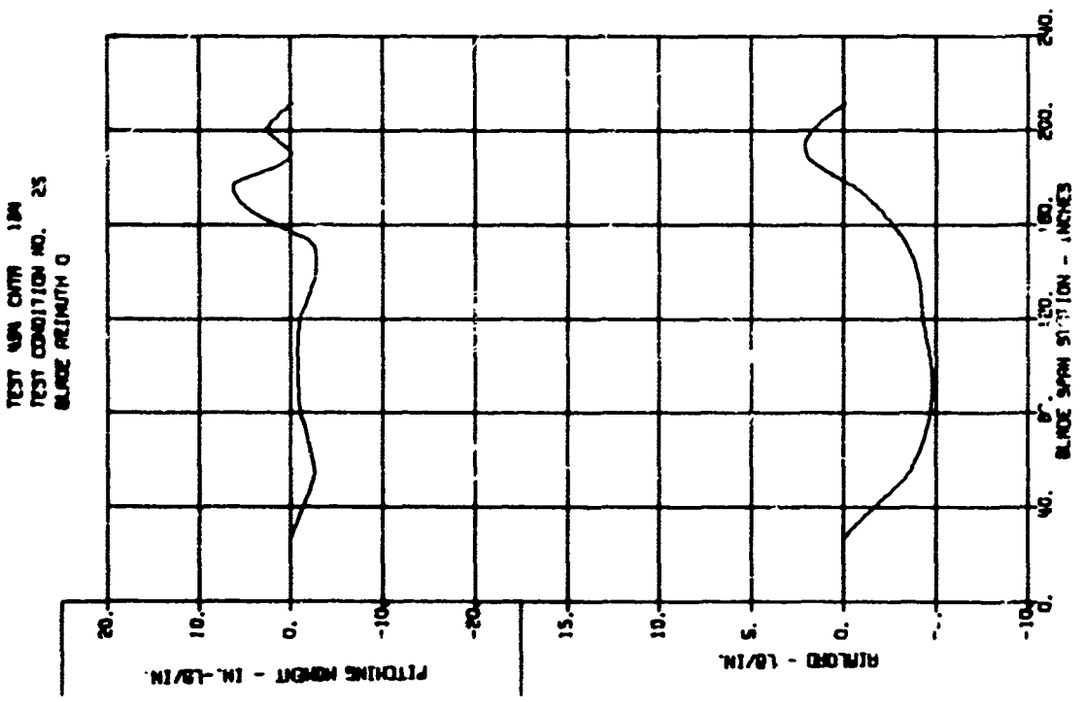

BLADE LOADS VERSUS SPAN - DYNAMIC COMPONENTS

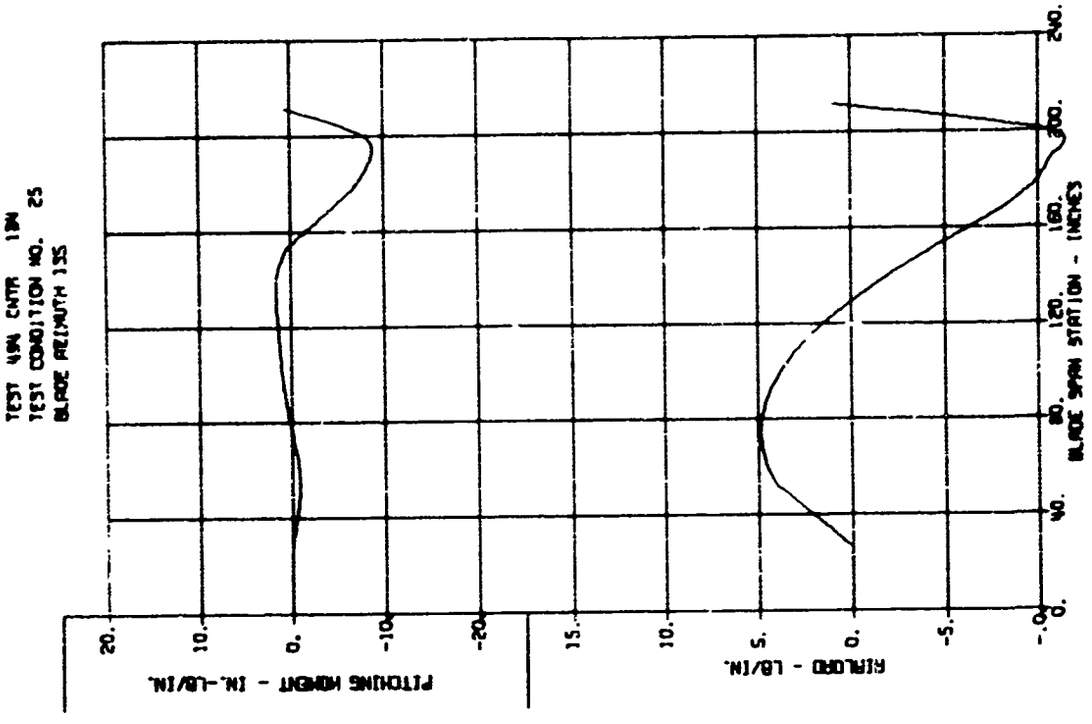

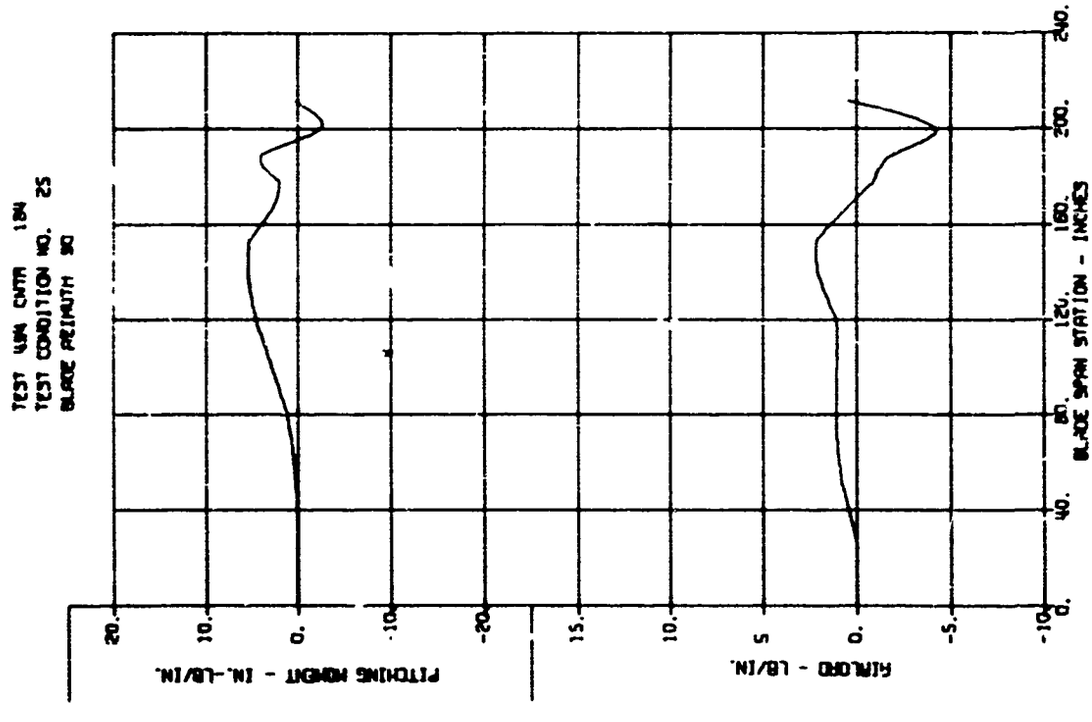

BLADE LOADS VERSUS SPAN - DYNAMIC COMPONENTS

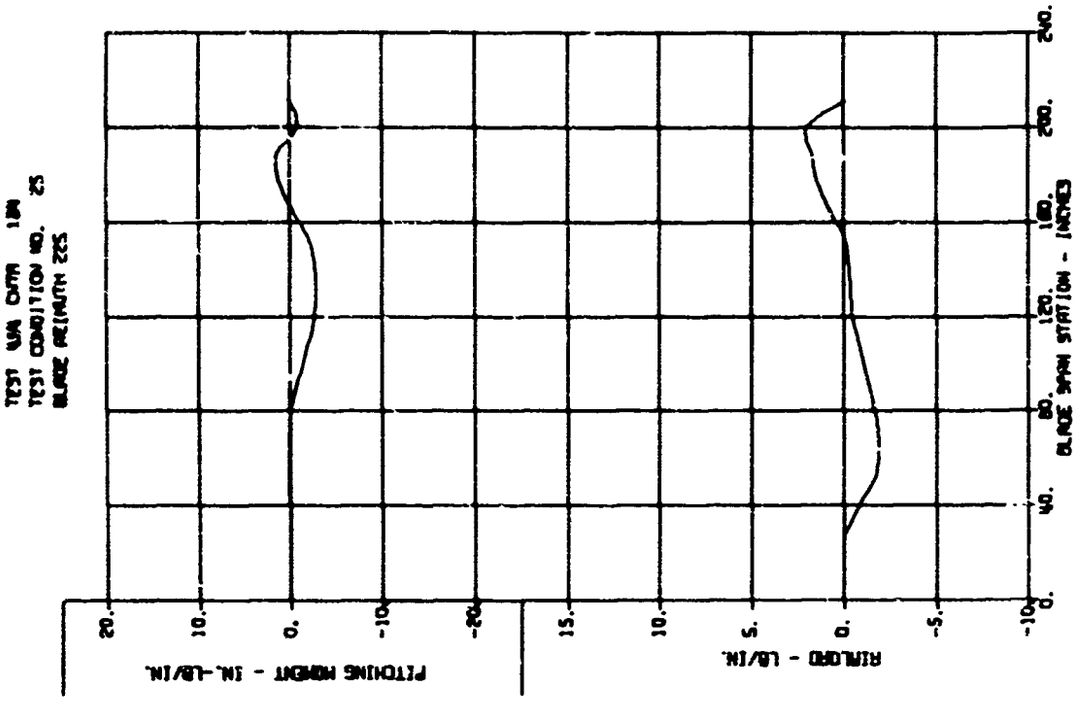

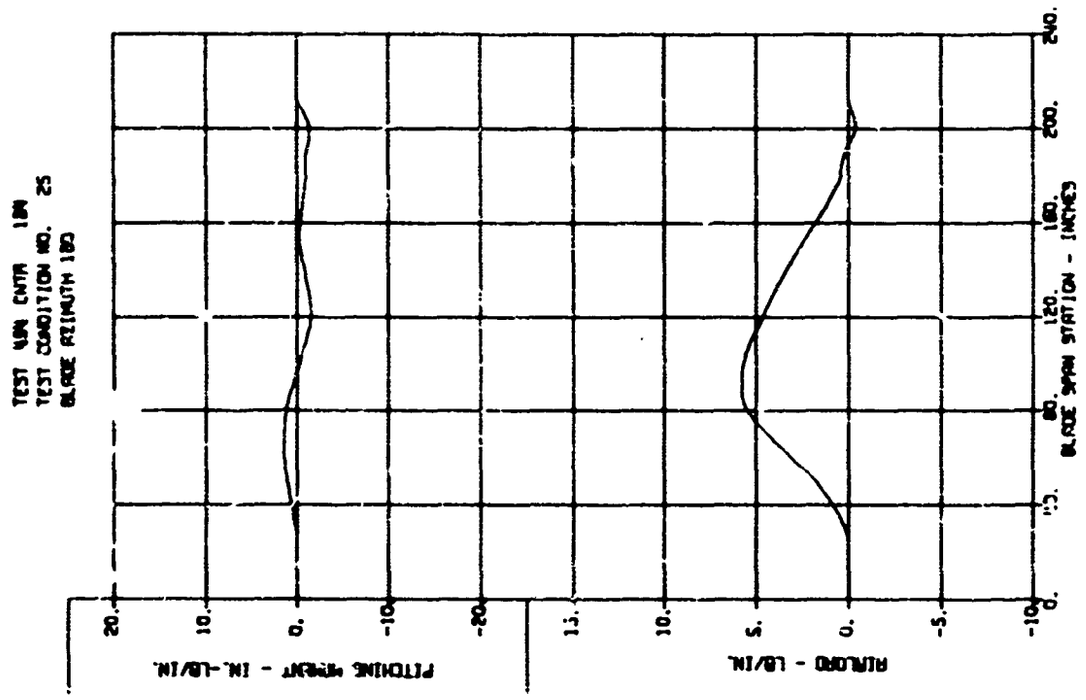

BLADE LOADS VERSUS SPAN - DYNAMIC COMPONENTS

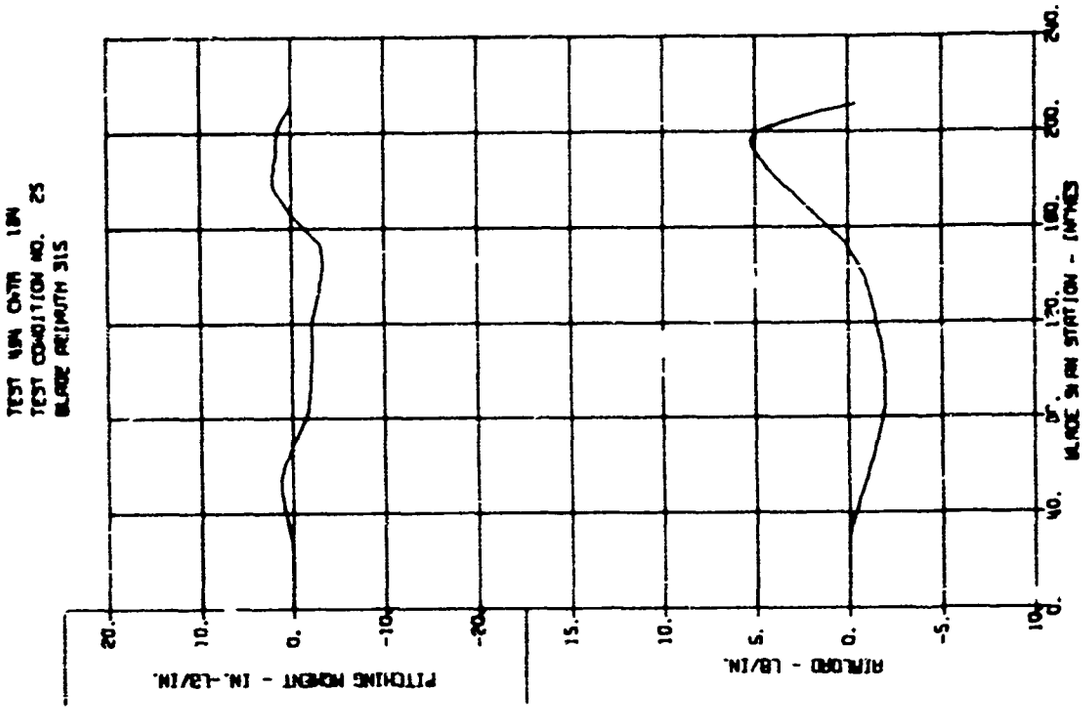

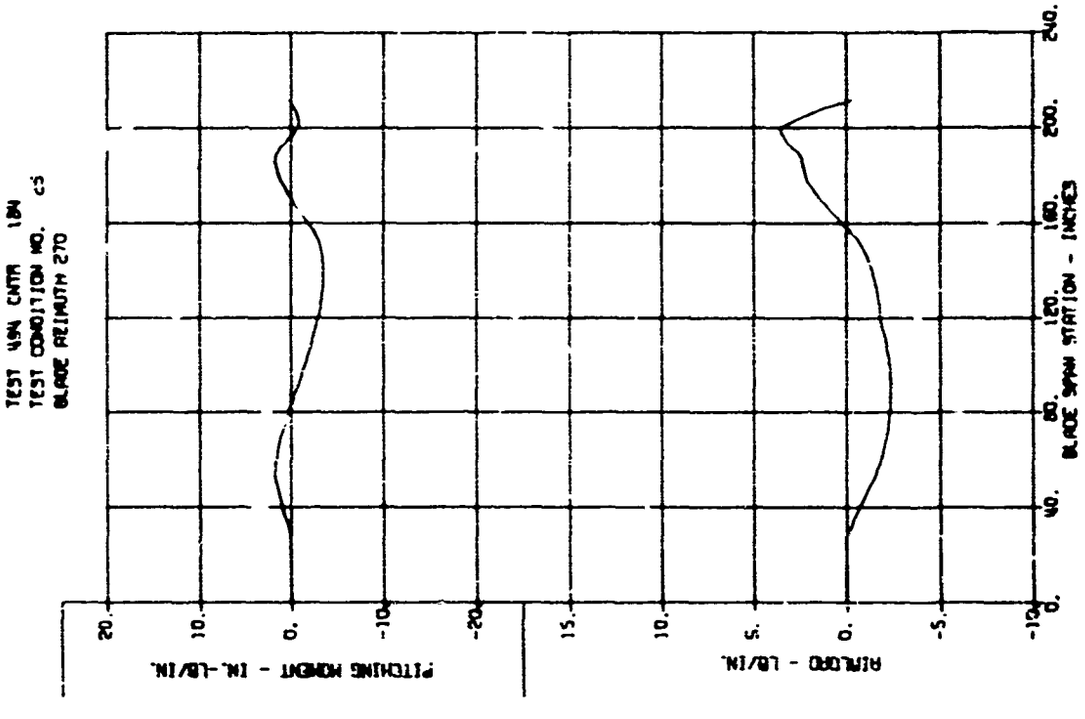

BLADE LOADS VERSUS SPAN - DYNAMIC COMPONENTS

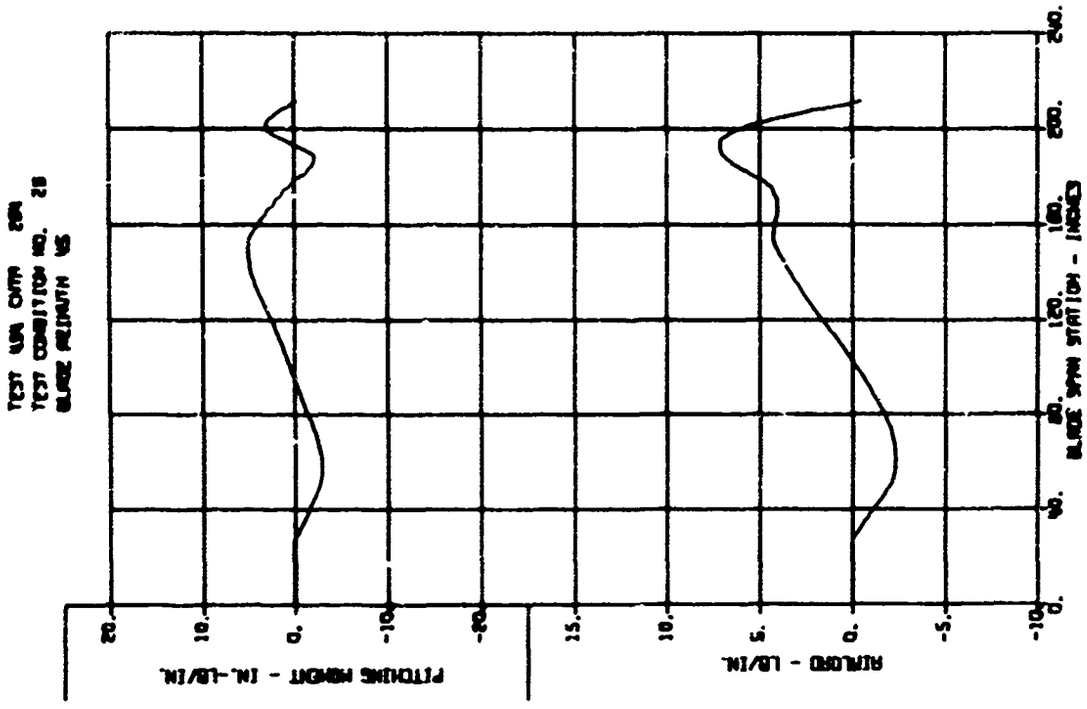

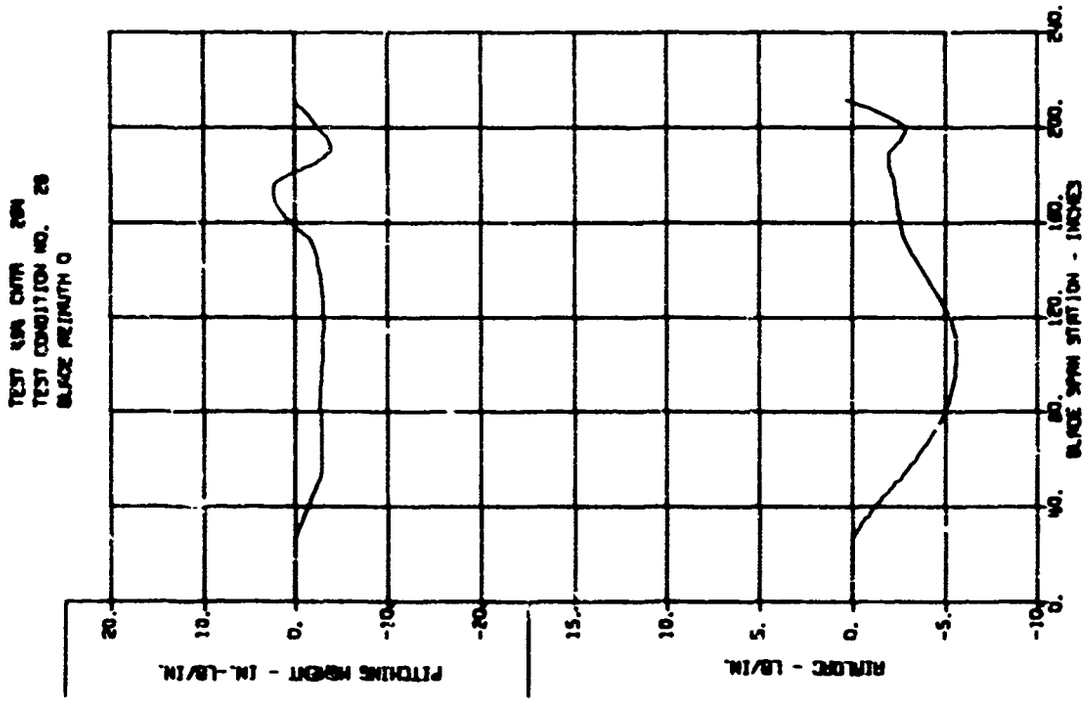

BLADE LOADS VERSUS SPAN - DYNAMIC COMPONENTS

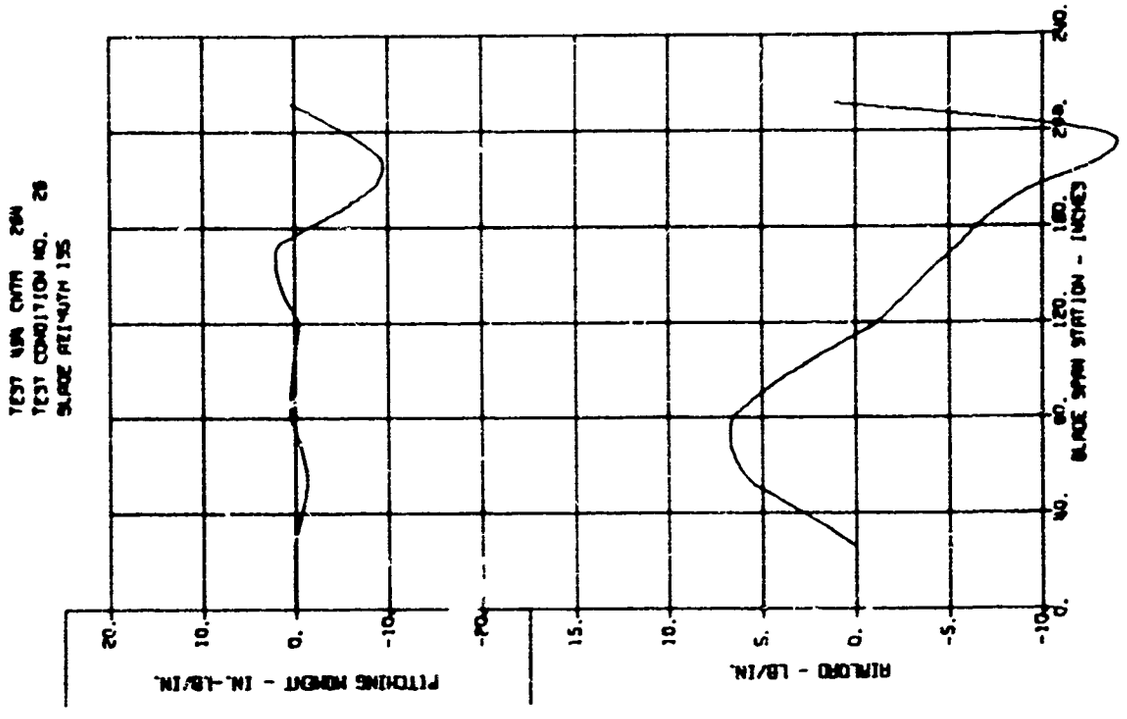

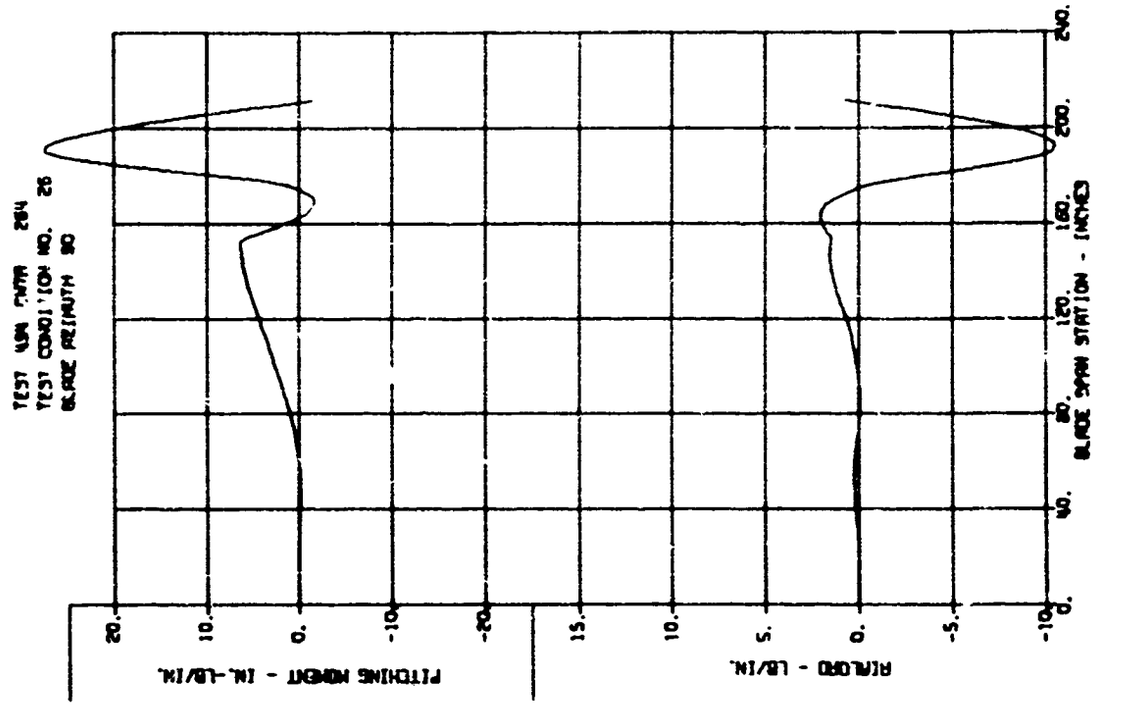

BLADE LOADS VERSUS SPAN - DYNAMIC COMPONENTS

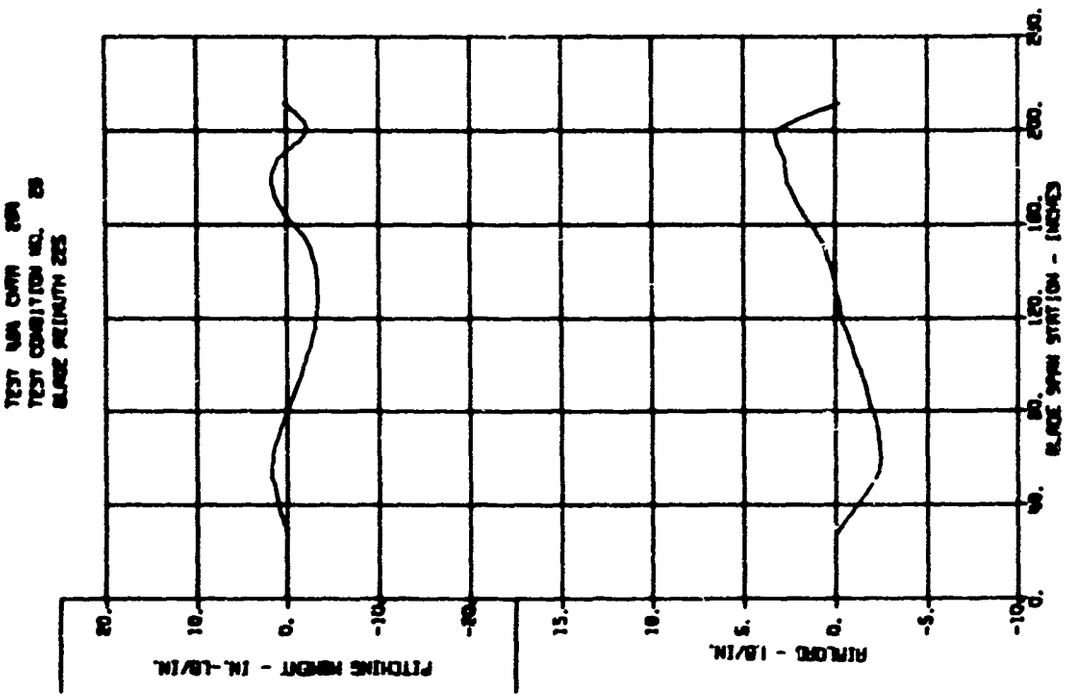

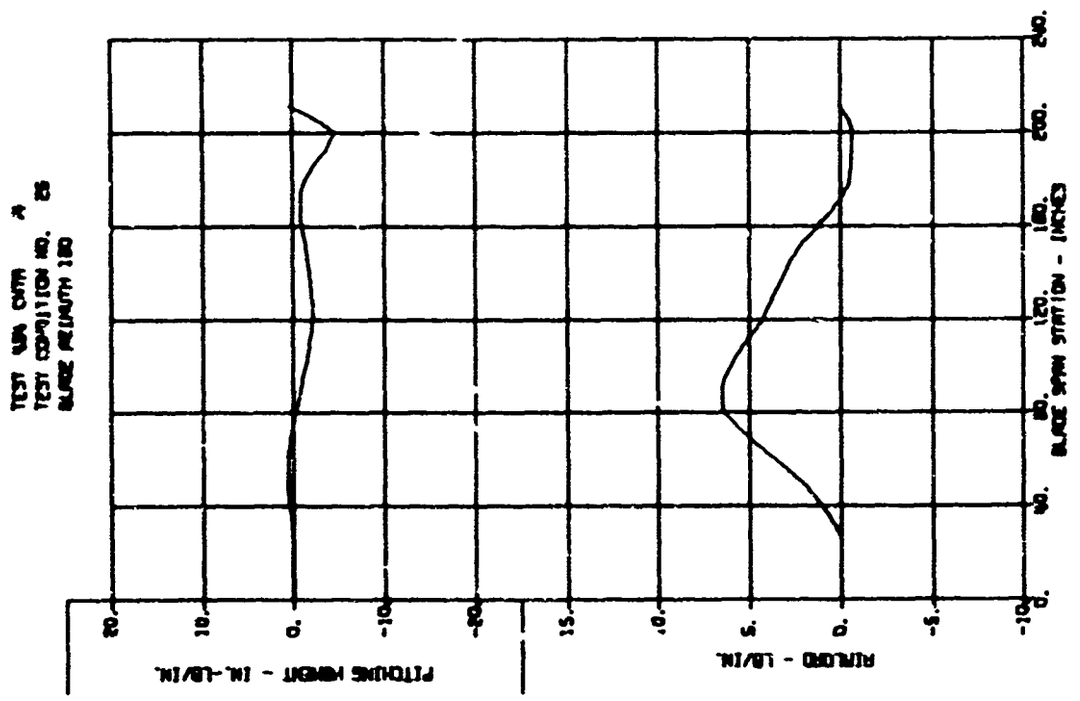

BLADE LOADS VERSUS SPAN - DYNAMIC COMPONENTS

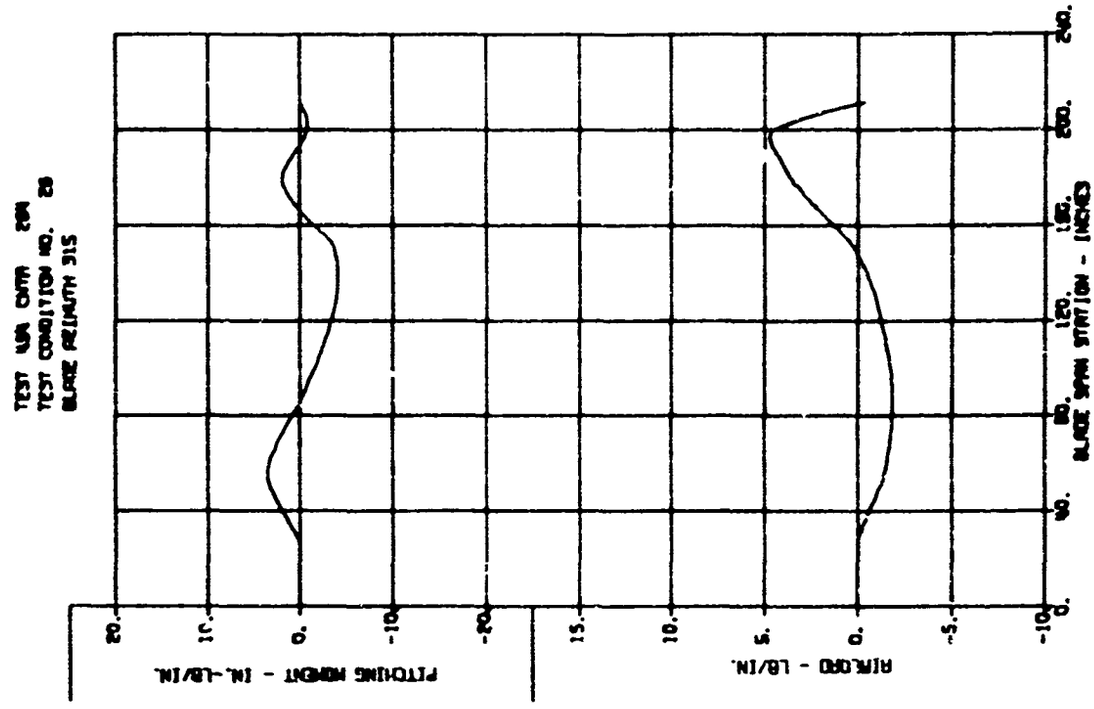

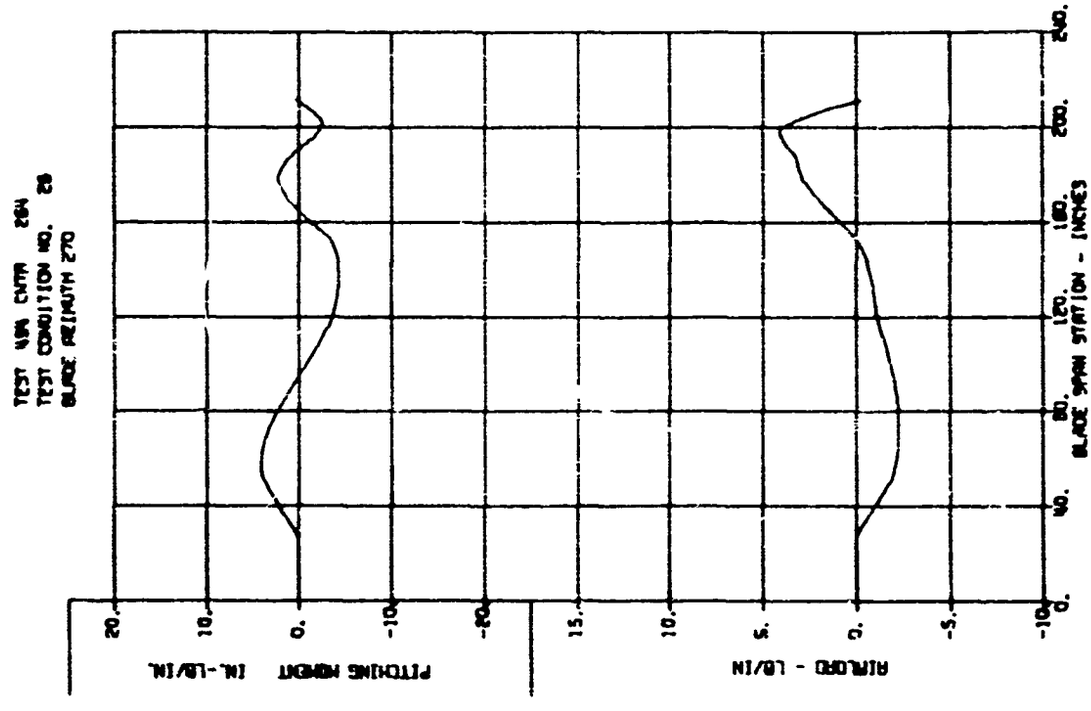

BLADE LOADS VERSUS SPAN - DYNAMIC COMPONENTS

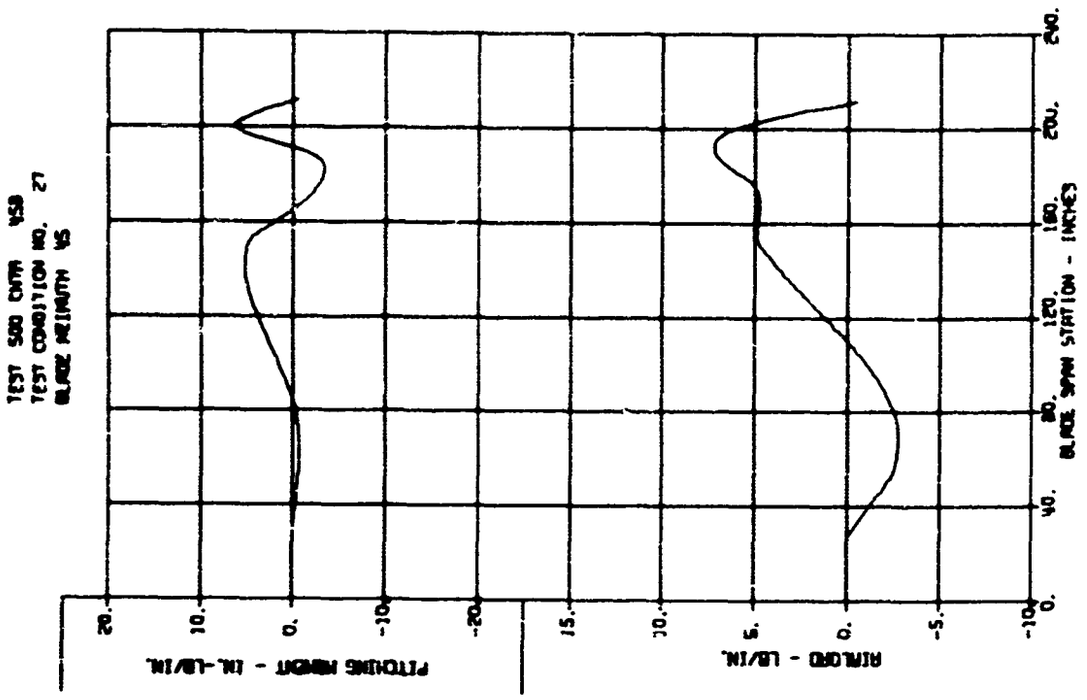

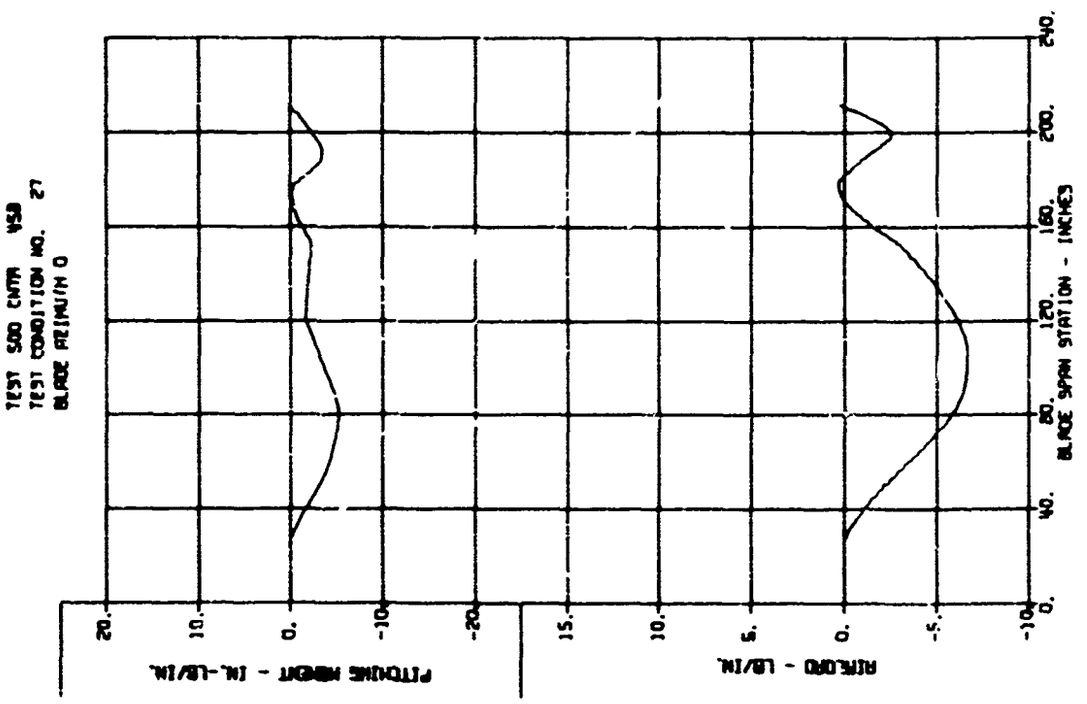

BLADE LOADS VERSUS SPAN - DYNAMIC COMPONENTS

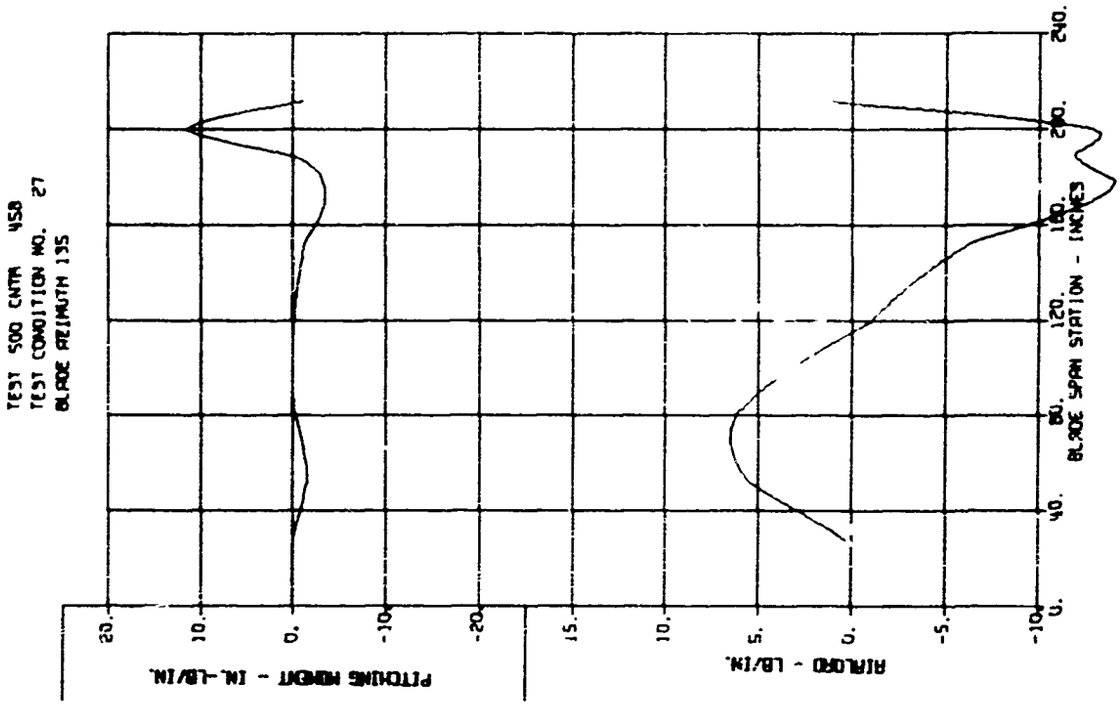

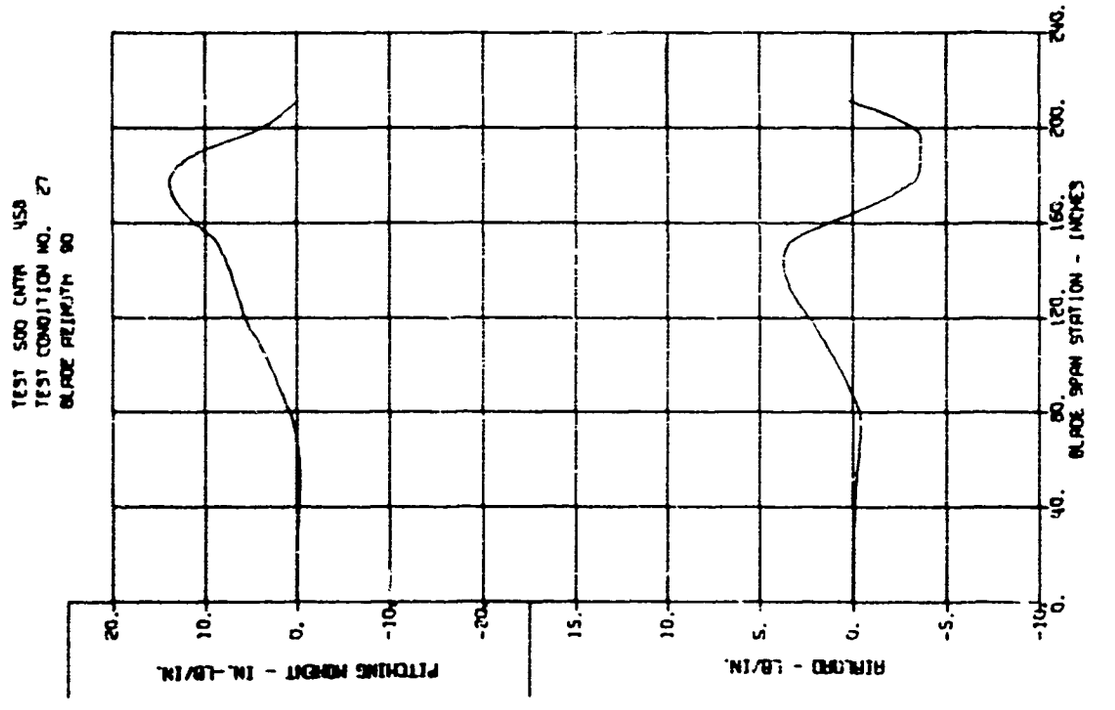

BLADE LOADS VERSUS SPAN - DYNAMIC COMPONENTS

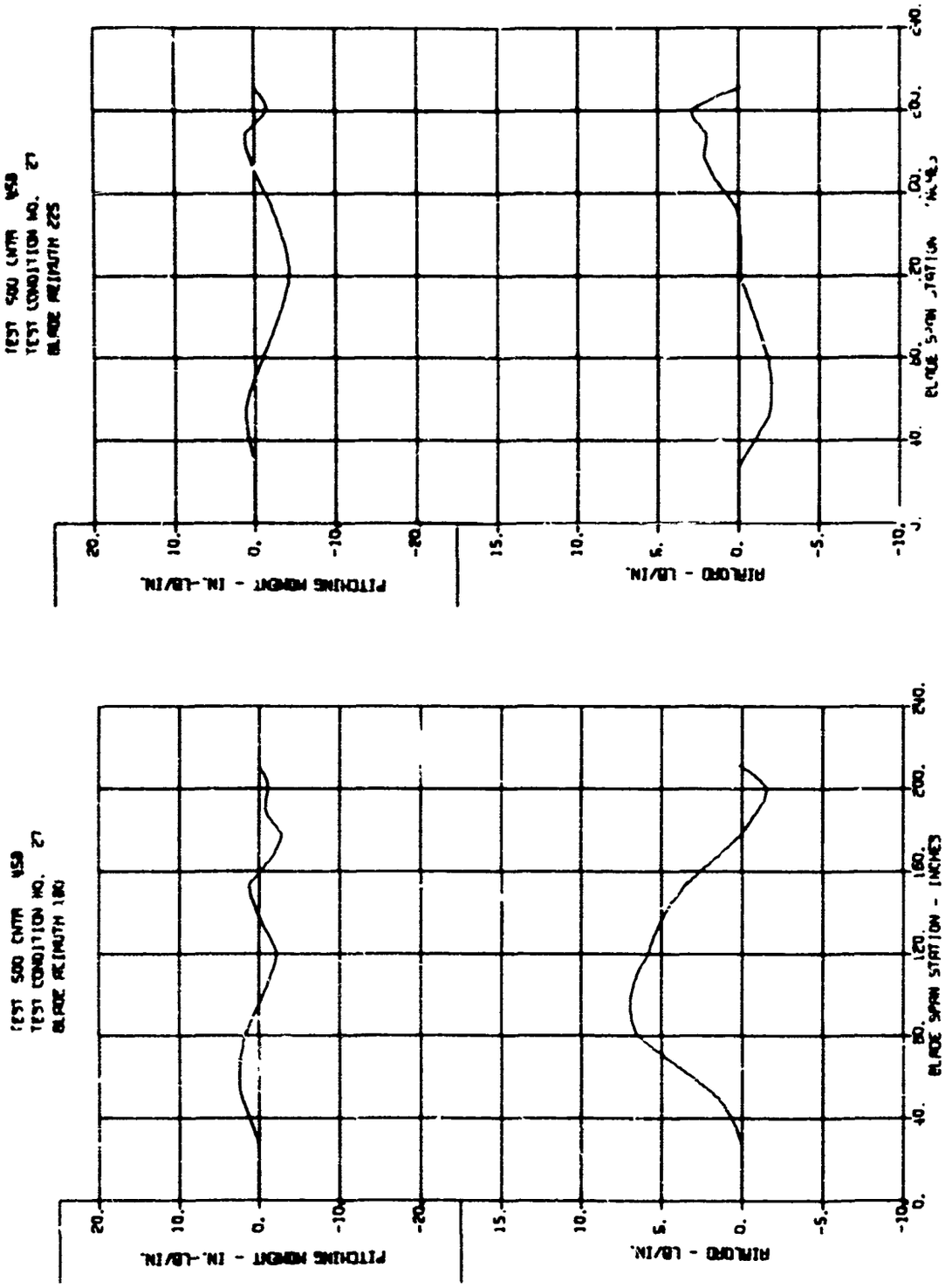

BLADE LOADS VERSUS SPAN - DYNAMIC COMPONENTS

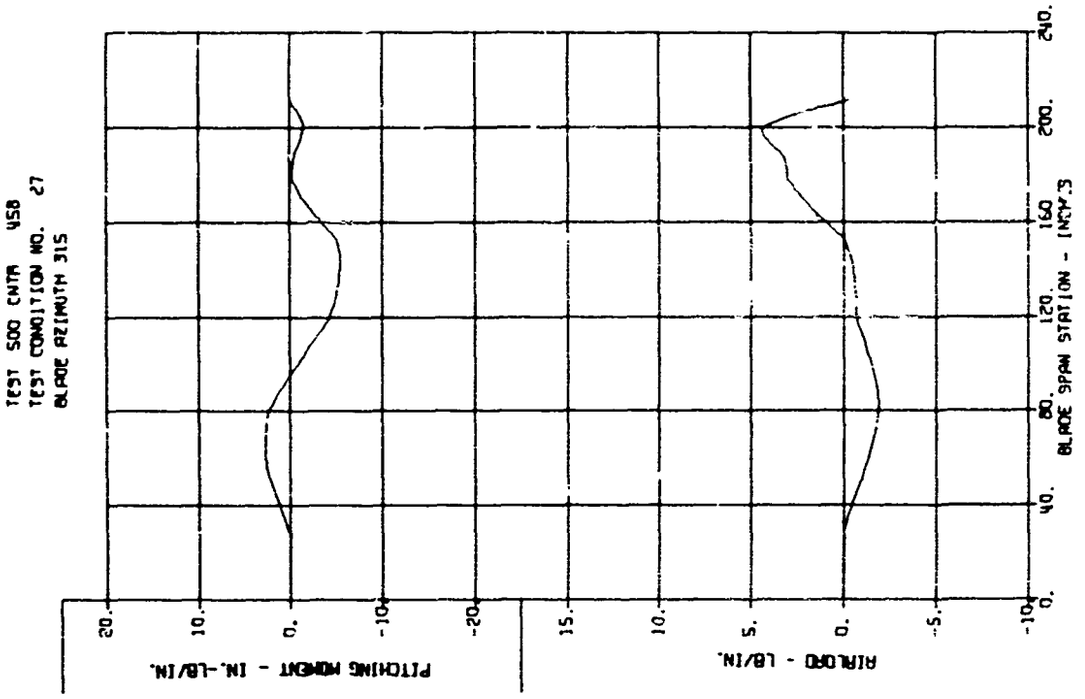

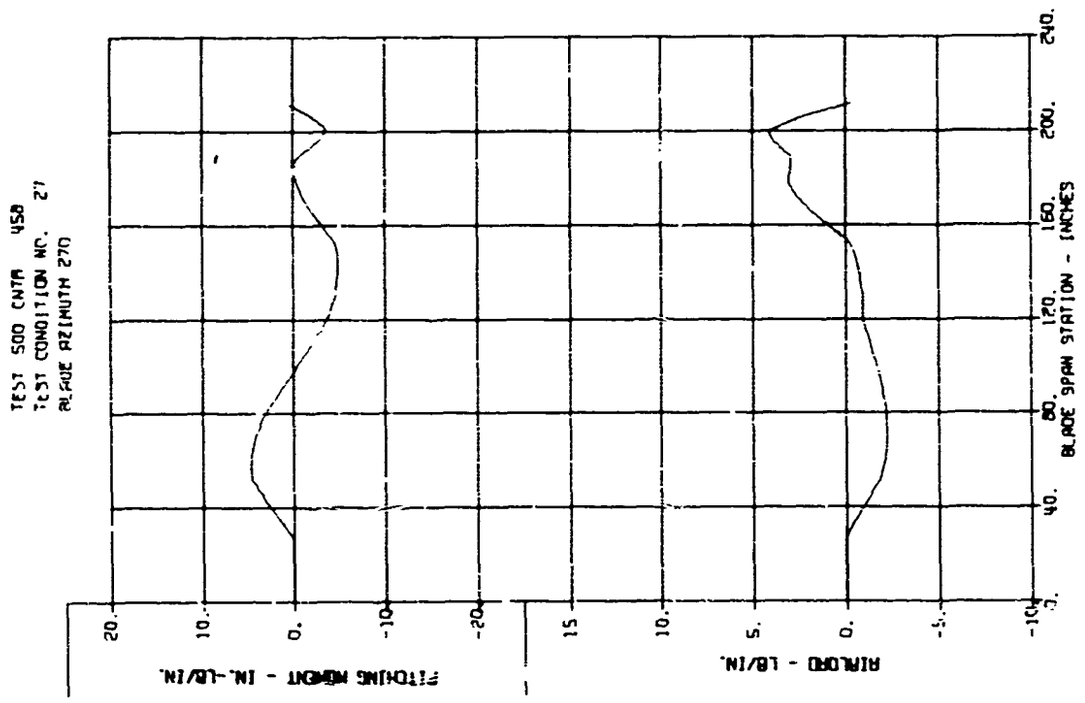

BLADE LOADS VERSUS SPAN - DYNAMIC COMPONENTS

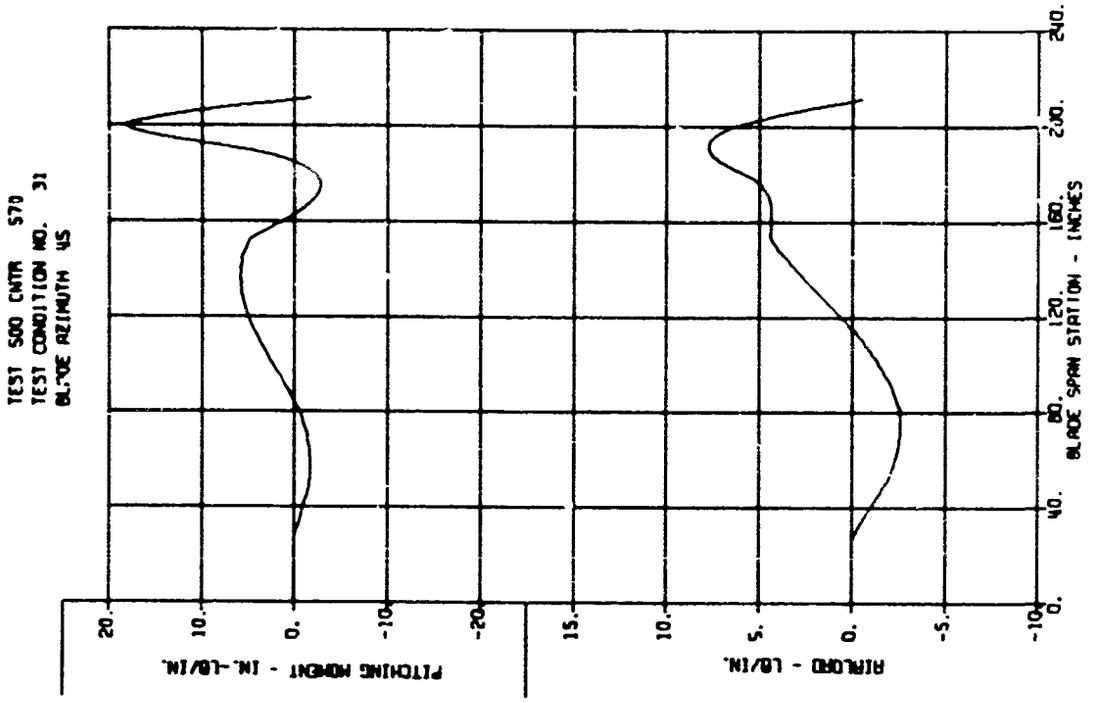

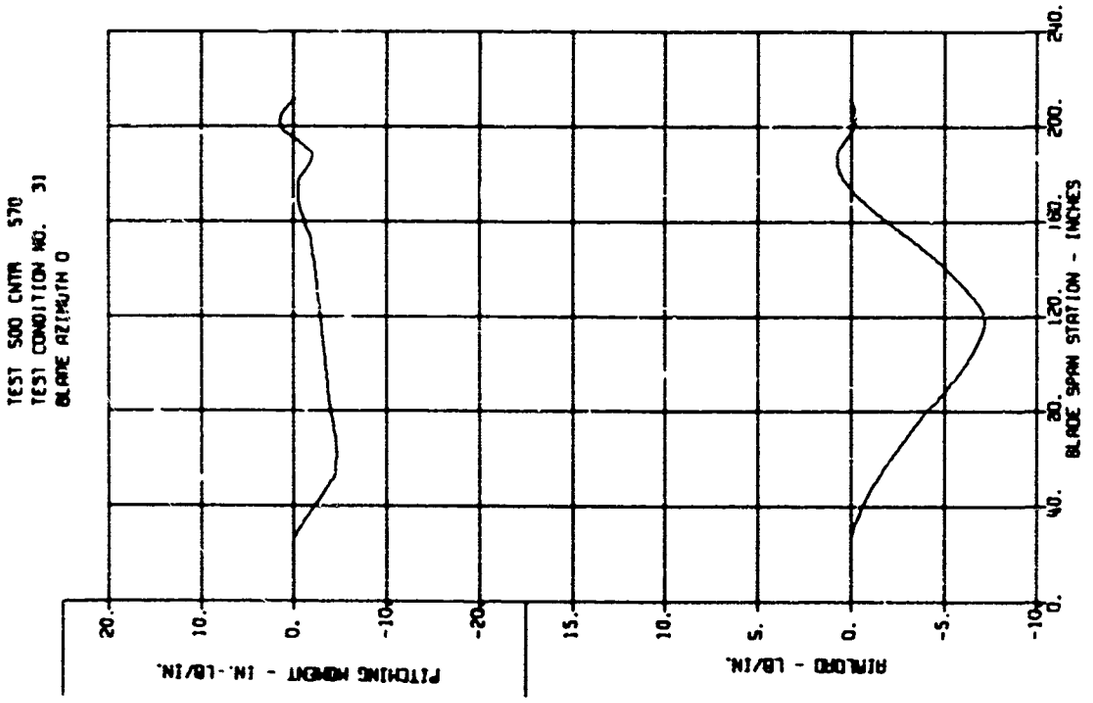

BLADE LOADS VERSUS SPAN - DYNAMIC COMPONENTS

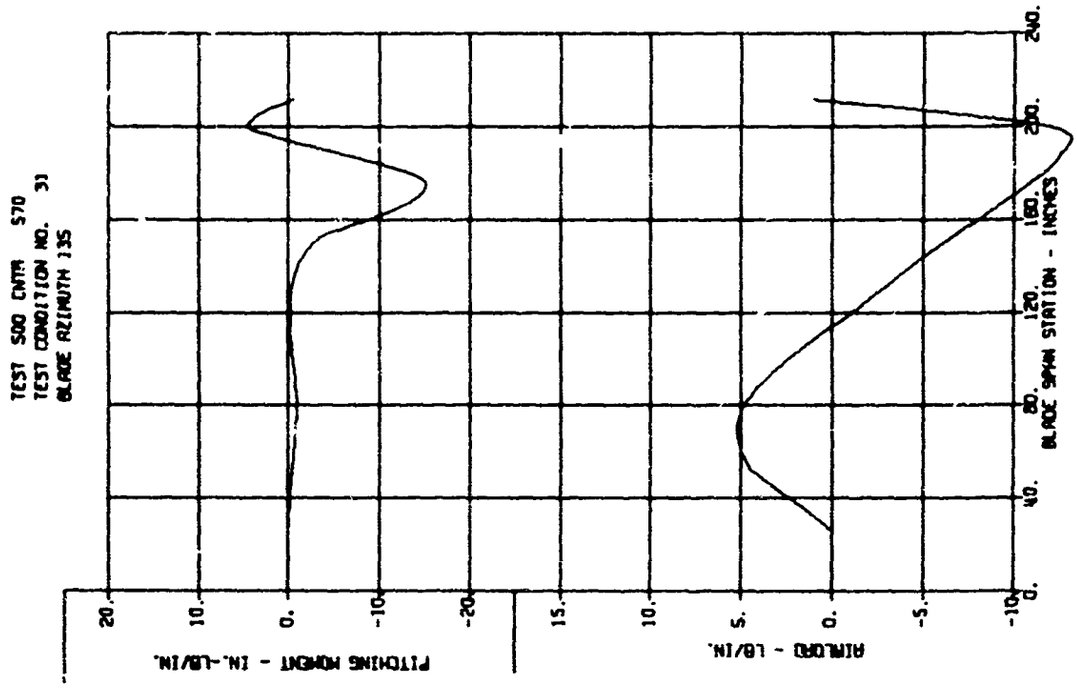

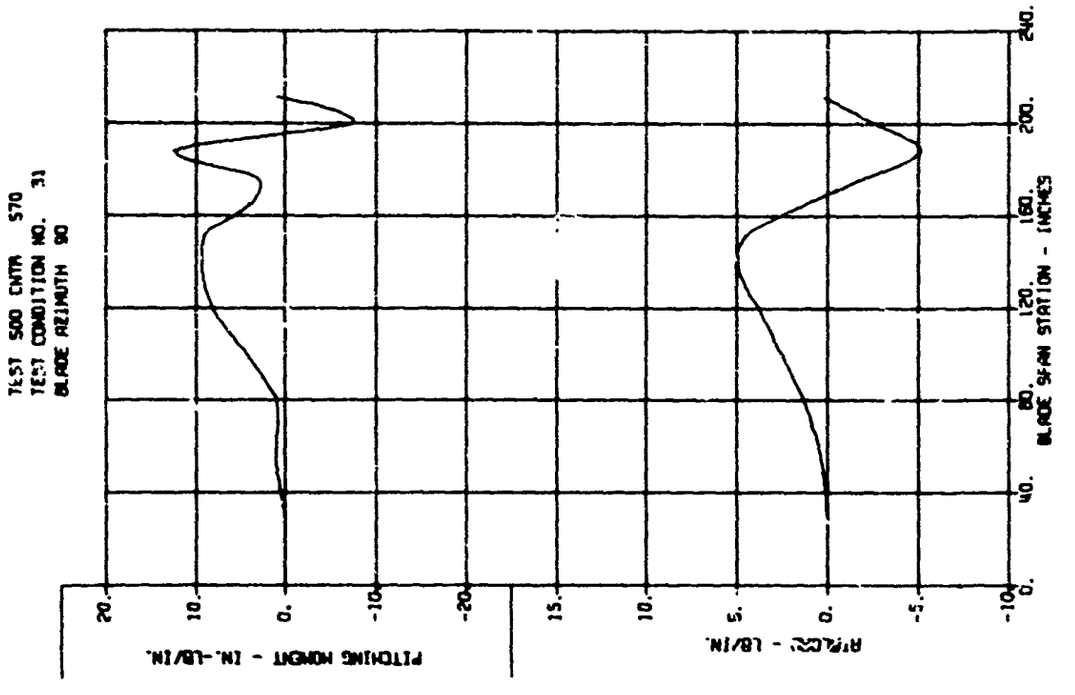

BLADE LOADS VERSUS SPAN - DYNAMIC COMPONENTS

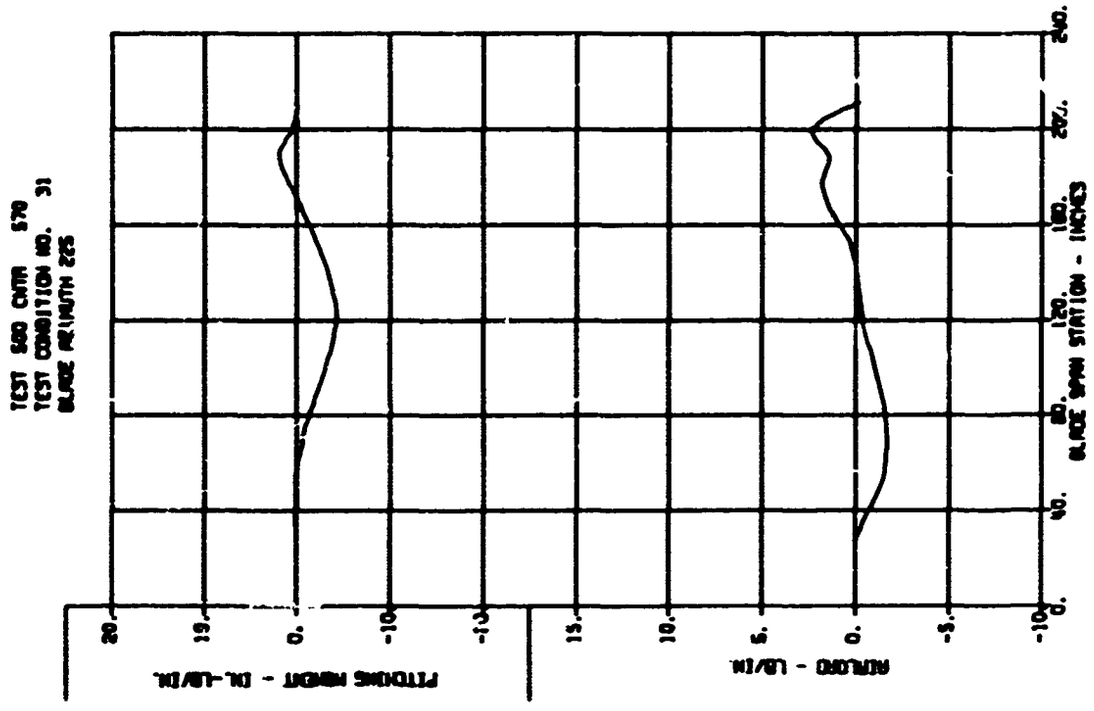

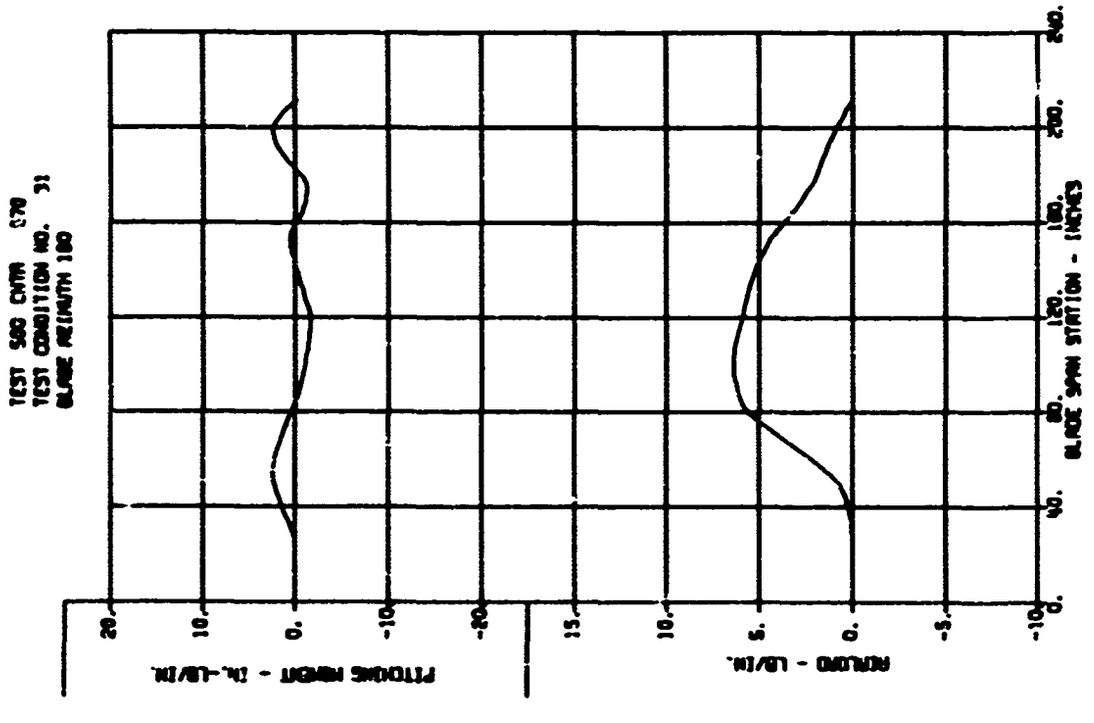

BLADE LOADS VERSUS SPAN - DYNAMIC COMPONENTS

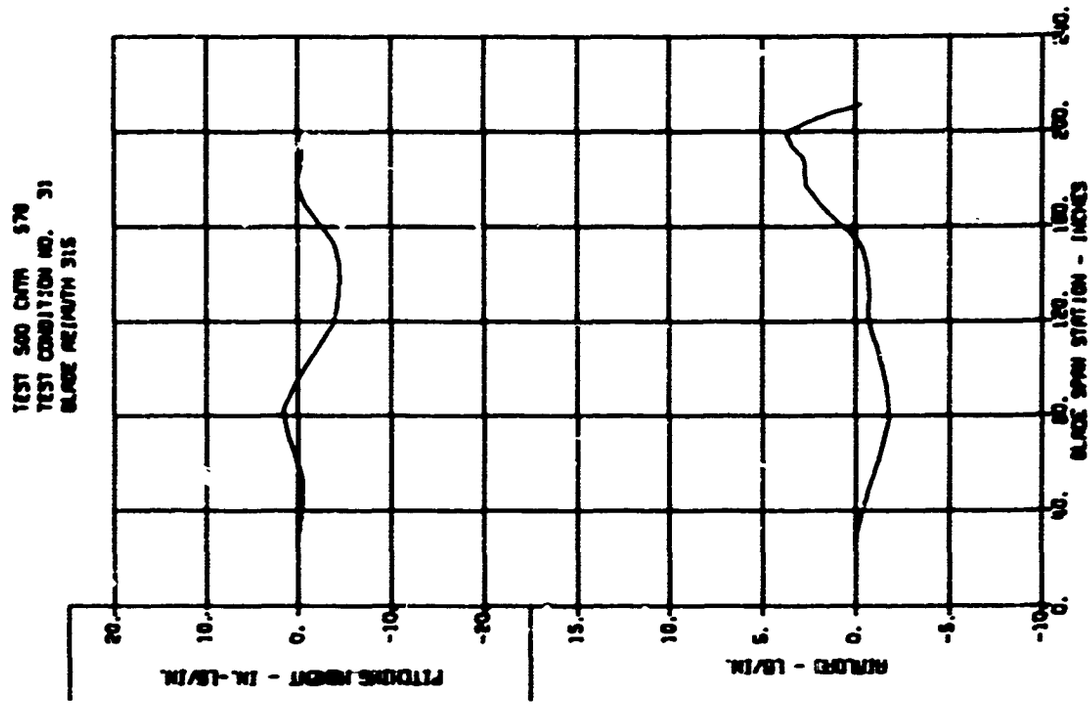

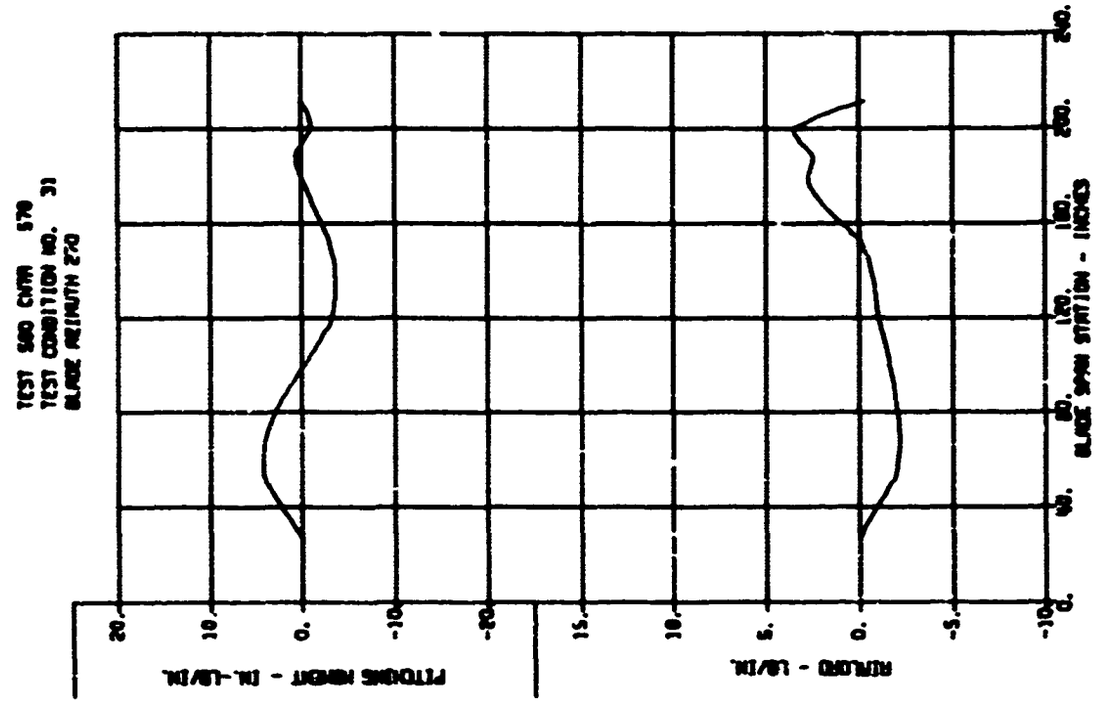

BLADE LOADS VERSUS SPAN - DYNAMIC COMPONENTS

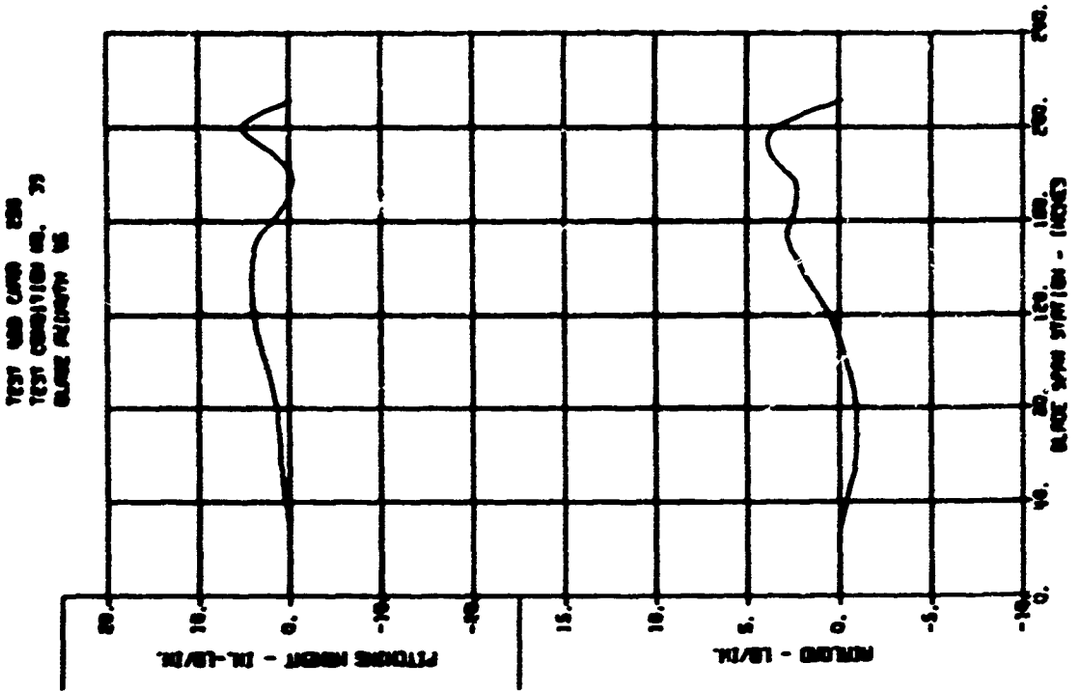

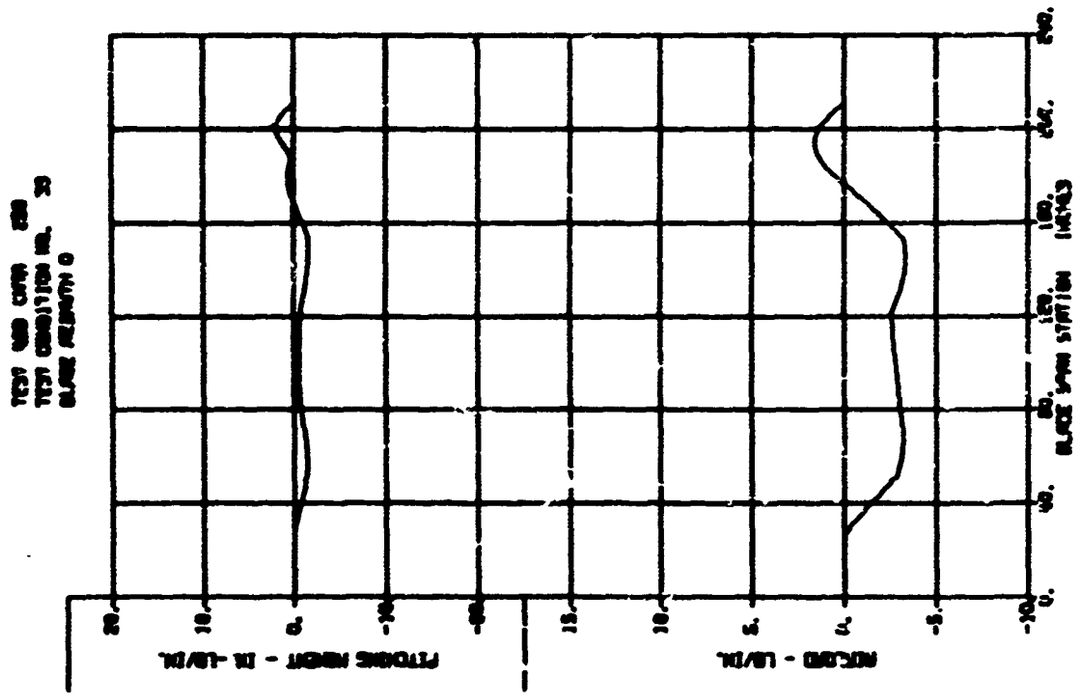

BLADE LOADS VERSUS SPAN - DYNAMIC COMPONENTS

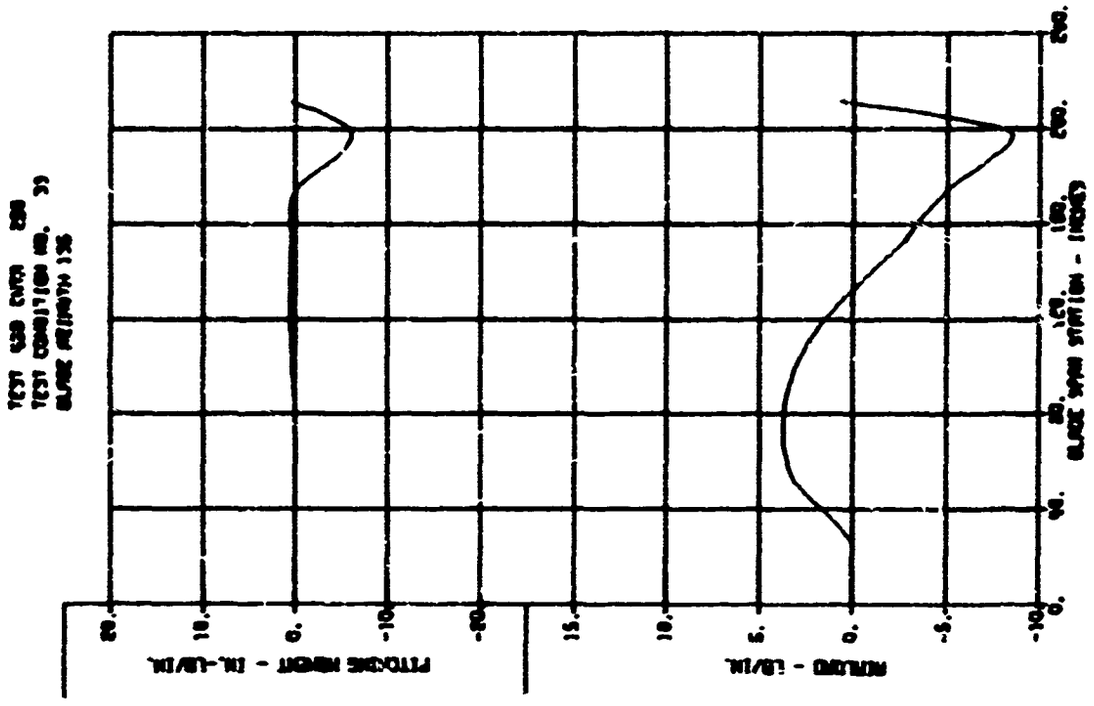

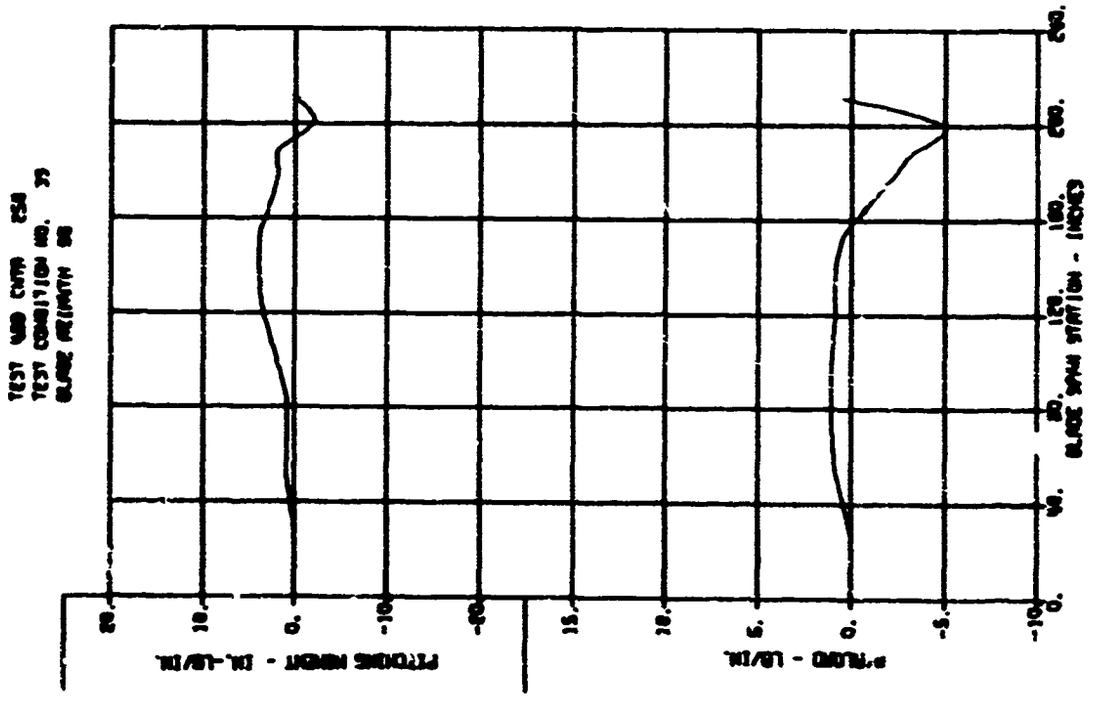

BLADE LOADS VERSUS SPAN - DYNAMIC COMPONENTS

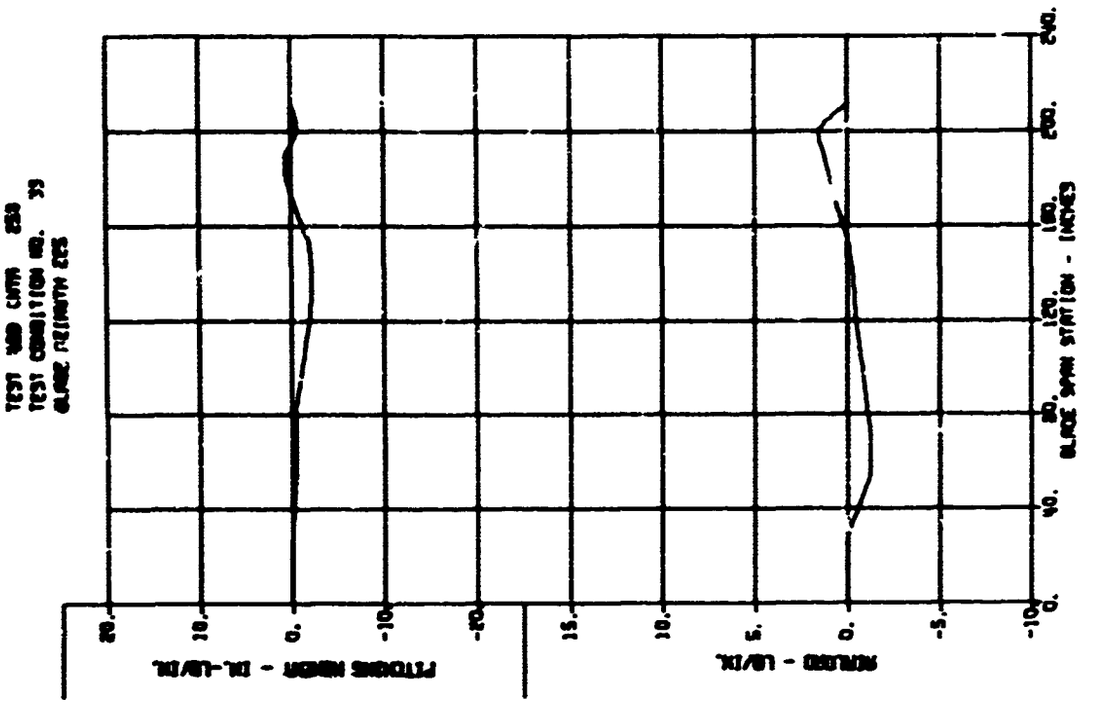

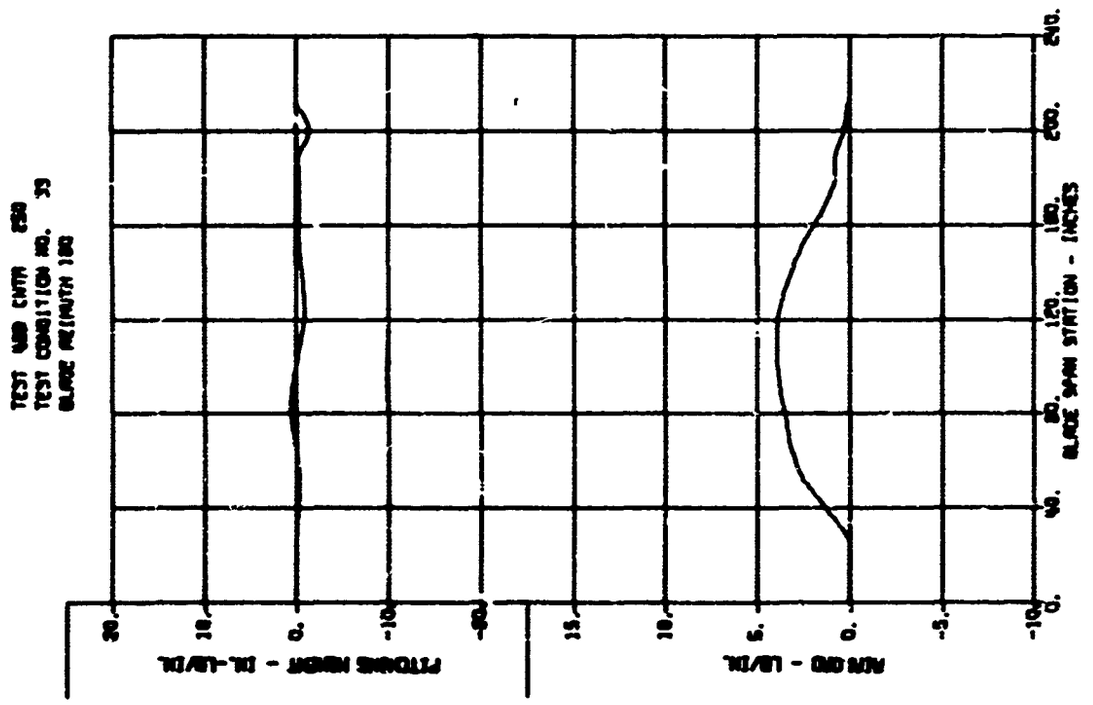

BLADE LOADS VERSUS SPAN - DYNAMIC COMPONENTS

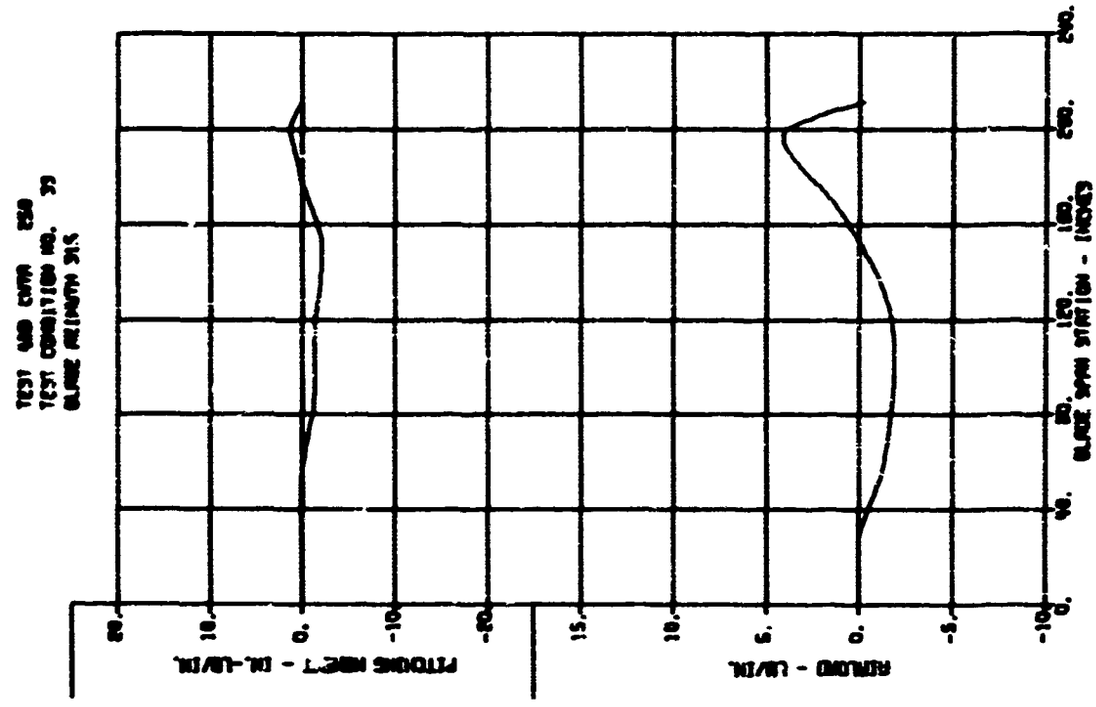

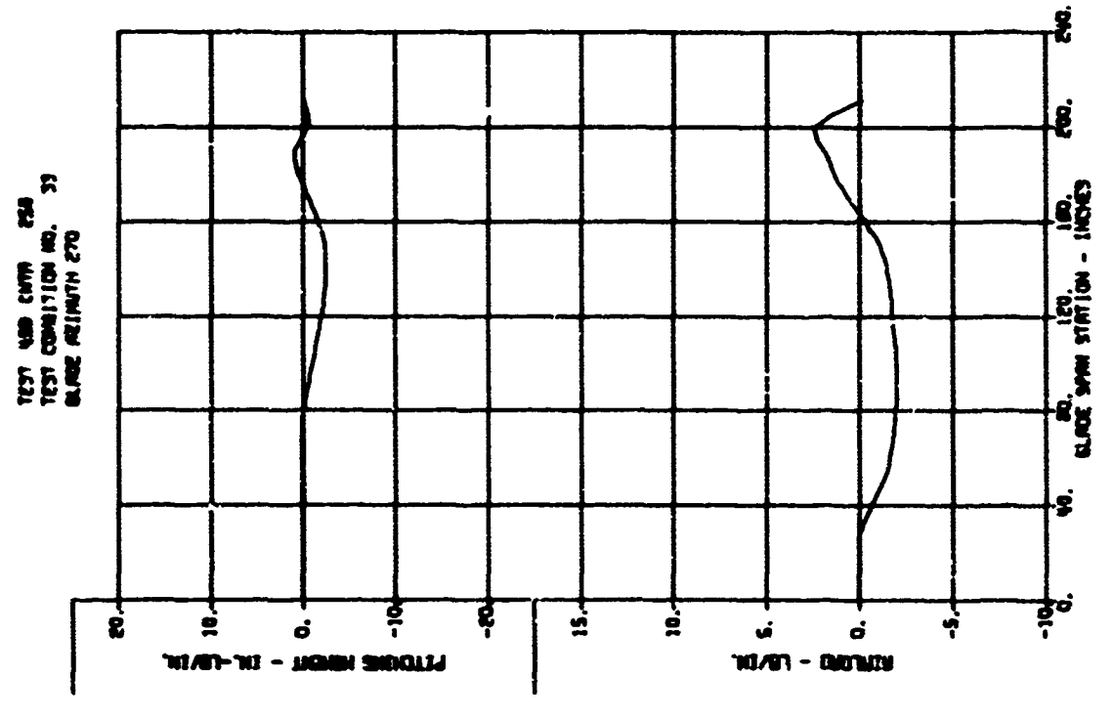

BLADE LOADS VERSUS SPAN - DYNAMIC COMPONENTS

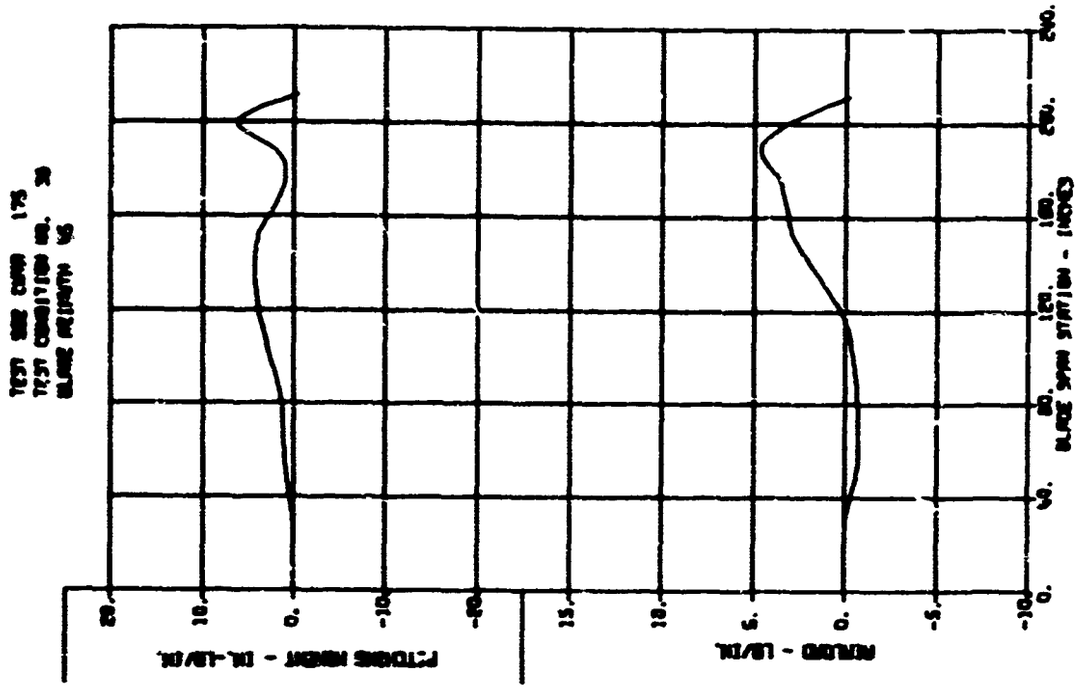

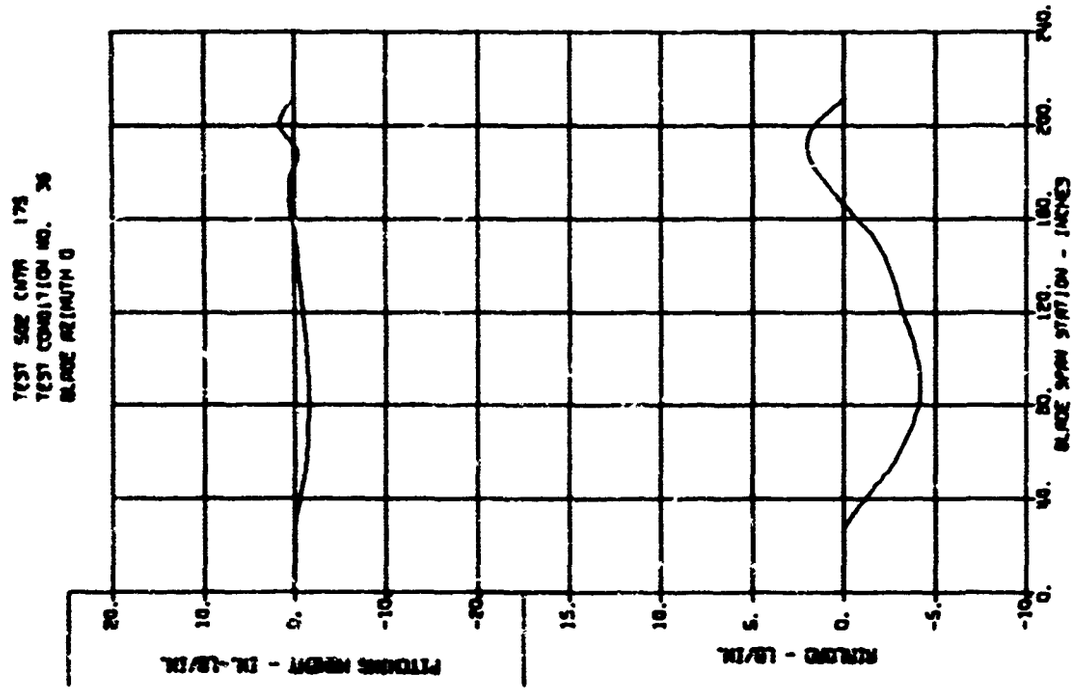

BLADE LOADS VERSUS SPAN - DYNAMIC COMPONENTS

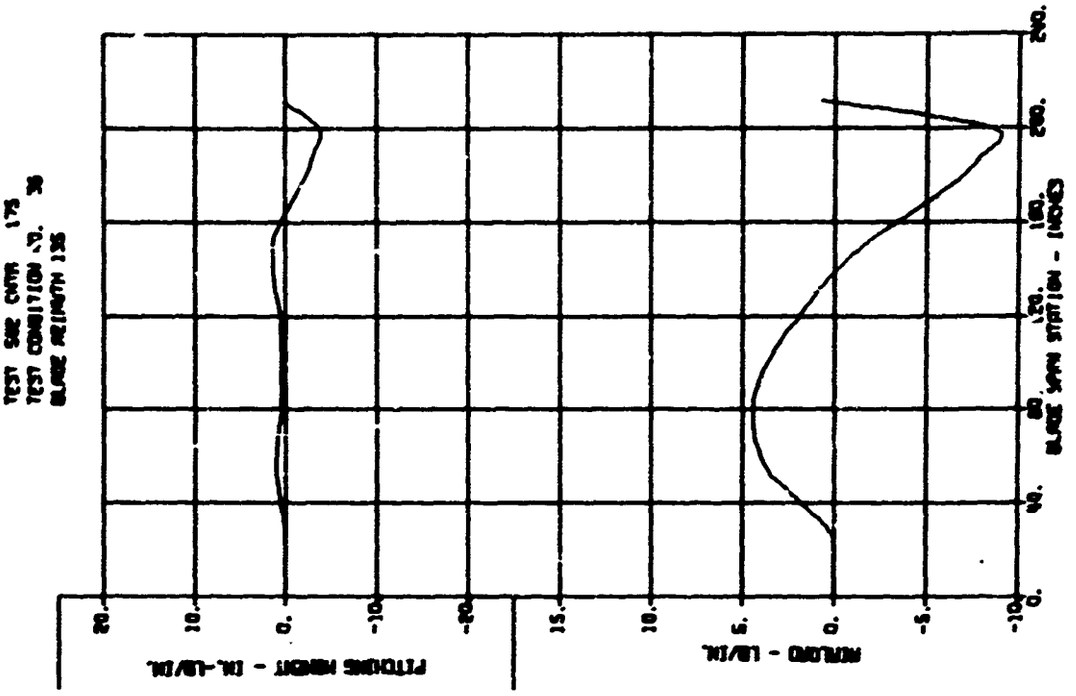

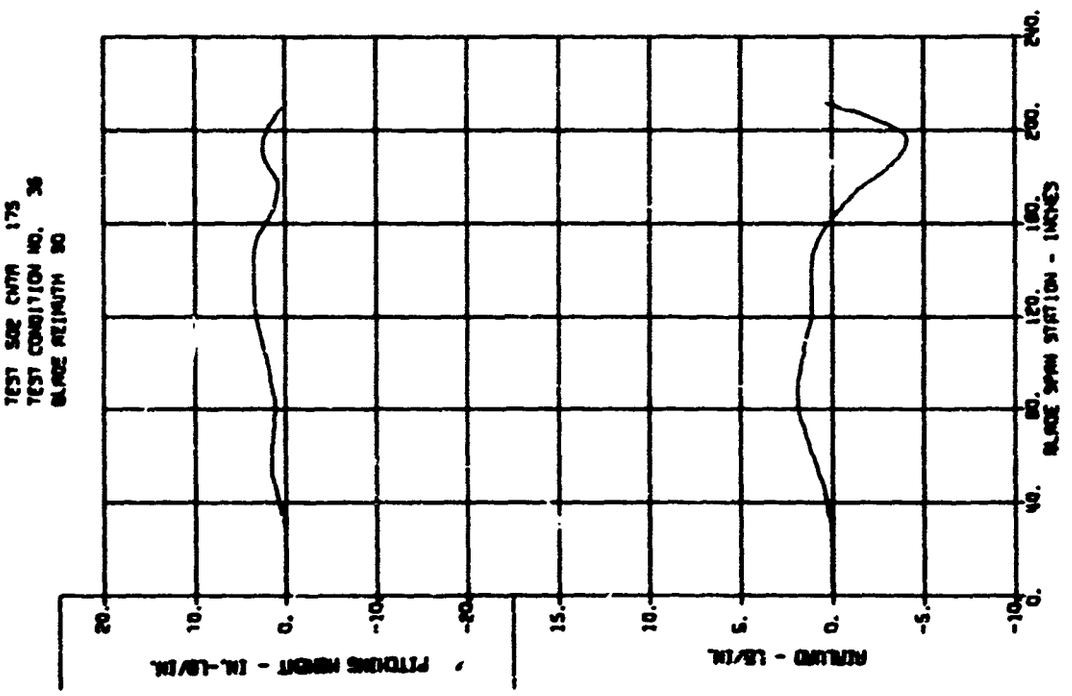

BLADE LOADS VERSUS SPAN - DYNAMIC COMPONENTS

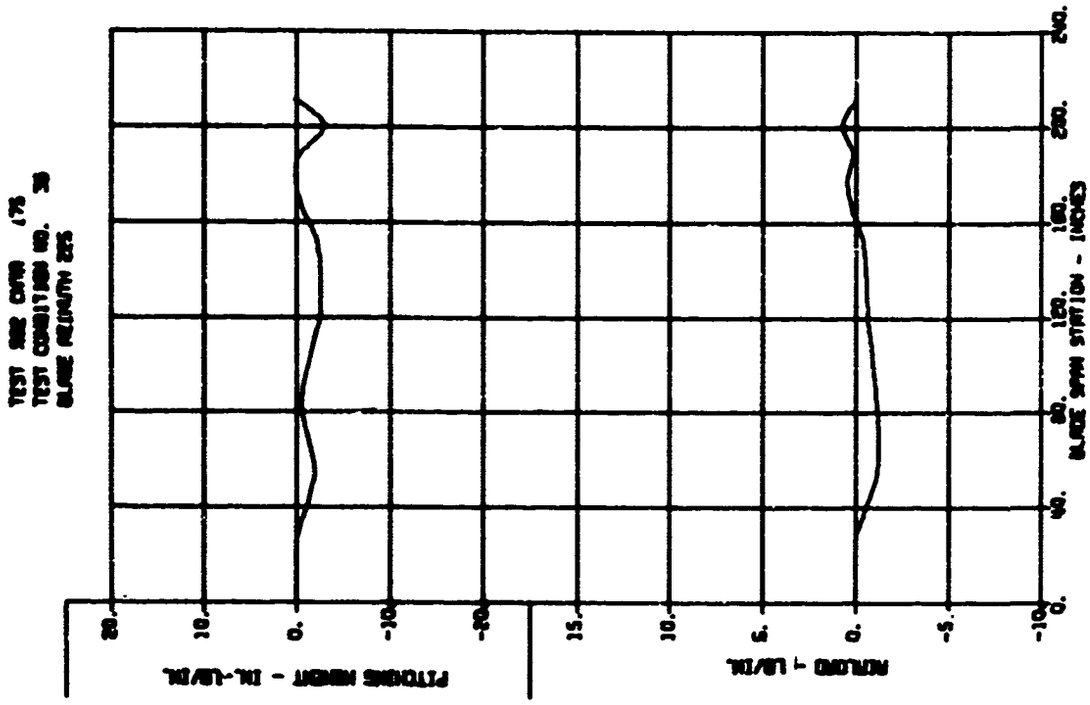

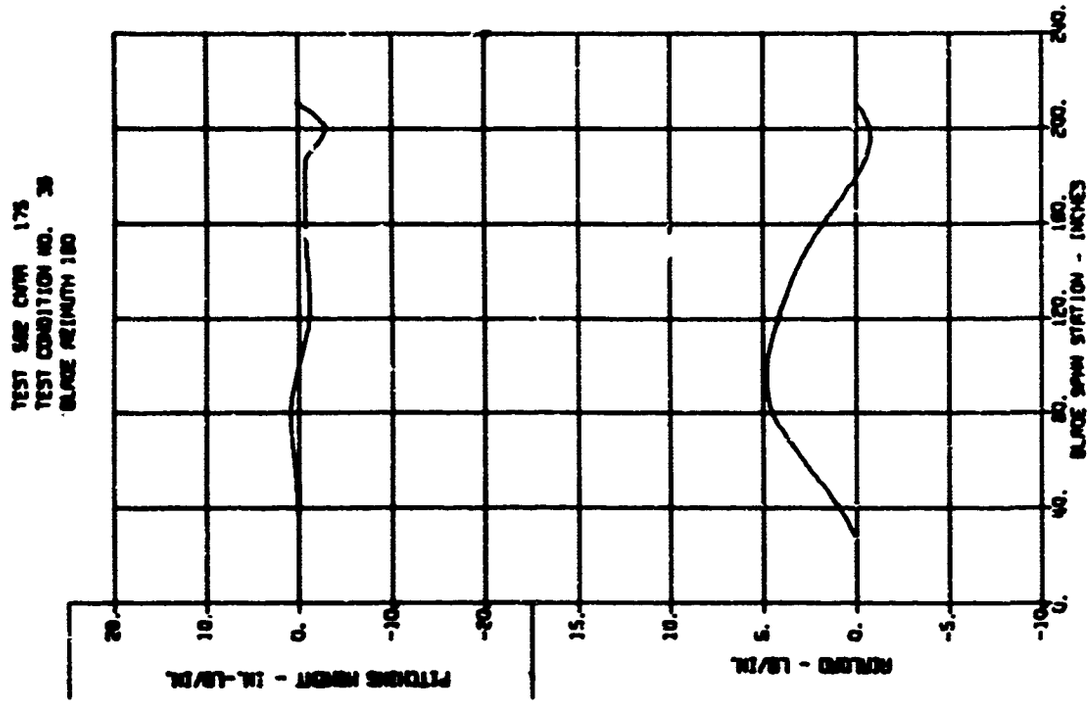

BLADE LOADS VERSUS SPAN - DYNAMIC COMPONENT

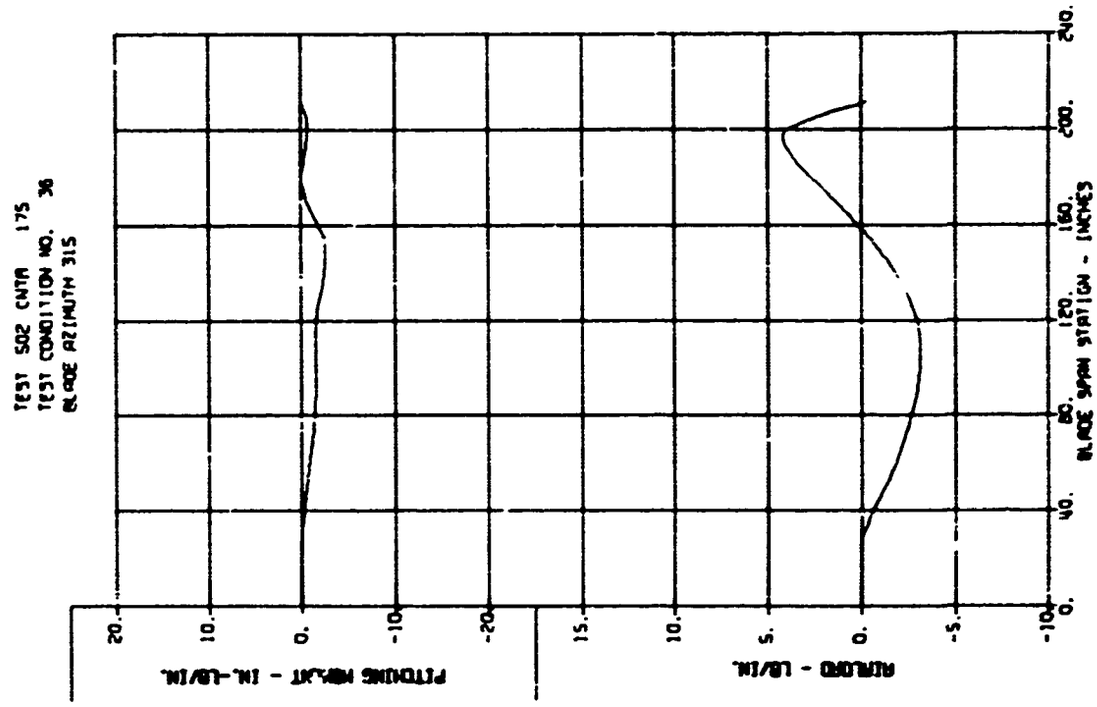

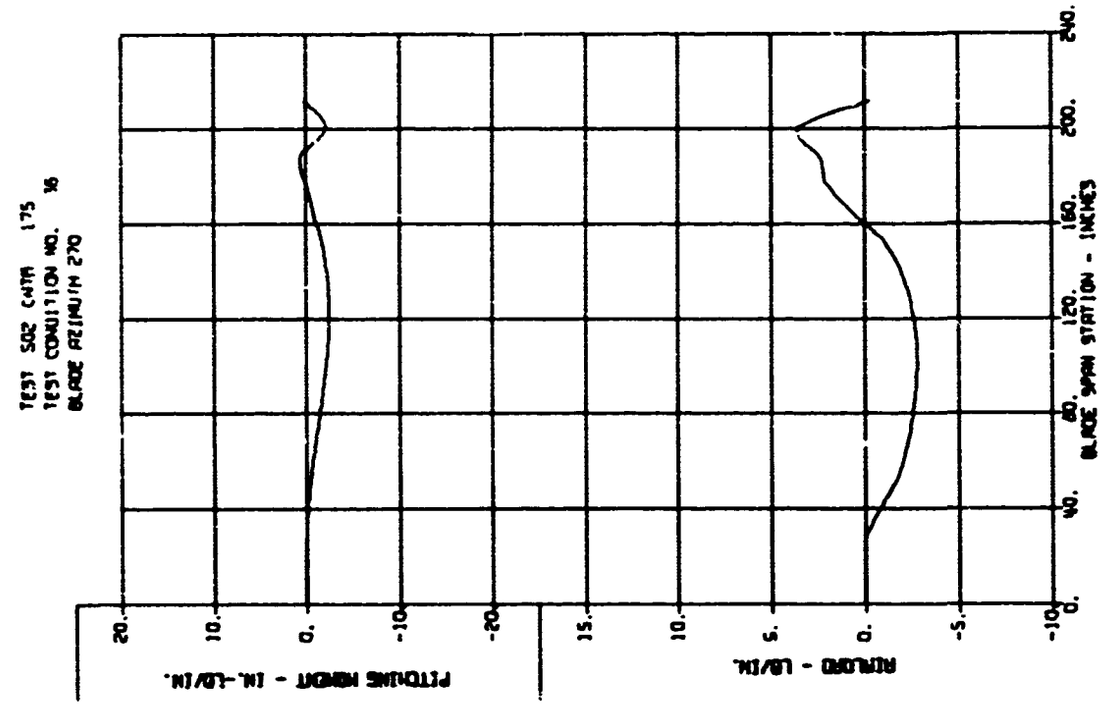

BLADE LOADS VERSUS SPAN - DYNAMIC COMPONENTS

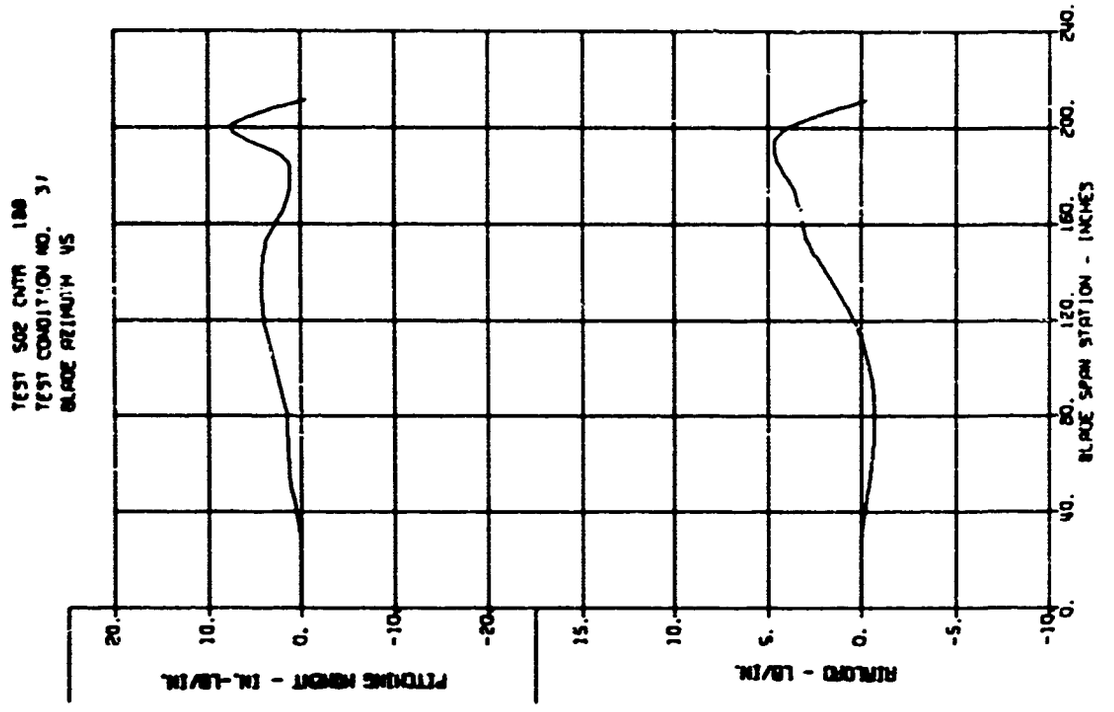

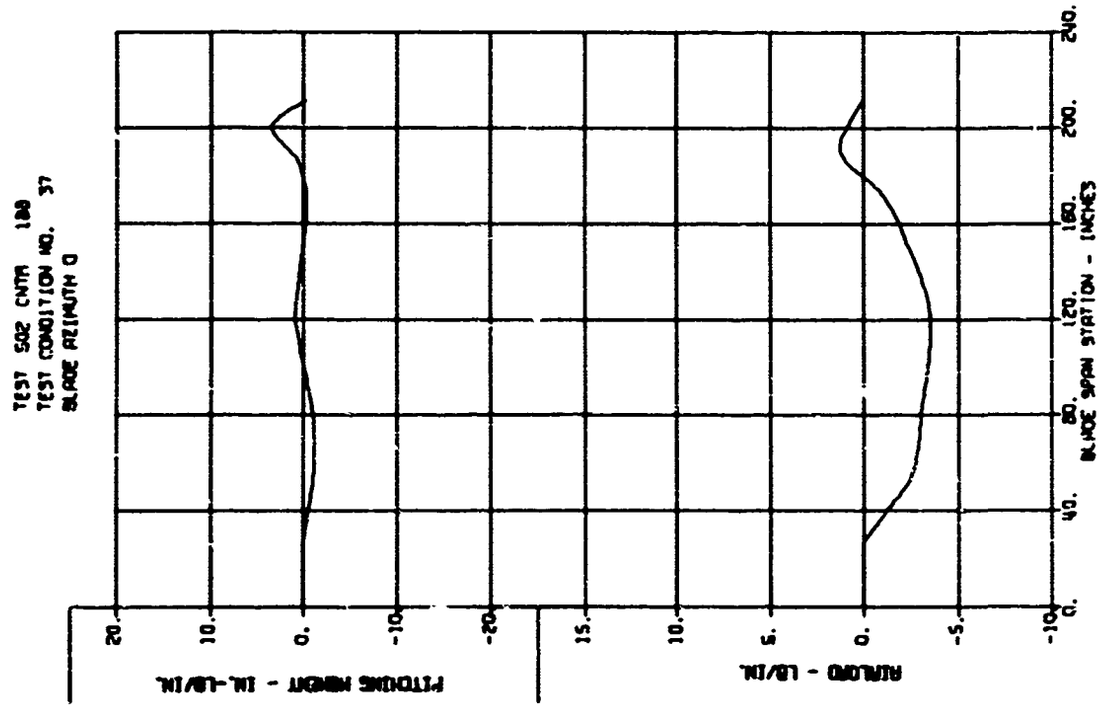

BLADE LOADS VERSUS SPAN - DYNAMIC COMPONENTS

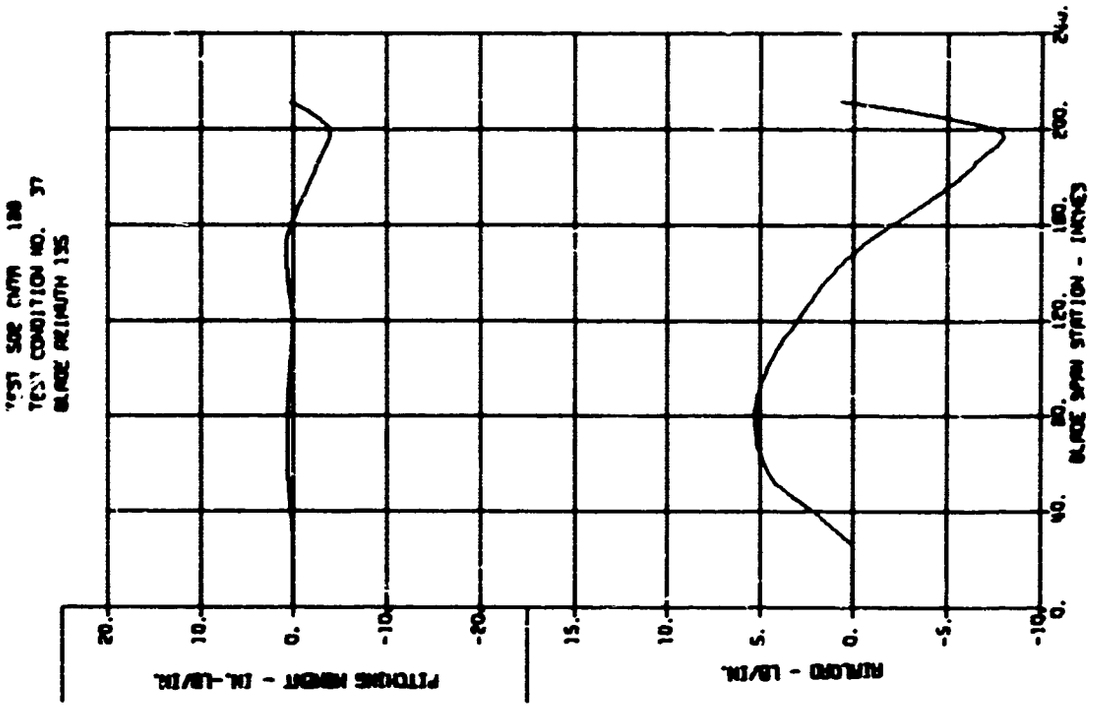

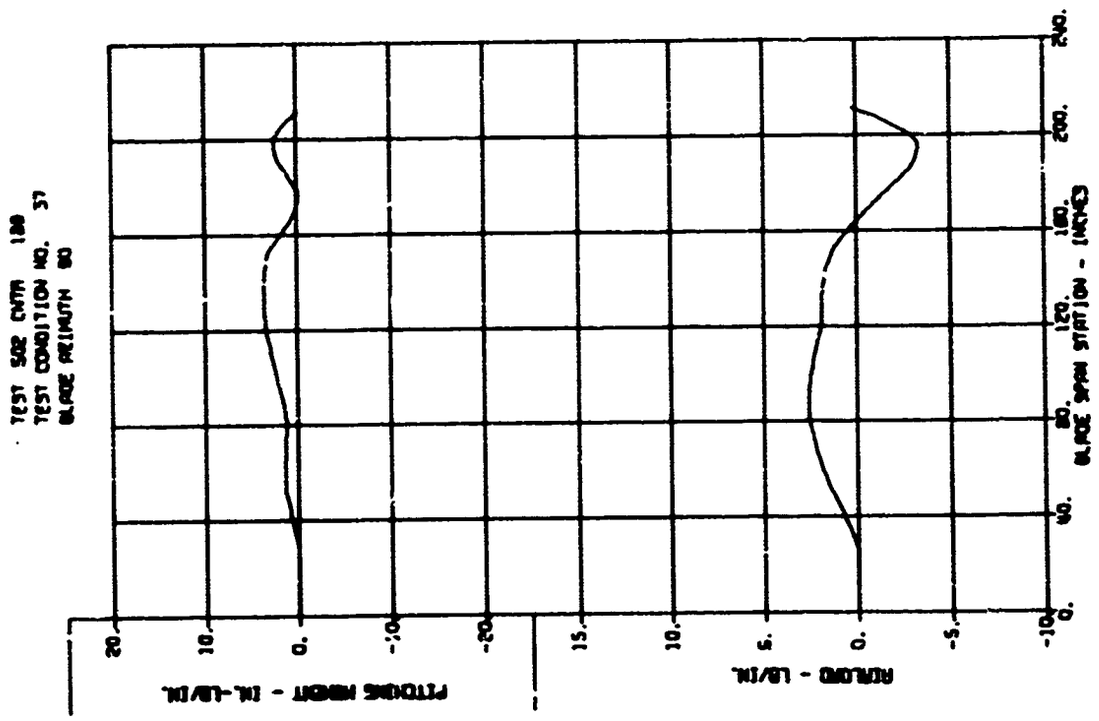

BLADE LOADS VERSUS SPAN - DYNAMIC COMPONENTS

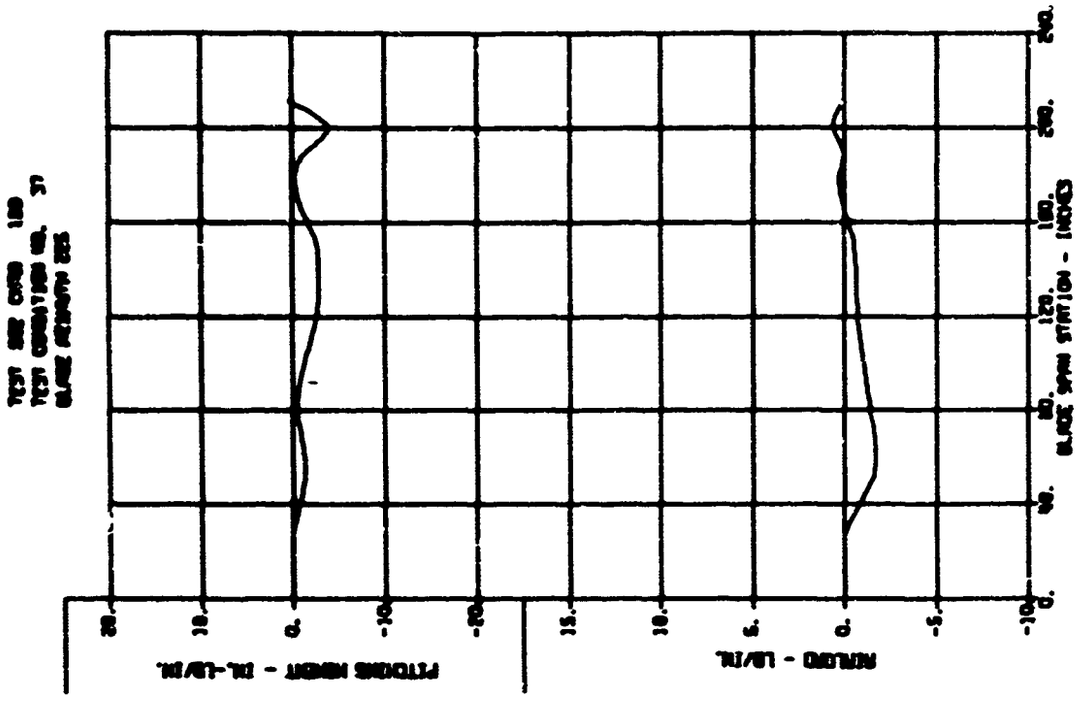

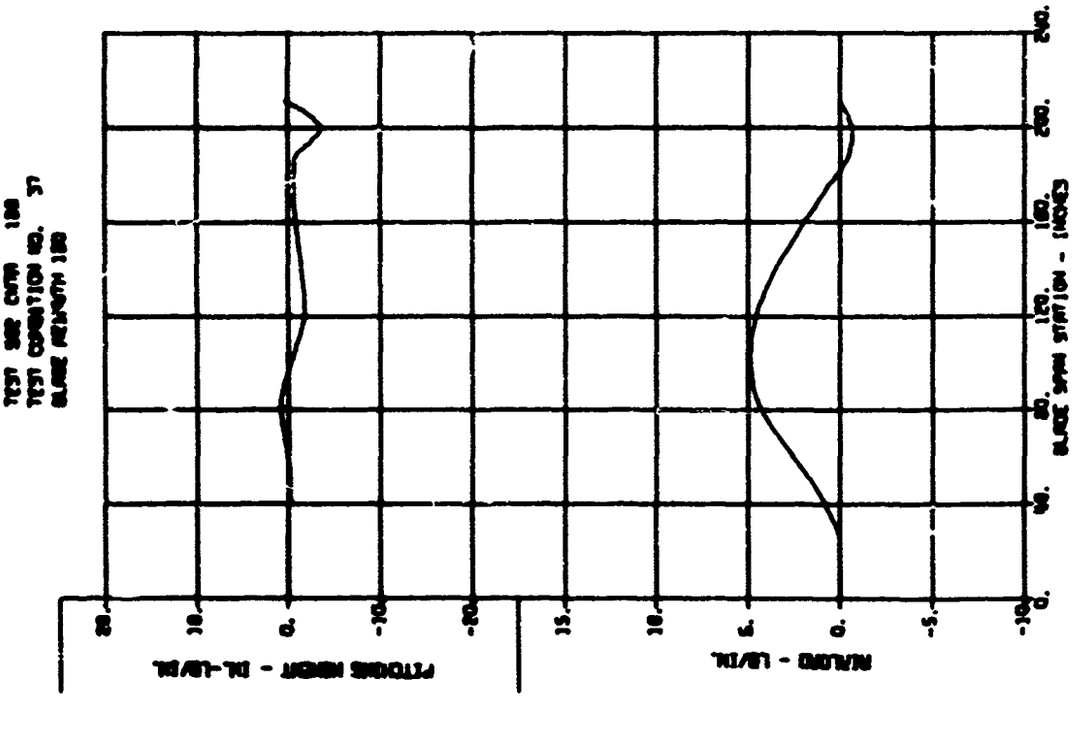

BLADE LOADS VERSUS SPAN - DYNAMIC COMPONENTS

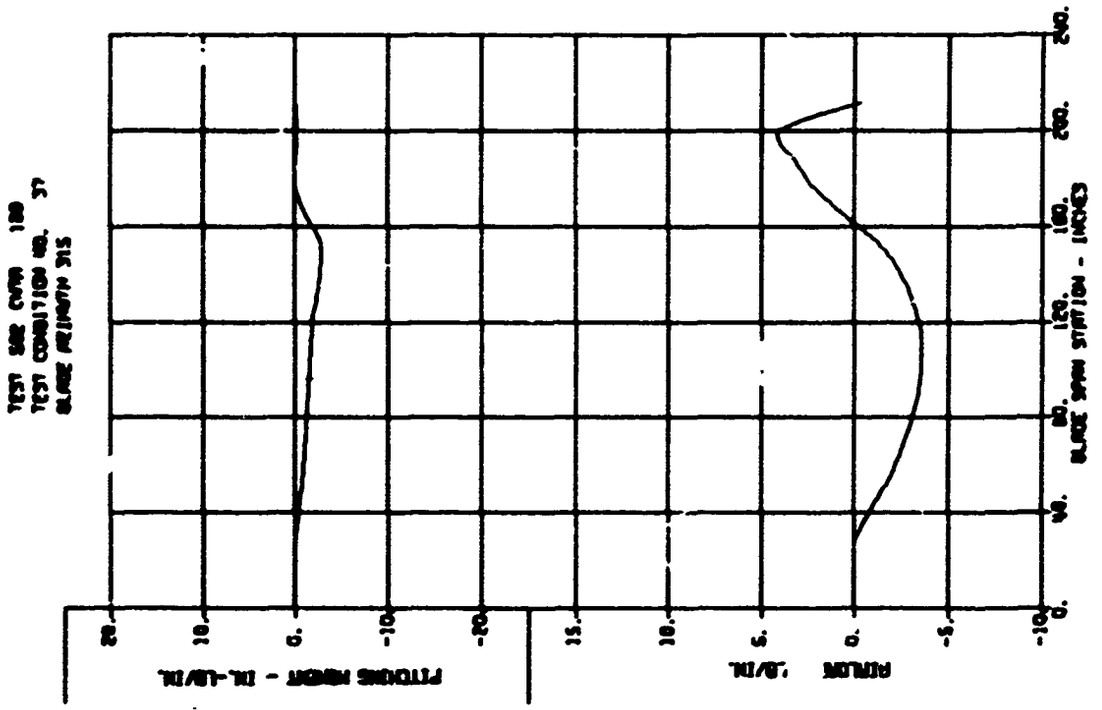

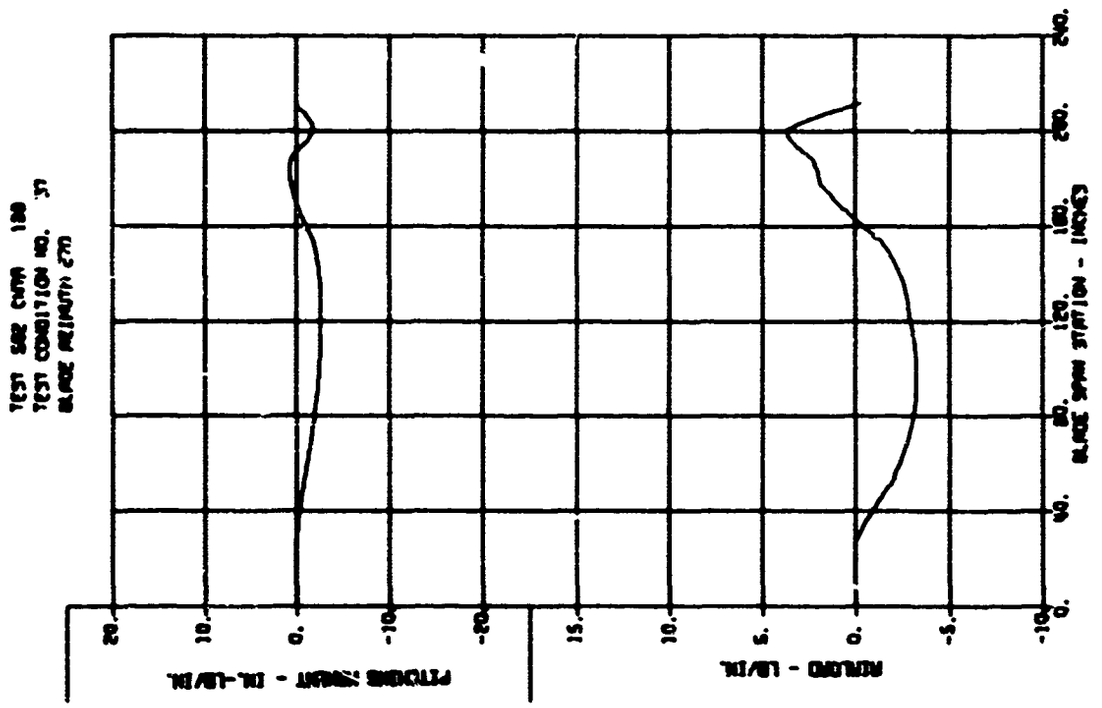

BLADE LOADS VERSUS SPAN - DYNAMIC COMPONENTS

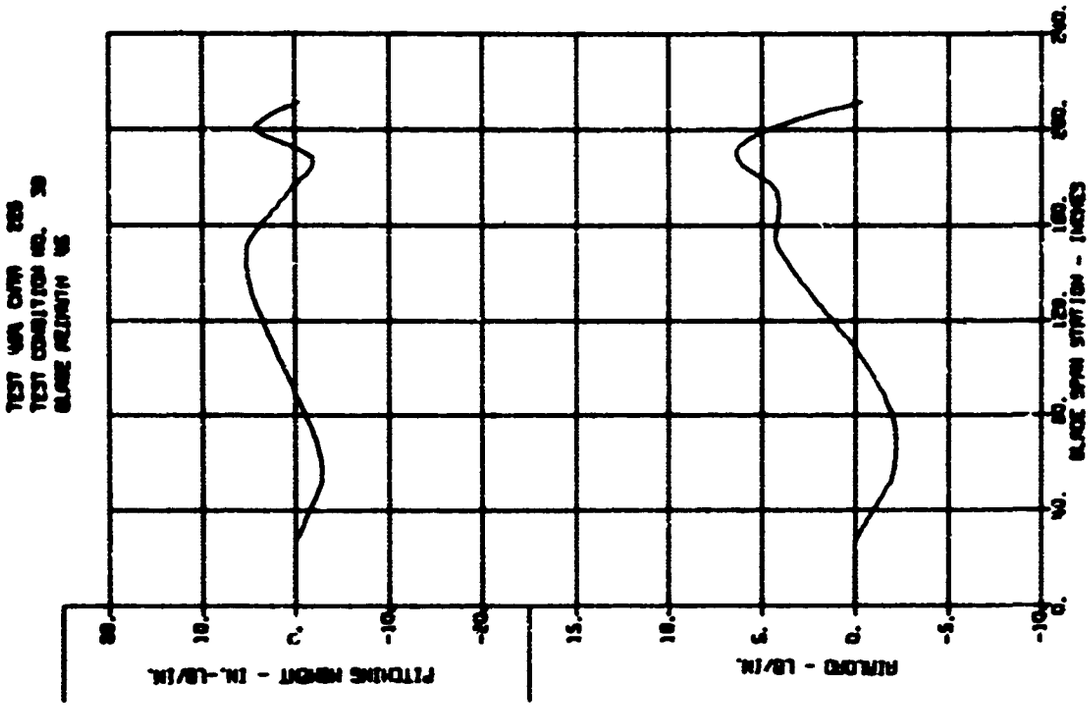

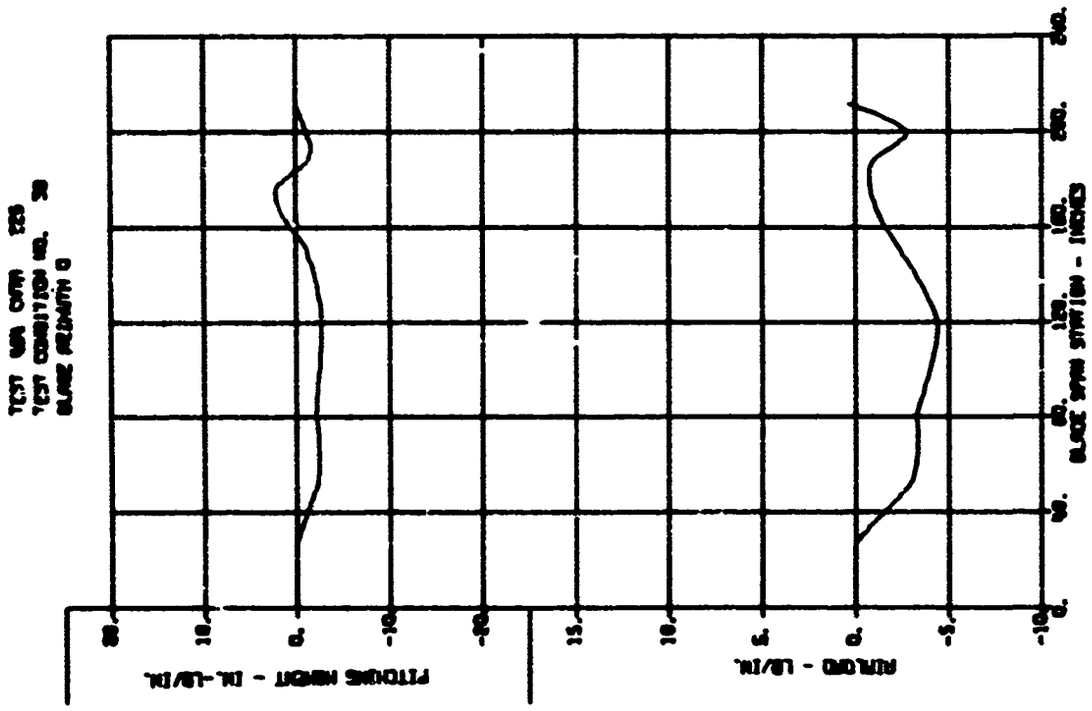

BLADE LOADS VERSUS SPAN - DYNAMIC COMPONENTS

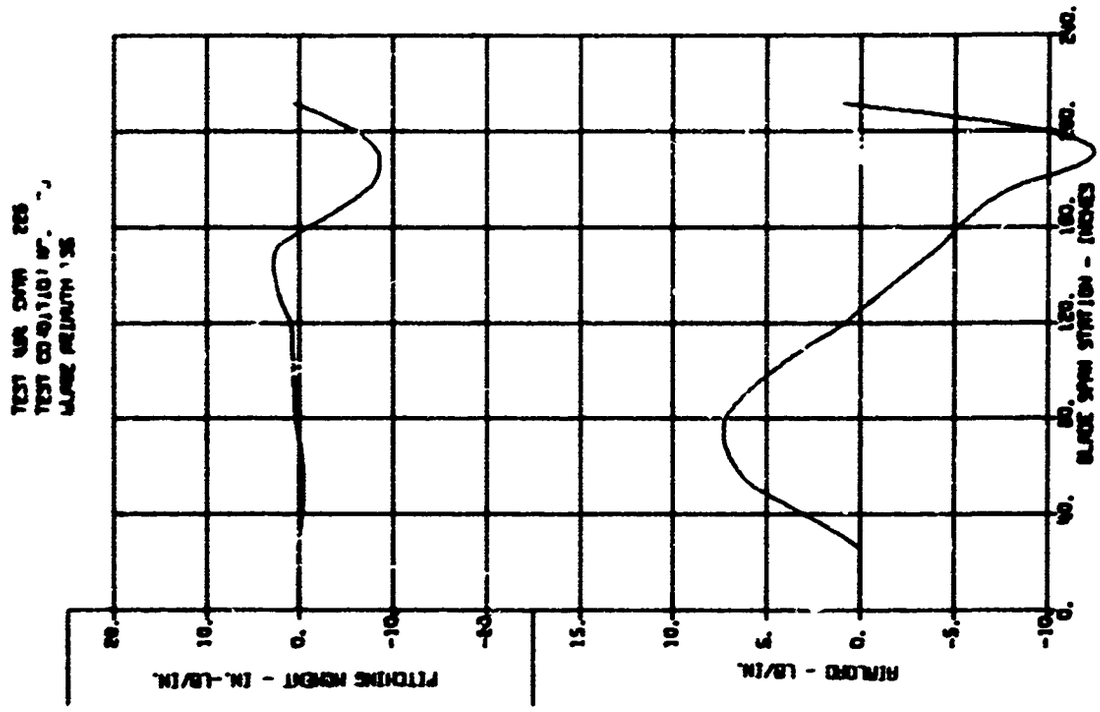

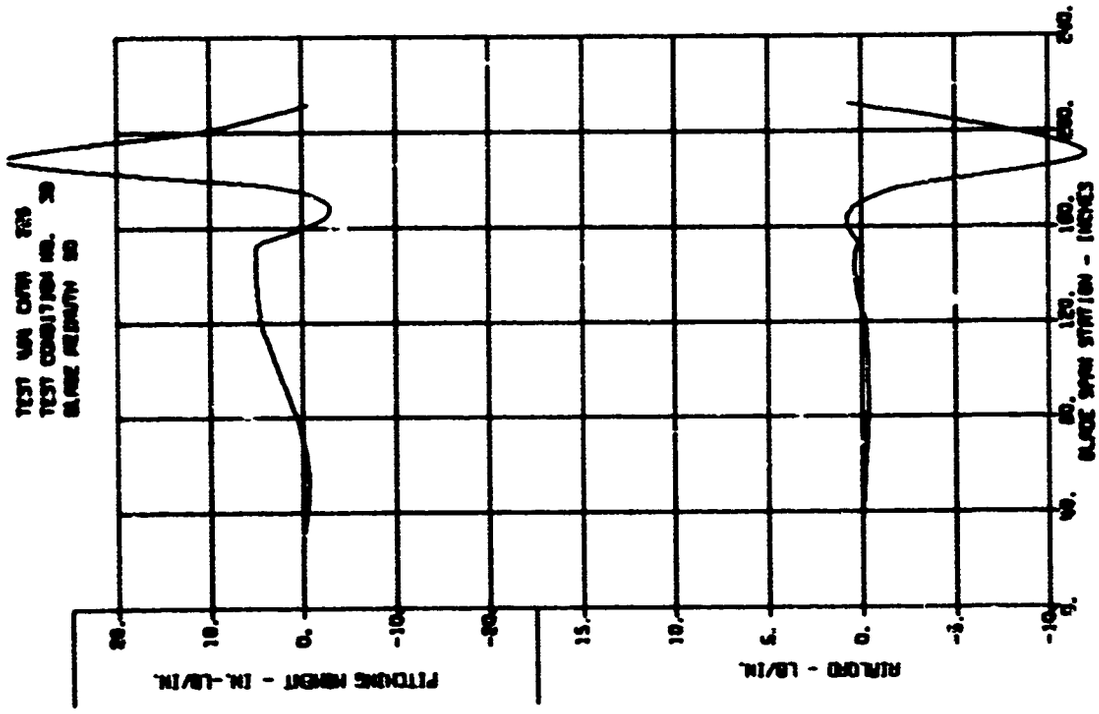

BLADE LOADS VERSUS SPAN - DYNAMIC COMPONENTS

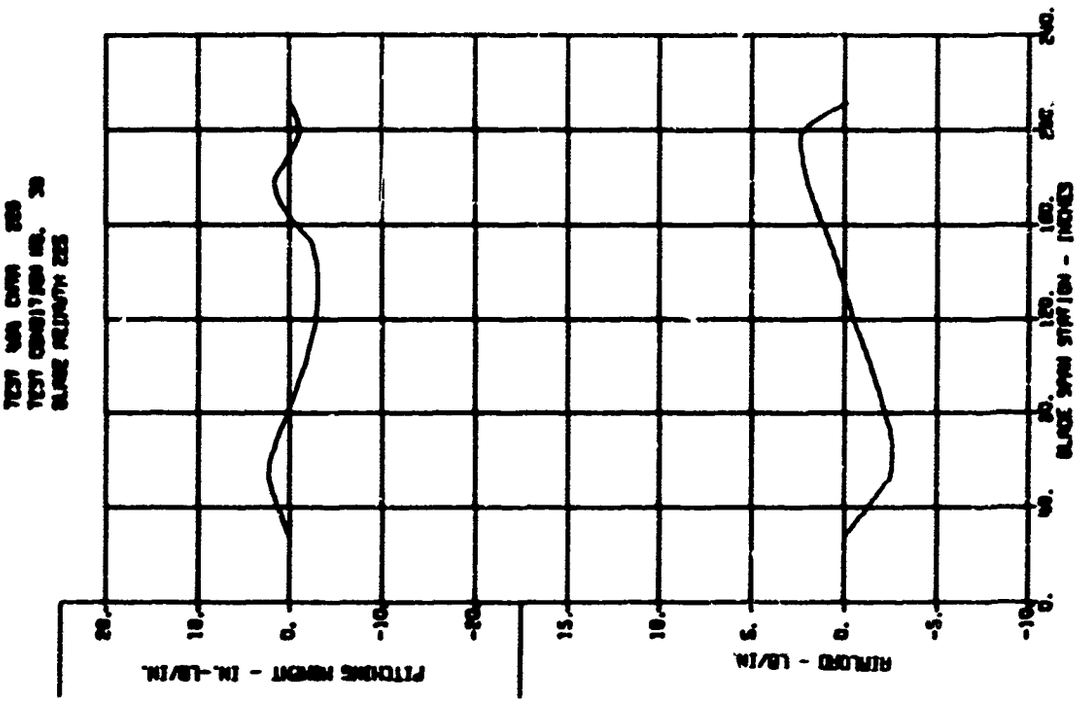

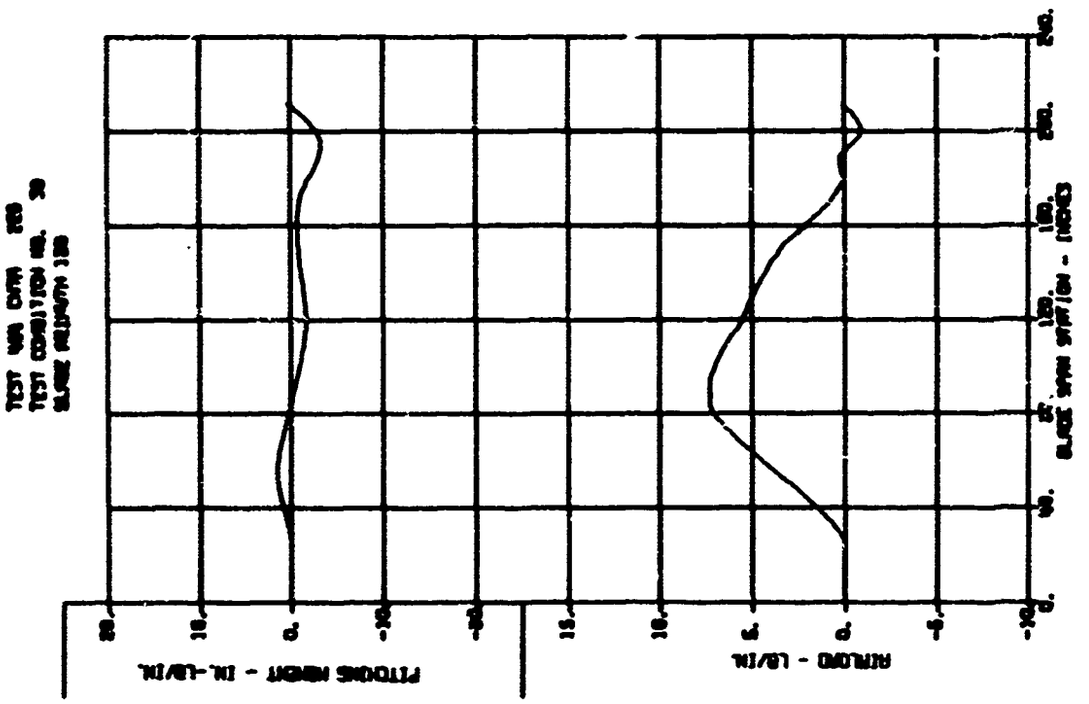

BLADE LOADS VERSUS SPAN - DYNAMIC COMPONENTS

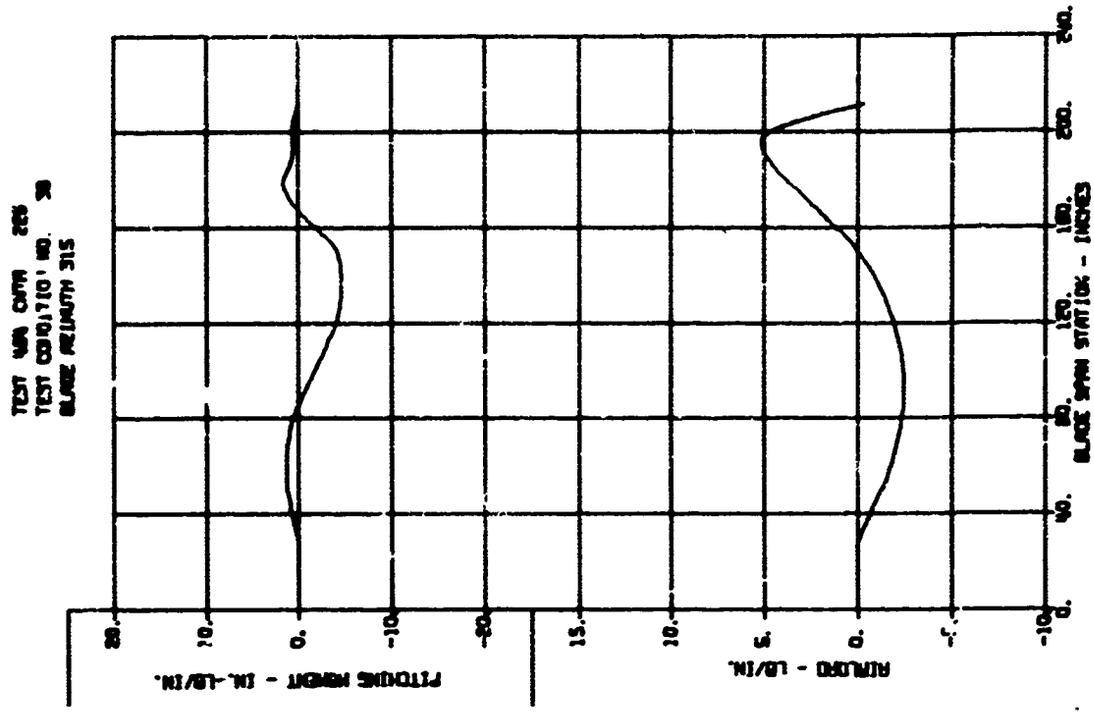

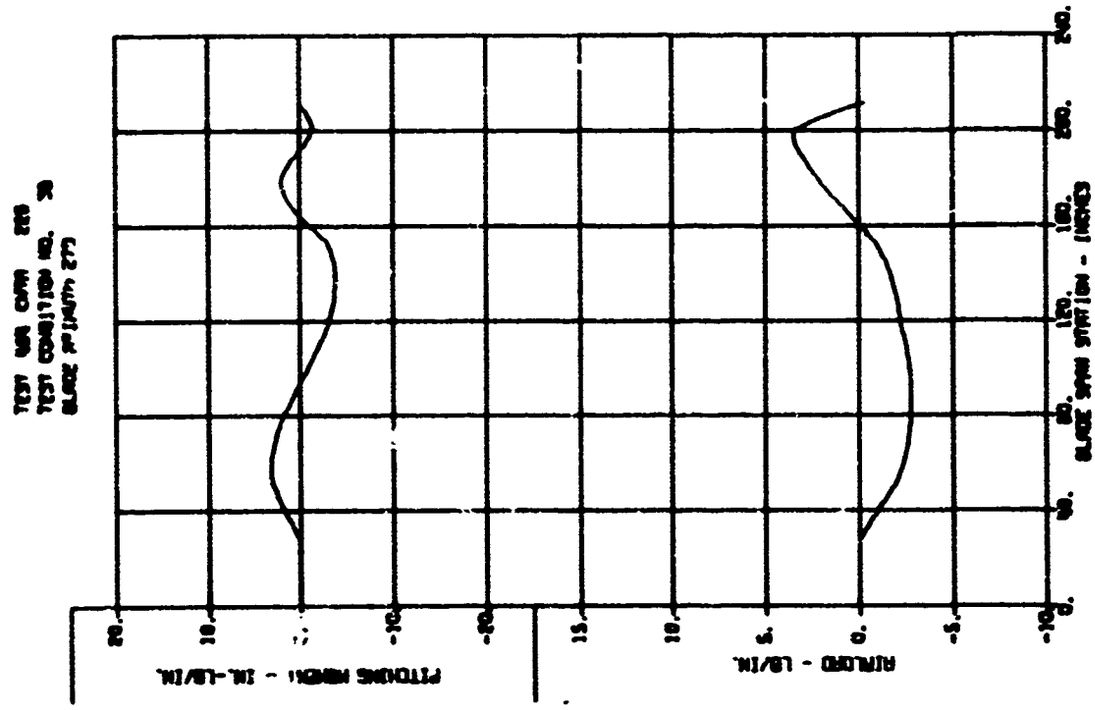

BLADE LOADS VERSUS SPAN - DYNAMIC COMPONENTS

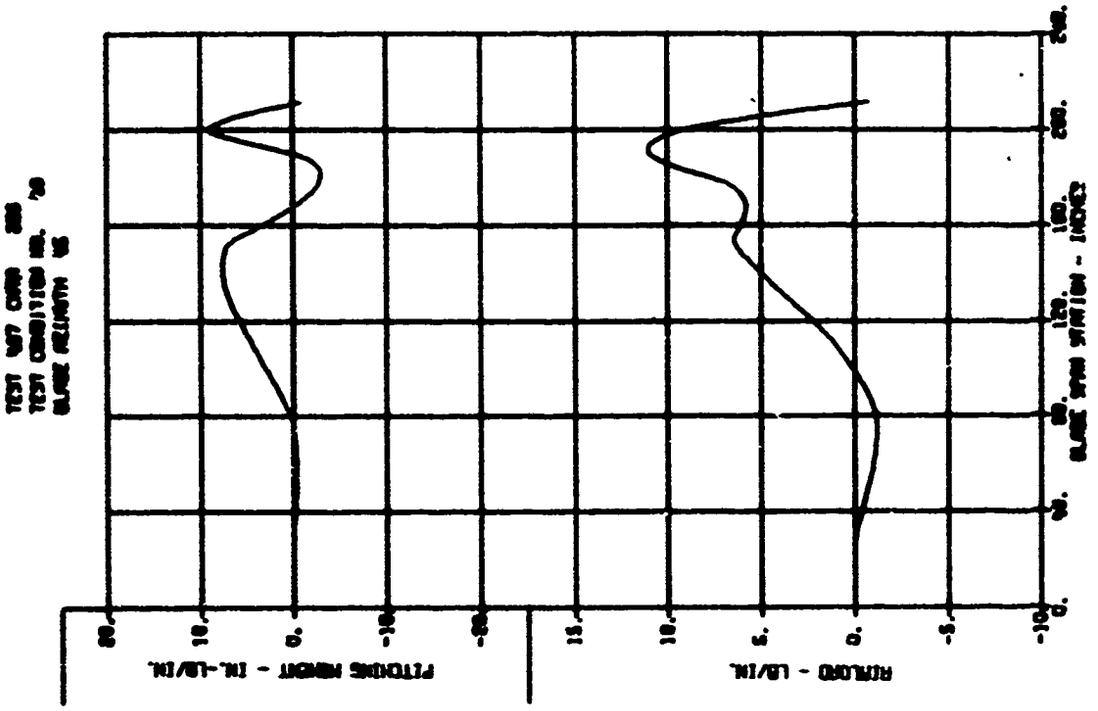

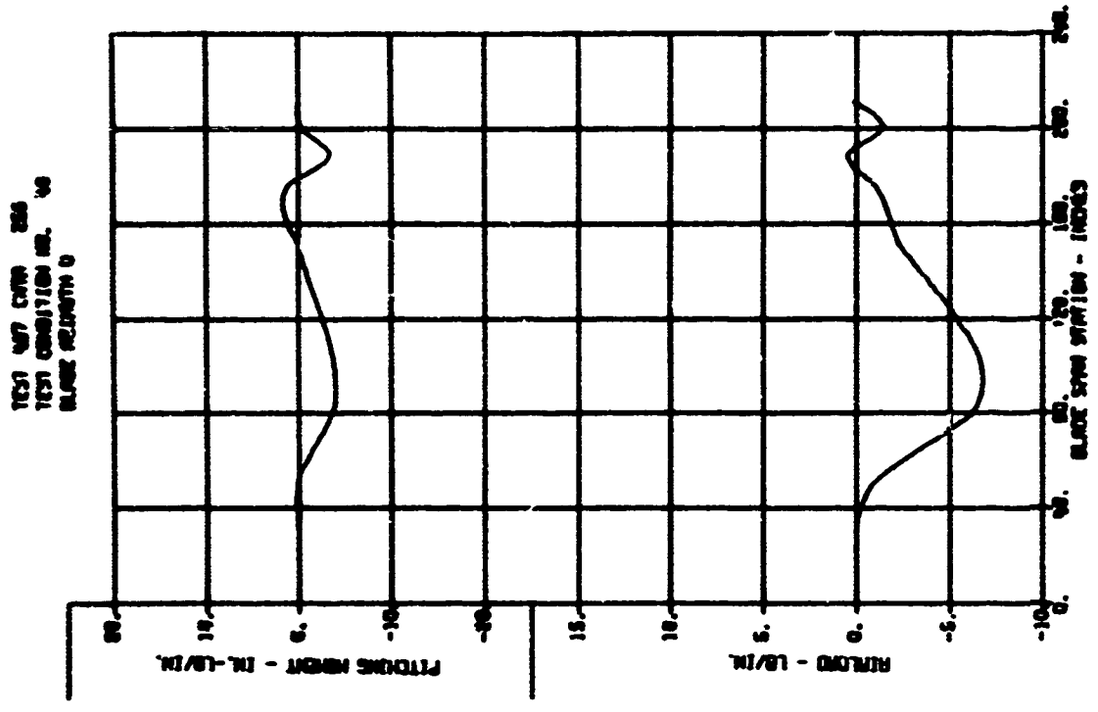

BLADE LOADS VERSUS SPAN - DYNAMIC COMPONENTS

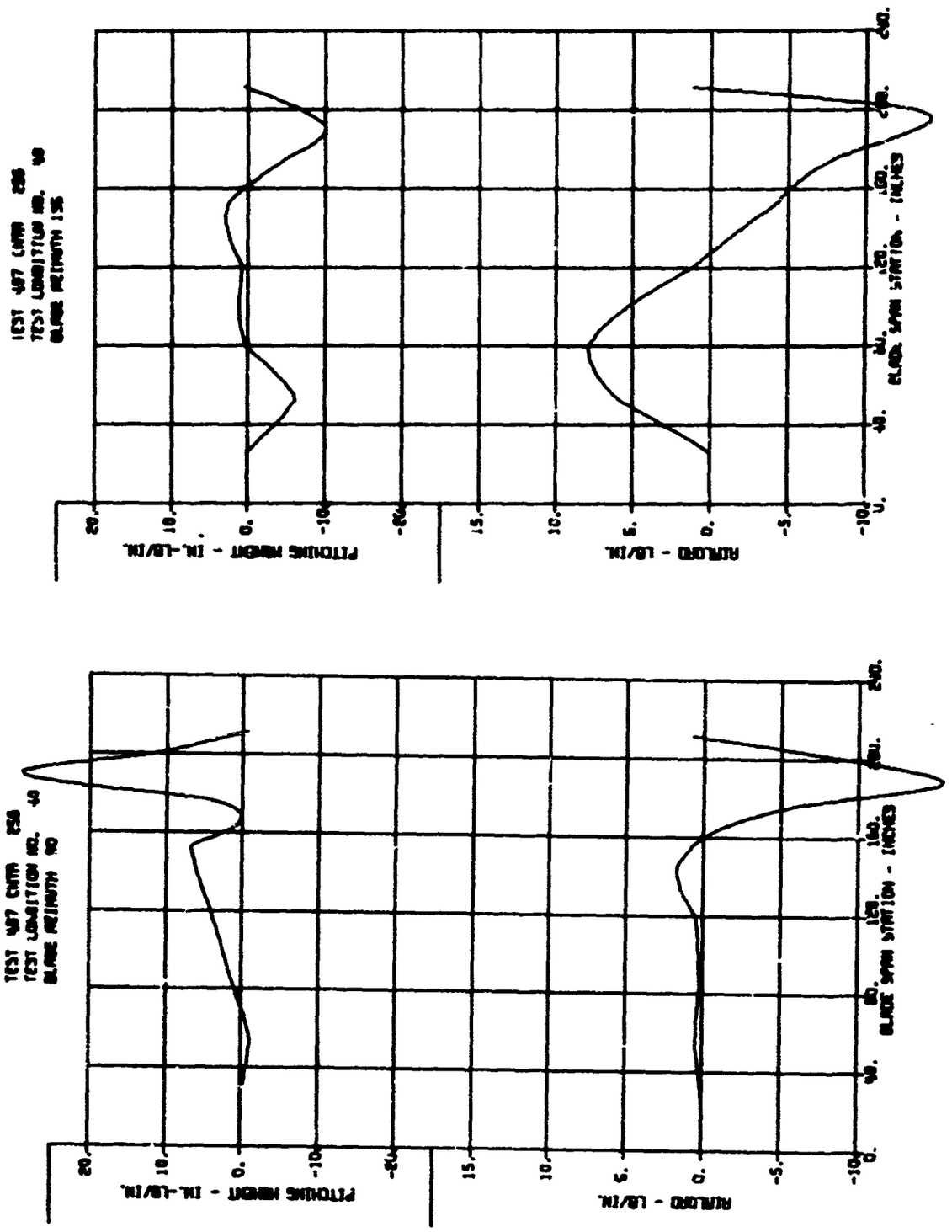

BLADE LOADS VERSUS SPAN - DYNAMIC COMPONENTS

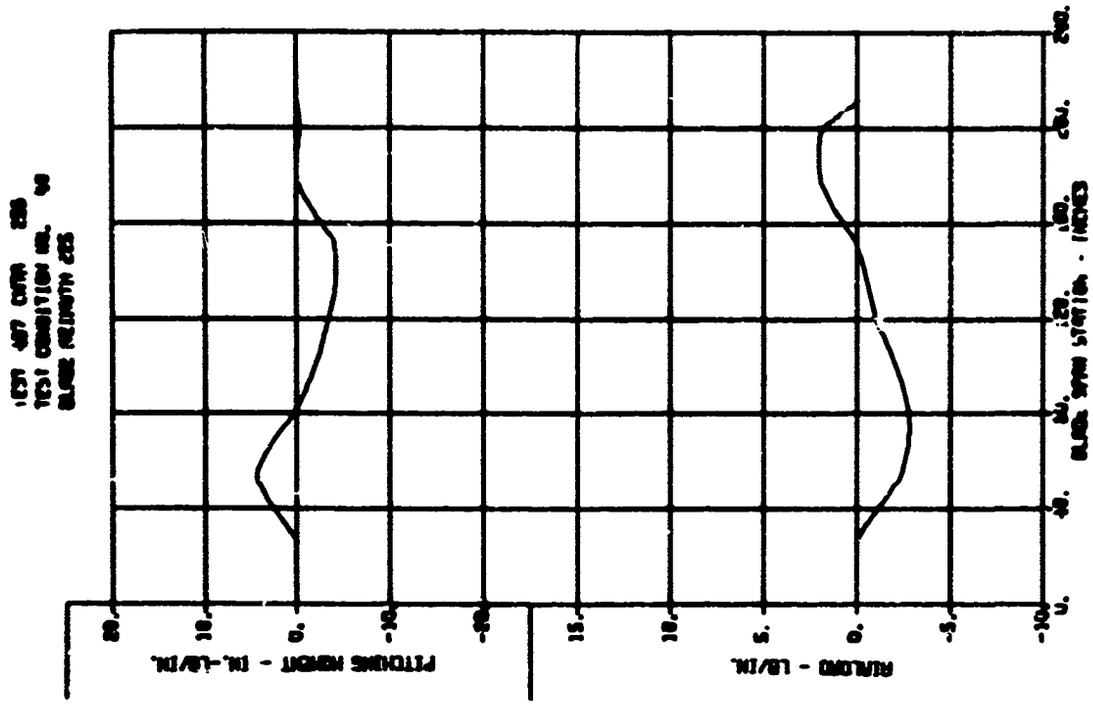

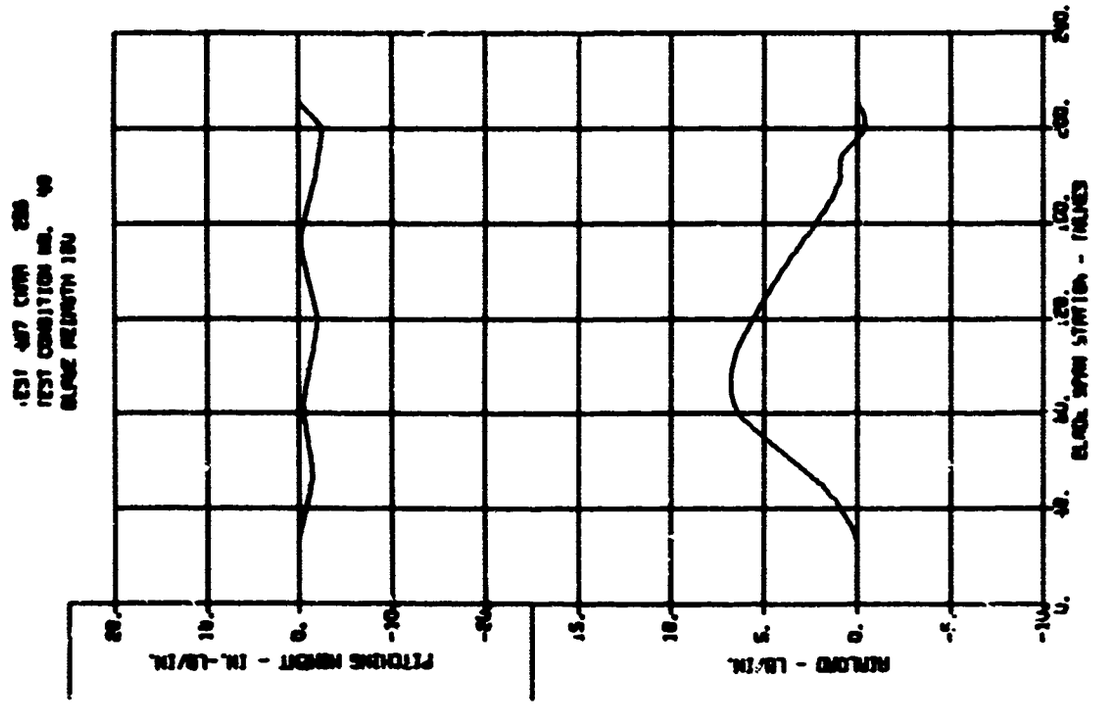

BLADE LOADS VERSUS SPAN - DYNAMIC COMPONENTS

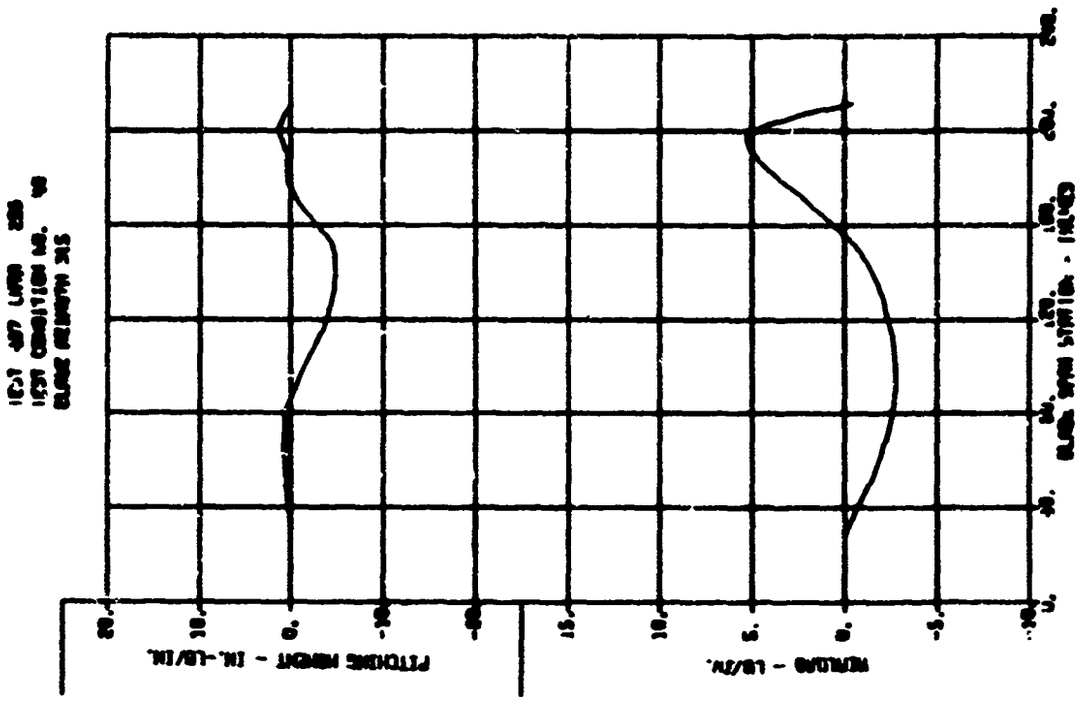

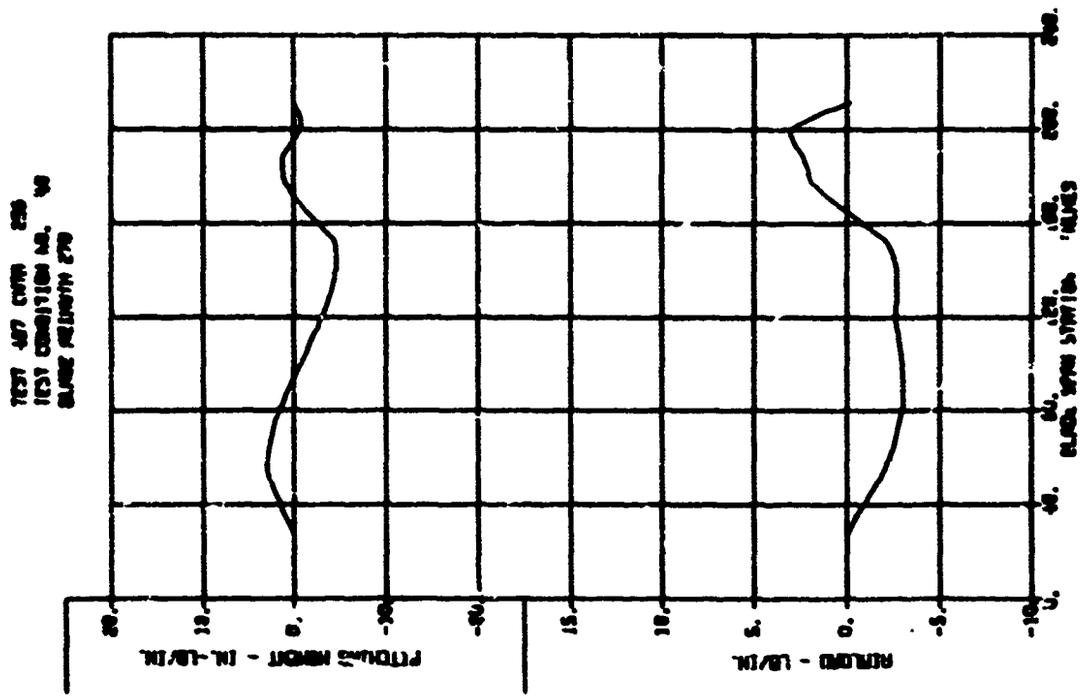

BLADE LOADS VERSUS SPAN - DYNAMIC COMPONENTS

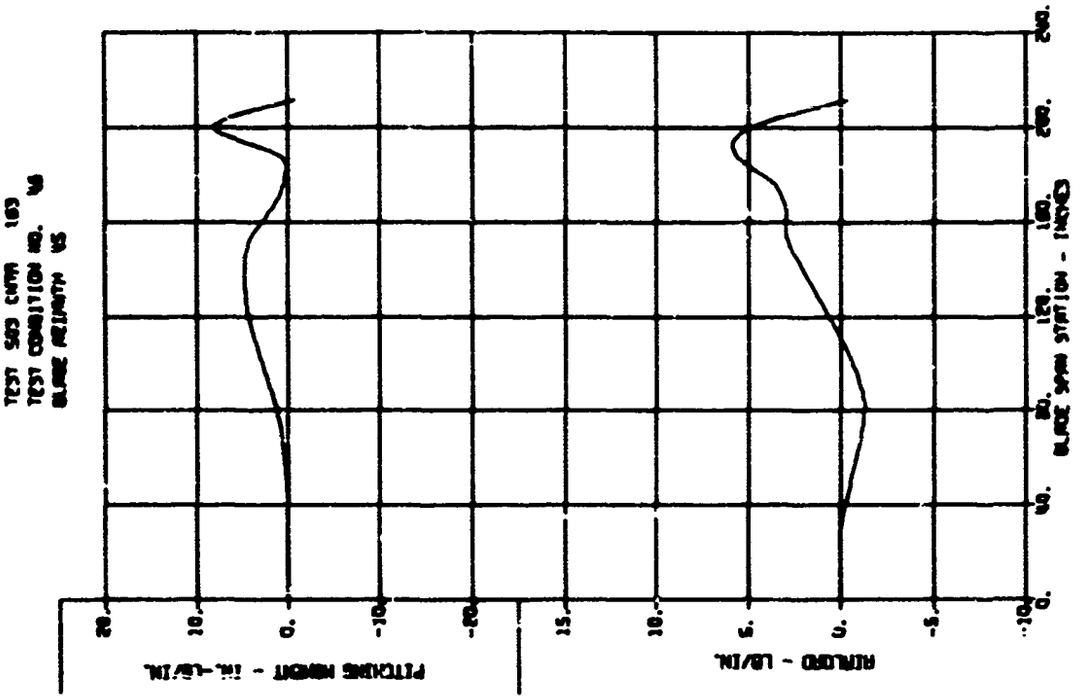

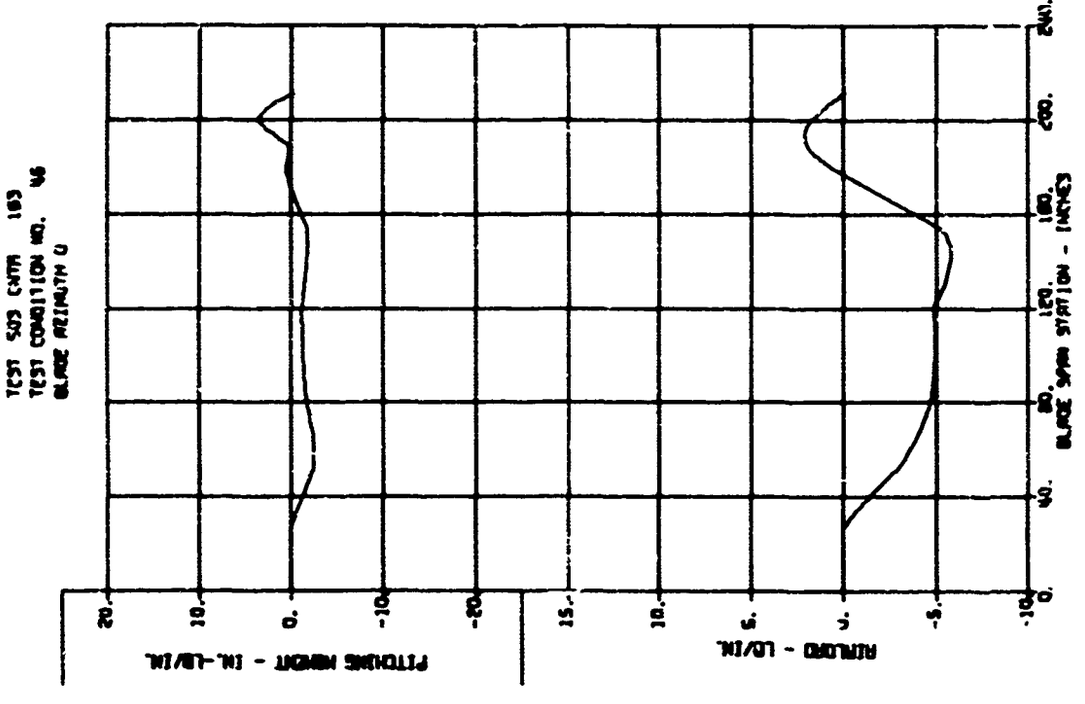

BLADE LOADS VERSUS SPAN - DYNAMIC COMPONENTS

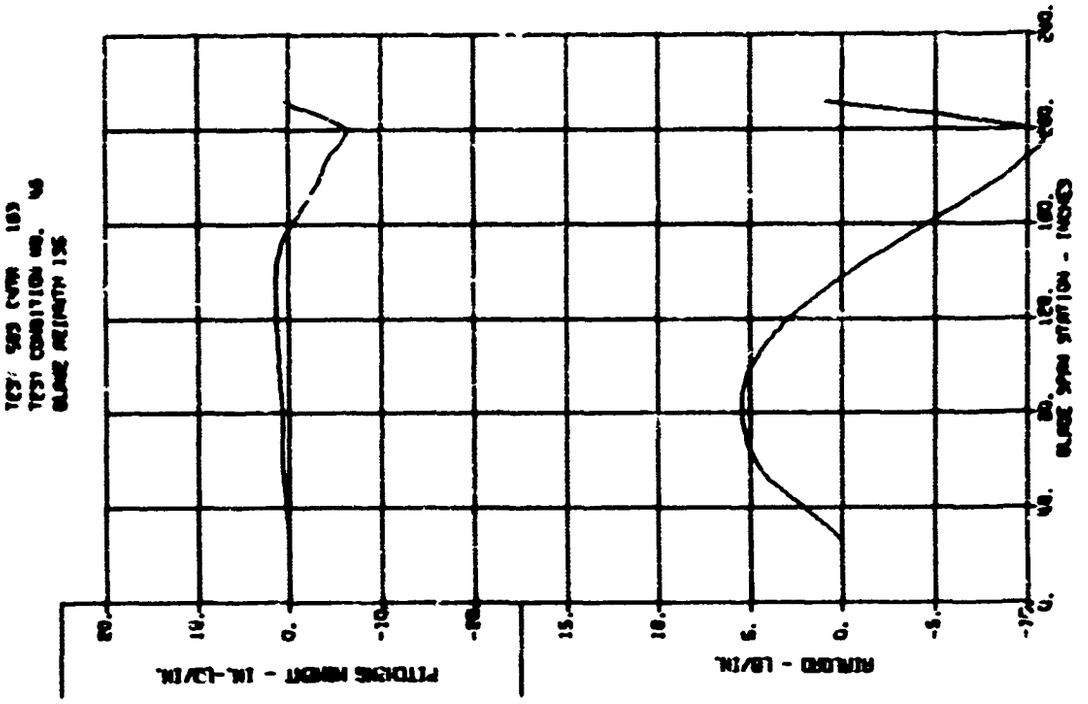

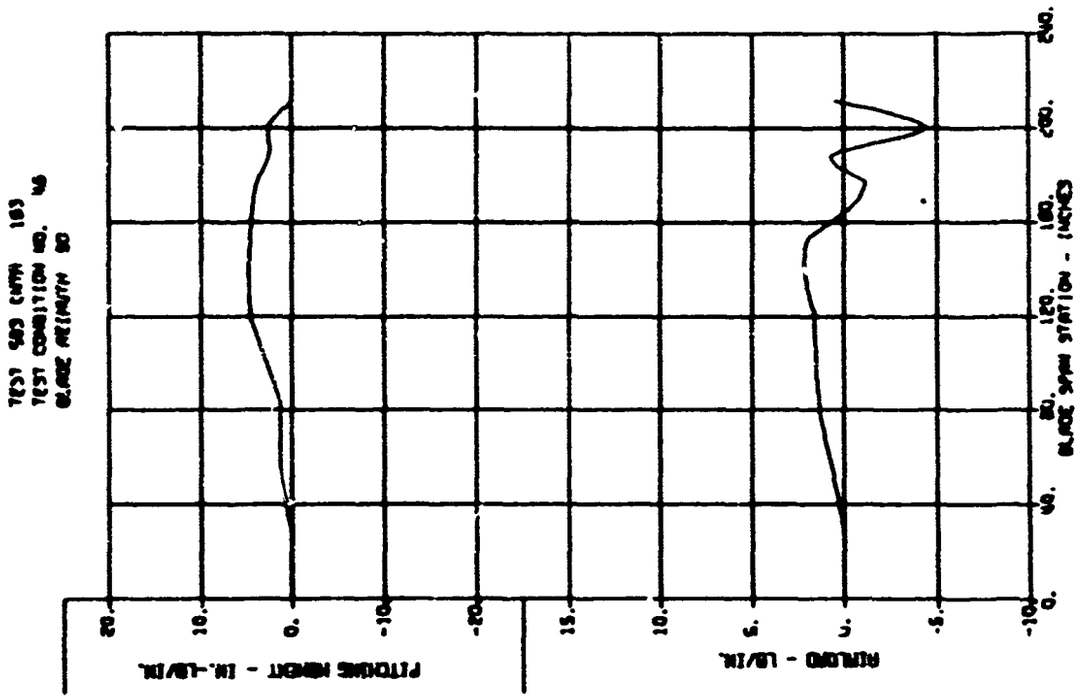

BLADE LOA.3 VERSUS SPAN - DYNAMIC COMPONENTS

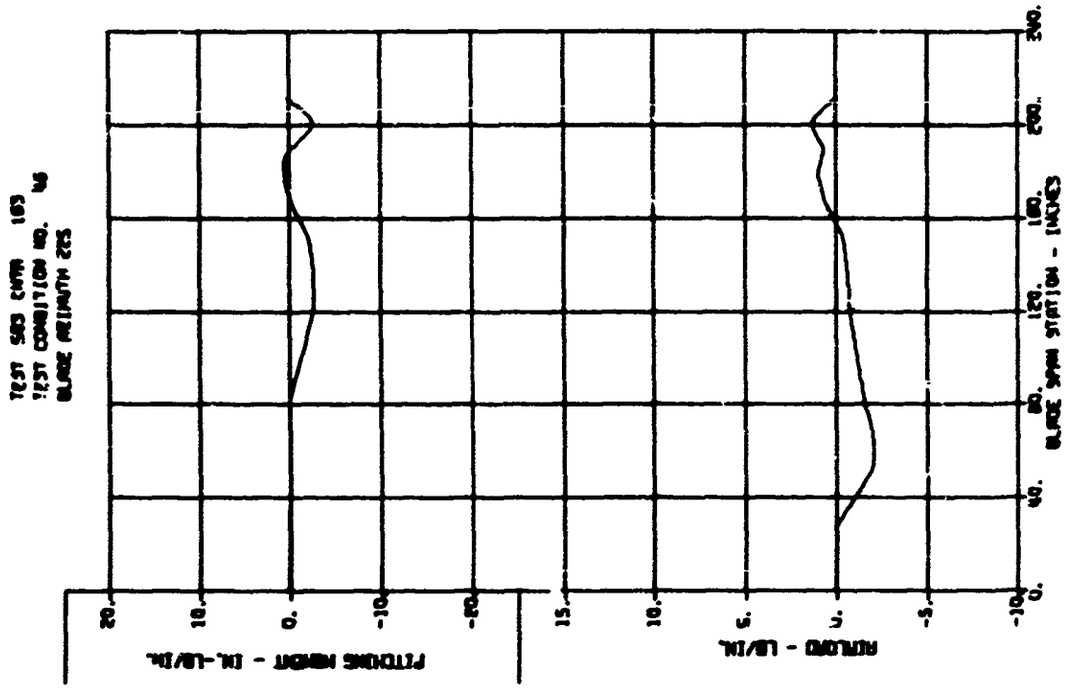

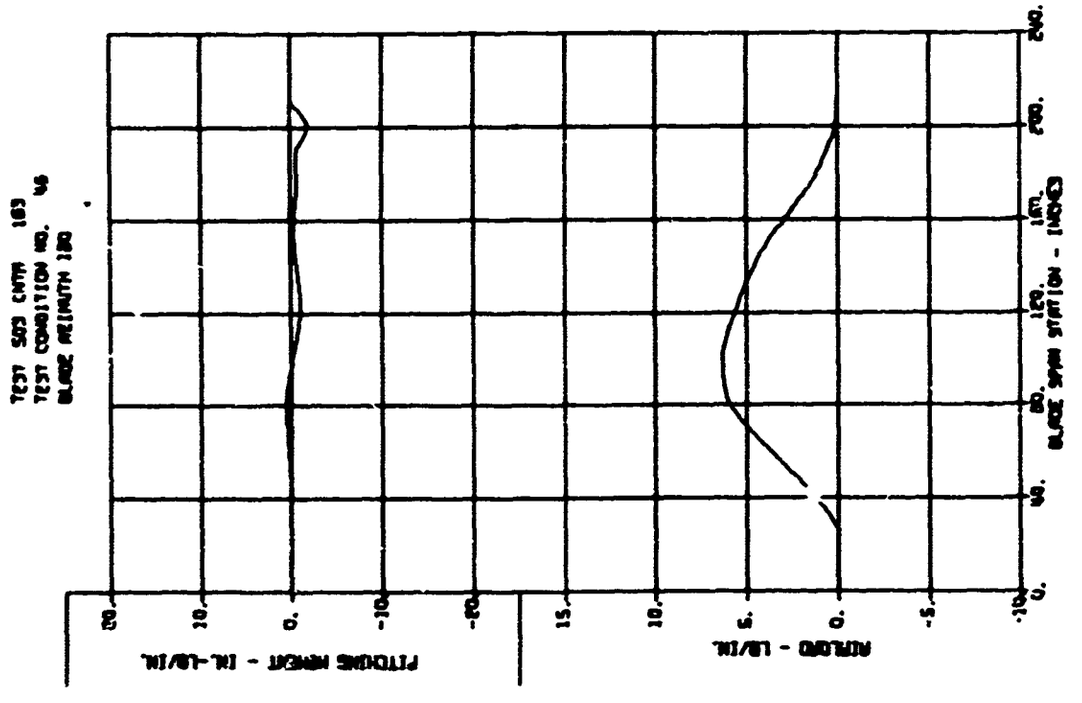

BLADE LOADS VERSUS SPAN - DYNAMIC COMPONENTS

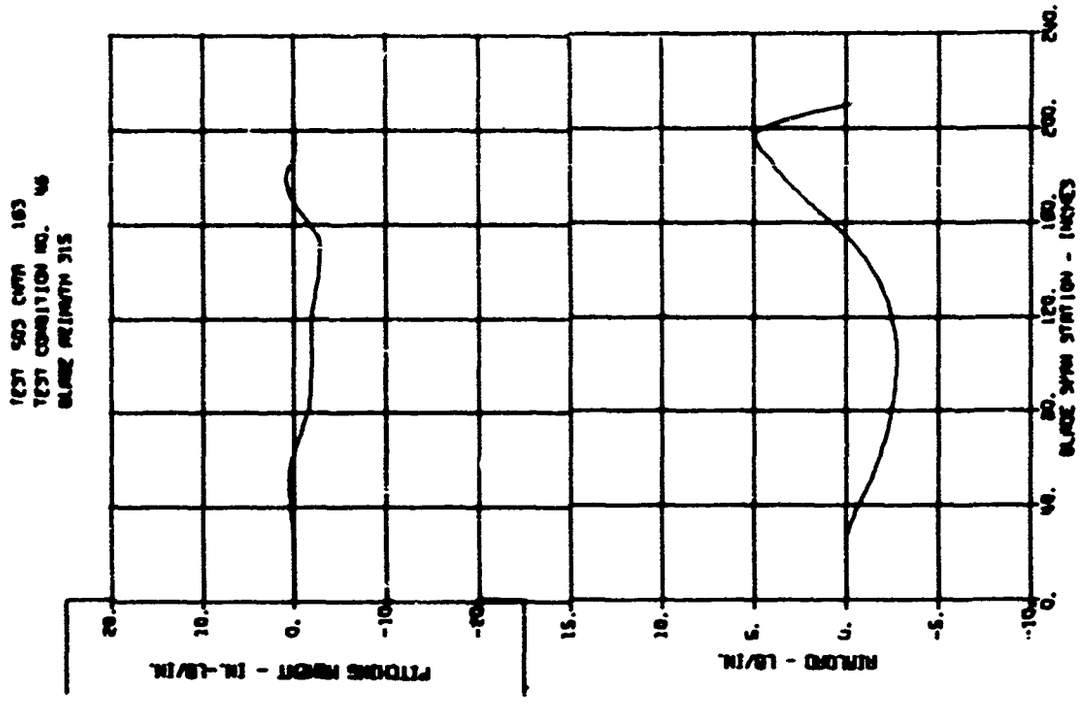

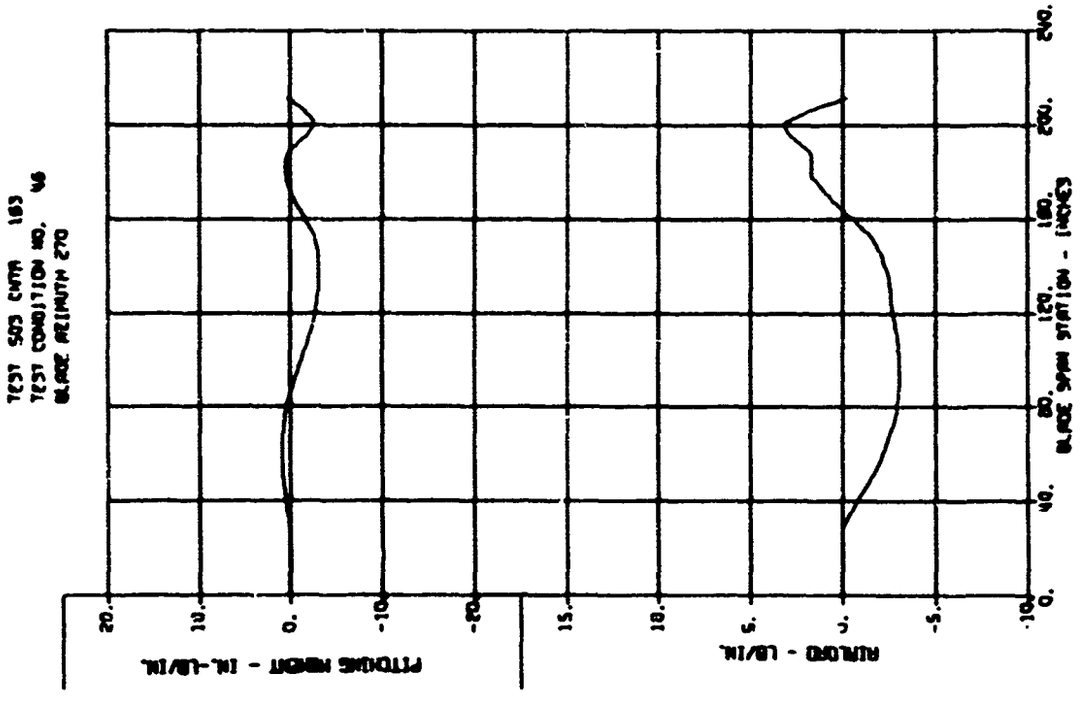

BLADE LOADS VERSUS SPAN - DYNAMIC COMPONENTS

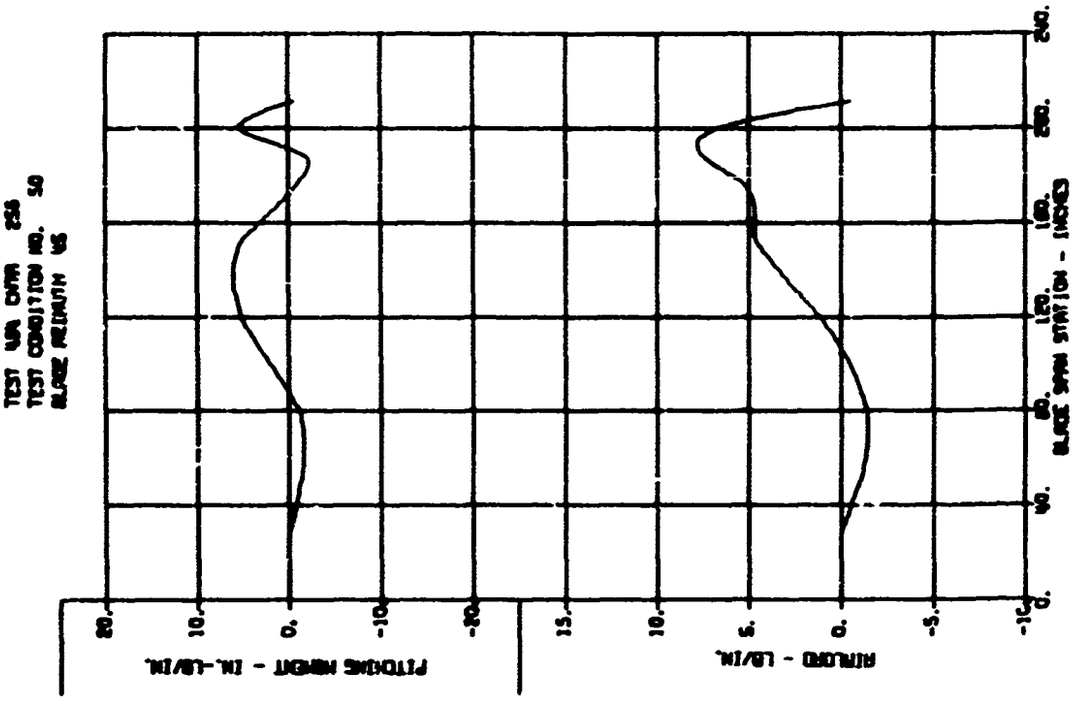

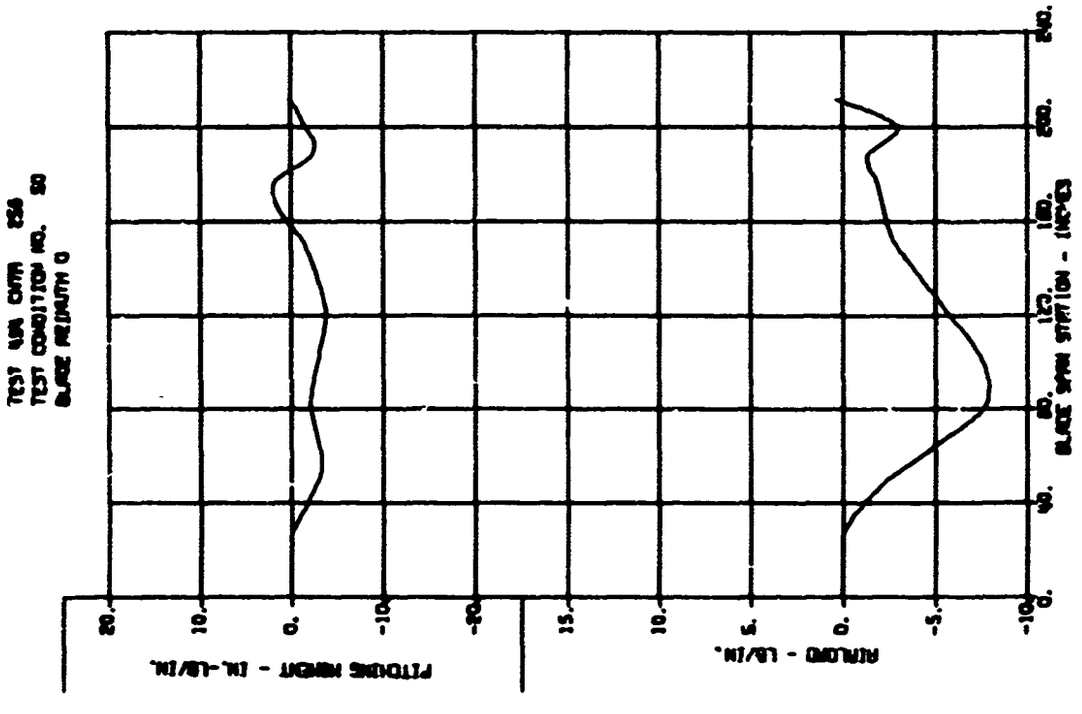

BLADE LOADS VERSUS SPAN - DYNAMIC COMPONENTS

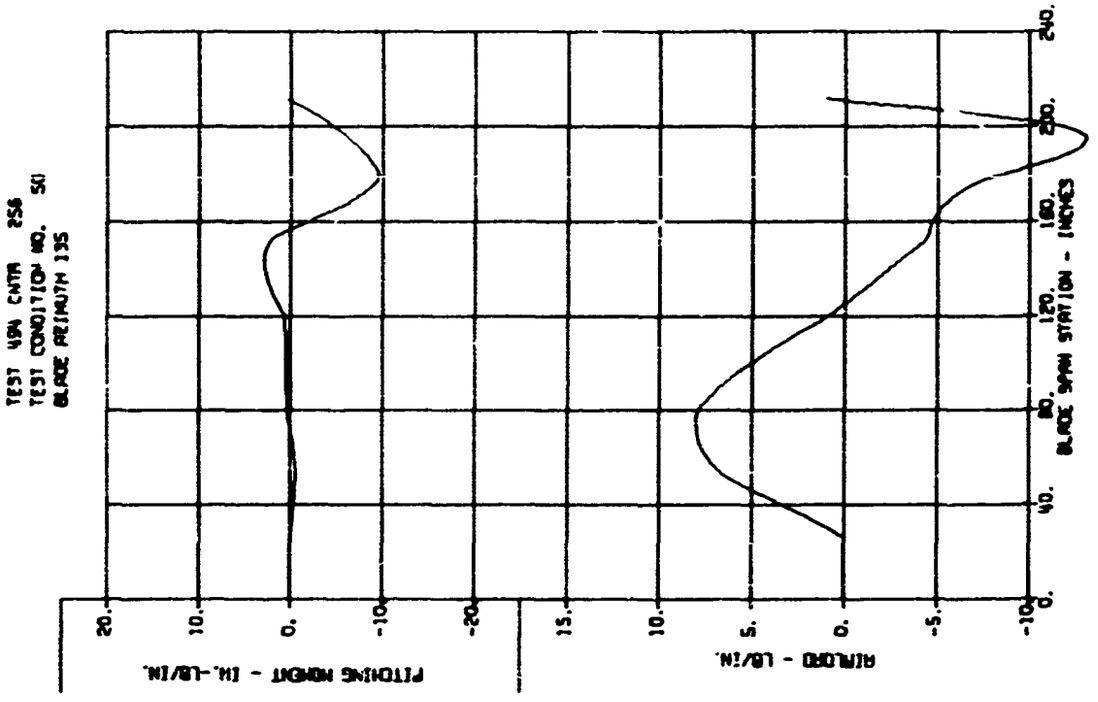

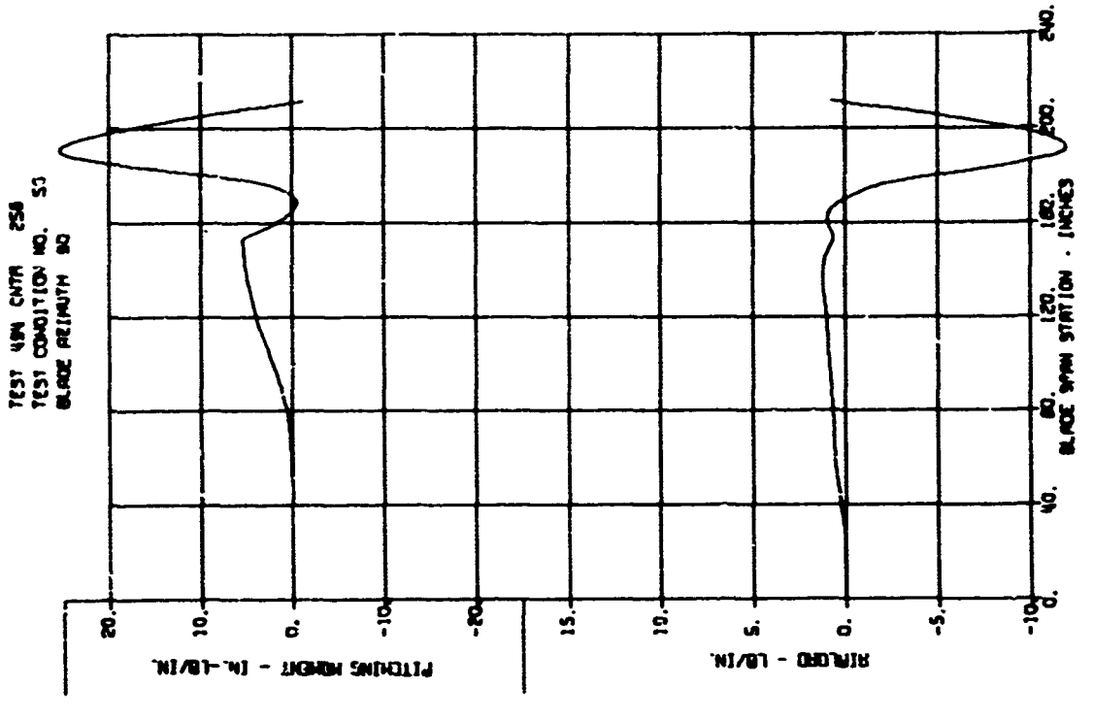

BLADE LOADS VERSUS SPAN - DYNAMIC COMPONENTS

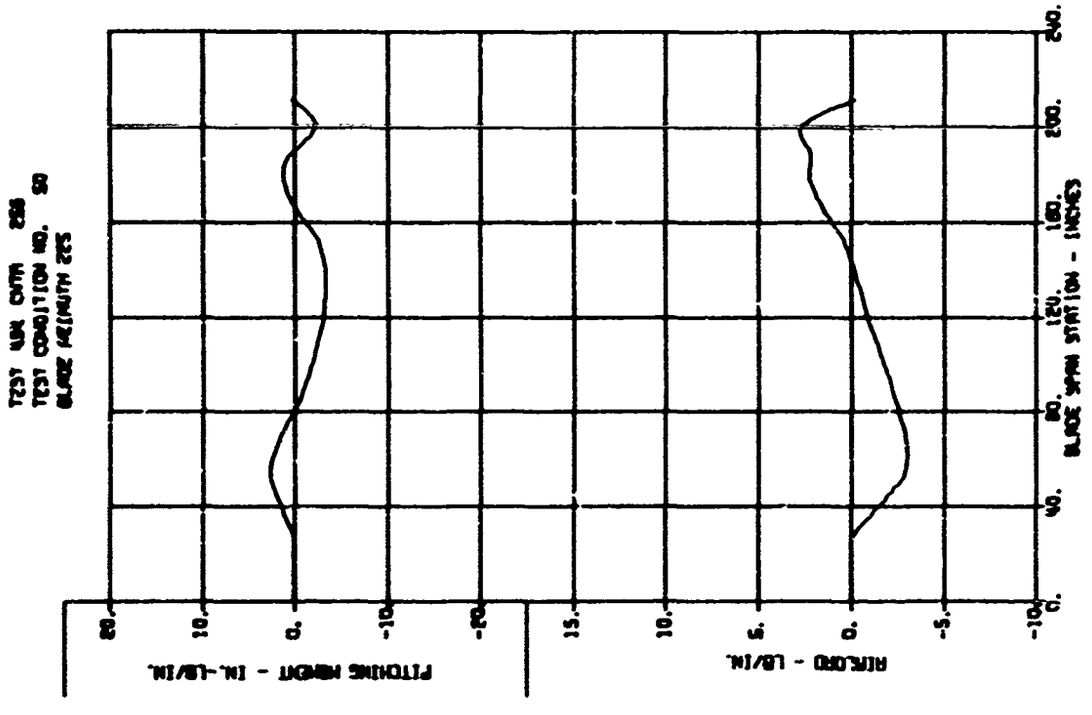

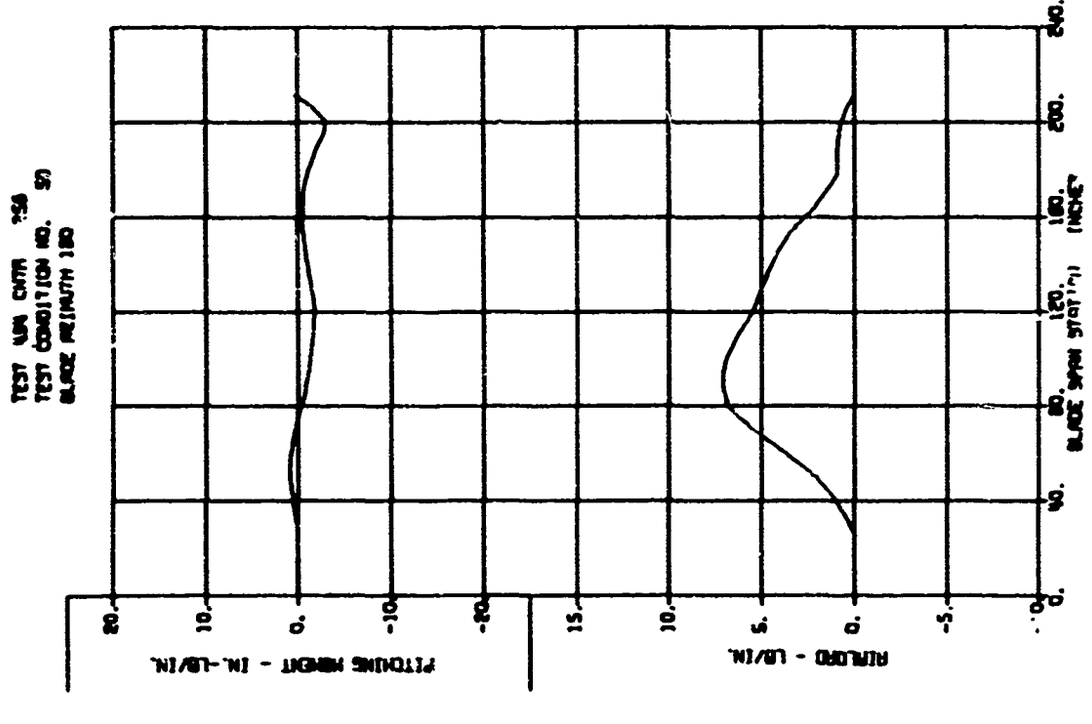

BLADE LOADS VERSUS SPAN - DYNAMIC COMPONENTS

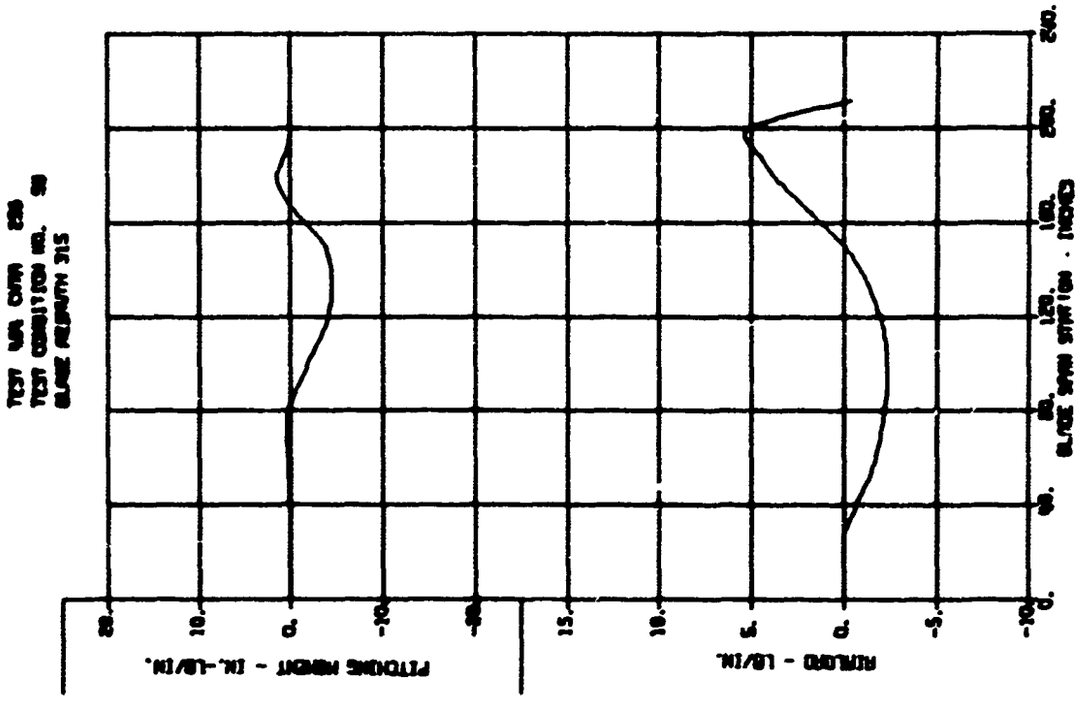

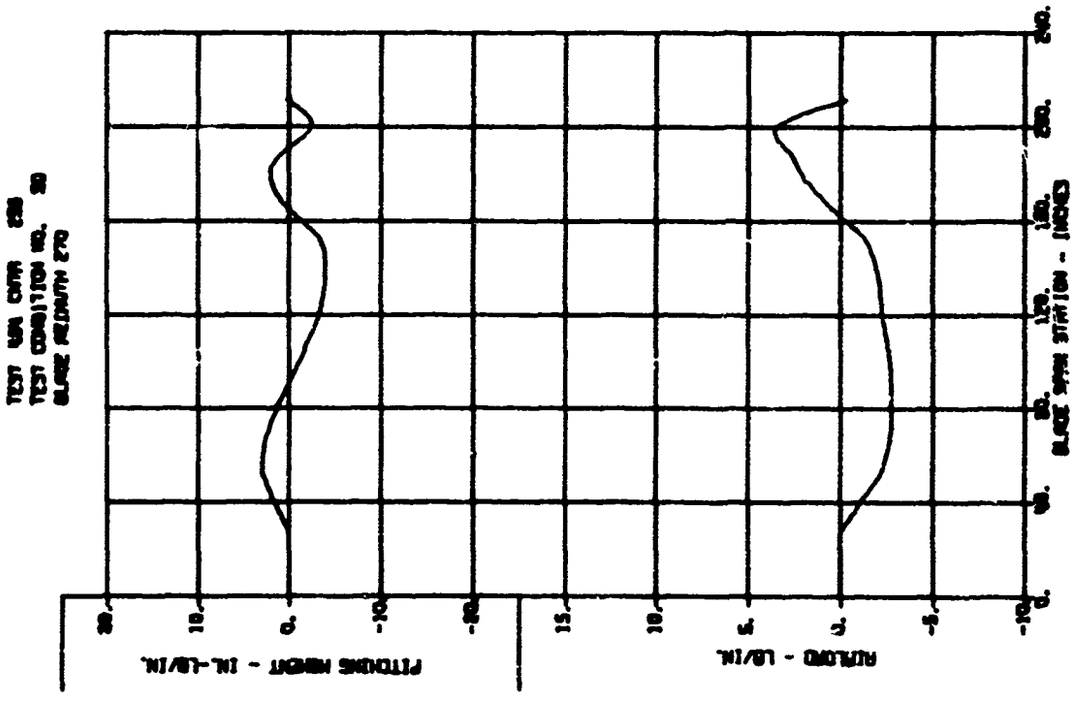

APPENDIX III

BLADE LOADS VERSUS SPAN - STATIC COMPONENTS

This appendix contains the plottings of the static components of the air-loads (in pounds per inch) and pitching moments (in inch-pounds per inch) versus blade station for the 20 test conditions selected for full analysis. The identification "Blade Azimuth 360" means, in this case, that the static component is valid for all azimuth positions 0 through 360 degrees.

The corresponding dynamic components are shown in Appendix II. Tabulated data of the blade loads are listed in Appendix VII.

BLADE LOADS VERSUS SPAN - STATIC COMPONENTS

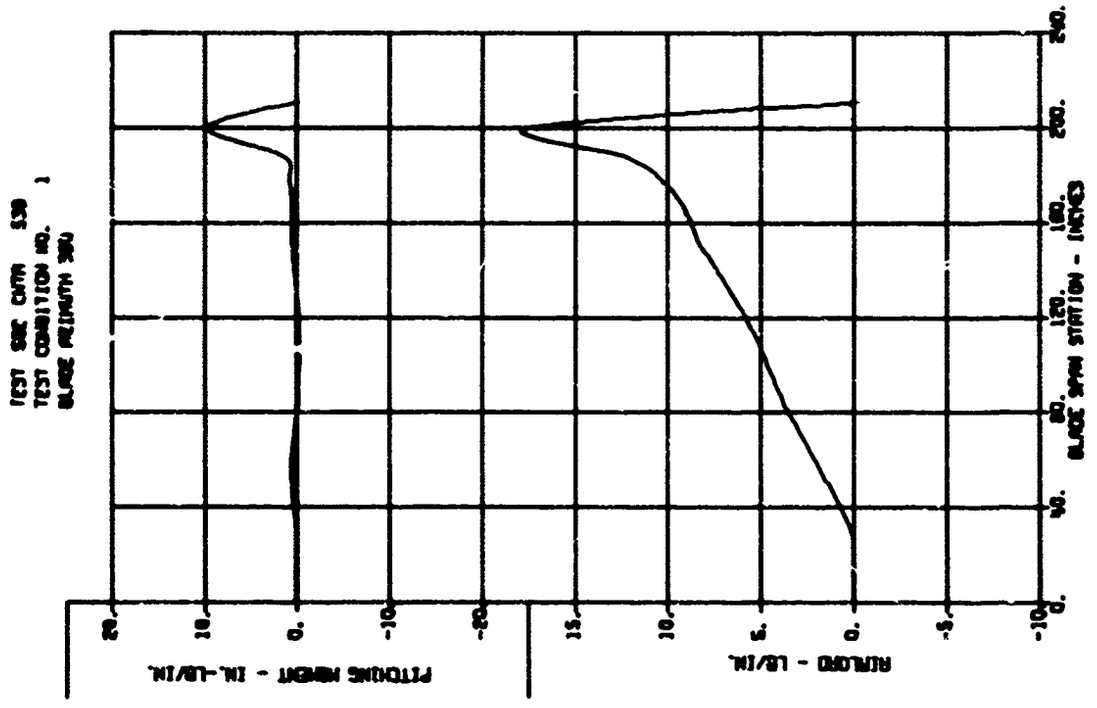

BLADE LOADS VERSUS SPAN - STATIC COMPONENTS

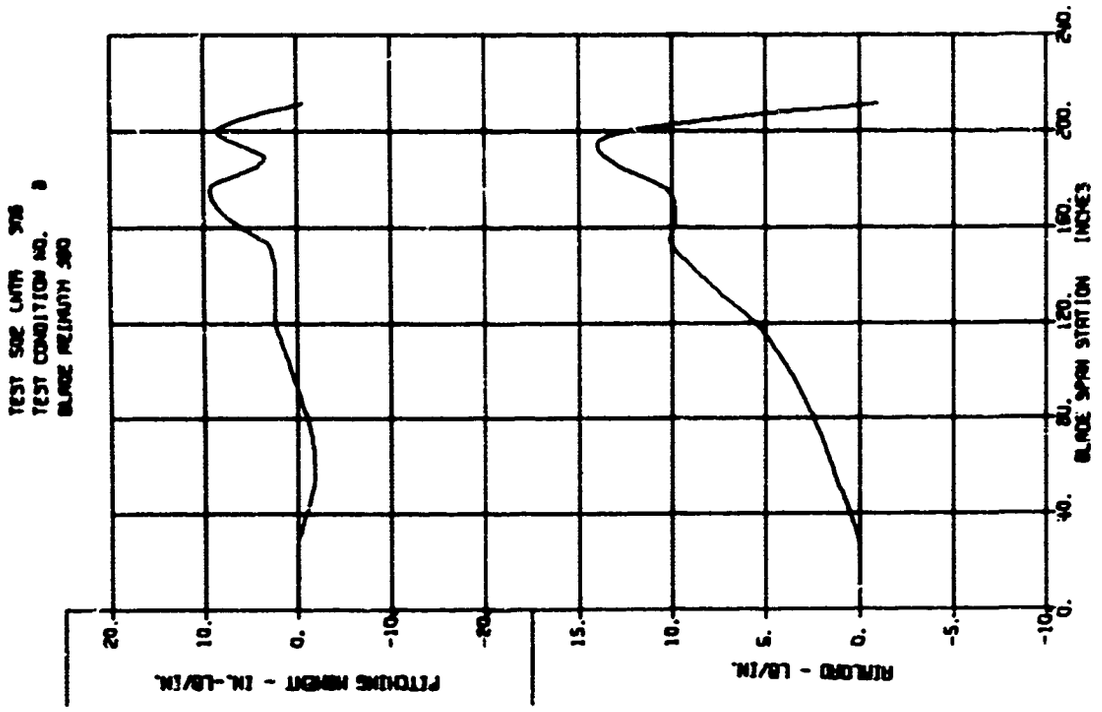

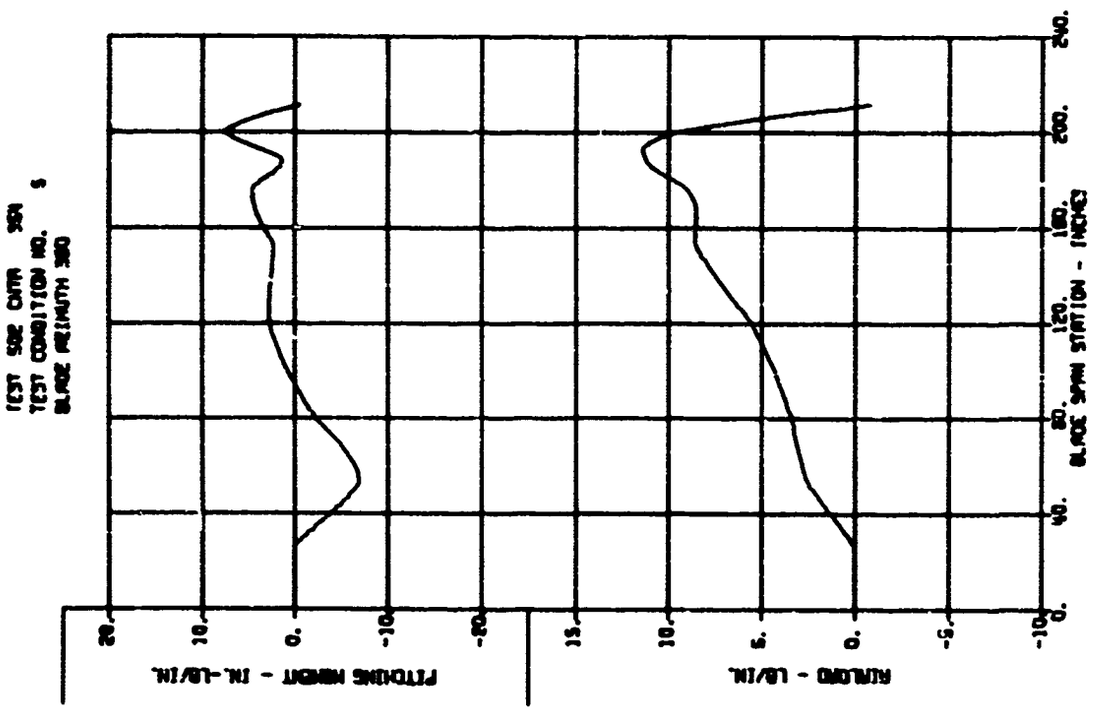

BLADE LOADS VERSUS SPAN - STATIC COMPONENTS

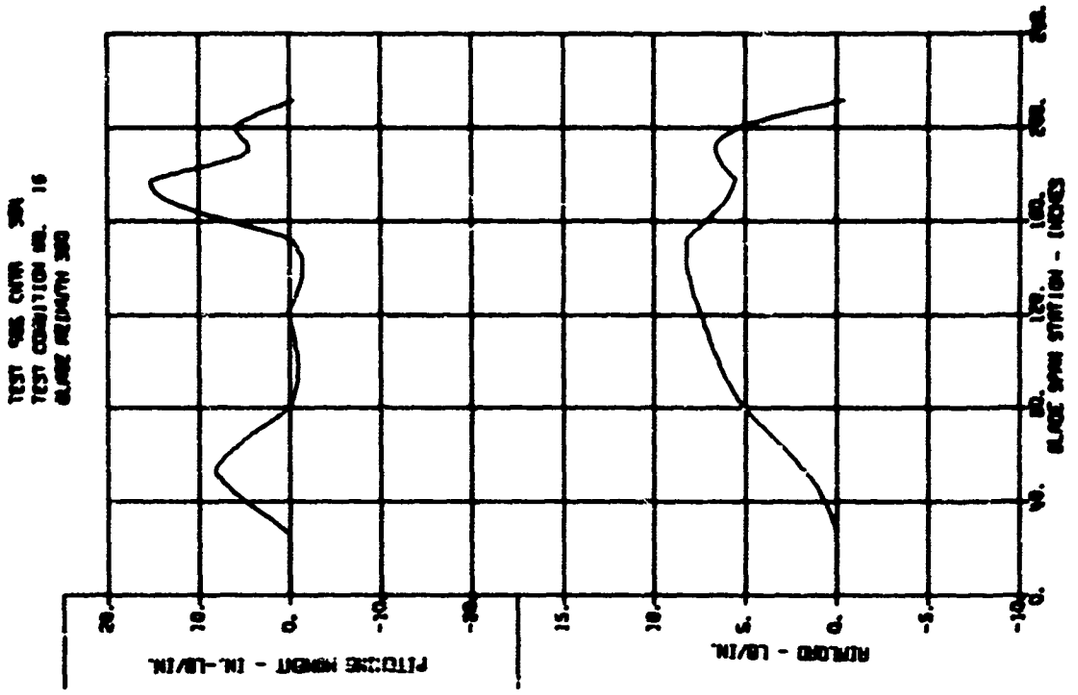

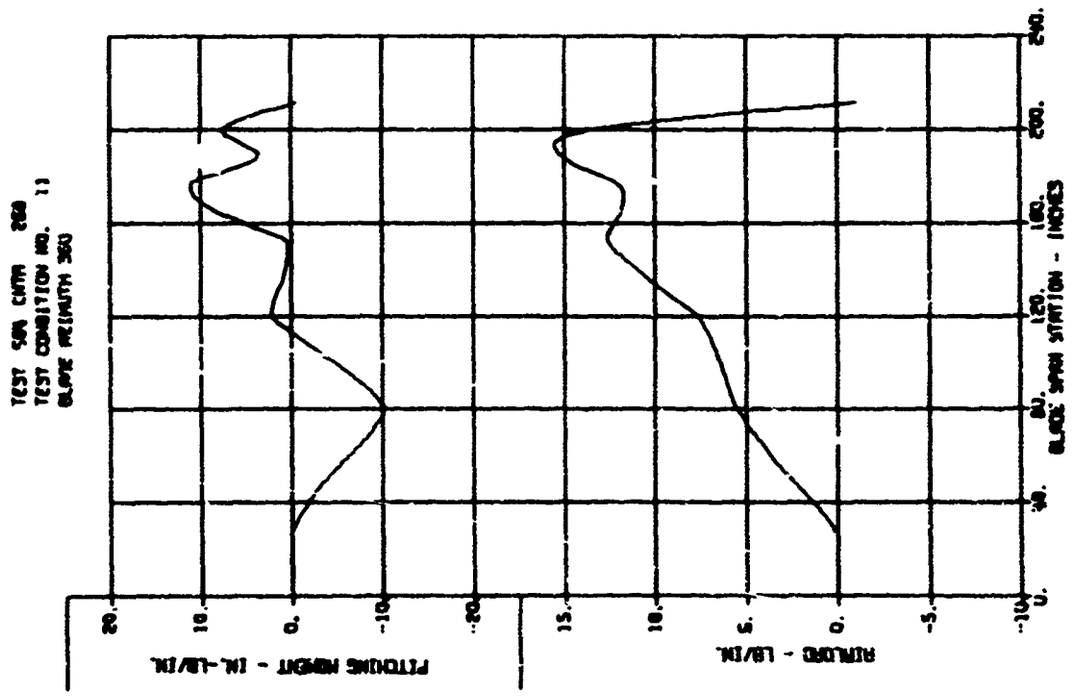

BLADE LOADS VERSUS SPAN - STATIC COMPONENTS

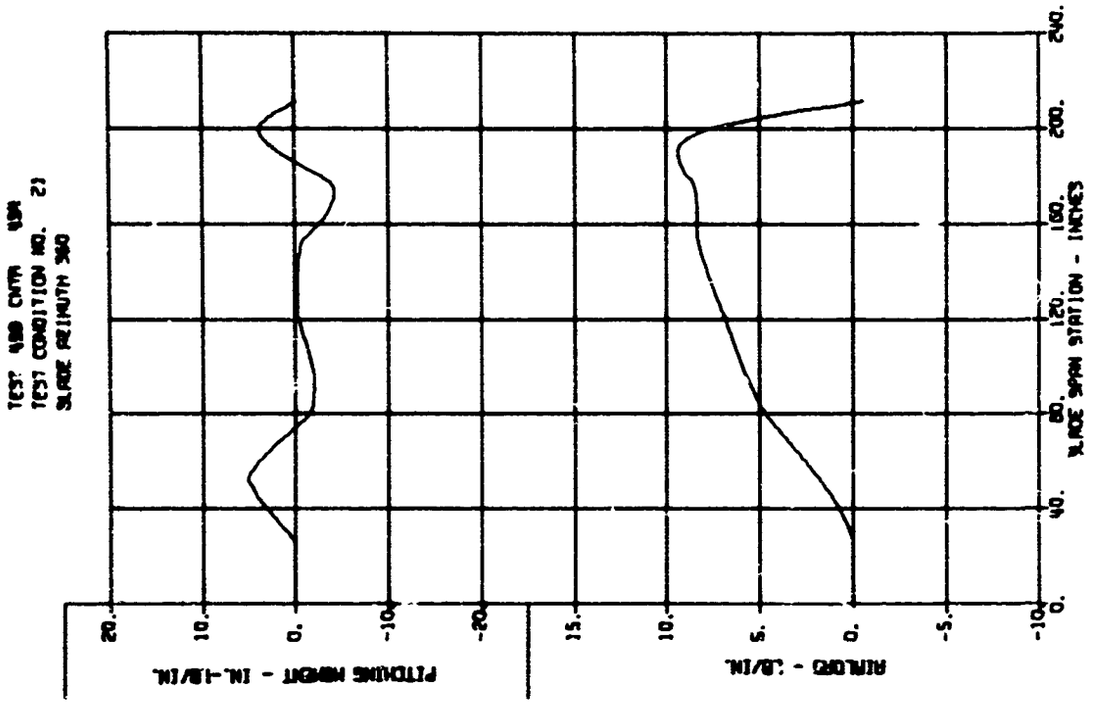

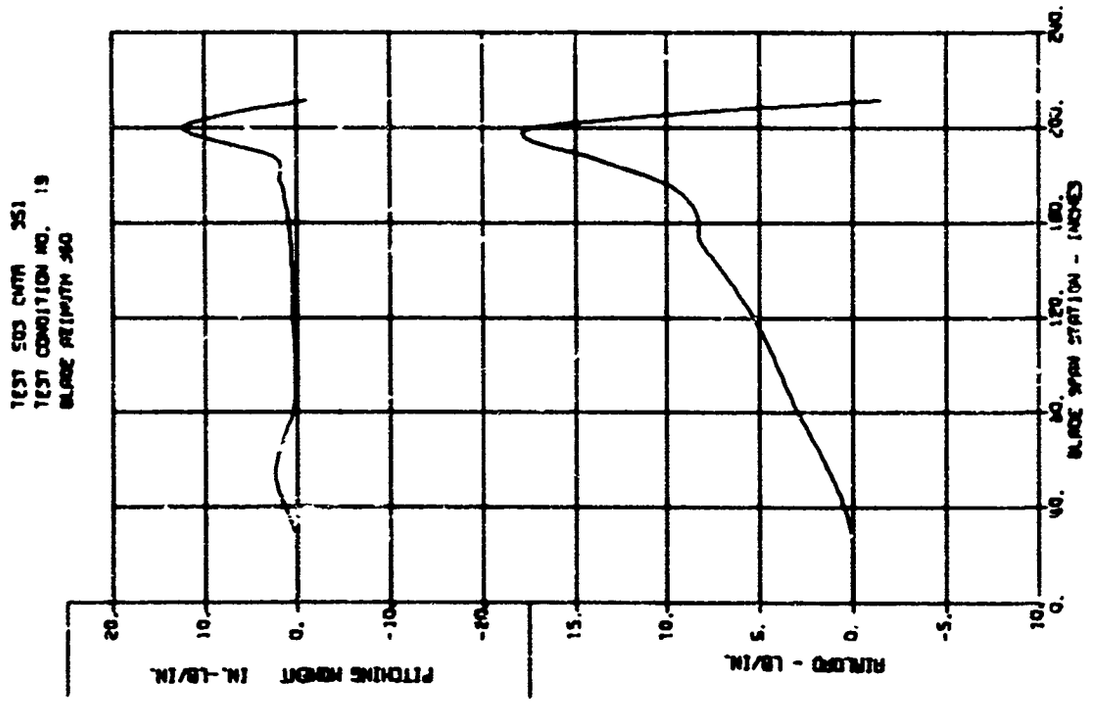

BLADE LOADS VERSUS SPAN - STATIC COMPONENTS

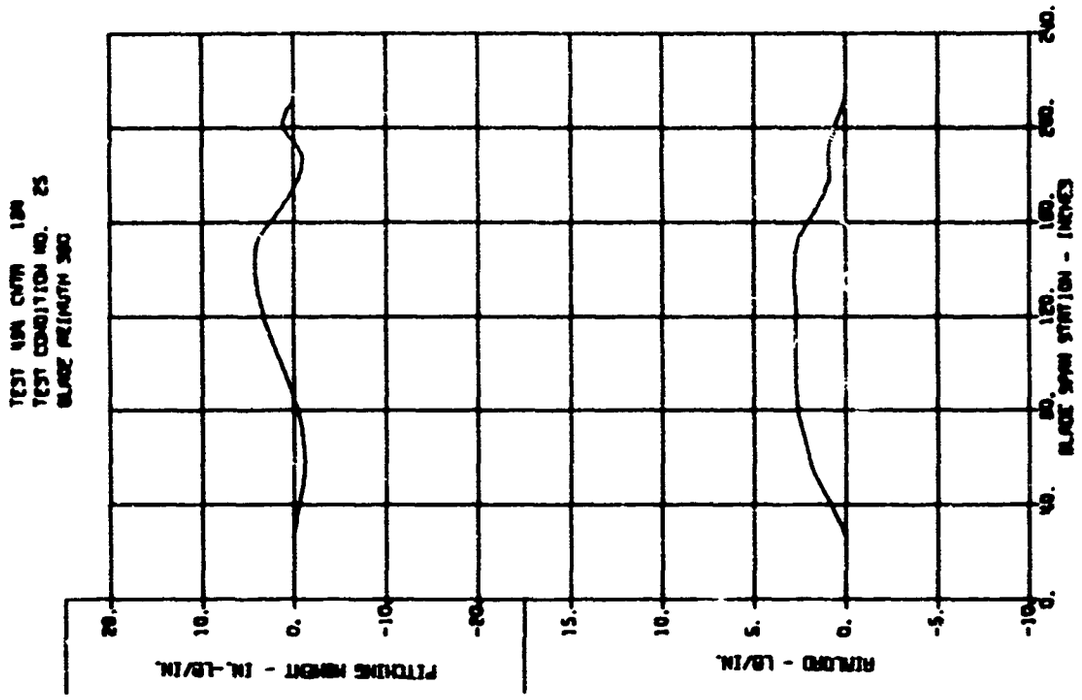

BLADE LOADS VERSUS SPAN - STIATIC COMPONENTS

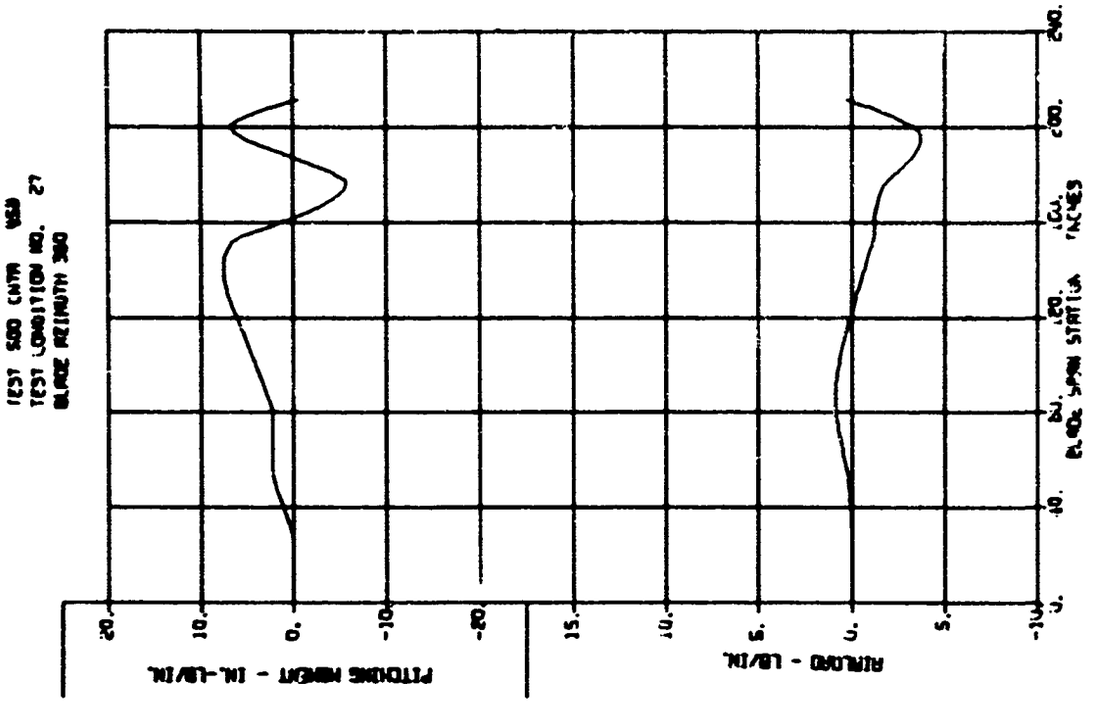

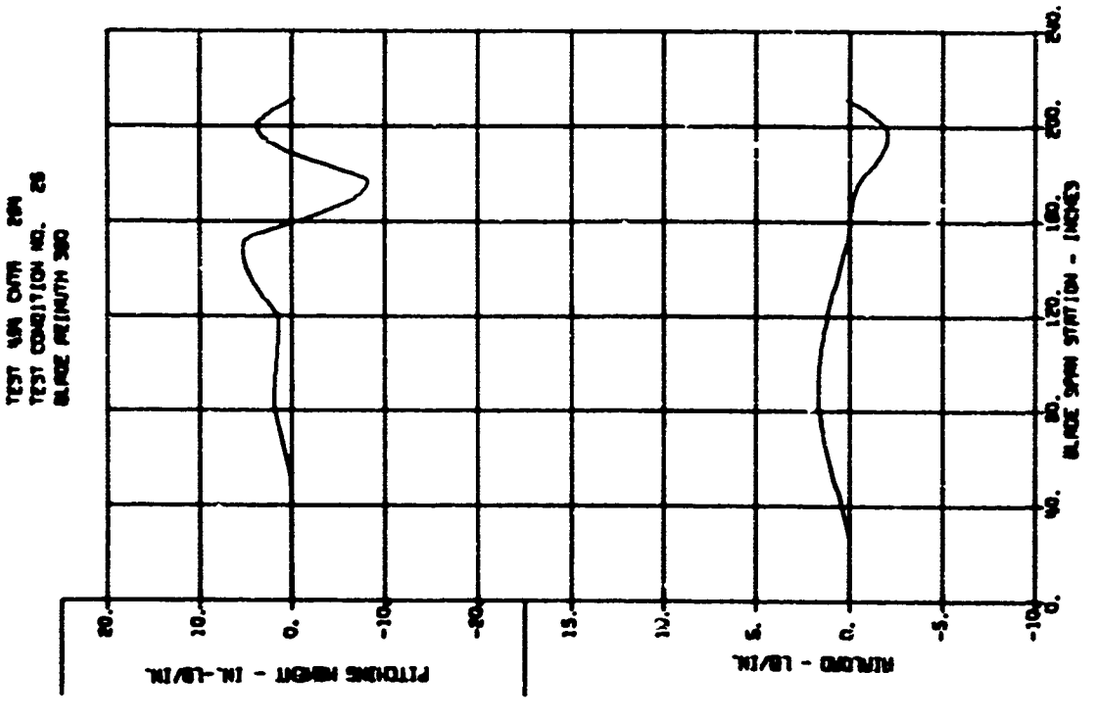

BLADE LOADS VERSUS SPAN - STATIC COMPONENTS

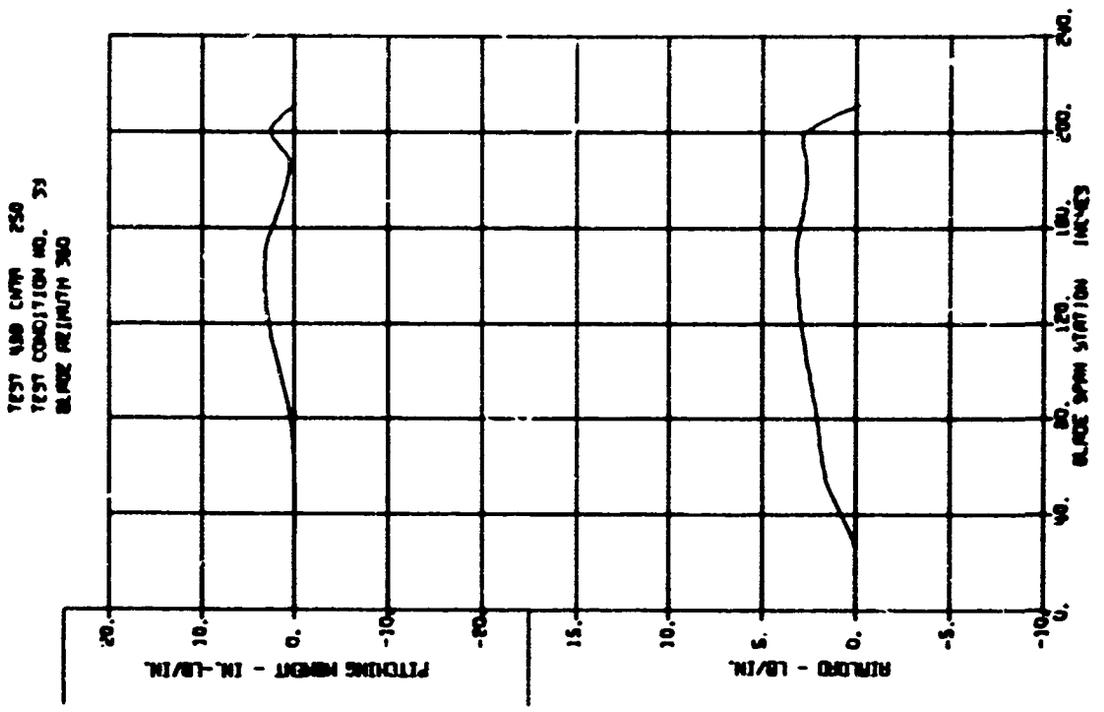

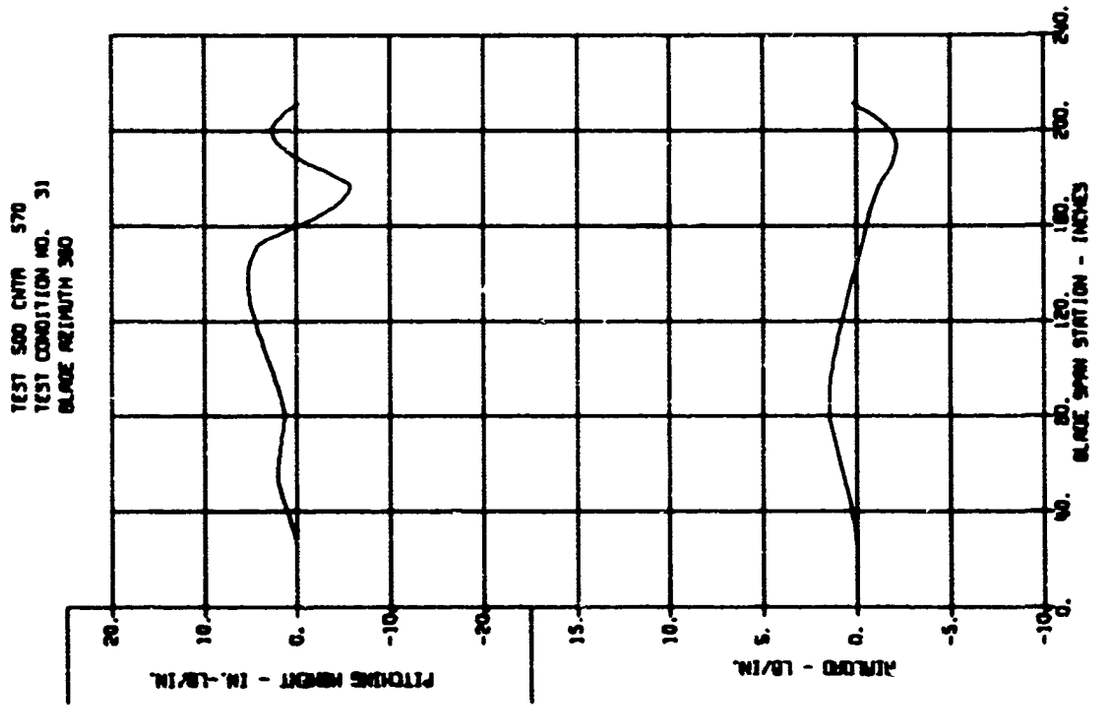

BLADE LOADS VERSUS SPAN - STATIC COMPONENTS

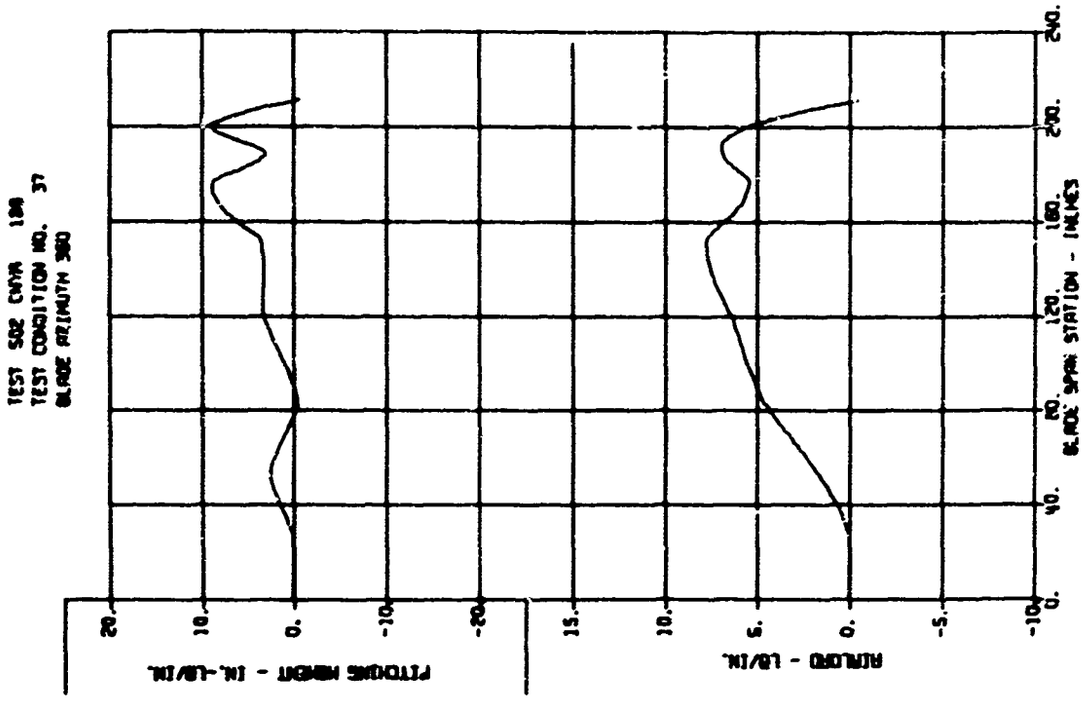

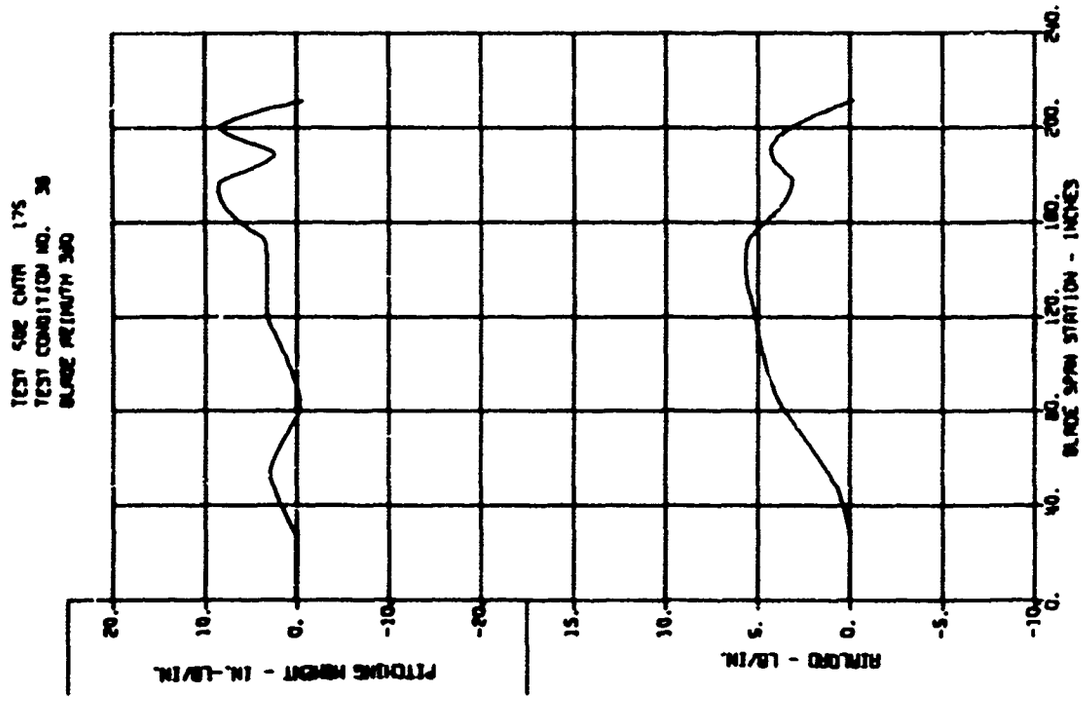

BLADE LOADS VERSUS SPAN - STATIC COMPONENTS

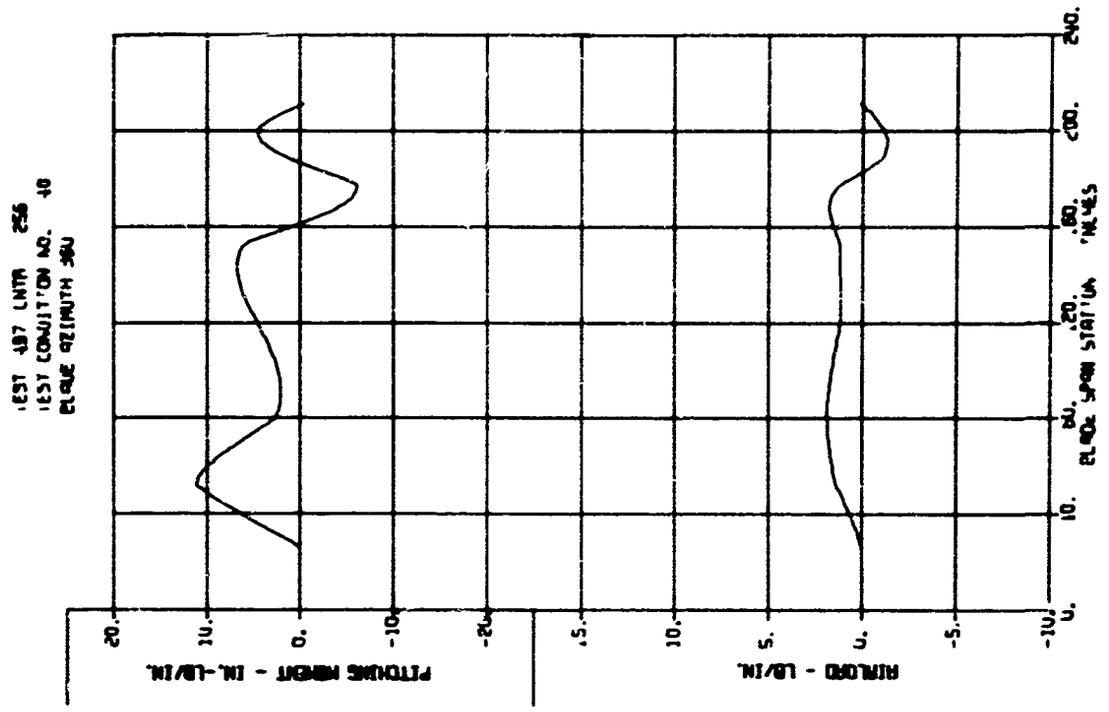

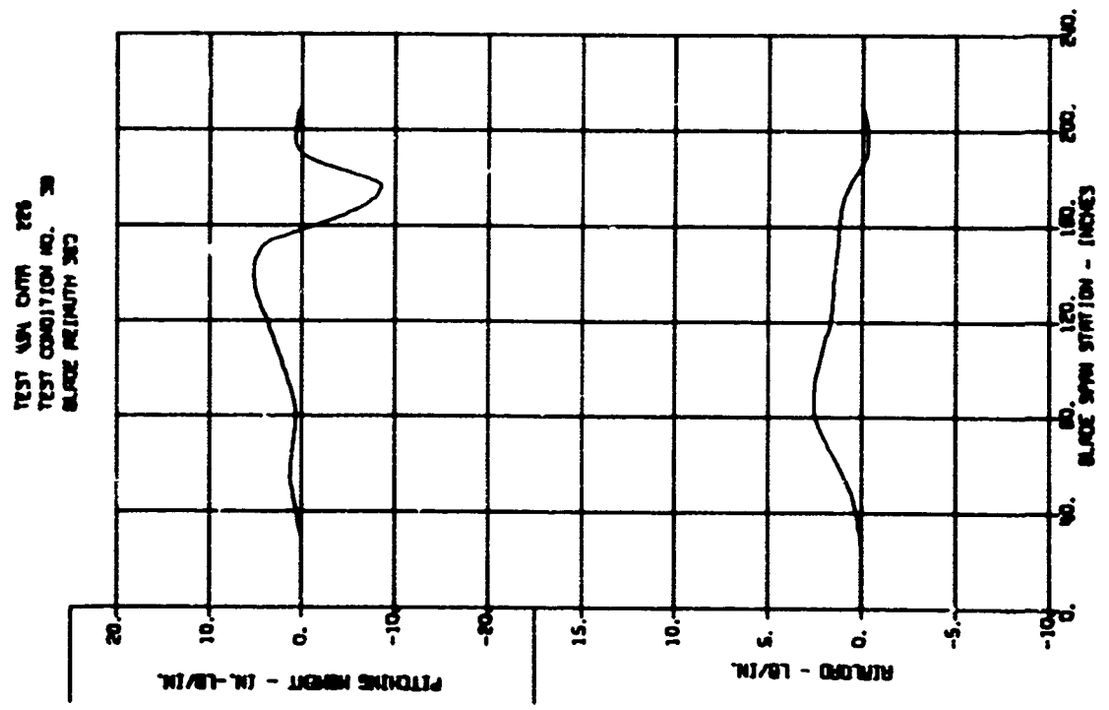

BLADE LOADS VERSUS SPAN - STATIC COMPONENTS

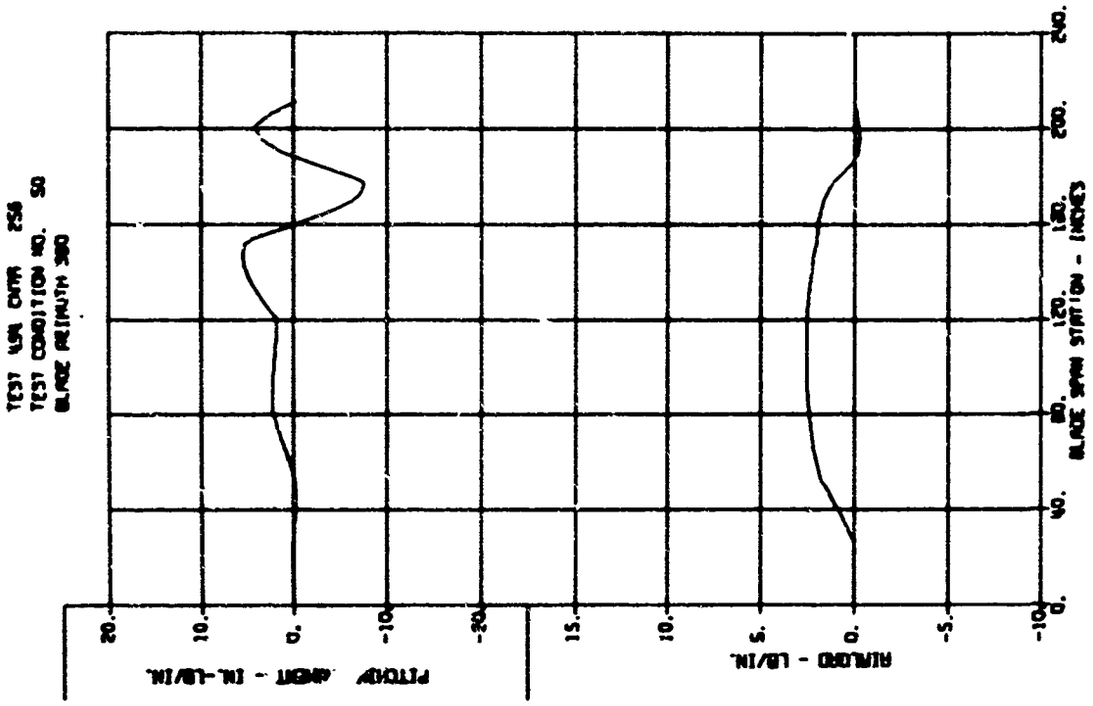

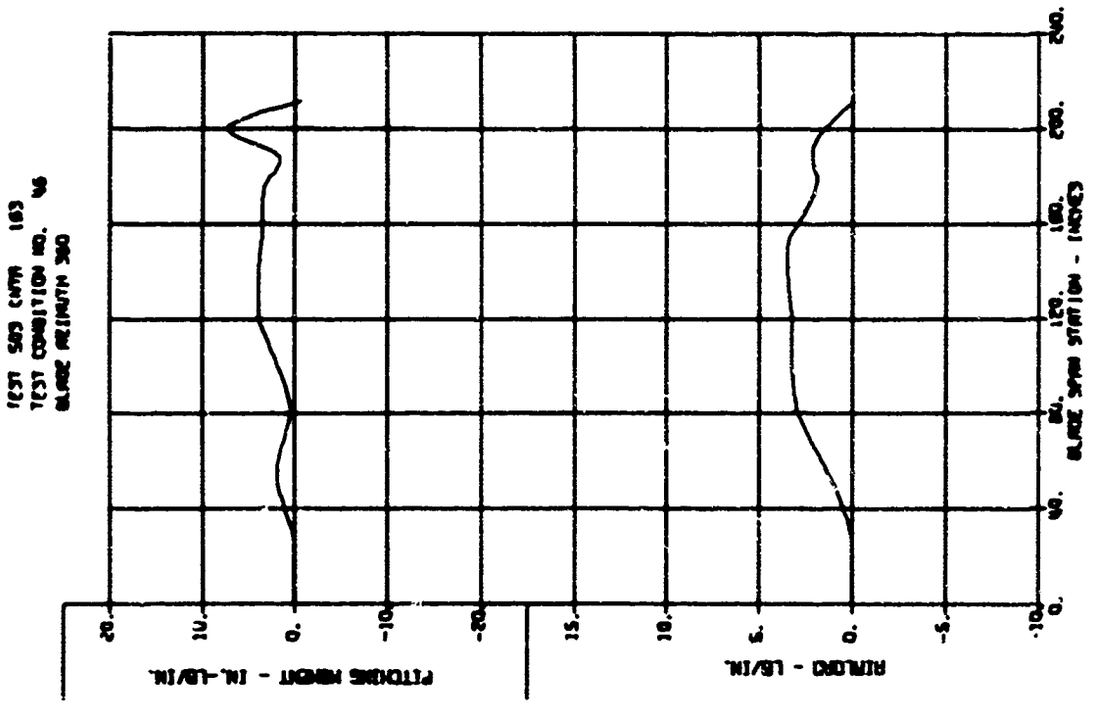

APPENDIX IV

BLADE LOAD HARMONICS VERSUS SPAN

The spanwise distribution of the steady-state term and the first three harmonic components of the blade loads (in pounds per inch) are presented in this appendix for the selected 20 conditions.

The symbols used for identification are:

A0 steady-state term

A1 cosine term of 1st harmonic

B1 sine term of 1st harmonic

A2 cosine term of 2nd harmonic

B2 sine term of 2nd harmonic

A3 cosine term of 3rd harmonic

B3 sine term of 3rd harmonic

BLADE LOAD HARMONICS VERSUS SPAN

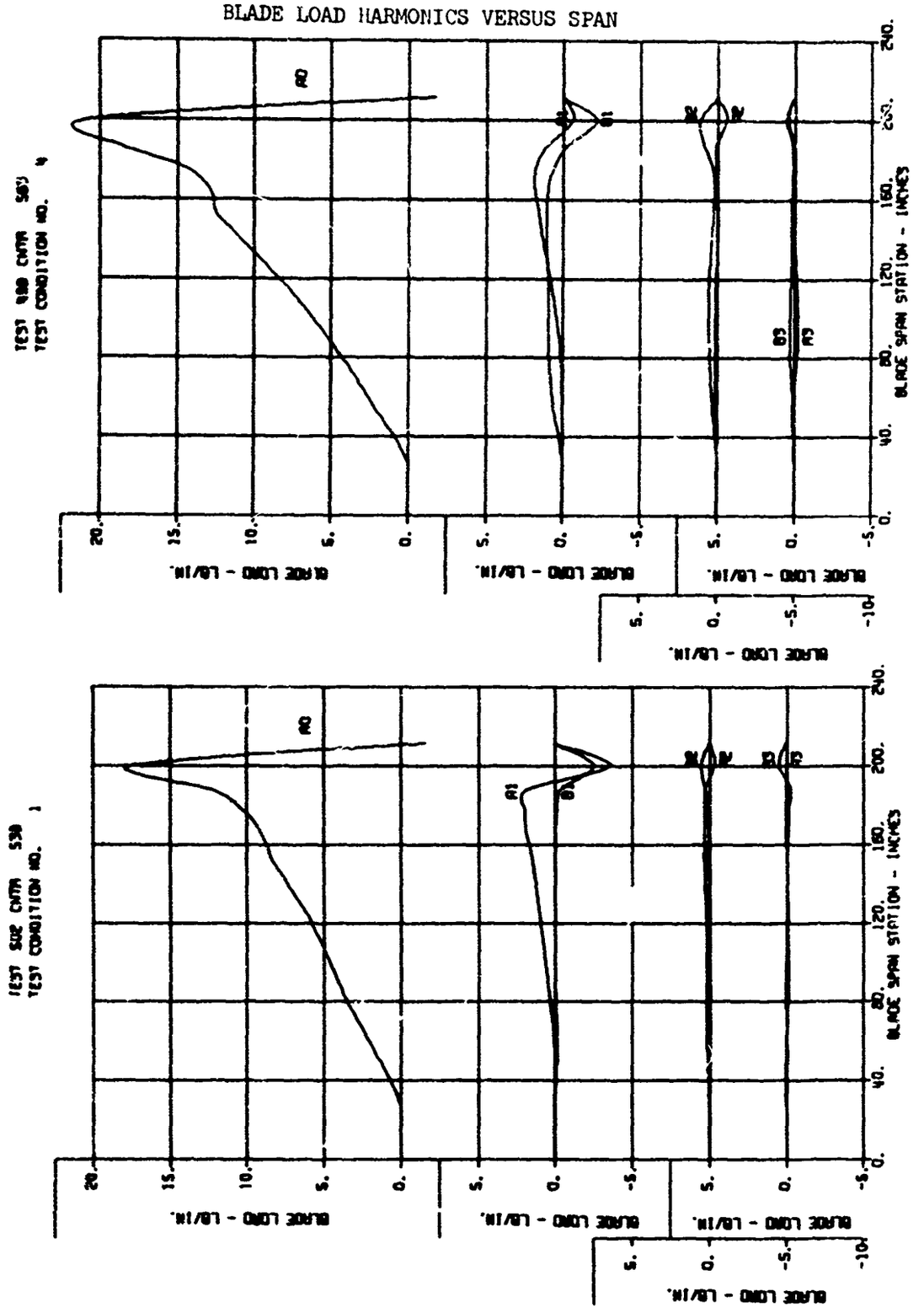

BLADE LOAD HARMONICS VERSUS SPAN

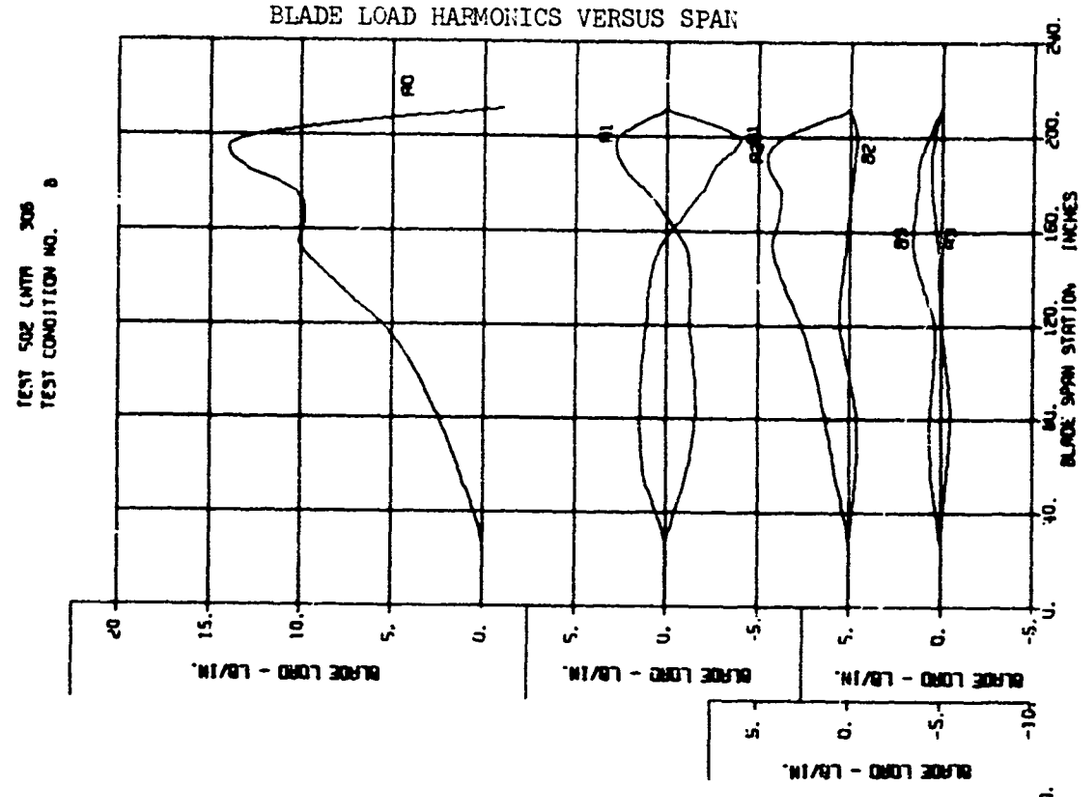

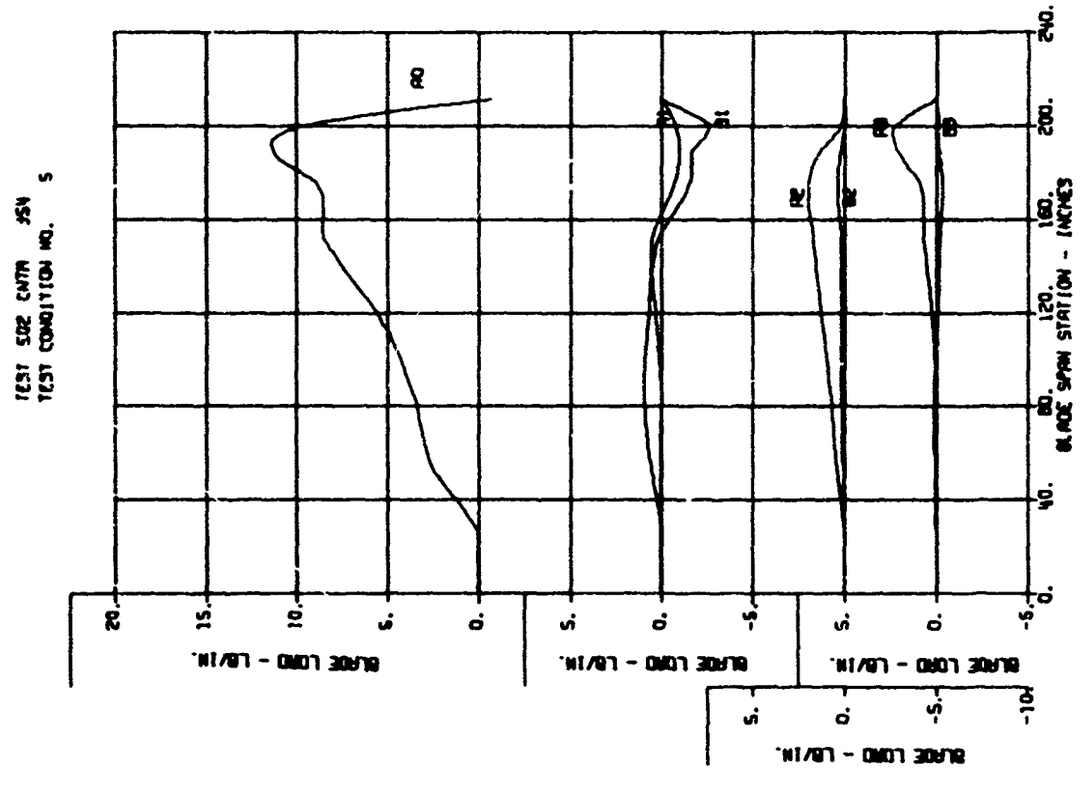

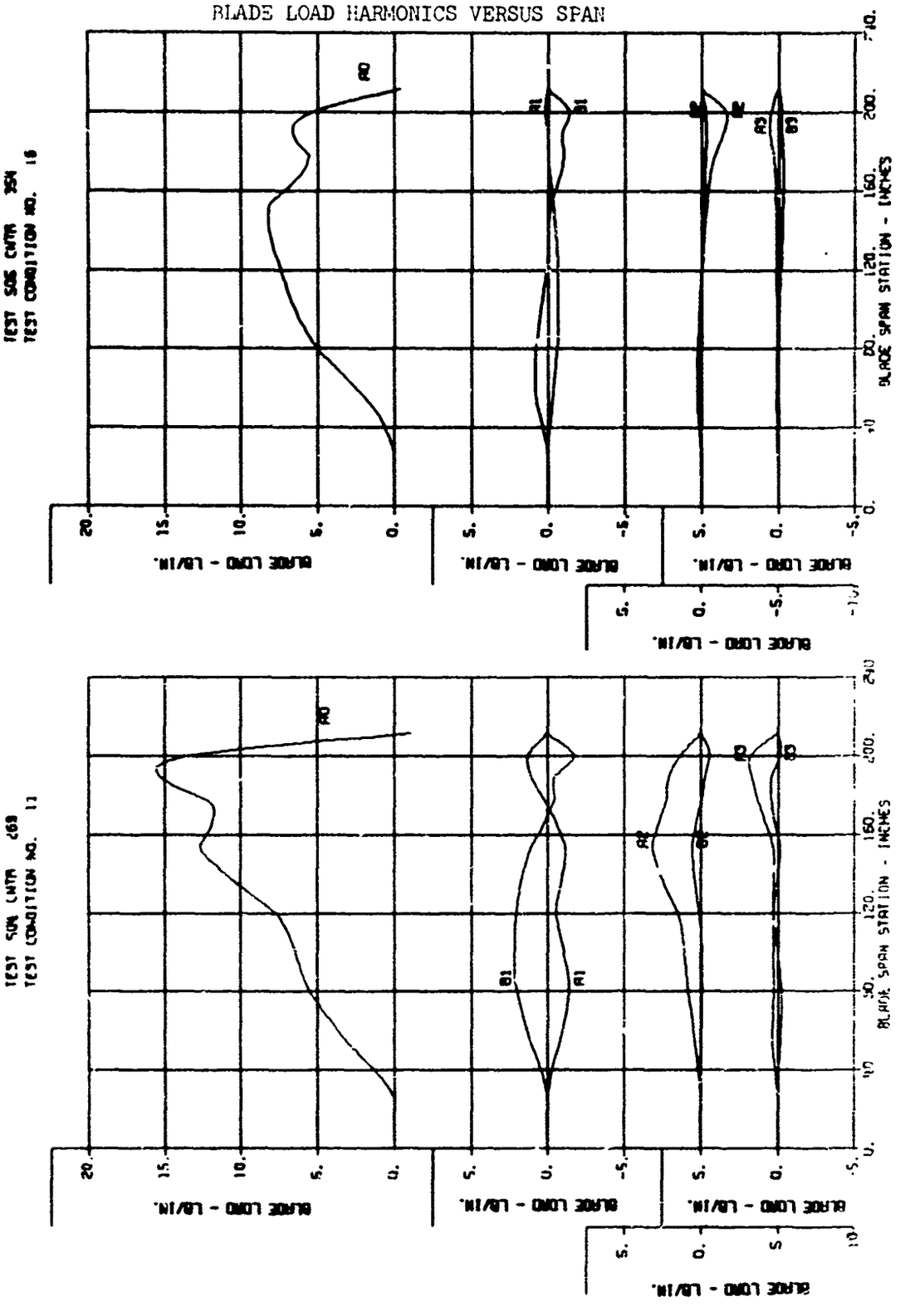
BLADE LOAD HARMONICS VERSUS SPAN
TEST SUN CNTR 359
TEST CONDITION NO. 16
BLADE LOAD - LB/IN.
BLADE SPAN STATION - INCHES
TEST SUN CNTR 269
TEST CONDITION NO. 11
BLADE LOAD - LB/IN.
BLADE SPAN STATION - INCHES

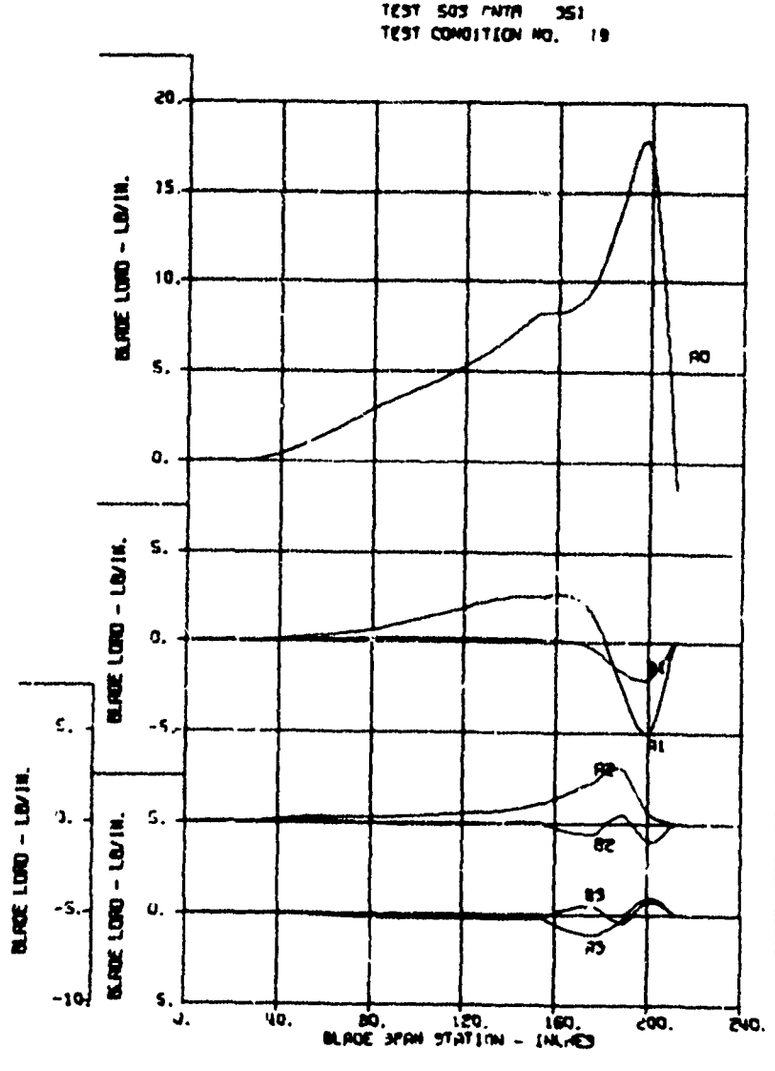

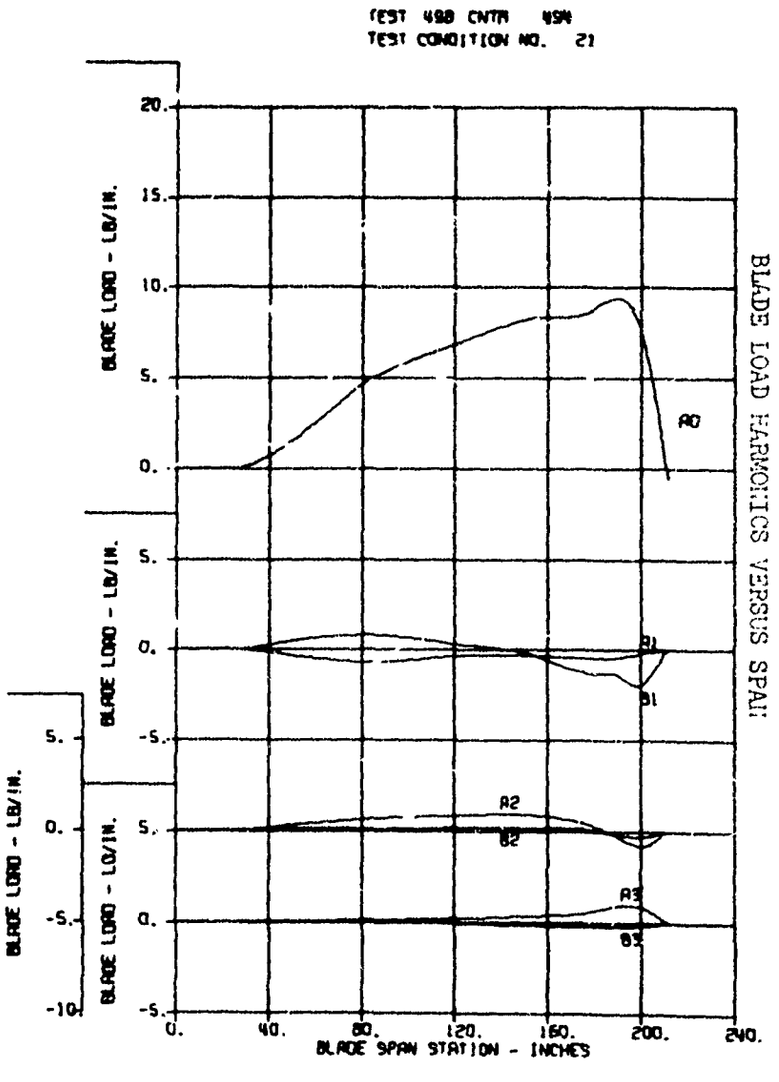

BLADE LOAD HARMONICS VERSUS SPAN

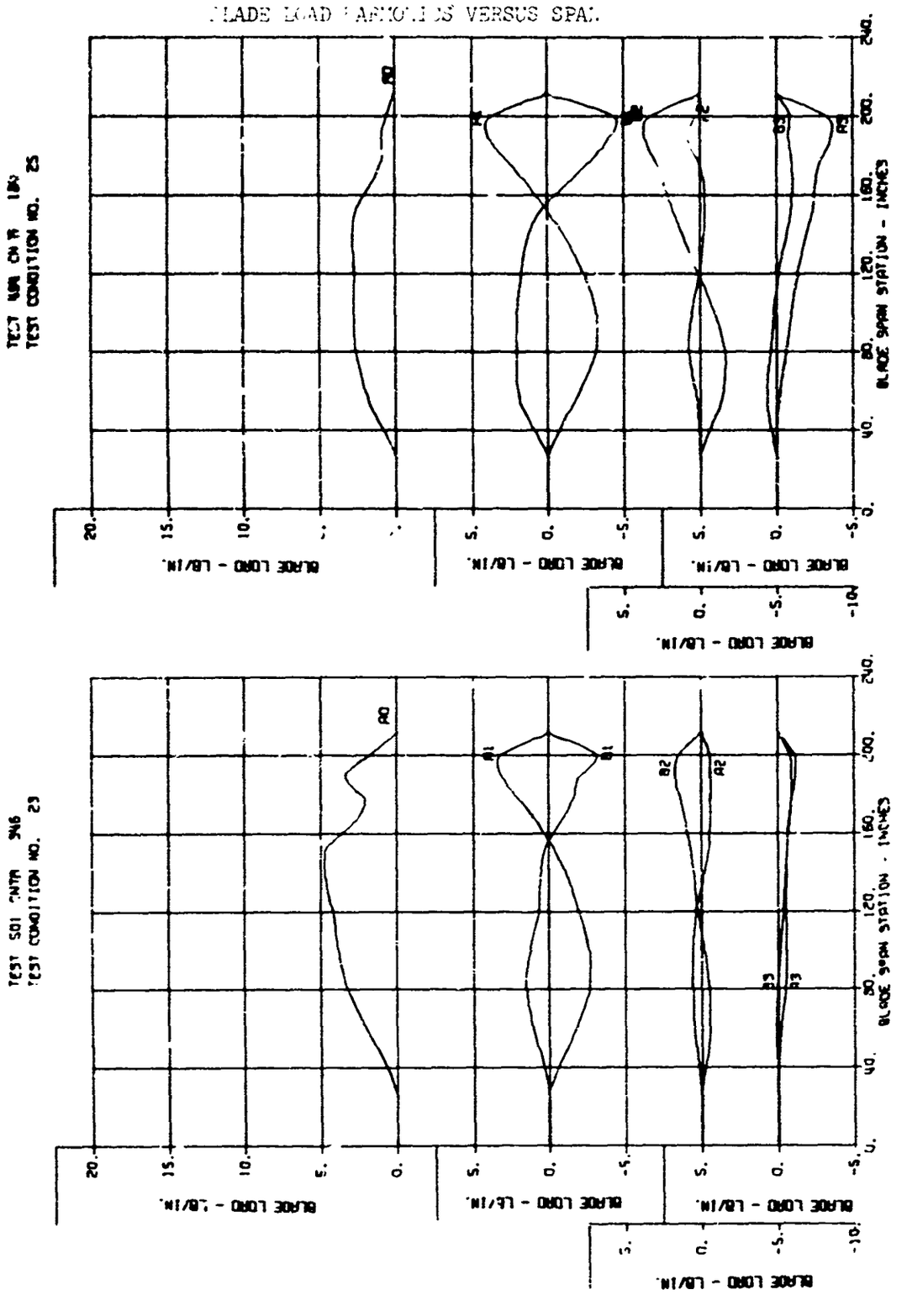
BLADE LOAD HARMONICS VERSUS SPAN
TEST CONDITION NO. 23
BLADE SPAN STATION - INCHES
BLADE LOAD - LB/IN.
TEST CONDITION NO. 23
BLADE SPAN STATION - INCHES
BLADE LOAD - LB/IN.

BLADE LOAD HARMONICS VERSUS SPAN

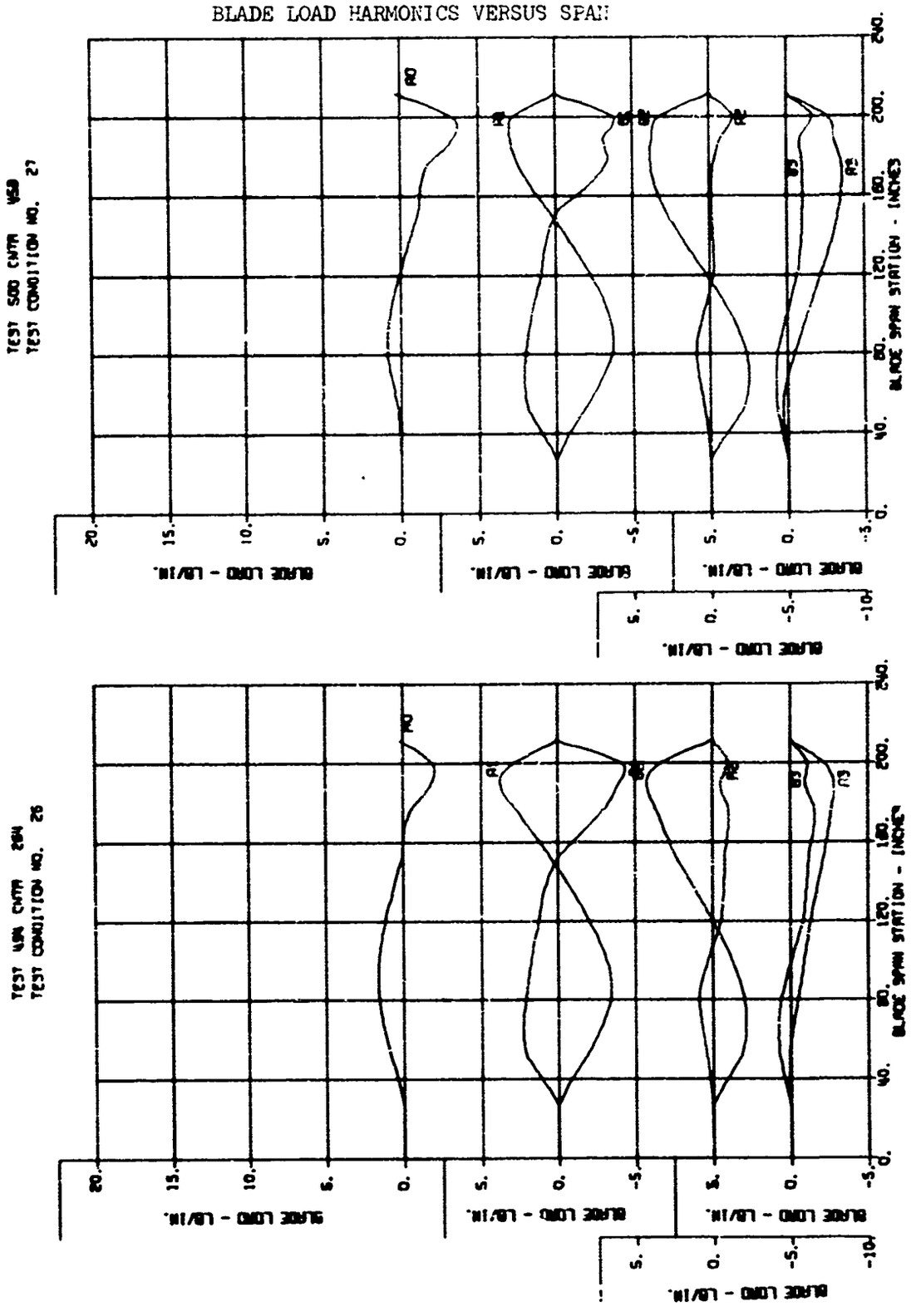

BLADE LOAD HARMONICS VERSUS SPAN

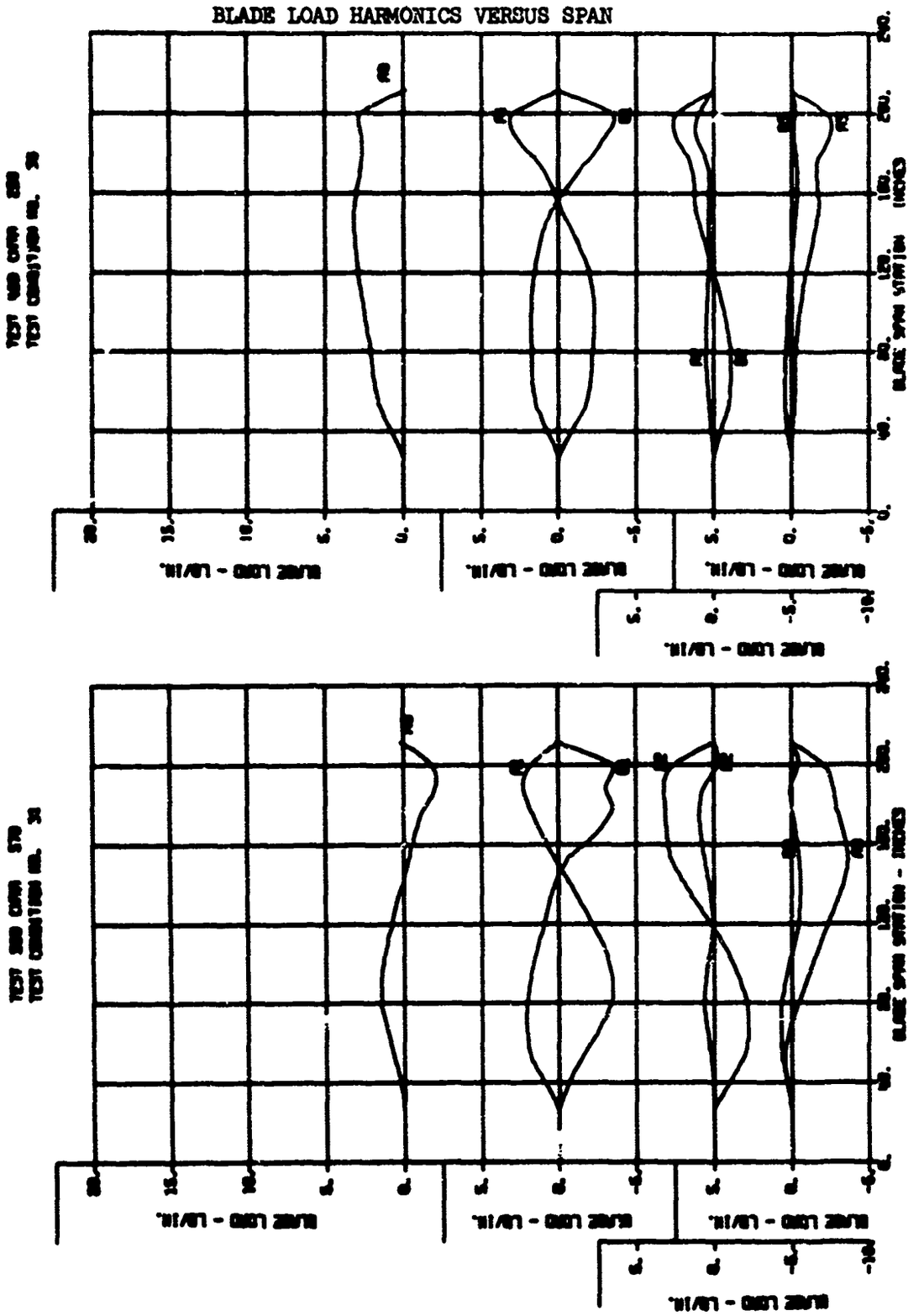

BLADE LOAD HARMONICS VERSUS SPAN

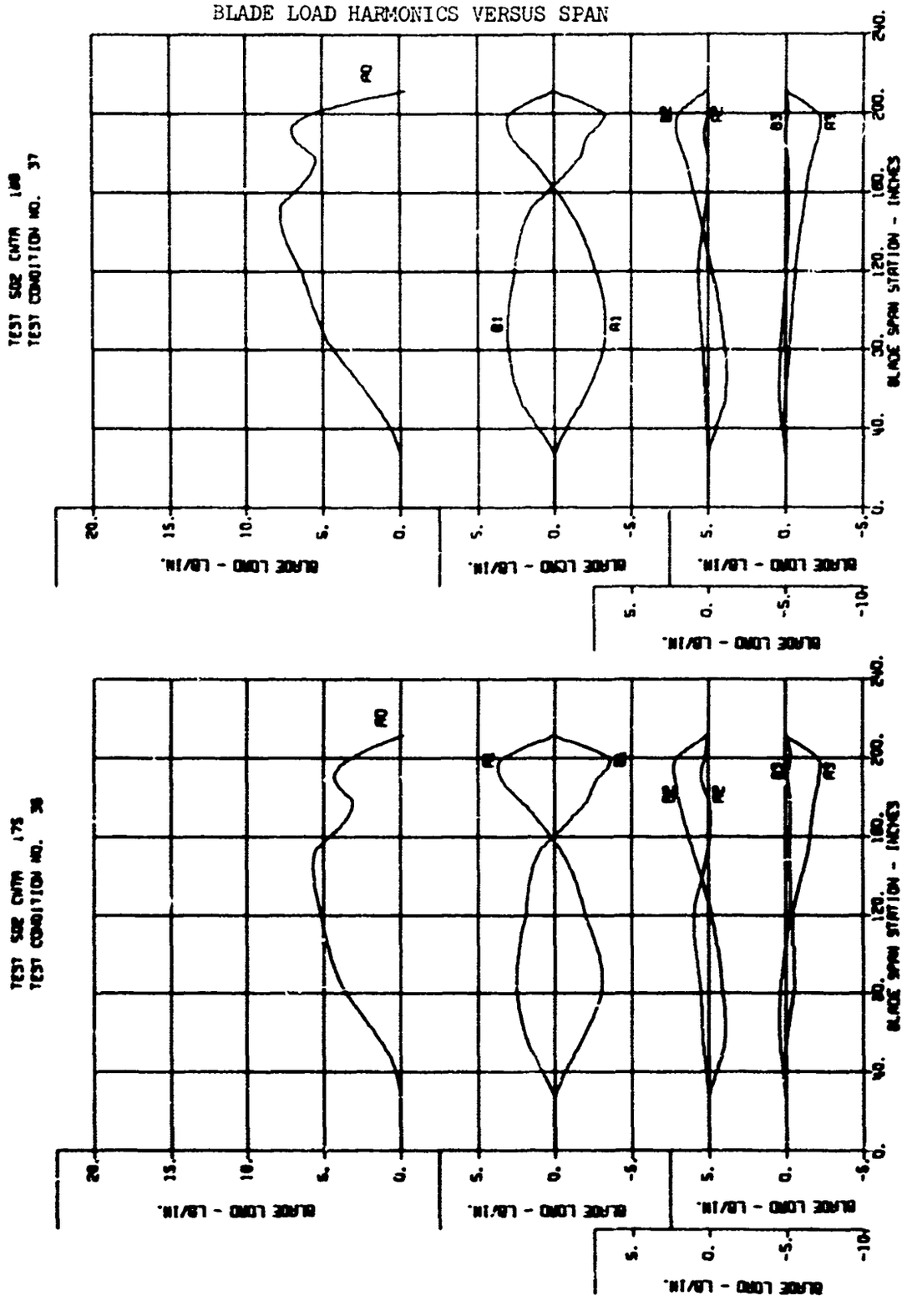

BLADE LOAD HARMONICS VERSUS SPAN

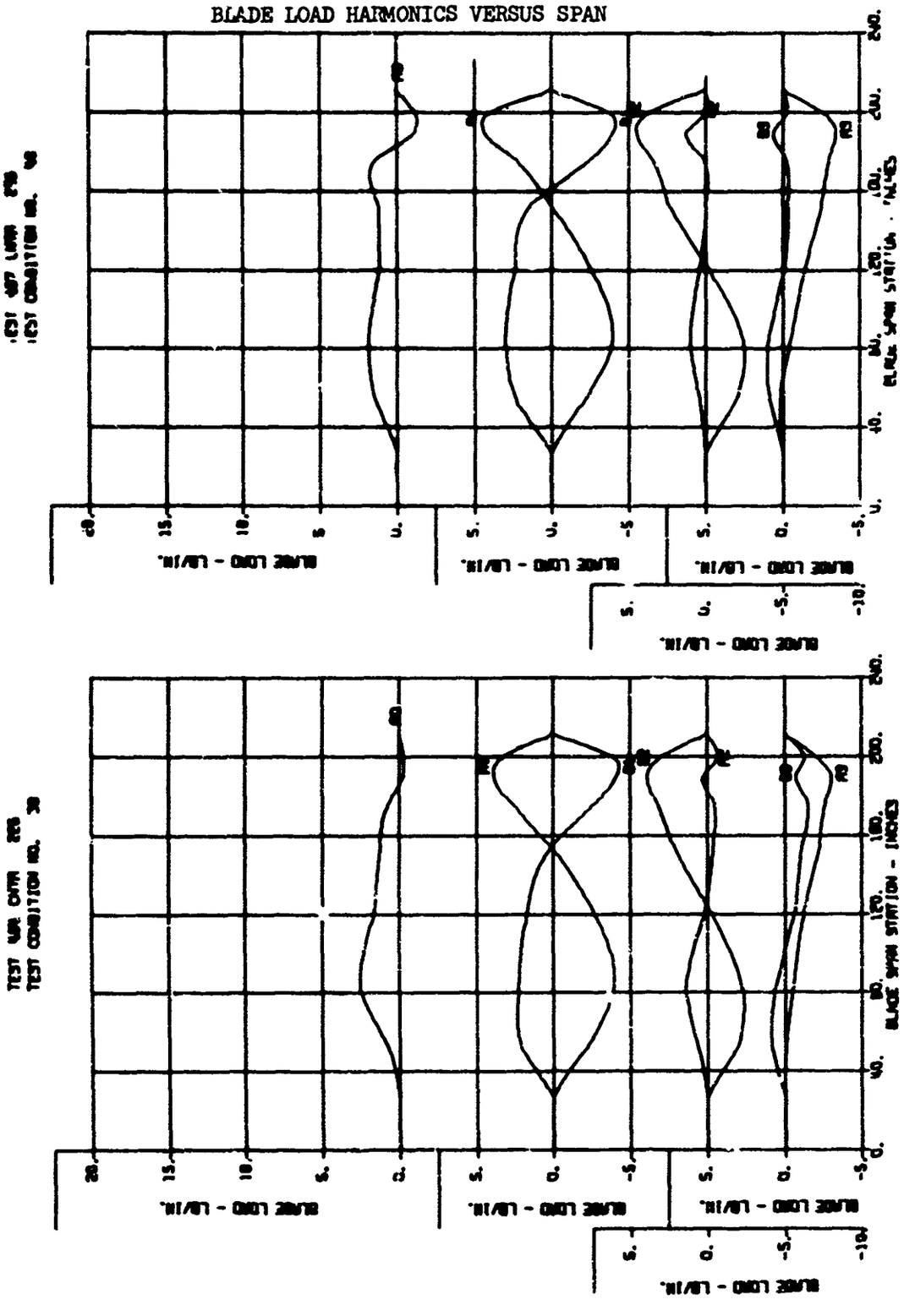

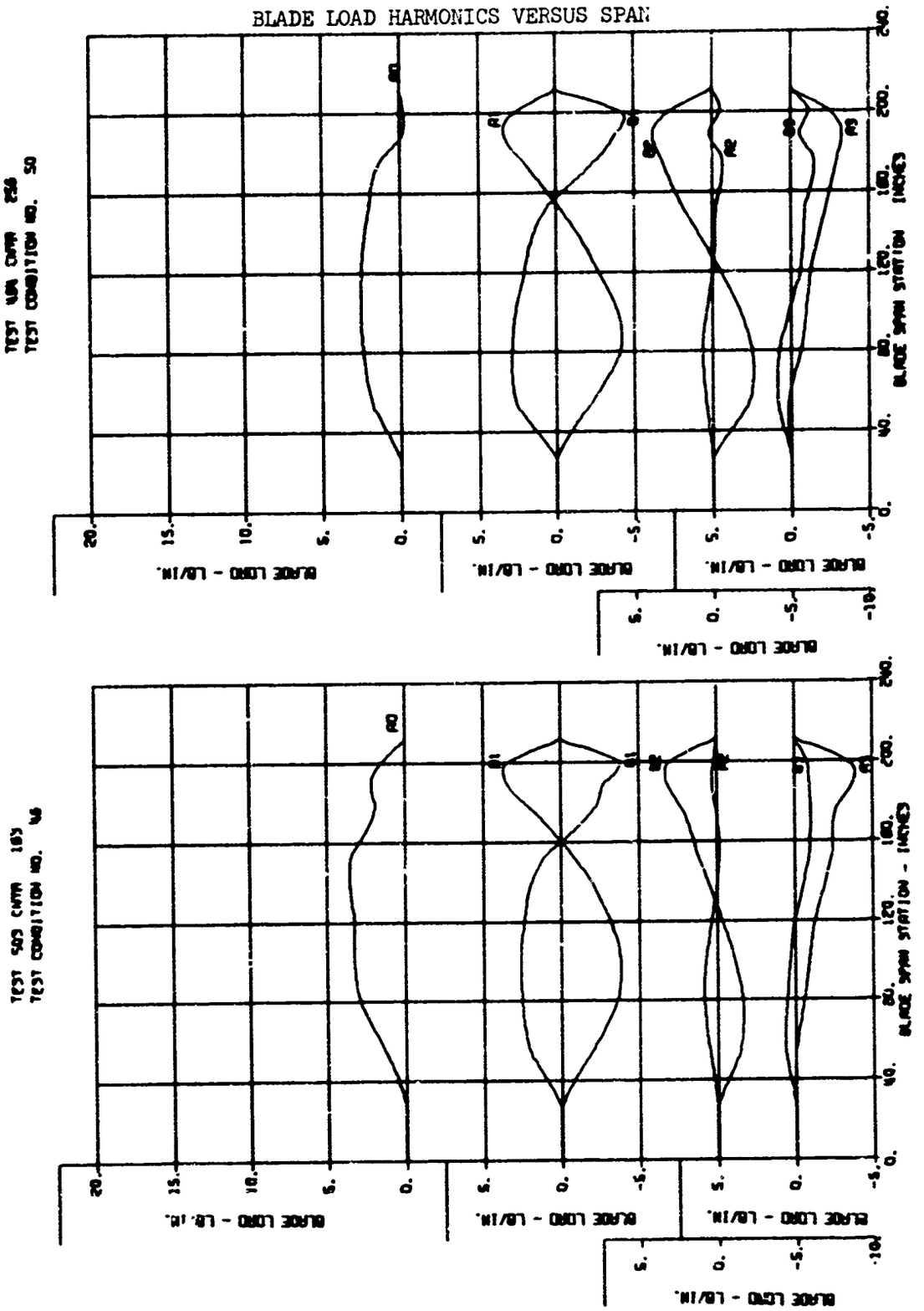
BLADE LOAD HARMONICS VERSUS SPAN
TEST WBA CHRN 256
TEST CONDITION NO. 50
BLADE SPAN STATION - INCHES
BLADE LOAD - LB/IN.
TEST SQS CHRN 183
TEST CONDITION NO. 48
BLADE SPAN STATION - INCHES
BLADE LOAD - LB/IN.

UNCLASSIFIED

Security Classification

DOCUMENT CONTROL DATA - R & D

(Security classification of title, body of abstract and indexing annotation must be entered when the overall report is classified)

1. ORIGINATING ACTIVITY (Corporate author)
Lockheed-California Company
Burbank, California

2a. REPORT SECURITY CLASSIFICATION
Unclassified

2b. GROUP

3. REPORT TITLE
In-Flight Measurement and Correlation With Theory of Blade Airloads and Responses on the XH-51A Compound Helicopter Rotor - Volume I, Measurement and Data Reduction of Airloads and Structural Loads

4. DESCRIPTIVE NOTES (Type of report and inclusive dates)
Final Technical Report

5. AUTHOR(S) (First name, middle initial, last name)
E. A. Bartsch

6. REPORT DATE	7a. TOTAL NO. OF PAGES	7b. NO. OF REFS
May 1968	179	5

8a. CONTRACT OR GRANT NO.	9a. ORIGINATOR'S REPORT NUMBER(S)
DA 44-177-AMC-357(T)	USAAVLABS Technical Report 68-22A
b. PROJECT NO. Task 1F125901A14608	
c.	9b. OTHER REPORT NO.(S) (Any other numbers that may be assigned this report) LR 21072
d.	

10. DISTRIBUTION STATEMENT
This document has been approved for public release and sale; its distribution is unlimited.

11. SUPPLEMENTARY NOTES	12. SPONSORING MILITARY ACTIVITY
Volume I of a 3-volume report	U.S. Army Aviation Materiel Laboratories Fort Eustis, Virginia

13. ABSTRACT

This report presents the results of a two-phase research program consisting of (1) in-flight measurement of aerodynamic pressures and structural loads on a compound, rigid-rotor helicopter and (2) correlation of these data with theoretical results.

Flight test data obtained in Phase I and recorded on an oscillograph were read on an oscillograph reading machine and were processed in an automatic data reduction program. This data processing consisted of integration of the pressure data to obtain the distribution of aerodynamic lift and pitching moments over the rotor blade, as functions of azimuth position. Airload and structural load data were harmonically analyzed.

Output of the data reduction program was used in Phase II as input to the correlation program. The measured airloads were used to compute the theoretical bending and torsion responses of the blade. The measured torsion moments were used in the theoretical prediction of the airloads. The results of the applied theories are compared with the flight measurements.

DD FORM 1 NOV 68 1473 REPLACES DD FORM 1473, 1 JAN 64, WHICH IS OBSOLETE FOR ARMY USE.

UNCLASSIFIED

Security Classification

14. KEY WORDS	LINK A		LINK B		LINK C	
	ROLE	WT	ROLE	WT	ROLE	WT
Compound Helicopter						
Differential Pressure Measurements						
Dynamic Response						
Harmonic Analysis						
Helicopter						
High Advance Ratio						
Modes of Vibration						
Pressure Measurements						
Rigid Rotor						
Rotor Loads						
XH-51A						